Ph.D. Thesis

POLITECNICO DI TORINO

Dottorato di Ricerca in Scienza e Tecnologia dei Materiali

"Composite Materials reinforced by Carbon Nanotubes"

Tutor:

Matteo Pavese

Coordinator:

Prof. Claudio Badini

Candidate:

Silvia Marchisio

February 2013

CONTENT

CHAPTER 1: AIM OF THE WORK

The work of this Ph.D. thesis has been realised in the field of a promising and largely studied technological material: the carbon nanotubes (CNTs). After a first observation they were "re-discovered" at the beginning of the 90s and immediately started to cover a fundamental role in several scientific branches, from Physics to Chemistry, going through Medicine and Biology. In the Material Science and Engineering field a large number of studies have been conducted on carbon nanotubes, as a consequence of their extraordinary physical, technological and mechanical properties. For what concerns this thesis, they have been largely investigated as reinforcement materials in composites. Since 1991 a large number of attempts have been conducted, trying to exploit the outstanding potential of this carbonaceous material, in order to improve the properties of several matrices. The most important application is the production of polymer matrices composites (PMCs), but in last decades an increasing number of metal matrix ones (MMCs) have been presented and recently also ceramic matrix (CMCs) applications have been attempted. Despite massive efforts focused on CNTs-composites, the potential of employing this reinforcement materials has not yet been fully exploited. This lack is substantially due to the difficulties associated with the dispersion of entangled carbon nanotubes during processing and poor interfacial interaction between CNTs and matrix materials. The dispersion states of the nanotubes involve complicated phenomena, since the carbon nanotubes are produced in bundles or bundle aggregations. The states are affected by at least two competitive interactions: (1) the interactions of van der Waals forces, among carbon nanotube threads, and (2) the interactions between carbon nanotube threads and dispersion medium. The characteristics of single carbon nanotube and of bundles of carbon nanotubes are completely different. CNTs must be uniformly dispersed to the level of isolated tubes individually wetted by the matrix. This is necessary in order to achieve efficient load transfer to the reinforcement network. This also results in a more uniform stress distribution and minimises the presence of stress concentration centres.

Because of these reasons the very first aspect of this work has been the study of the dispersion state of nanotubes. The aim of the experiments was not only to obtain a good dispersion and distribution of the CNTs, but also to evaluate their dispersion grade. Indeed, due to their nanosize and to their carbonaceous nature, few simple experimental techniques result suitable for this purpose. In addition, the objective was also to use dispersion techniques which do not imply the utilisation of

high amount of solvents, reagents or surfactants, and so the aim was to develop a process as simple, low costs and as environmental friendly as possible.

The second part of the work consisted in the application of the carbon nanotubes to the production of new materials for technological applications, with improved mechanical properties. Three composite materials with different matrices have been designed, developed and produced: a polymer matrix composite, a ceramic matrix and a metal matrix one.

Also in these cases the aim of the work was the tuning of simple and possibly low costs production systems.

For PMCs a polyvinyl butyral matrix has been used and the composites were obtained by a deeply studied technique in the research group: the tape casting technology. The same approach was also used in the case of CMCs: tape casted silicon carbide matrix composites reinforced by carbon nanotubes have been produced. Finally a third matrix has been experimented: MMCs were investigated starting from pure aluminium powders. For Al matrix composites a particular technique was used: the sintering was obtained starting from a powder metallurgy approach and exploiting electric current and pressure (Electric Current Assisted Sintering approach).

For all the three different composite materials, after the development of the production route and the preparation of several specimens, a characterization step followed. The materials were characterized in terms of physical properties, morphology and microstructure, and mechanical behaviour.

CHAPTER 2: CARBON NANOTUBES AND THEIR ROLE AS REINFORCEMENT IN COMPOSITE MATERIALS

2.1. CARBON NANOTUBES

2.1.1. ALLOTROPY OF THE CARBON ELEMENT

The concept of carbon polymorphism was introduced for the first time in Mistscherlich's papers in1822 (Mitscherlich, 1822 Mitscherlich, E., 1822. Annales de Chimie, 19, 350–419). In Chatelier's book « Leçons sur le Carbone » (Le Chatelier, 1926), he affirmed *« Le carbone non combiné se présente sous des forms très curieuses: carbone amorphe, graphite et diamant »* (« Uncombined carbon is found under very inquiring forms: amorphous carbon, graphite and diamond"). After the discovery of the X-Ray diffraction in 1912, these two fundamental crystal structures (cubic diamond and hexagonal graphite) were identified and characterized. In the middle of next century the so called "Amorphous carbons" were deeply studied and moreover several new carbon polymorphic phases were identified and sintered. In Sixties, Russian scientists noticed one dimension chain like carbon structures, called carbynes (Donnet et al., 2000; S.-Y. Li, Zhou, Gu, & Zhu, 2000); in 1985 a large family of spherical carbon structures, called fullerenes, was discovered (H W Kroto, Heath, O'Brien, Curl, & Smalley, 1985); finally in 1991 a curved form of graphene (graphene refers to an atomic layer of graphite), the so called carbon nanotube, was identified (Bethune et al., 1993; S Iijima & Ichihashi, 1993; Sumio Iijima, 1991).

Even if carbon nanotubes were probably observed in the previous decades, mostly by Russian researchers, the date of 1991 is the most important in the history of such a material, since it was the data the carbon nanotubes were re-discovered as a promising material for technological applications. This was due both to the technological development that allowed at that time the exploitation of nano-sized materials but also to the instrumentation development that allowed complete characterisation of these materials. The previous observations of similar materials could not be complete and were generally neglected to the apparent little interest in such a material (Monthioux & Kuznetsov, 2006).

Crystalline Form	Diamonds	Graphites	Carbynes*	Fullerenes, Nanotubes
Hybridization	sp^3	sp^2	sp^1	$sp^{2+\epsilon}$
Coordinance z	4	3	2	3
Physical dimensionality D	3	2	1	0 and 1
Bond length (Å)	1.54	1.40	1.21	1.33 to 1.40
Bond energy (eV/mole)	15	25	35	> 25

* Also mixed sp^1 and sp^3 hybridizations (α form)

Table 1 - Schematic classification of the different forms of carbon (Loiseau, Launois, Petit, Roche, & Salvetat, 2006)

Allotropic forms of elemental carbon are divided into thermodynamically stable and metastable phases. The thermodynamic phase diagram of the carbon is shown in Figure 1. It has been elaborated after several decades of experimental works (Bundy, 1996).

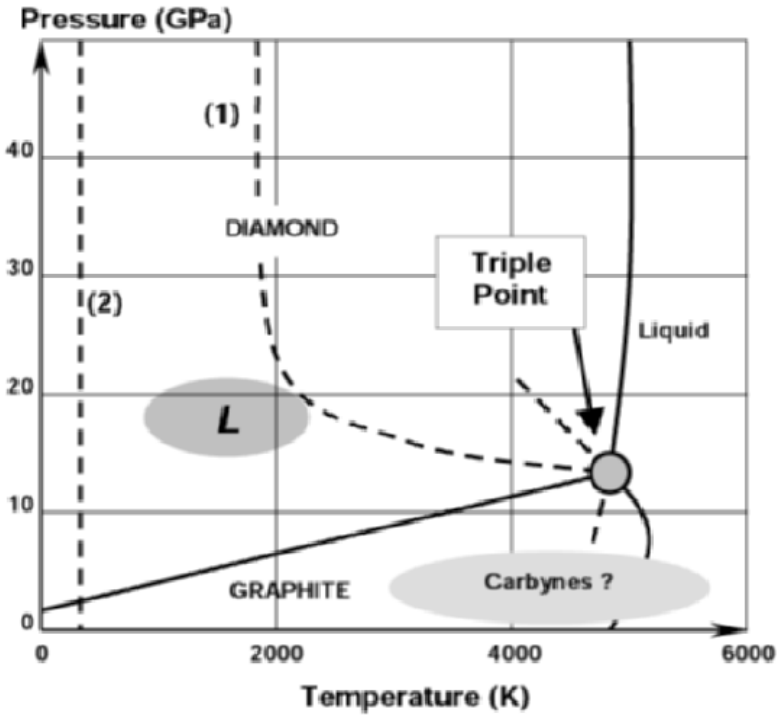

Figure 1 - Thermodynamic phase diagram of the carbon element. Solid lines represent equilibrium phase boundaries and dotted lines the kinetic transformations; L is for Lonsdaleite phase (Bundy, 1996)

At ambient temperatures and pressures the hexagonal graphite is the stabile phase (with the existence of a polytype, a rhombohedral variety under metastable conditions). The cubic diamond phase is stable under high pressures; a hexagonal phase known as Lonsdaleite is found under specific conditions. The carbyne phase should exist at high temperature, below the melting line of graphite. All the phase transformations are considered as theoretically reversible. Under this frame it does not

appear evident to include in the same diagram the new molecular carbon phases, fullerenes and nanotubes which are not classical extended solids but can form themselves crystalline structures.

During last decades several theoretical models have been developed to predict new carbon species with particular properties (Cohen, 1994, 1998). These models are based on the calculation of enthalpy (as the excess of cohesion energy at zero Kelvin). One important parameter is the bulk modulus B_0

$$B_0 = -V_0 \left(\frac{dP}{dT}\right)_{T\to 0}$$

A useful semi-empirical expression has been proposed by Cohen (Cohen, 1994):

$$B_0 = \frac{N_c}{4}(1972 - 220\lambda)d^{-3.5}$$

where N_c is the average coordination number of the compound considered, d the average bond length and λ is an ionization factor which is zero for pure carbons. For short d and large bond energy we obtain large compressibility factors and thus high cohesion energies. The highest density of strong covalent bonds is associated with super hard compounds with low compressibility factors, whereupon diamond is such hard material.

However in new phase materials, such as carbon nanotubes, the total cohesion energy can be decreased by curving the graphene sheets and forming closed structures as cylinders. A topological classification for curved surfaces, in non-Euclidian geometry, was proposed by Schwarz (Schwarz, 1890). A simple approach is to define a mean (H) and a Gaussian (K) curvatures proportional to the inverse of a length and a surface, respectively. As proposed by Mackay and Terrones (Mackay& Terrones, 1991), the following geometrical shapes may exist:

– K >0 (spheres) as fullerenes

– K = 0 (planes or cylinders if H = 0), as nanotubes

– K <0 (saddle): “Schwarzites”.

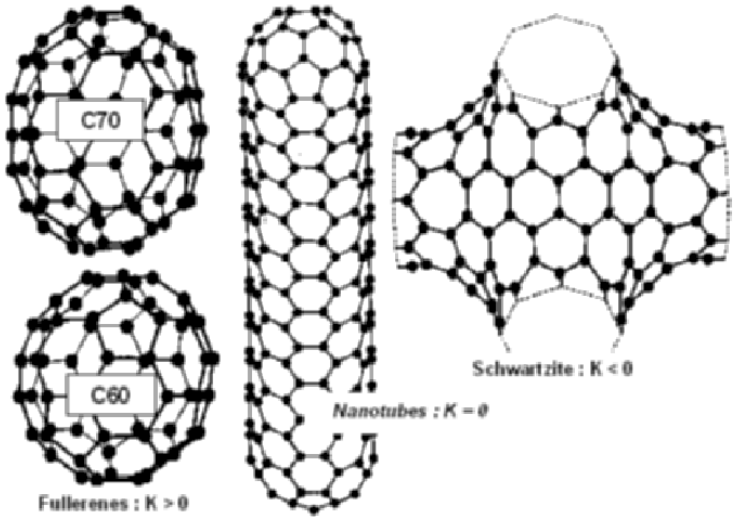

Figure 2 - Examples of curved graphene varieties classified through their gaussian curvature *K*

Negatively curved carbon networks belong to the class of periodic minimal surfaces and they have been called "Schwarzites", in honour of Schwartz. This curvature is made possible by introducing seven or eight member rings in addition to the usual six members for planar surfaces. In spite of different attempts, these big unit cells have not been observed experimentally. The same holds for a positive curvature owing to a five member ring (case of C_{60}).

Infinite single-wall nanotubes are cylindrical shaped with carbon atoms organized in a honeycomb lattice. Their coordination number is three (z = 3) and the surface curvature induces some s-p hybridization. Single-wall carbon nanotubes (SWCNTs) can be ideally constructed rolling a graphene sheet. Because of this construction it is possible to characterize the CNT structure with a pair of integers (*n,m*). These indices define the so-called "chiral vector":

$$\vec{C} = n\overrightarrow{a_1} + m\overrightarrow{a_2}$$

which joins two crystallographically equivalent sites of the nanotube on the graphene sheet, $(\overrightarrow{a_1},\overrightarrow{a_2})$ being the graphene basis where $a = |\overrightarrow{a_1}| = |\overrightarrow{a_2}| \approx 2.49$ Å. The conventional basis chosen in crystallography for a graphene sheet is a basis $(\overrightarrow{a_1},\overrightarrow{a_2})$ where the angle between the vectors is 120° (Hamada, Sawada, & Oshiyama, 1992). The angle between reciprocal vectors $\overrightarrow{a_1}^*$ and $\overrightarrow{a_2}^*$ is 60° and allows one to use the well-known (h, k, $l = -h - k$) notation: the wave-vectors are equivalent for circular permutations of the h, k, l indices which describe three-fold rotations. However, the basis which is the most frequently used in nanotube literature is the one with $(\overrightarrow{a_1},\overrightarrow{a_2})$ =60° (Robertson, Brenner, & Mintmire, 1992).

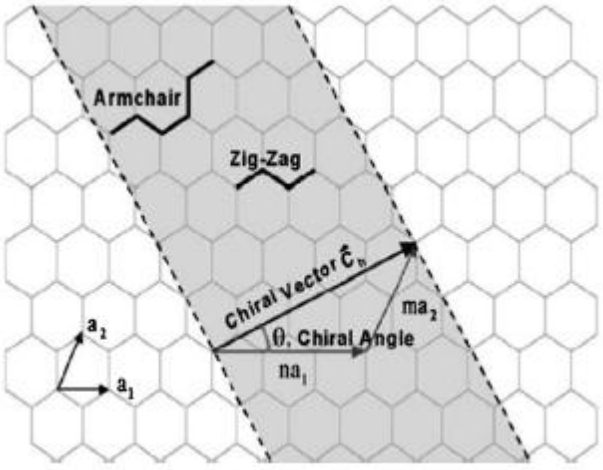

Figure 3 - Schematic diagram showing how a hexagonal sheet of graphene
is rolled to form a CNT with different chiralities (Erik T Thostenson, Ren, & Chou, 2001)

The nanotube is obtained by cutting a ribbon of perpendicular basis $\overrightarrow{C}$ in the sheet and by rolling it up, as shown in Figure 3 - Schematic diagram showing how a hexagonal sheet of graphene. The tube circumference could be written as:

$$\vec{C} = |\vec{C}| = a\sqrt{n^2 + m^2 + nm}$$

The hexagons orientation on the tube surface is characterized by the "chiral angle" θ:

$$\theta = \arctan\left(\sqrt{3}m/(2n + m)\right)$$

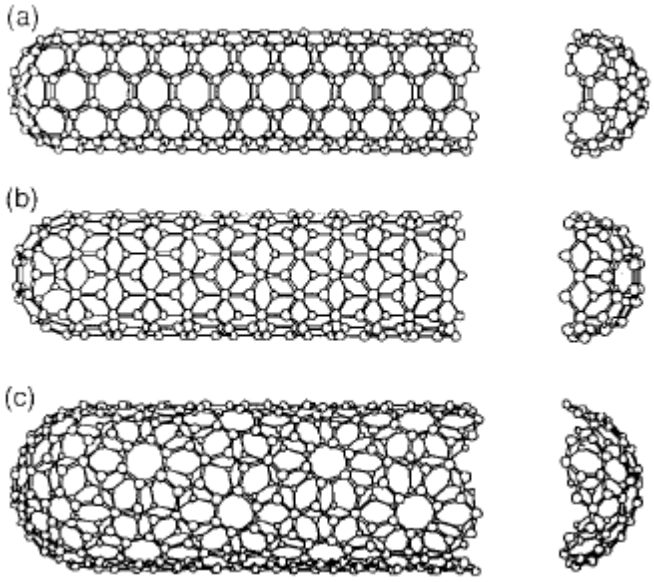

Figure 4 - A schematic theoretical model for single-wall carbon nanotube
with different chiralities (Dresselhaus, Dresselhaus, & Saito, 1995)

Different chiral angles correspond to as many chiralities of the carbon nanotubes. A schematic theoretical model for a single-wall carbon nanotube is shown in Figure 4, with the tube axis normal to: (a) the θ = 30° direction (an "armchair" tubule), (b) the θ = 0° direction (a "zigzag" tubule), and (c) a general direction *B* with 0°<|θ| < 30° (a "chiral" tubule). The actual tubules shown in the figure correspond to (*n,m*) values of: (a) (5,5), (b) (9,0), and (c) (10,5).

2.1.2. CARBON NANOTUBES SYNTHESIS METHODS

The history of carbon nanotubes discover started in 1965 with the synthesis of C_{60} molecules by Kroto et al. (Harold W. Kroto, Heath, O'Brien, Curl, & Smalley, 1985), involving the ablation of a graphite target by a pulsed laser. However, the spread on a large scale of the research on fullerenes began only in 1990 with the introduction of the mass production route invented by Krätschmer and Huffman (Krätschmer, Lamb, Fostiropoulos, & Huffman, 1990). This synthesis was based on an electric arc generated between two electrodes made in graphite under helium atmosphere. Thanks to this simple technique several research groups started to investigate the C_{60} molecules and was promptly clear that those were not the only species produced during the synthesis. In fact C_{70} molecules (rugby ball shaped) were observed in the soot produced by the electric arc, and afterwards, changing the electric supply from alternating to continuous current, strange filamentous species were found on the electrodes. The first scientist interested in these anomalous formations has been Iijima in 1991: using a high-resolution transmission electron microscope he identified tubular structures of crystallized carbon and named them nanotubes. This extraordinary discover caused a great uproar inside the research community and the publication of Iijima on Nature (Sumio Iijima, 1991) can be considered as a true breakpoint in the history of carbon.

As a matter of fact this was not the first CNTs observation: Bacon in the Sixties (Bacon, 1960) and Endo in the Seventies (Oberlin, Endo, & Koyama, 1976) studied tubular undesired by-product in industrial chemical processes, and the thinner filaments were therefore very close to the present nanotubes. However, they did not attract so much interest because in those years there were no techniques to study and to use nanometric sized objects. This context was completely changed in 1991 and several methods have been introduced to produce carbon nanotubes up to the present. The various synthesis methods are generally classified into two main categories depending on the temperatures reached during the process: high-temperature and medium-temperature routes. The former are based on the vaporization of a graphite target whereas latter are based on Combustion Chemical Vapour Deposition (CCVD) processes.

2.1.2.1. HIGH-TEMPERATURE METHODS FOR THE SYNTHESIS OF CARBON NANOTUBES

High-temperature methods grow out from the Krätschmer and Huffman production route (Krätschmer et al., 1990). They all involve graphite sublimation in a reduced or inert atmosphere, to temperatures above 3200°C and vapour condensation under a high temperature gradient. Several high-temperature techniques have been developed, with different methods used for sublimating graphite.

- **The Electric Arc Discharge Technique**

This method is based on an arc discharge generated between two graphite electrodes placed face to face in the instrument chamber under a partial pressure of helium or argon (typically 600 mbar). The electric discharge rises the temperature up to 6000°C. This temperature allows the graphite to sublimate. Because of the very high pressure reached during the process, carbon atoms are ejected from the electrodes and can form a plasma. These atoms move toward colder zones within the chamber, and a nanotube deposit on the cathode follows.

Iijima used an apparatus of this kind in his early experiments. He used DC arc discharge in argon consisting of a set of carbon electrodes, with temperature of 2000–3000°C in nominal conditions of 100 A and 20 V. It produced multiwall nanotubes in the soot. Later, single-wall carbon nanotubes were grown with the same set-up by adding to the electrodes suitable catalyst particles, e.g. of Fe, Co, Ni or rare-earth metals (Loiseau et al., 2006)

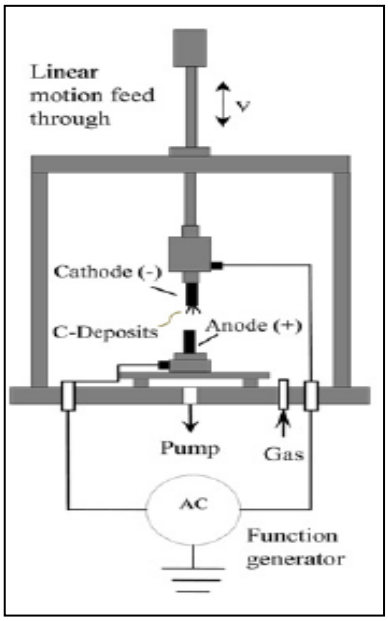

Figure 5 - A typical arc-discharge apparatus (Merchan-Merchan, Saveliev, Kennedy, & Jimenez, 2010)

The working conditions hugely influence the carbon nanotubes properties: in presence of small amounts of transition metals such as Fe, Co, Ni in the graphitic anode material (and leaving the cathode as pure graphite) single-wall carbon nanotubes result the main product. A hydrocarbon gas introduced into the arc discharge is more favourable to yield CNTs than fullerenes (Y Ando, 1994). In absence of such catalysts, the formation of multiwall carbon nanotubes is favoured.

- **Laser Ablation**

The sublimation of the graphite could be obtained by ablation with a focused laser beam in an inert atmosphere at low pressure. Two kinds of methods were developed: the former uses a pulsed laser (Yoshinori Ando, Zhao, Sugai, & Kumar, 2004; Guo et al., 1992; Thess et al., 1996) the latter a continuous one (Maser, 1998; Munoz et al., 2000).

The main differences with the arc method are:

– The material is subjected to a laser ablation instead of an arc discharge.

– No tube of reasonable length has ever been synthesized without some catalysing particles. This implies that a certain local anisotropy is necessary to grow a nanotube.

– Particles are collected through a carrier gas on a cool plate far from the target. A secondary heating is usually added.

The pulsed laser (PL) is characterized by a higher light intensity (100 kW/cm^2 compared with 12 W/cm^2). In the pulsed laser configuration (Figure 6), the target is vaporized in a high temperature argon buffer gas by a Nd-YAG laser pulse.

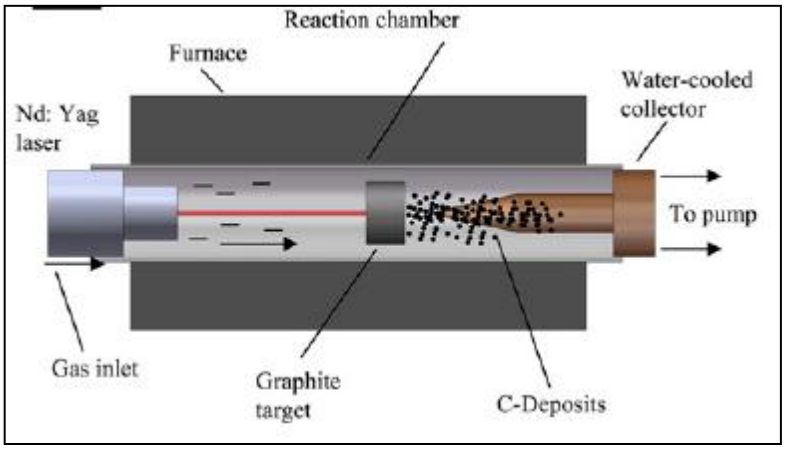

Figure 6 -A typical pulsed laser ablation apparatus (Merchan-Merchan et al., 2010)

The main advantages of PL technique include SWNT formation and diameter control. The SWNT diameter can be varied by controlling the temperature, catalyst composition, and gas flow rate

(Bandow et al., 1998; H. Kataura et al., 2000; Sen et al., 2000). At higher temperatures, SWNT diameters enlarge. Equally, an increasing in the nanotube diameter is observed as a consequence of the introduction of a Ni-Y catalyst, while applying a Rh-Pd catalyst reduces the diameter (Avigal& Kalish, 2001; Hiromichi Kataura et al., 1998). Disadvantages of the PLV method include the limited scale of SWNT production and the presence of large amounts of contaminants such as catalytic particles and amorphous carbon.

In the continuous laser configuration a 2-kW continuous-wave CO_2 laser is focused on the target, heating it up to 3000–3500 K. An inert gas (He, Ar, N_2) flows from the bottom to the top of the reactor chamber removing the produced soot inside the quartz tube.

- **Vaporisation induced by a solar beam**

A particular method investigated in last years involves a solar furnace in which the sunlight is focused on a graphite sample to vaporize the carbon. The soot is then condensed in a cold dark zone of the reactor. The sunlight is collected by a flat tracking mirror and is reflected towards a parabolic mirror which focuses the solar radiation directly on the graphite target (Figure 7). Under clear-sky conditions, temperatures of around 3000K can be reached at the 2-kW set-up of the solar station and the evaporation process can start. At the beginning only fullerenes were produced with this technique (Laplaze et al., 1994), but since 1998 also nanotubes were obtained, just by changing the target composition and adjusting the experimental conditions (Laplaze et al., 1998).

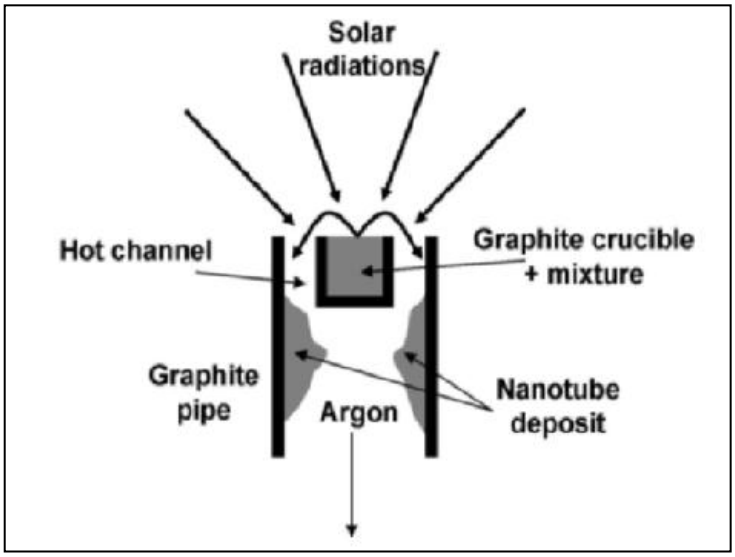

Figure 7 - Principle of the solarfurnace technique (Loiseau et al., 2006)

2.1.2.2. SYNTHESIS OF MWNT AND SWNT VIA MEDIUM-TEMPERATURE ROUTES

- **Chemical Vapor Deposition (CVD)**

The main problem of the high-temperature techniques is the very low production yield obtained during the process. This problem can be solved using a different technique based on a catalytic chemical vapour deposition. This method derives directly from a particular technique used since 1950 to produce carbon filaments and to study kinetic behaviour of carbon decomposition processes. The chemical reactions involved in the production of carbon (such as the disproportionation of CO) would be infinitely slow or would produce non-filamentary carbon (by decomposition of hydrocarbons) without small particles of metal like Fe, Co or Ni. Each filament is generated from one catalytic particle, located either at the base or at the tip of the filament. The first aim in order to synthesize CNT has been to decrease the size of the catalytic particles. The second aim has been to adjust the conditions of the reaction, often by modifying the value of the physical parameters or the nature of the reacting gas. The main problem connected with nanoparticles is their coalescence at the temperatures reached during the hydrocarbons decomposition. Refractory metals could be used because they less coalesce than other metals. However, Co, Fe, Ni nanoparticles, alone or associated with Mo, V or W, are much more active. One common solution is the deposition of the metal nanoparticles on finely divided or highly porous powders. Nonetheless this resolution is efficient only with reaction temperatures not too high (Cassell, Raymakers, Kong, & Dai, 1999; Nikolaev et al., 1999). Another way is to generate the metal nanoparticles in-situ inside the reactor, preferentially at the reacting temperature, either from an organometallic (Ci et al., 2001; Nikolaev et al., 1999; Zhu et al., 2002) or from a solid, by the selective reduction of an oxide solid solution (Bacsa et al., 2000; Flahaut et al., 1999) or of an oxide compound (Ning et al., 2002). Depending on the maximal temperature permitted to avoid or limit the coalescence of the catalytic particles, the carbonaceous gas can be either CO or hydrocarbons. Generally, the carbonaceous gas is mixed with an inert gas (Ar, He or N_2) or with H_2 that allows to act on the hydrodynamic parameters or/and to modify the thermodynamic conditions.

A lot of strategies have been used to adapt the CCVD methods to the synthesis of CNT, including horizontal furnace, fluidized bed reactor, vertical furnace, and basic plasma enhanced CVD. All the parameters, related either to the catalyst or to the reaction conditions, are important and may interact. It is very important to tune correctly these parameters to obtain the final sought products.

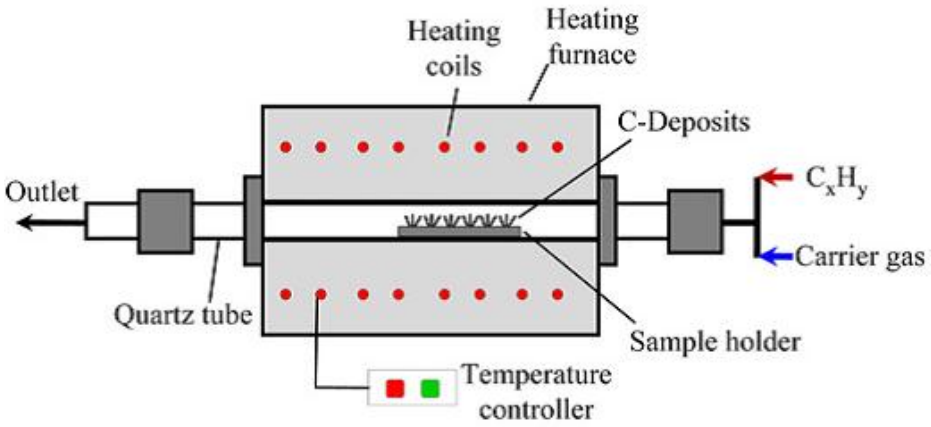

Figure 8 - Example of a CCVD apparatus (Merchan-Merchan et al., 2010)

2.1.3. MECHANICAL PROPERTIES OF CNTs

In treating the problem of single-nanotube mechanical properties, the main problem is whether macroscopic equations can be applied to a giant elongated molecule. One important engineering parameter is the Young's modulus, *E*, which is constant for a given material. The unusual fact with nanotubes is that E is expected to vary slightly with the diameter, since curvature modifies C–C bond hybridization hence stiffness. Some difficulties arise because of the practical interest in treating a nanotube like a continuous medium, which implies determining the shell thickness. Good approximations have been obtained during last decades: Young's modulus and thickness of a single-wall nanotube are not very different from that of a single graphene sheet and multiwall nanotubes are very similar to bulk graphite or carbon fibres. However, it is important to understand if the classical elasticity is applicable to the nanotubes. Harik (Harik, 2002) discussed specifically the applicability of Euler beam model to carbon nanotubes. The deformation of a homogeneous elastic beam is described by the Bernouilli-Euler equation (Landau, Lifshits, Kosevich, & Pitaevskii, 1986):

$$\frac{d^2z}{dx^2} = -\frac{M(x)}{EI}$$

where *M(x)* is the bending moment at *x* and *I* the areal moment of inertia shape dependent parameter, which can be express, in the tube case, as:

$$I = (\pi/64)((D_O)^4 - (D_i)^4)$$

With D_O the outer diameter and D_i the inner diameter of the tube.

The Bernoulli-Euler equation can be used to calculate the deflection of a long beam of length *L* clamped at one end and submitted to the force *F* at the other end:

$$\delta = \frac{FL^3}{3EI}$$

Although elongation (or contraction) of a beam depends only on its cross-section area (*A*), the flexural behaviour is strongly influenced by the cross-section shape. Axial and lateral deformations can all be described using only the Young's modulus, in the case that the beam aspect ratio is larger than 10. For aspect ratios smaller than 10, a shearing component must be added to the deflection formula:

$$\delta_s = \frac{f_s FL}{GA}$$

with *G* the shear modulus, and f_s the shear coefficient, beam shape dependent (Gere & Timoshenko, 1990).

Concerning a single-wall nanotube, lots of studies have been conducted trying to answer whether it can be described as a homogeneous tube made from an isotropic shell of finite thickness *t*. As a first approximation the carbon nanotubes could be described as homogeneous isotropic continuous shells of thickness *t*, and all their elastic deformations can be calculated knowing the Young's modulus, *E*, and the Poisson ratio, ν. Supposing the tube to be equivalent to a sheet of width $2\pi R$, *E* and *t* can be deduced from the bending rigidity (*D*) and in-plane stiffness (*C*) of a graphene plate:

$$D = \frac{Et^2}{12(1-\upsilon^2)}$$

And

$$C = Et$$

D, *C* and ν are characteristics parameters of graphene determined by C–C bond rigidity, that can be calculated independently from *t*. The bending rigidity of a graphene sheet is determined by inversion configuration of the C–C bonds (Odegard, Gates, Nicholson, & Wise, 2002). Without this term, the bending rigidity of the graphene sheet would be zero. Combining the two previous equations, it is possible to find $E \approx 5$ TPa and $t \approx 0.07$ nm. The effective thickness of a single shell nanotube, using this approximation, is less than 0.1 nm, not so far from a single graphene layer (however many authors use $t = 0.34$ nm and $E = 1$ TPa, since it compares directly with bulk graphite values). An error is made

using this model because a nanotube has an effective flexural rigidity, *EI*, with *I* the moment of inertia, much higher than that of a graphene sheet. In particular *EI* could be express as:

$$EI = E\frac{\pi D_o^4}{64}\left(1-\left(\frac{D_i}{D_o}\right)^4\right) = E\frac{\pi D_o^4}{64}(1-\left(1-\left(\frac{2t}{D_o}\right)\right)^4)$$

And if $2t \ll D_o$, $\left(1-(2t/D_o)\right)^4 \approx 1-4(2t/D_o)$, with

$$EI = \frac{\pi}{8}D_o^3 Et = \frac{\pi}{8}D_o^3 C$$

These formulas mean that for a SWCNT of large diameter the bending rigidity is governed by the in-plane stiffness of the graphene sheet. Thus a SWNT can be approximated by a shell of thickness $t = t_G$ = 0.34 nm with $E = E_G$ = 1 TPa. Obviously this is a mere approximation.

Unfortunately also the continuum approach is an approximation, since defining the thickness of one-atom-thick layers does not have a rigorous physical meaning, even if the notion of an electronic density cloud is used. Arroyo and Belytschko (Arroyo & Belytschko, 2002) proposed a method to describe one-atom-thick layer deformations extending hyper-elastic models used for bulk materials. It is clear that continuum models show several limitation, especially in the non-linear elastic regime.

For a two-layer structure, considered as and anisotropic shell, the thickness could be considered $t_D = t + d_i$, where d_i is the interlayer thickness. The starting supposition is that slidings are not allowed between the layers, because of the Van der Waals forces. In this more complex situation the bending stiffness is determined by the in-plane stiffness of the C-C bonds (Srolovitz, Safran, & Tenne, 1994).

Young's modulus could be express as a function of the number of shells N (Tu& Ou-Yang, 2002):

$$E_N = \frac{N}{N-1+(t/d_i)}\frac{t}{d_i}E$$

SWNTs usually exist grouped in bundles. While covalent C–C bonds ensure strong intra-tube stiffness, transverse properties are governed by Van der Waals forces very similar to those at work in graphite interplane cohesion. The SWNTs aggregate is thus highly anisotropic, with low torsion and shear moduli. Elastic constants can be approximated with classical elasticity theory using those of graphite. In addition, the various forms of carbon structures are characterized by different Young's modulus according to their structure. In fact the perfect isotropy of the elastic behaviour of the graphene sheets is correlated with their hexagonal symmetry. As the sheet is into a tube, the bending strain

induces distortion of the C–C bonds, resulting in a hybridization of the σ bonds, which increases as the diameter decreases. So it is clear that both the diameter and the helicity of the tubes could affect their elastic properties.

- **Non-linear elastic regime**

Carbon nanotubes exhibit an extraordinary capability to carry high strength without breaking. This phenomenon could be studied only assuming a non-linear regime. At high strain the hexagonal lattice symmetry is broken and differences appear as a function of chirality.

A good estimation of ideal strength of carbon nanotubes is calculated by the Orowan-Polanyi equation which states that ultimate limit to elasticity is reached when strain energy equals the energy needed to separate two crystallographic planes in 3d or lines in 2d:

$$\sigma_{th} = \sqrt{\frac{E\gamma}{a}}$$

In which γ is the surface energy and a the interplane separation. Using typical values for graphite this equation leads to σ_{th} ≈300 GPa taking E ≈5 TPa or ≈150 GPa with E ≈1 TPa, and it represents an upper limit of the theoretical strength, since the real nanotubes exhibit defects that lower their properties. As in other materials, also their strength strictly depends on their ability to prevent initiation and propagation of defects. They are quantified by a formation energy and an activation barrier and they are temperature dependent. While grain boundary has hardly an equivalent in a nanotube, cracks may be present in the form of non-bonding trapped states (Dumitrică, Belytschko, & Yakobson, 2003) and elongated vacancy clusters (Belytschko, Xiao, Schatz, & Ruoff, 2002).

Because of their 2d structure, extended defects like dislocation lines or loops are obviously absent, however correspondent large defects has been noticed, e.g. (5–7) pentagon-heptagon pairs (Lauginie & Conard, 1997).

Another extended defect in SWCNTs involves the formation of (5-7-7-5) defect pairs by a 90° bond rotation, known as the Stone-Wales (S-W) transformation. This transformation requires high temperature or long time under normal strain conditions (less than a few %). When strain increases S-W defect formation energy and activation barrier decrease (Buongiorno Nardelli, Yakobson, & Bernholc, 1998).

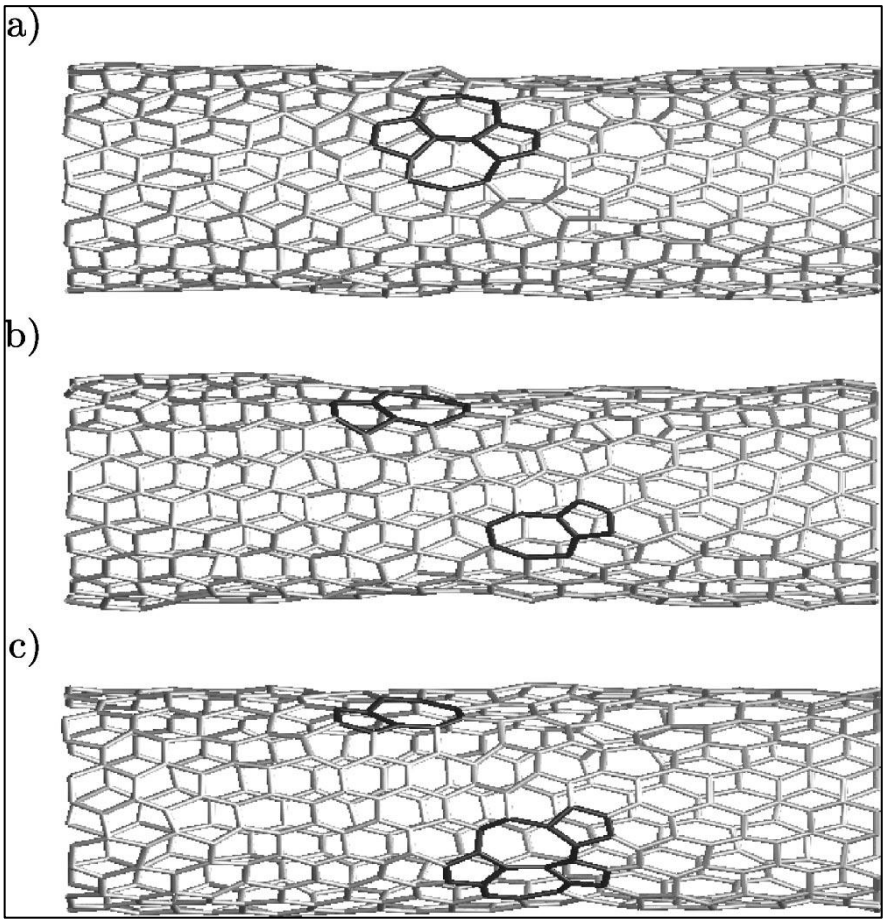

Figure 9– Time evolution of a particular (5-7-7-5) defect from a classical simulation for a (10,10) carbon nanotube at 2000 K under 10% uniaxial strain. The defect structure is highlighted in black. a) Formation of the pentagon-heptagon defect whose evolution in time will be followed (*t*=1.5 ns). b)The defect splits and starts diffusing (*t*=1.6 ns), note that a (10,10)/(10,9)/(10,10) heterojunction has formed; c) Another bond rotation has led to the formation of a (5-7-5-8-5) defect (*t*=2.3 ns) (Buongiorno Nardelli et al., 1998)

Due to the presence of C-C covalent bonds the CNTs are characterised by high Peierls barriers, which ensure no plastic deformations at room temperature and a fragile rupture. It is possible to observe the spontaneous formation of cracks via a bond-breaking bifurcation state when nanotubes are under tension (Dumitrică et al., 2003). This occurs when strain energy per bond approaches the cohesive energy so that a C–C bond starts to switch between a bonding and a non-bonding state.
Therefore, time or energy are requested for plastic deformation, via Stone-Wales transformation. It is supposed to dominate at high temperature and for long times. Brittle failure is expected at room temperature. It is certainly a peculiar characteristic of nanotubes to show plasticity, because of their capacity to sustain high strain, which reduces both formation energy and activation barrier of S-W transformation.

- **Experimental results**

The theoretical analysis of the CNTs mechanical behaviour must be supported by experimental results. Experimental methods and principles used are not conceptually different from those used

with macroscopic materials. However, they differ from common testing tools because they measure nanometer size displacement and nanoNewton forces. Measurements in the nanoscale range always involve further problems because of the very small dimension of the tested materials.

Ultrasonic tests and sonic resonances are routine methods for the measurement of elasticity in solids. Longitudinal wave velocity in a bar is expressed by:

$$v_1 = \sqrt{\frac{E}{\rho}}$$

Where ρ is the material density. Unfortunately, this technique is not easily applicable to the nanometer scale.

Classical elasticity could be useful to calculate vibration frequencies and amplitudes of a bar, in which the vibration modes depend on the elastic constants of the material. The general equations are known as Timoshenko's beam equations (Timoshenko, Young, & Weaver, 1964). They are reprocessing of Bernouilli-Euler formula, in which shear and torsion effects are introduced. Shear deformation and rotatory inertia have a small effect on the first mode of vibration but must be incorporated in higher modes (Antes, 2003; Schanz & Antes, 2002).

As a first order approximation, Bernouilli-Euler formula can be used to calculate the Young's modulus. For a nanotube clamped at one end:

$$E = \frac{16\pi L^2 f_n}{\beta_n^2} \frac{\rho}{D_i^2 + D_o^2}$$

where f_n is frequency of vibration for transversal mode n and β_n is solution to $\cos\beta_n \cosh\beta_n = -1$, and so $\beta_1 = 1.88$, $\beta_2 = 4.69$, $\beta_3 = 7.85$, $\beta_4 = 11$, $\beta_n = (n - 1/2)\pi$ for $n \geq 5$. Both thermal and stimulated transversal vibrations of a nanotube were measured using a TEM. Vibration resonances can also be measured by field emission. The tension applied by an electric field was used to tune resonances by up to a factor of 10 (Purcell, Vincent, Journet, & Binh, 2002).

Also the atomic force microscope (AFM) could be a useful method to evaluate the mechanical properties of the carbon nanotubes. This technique in its initial conception was designed to measure and record images of flat surfaces with atomic resolution. Its use has then been extended especially in the field of nanomechanics. Indeed, its special ability is to simultaneously measure a displacement (by the vertical piezoelectric tube) and a force (by the cantilever deflection). AFM could measure stiffness and strength, in bending and in tension (B. J. Salvetat et al., 1999; Wong, 1997; M.-F. Yu, 2000) for MWNT and SWNT ropes, confirming the high Young's modulus and exceptional strength predicted by theory.

2.2. COMPOSITE MATERIALS

Composites are produced when two or more materials or phases are used together to give a combination of properties that cannot be obtained otherwise. In nature several composites already exist, furthermore a particular interest has been devoted, since last century, toward syntetic composite materials, in particular with fibres. These materials are designed so to take advantage of the properties of all the components involved and may be selected to give unusual combinations of stiffness, strength, weight, high-temperature and corrosion resistance, hardness or conductivity.

As anticipated the "composites" concept is not a human invention. Wood is a natural composite material consisting of one species of polymer — cellulose fibres with good strength and stiffness — in a resinous matrix of another polymer, the polysaccharide lignin. Bones, teeth and mollusc shells are other natural composites, combining hard ceramic reinforcing phases in natural organic polymer matrices. Man was aware, even from the earliest times, of the concept that combining materials could be advantageous, however only in the last half century the science and technology of composite materials have intensely developed (Matthews & Rawlings, 1999).

Materials called now-a-days "composites" are produced dispersing in a particular material a second species, generally previously sintetized. The body constituent gives the composite its bulk form, and it is called the matrix. The other component is a structural constituent, sometimes called the reinforcement, which determines the internal structure of the composite.

Generally speaking is very difficult to define "composite materials". They differ from traditional materials because:

- They were hystorically born later
- Their properties are not exactly governed by the conventional laws of materials
- Their microstructure and properties have been accurately projected
- Frequently their properties are entirely new and exclusive

So we can define a "composite" as a material brought about by combining materials differing in composition or form on a macroscale for the purpose of obtaining specific characteristics and properties (Callister, 2007).

Although there are many materials projected and used for their physical properties (e.g. superconductors), most composites are designed to improve their mechanical properties.

There are many ways to classify composites, including schemes based upon: 1) materials combinations, such as polymer–matrix, or carbon nanotubes-reinforced composites; 2) bulk form characteristics, such as laminar composites or matrix composites; 3) distribution of constituents, such as continuous or discontinuous or 4) function, like structural or electrical composites.

There are five general types of composites when categorized by bulk form. Fibre composites consist of fibres. By definition, a fibre is a particle longer than 100 µm with an aspect ratio greater than 10:1. Flake composites consist of flakes. A flake is a flat, plate-like material. Particulate composites are characterized by the presence of particulates, which are roughly spherical in shape. In a filled composite, the reinforcement is continuous and often considered the primary phase, with a second material added through particular processes. Finally, laminar composites are composed of distinct layers. The layers may be of different materials, or the same material with different orientation.

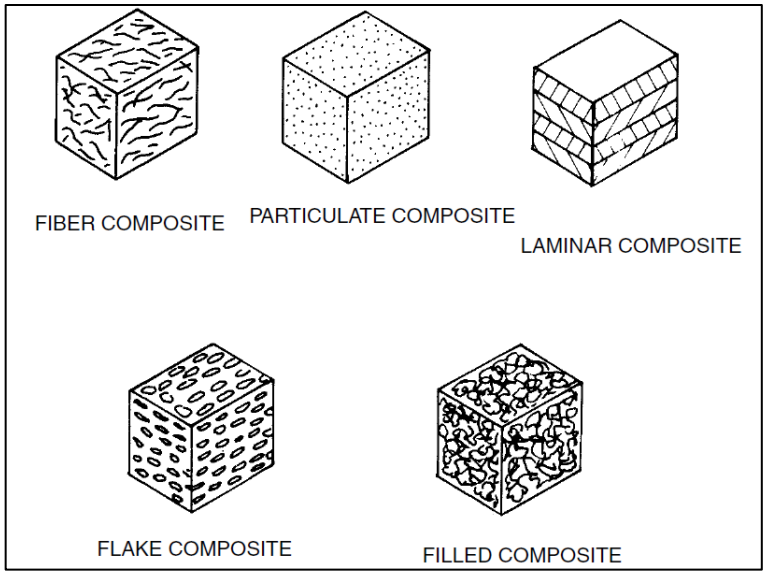

Figure 10 - Classes of composites.

The chemical composition of the composite constituents is not limited to any particular material class. There are metal–matrix, ceramic–matrix, and polymer–matrix composites.The terms metal, plastic and ceramic cover whole families of materials with ranges of properties as broad as the differences between the three classes. Using a very simplicistic approach we can say:

- Plastics are low density materials. They are characterized by good short-term chemical resistance but they exhibit low thermal stability resistance to environmental degradation (e.g. photo-chemical effects of sunlight). Their poor mechanical properties are counterbalanced by their easily fabrication and join.
- Ceramics have great thermal stability and are resistant to most forms of attack (abrasion, wear, corrosion). They are very rigid and strong because of their chemical bonding and they are also brittle and can be formed and shaped only with difficulty.
- Metals are mostly of medium to high density. They exhibit good thermal stability and alloying could provide them a good corrosion resistance. They have useful mechanical properties and

high toughness, and they are moderately easy to shape and join. They are also characterized by ductility and resistance to cracking.

Composite materials were born so to exploit the advantages of these materials and to overcome their defects.

In a composite the matrix performs different roles. First of all, the matrix binds the fibres (or the other reinforcements) together. Loads applied to the composite are transferred into the fibres through the matrix, allowing the composite to withstand compression, flexural and shear forces as well as tensile loads. The ability to support loads of any kind depends on the presence of the matrix as the load-transfer medium, and the efficiency of this load transfer is directly related to the quality of the fibre/matrix bond. The matrix must also isolate the fibres from each other. Indeed the properties of the reinforcements well dispersed into the matrix are completely different from properties of bundles and aggregates of fibres. The matrix should protect the reinforcements from mechanical damage and from chemical or environmental attacks. In addition a ductile matrix enables a means of slowing down or stopping cracks that might have originated at broken fibres.

The problem with composites production is to develop proper methods to combining the matrix and the reinforcement in order to obtain suitable properties and shape of components. The range of techniques used to produce composites is verywide. Almost all of the basic metal, polymer and ceramic forming processes have been adapted to their class of composites, with more or less success. One of the most significant aspects of the production of composites, in particular for materials designed to withstand loads, is the nature of the interfaces between matrix and reinforcements. The interface between two solids, especially when thermal or chemical processes have been involved in putting them together, is rarely a simple boundary between two materials of quite different character. The properties of these “interphases” determine the manner in which stresses are transferred from matrix to fibres and most of the chemical, physical and mechanical properties of the composite. Control of interface regions is a crucial way to monitor and develop the mechanical response of composite materials. An important parameter to ensure a tight contact between matrix and reinforcement is the wettability. A liquid phase on a solid can flow on the surface and can create a broad layer (in other words, the liquid wets the solid) or it can be rejected and can form a spherical droplet (so the liquid does not wet the solid). Therefore, the wettability is a favourable condition to ensure a good physical contact between the components of the composite. In a first moment the liquid drop could be considered spherical shaped and exhibit a single contact point with the solid surface. Afterwards it can wet the surface. For every increase of the wetted surface dA, a new separation surface solid/liquid is formed, with its surface energy γ_{SL}, and the separation surface liquid/gas enlarges (with an increasing of the energy of the system proportional to

γ_{LV}). Nevertheless at the same time the separation surface between solid and gas decreases with an energy reduction proportional to γ_{SV}. An increase of the wetted surface dA is allowed only if the following condition is observed:

$$\gamma_{SL} dA + \gamma_{LV} < \gamma_{SV} dA$$

The process could proceed if an equilibrium condition is reached. In that case the surface tensions are balanced each others.

The equilibrium condition is expressed as:

$$\gamma_{SL} + \gamma_{LV} cos\theta = \gamma_{SV}$$

For ϑ<90° the wettability is ensured.

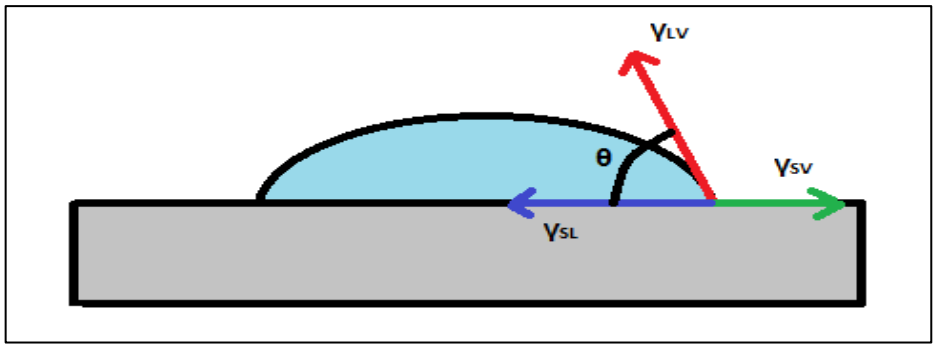

Figure 11 - Contact angle of a liquid droplet wetted to a rigid solid surface

Another fundamental point in the design and production of composites is the prediction of their mechanical behaviour. In particular, for short fibres reinforced composites, lots of theoretical work had been carried out since the 1950s in order to model the mechanical properties of composites. Since some of these models (Tucker & Liang, 1999) are quite sophisticated, we will consider two of the simplest and most common. These are the rule of mixtures and the Halpin–Tsai equations.

- **Mixtures equation**

The simplest method to estimate the stiffness of a composite in which all of the fibres are aligned in the direction of the applied load (isotropic, elastic matrix filled with aligned elastic fibres that span the full length of the specimen) is to assume that the structure is a simple beam (Figure 12) in which the two components are perfectly bonded together so that they deform together.

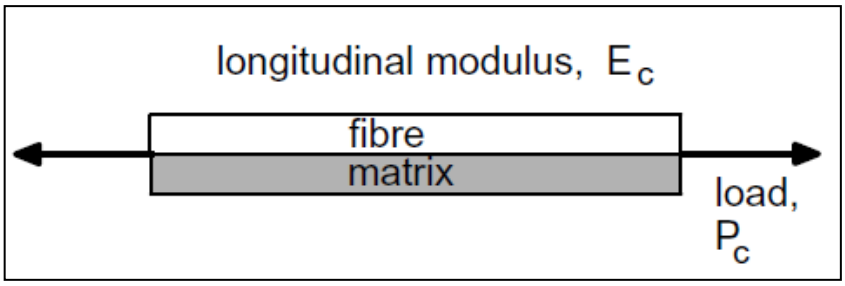

Figure 12 - Simplified parallel model of a unidirectional composite(Harris, 1999).

The assumptions of the mixture equation are:

$$\mathrm{V_f} + \mathrm{V_m} = 1$$

where V_f and V_m are respectively the volume fraction of the fibres and of the matrix. Moreover the load on the composite P_c is expressed as the sum of the loads on the components:

$$P_c = P_f + P_m$$

and the so called "iso-strain condition" is assumed:

$$\varepsilon_c = \varepsilon_f = \varepsilon_m$$

So the stress could be expressed as:

$$\sigma_c A_c = \sigma_f A_f + \sigma_m A_m$$

with A the cross-sectional area of the various components. On the basis of the iso-strain condition we can write:

$$\frac{\sigma_c A_c}{\varepsilon_c} = \frac{\sigma_f A_f}{\varepsilon_f} + \frac{\sigma_m A_m}{\varepsilon_m}$$

Or:

$$E_c = E_f V_f + E_m(1 - V_f)$$

This equation is referred to as the Voigt estimate, but is better known as the rule of mixtures. It makes the implicit assumption that the Poisson ratios of the two components are equal ($\nu_f = \nu_m$), thus overlooking elastic constraints caused by differential lateral contractions. More sophisticated models have been developed and they show that the mixtures equation tend to underestimate the true

stiffness of a unidirectional composite beam but for more practical purposes this difference is so small as to be negligible.

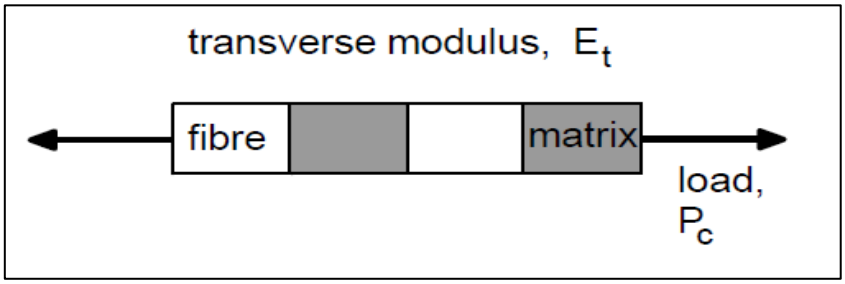

Figure 13 - Simple series model of a composite (Harris, 1999)

The transverse modulus, E_t, is calculated using a similar approach with a block model such as that shown in

Figure **13** with the same constraints as before, i.e. well-bonded components with similar Poisson ratios, and no visco-elastic response from the matrix. We consider now an 'iso-stress' model, so that $\sigma_c = \sigma_f = \sigma_m$. The total extension of the model is the sum of the extensions of the two components:

$$\varepsilon_c L_c = \varepsilon_f L_f + \varepsilon_m L_m$$

If the cross-sections of both phases are the same, $L \equiv V$, so dividing through by the stress (and remembering that $V_f + V_m = 1$) we have:

$$\frac{\varepsilon_c}{\sigma_c} = \frac{\varepsilon_f V_f}{\sigma_f} + \frac{\varepsilon_m V_m}{\sigma_m}$$

Or

$$\frac{1}{E_t} = \frac{V_f}{E_f} + \frac{V_m}{E_m}$$

This is the Reuss estimate, sometimes called the inverse rule of mixtures and the transverse modulus is therefore expressed as:

$$E_t = \frac{E_f E_m}{E_m V_f + E_f (1 - V_f)}$$

The problem with the Reuss model for the transverse case is that the geometry of the model does not resembles in any way that of a fibre composite perpendicular to the fibres. And it ignores

constraints due to strain concentrations in the matrix between the fibres, by assuming that the Poisson ratios of the phases are the same.

- **Halpin Tsai equation**

Another common model is that developed by Halpin and Tsai (Halpin & Kardos, 1976). The mixture rules seen before are extremely simplicistic. More rigorous approaches may give predictions of elastic properties that are closer to experimentally observed values than these simple models, but they are seldom easy to use in practice. Halpin and Tsai showed that many of the more rigorous mathematical models could be reduced to a group of approximate relationships of the form:

$$E_1 \approx E_f V_f + E_m(1 - V_f)$$

$$E_2 = \frac{(1 + \zeta\eta V_f)}{(1 - \eta V_f)} E_m$$

$$G_{12} = \frac{(1 + \zeta\eta V_f)}{(1 - \eta V_f)} G_m$$

Where the longitudinal stiffness of a unidirectional composite is E_1 and the transverse stiffness is E_2, G_{12} is the in-plane shear modulus, ζ is a factor, specific to a given material, that is determined by the shape and distribution of the reinforcement, and by the geometry of loading. The parameter η is a function of the ratio of the relevant fibre and matrix moduli and of the reinforcement factor ζ, thus:

$$\eta = \frac{\left(\frac{E_f}{E_m} - 1\right)}{\left(\frac{E_f}{E_m} + \zeta\right)}$$

2.2.1. METAL MATRIX COMPOSITES (MMCs)

A Metal Matrix Composite (MMC) is a composite material in which one constituent is a metal or alloy forming at least one percolating network. The other constituent is embedded in this metal matrix and usually serves as reinforcement. Metal matrix composites have been an attractive end goal for many materials engineers as an alternative to the traditional pure ceramic or pure metal materials. The idea of creating a material that has nearly the same high strength as the ceramics, but also a high fracture toughness due to the contribution from the metal, has lead to the development of a new family of metallo-ceramic composites (Breval, 1995). MMCs exhibit significant advantages compared

to conventional materials. The driving force behind the development of metal matrix composites is their capabilities to be designed to provide needed types of material behavior, such as their improved strength and stiffness (Ward, Atkinson, & Anderson, 1996; Ward-Close, Chandrasekaran, Robertson, Godfrey, & Murgatroyde, 1999), outstanding corrosion resistance (Blackwood, Chua, Seah, Thampuran, & Teoh, 2000; C. Chen & Mansfeld, 1997; Shimizu, Nishimura, & Matsushima, 1995), friction resistance (Akbulut, Durmam, & Yilmaz, 1998; Kennedy, Balbahadur, & Lashmore, 1997) and wear resistance (Berns, 2003), high electrical and thermal conductivity (Korab, Stefanik, & Kaveck, 2002; Weber, Dorn, & Mortensen, 2003), and high temperature mechanical behavior (Llorca, 2002; Z. Y. Ma & Tjong, 1999; Tjong & Ma, 1997). Metal matrix composites have been developed in order to make more resistant light metals, at relatively high temperatures and avoiding lightness decreasing as well, or with the aim to extend the temperature range in which superalloys with high density could be employed.

The most important metal matrices commonly used are low density alluminum, magnesium or titanium alloys. For particular applications copper matrix composites (with high thermal conductivity) or intermetallic matrix composites (for very high temperatures) have been developed. A particular interest has been direct to advanced metal matrix composites (MMC) with high thermal conductivity (TC) to effectively dissipate heat and tailorable coefficient of thermal expansion (CTE) to minimize thermal stresses, very promising for enhancing the performance, life cycle and reliability of electronic devices (Kaczmar, Pietrzak, & Włosiński, 2000; Mallik, Ekere, Best, & Bhatti, 2011).

In the present work we will study a particular metal used as a matrix: the alluminium. In the area of metal composites, aluminium has attracted intense interest because of its excellent strength, low density and corrosion resistance properties. The aluminum matrix composites are generally fabricated by the addition of a reinforcement phase to the matrix by the use of several techniques such as powder metallurgy, liquid metallurgy and squeeze-casting. The reinforcement phase is generally one of the following: continuous boron or graphite fibres, or hard particles such as silicon carbide or alumina, in discontinuous particulate or whisker morphology. The volume fraction of reinforced particles or whiskers is generally within the range 10-30%. Also aluminium alloys, such as the 2000, 5000, 6000 and 7000 alloy series, are commonly utilised materials in composite fabrication. Aluminium composites are widely employed in the aerospace industry (Deuis, Yellup, & Subramanian, 1998; Speer & Es-Said, 2004; Yan, Lifeng, & Jianyue, 2008).

2.2.2. POLYMER MATRIX COMPOSITES

To overcome the obvious defects of polymers, for example, low stiffness and low strength, and to expand their utilization for different applications, several fillers, such as fibres of variuos kind, particles, such as micro-/nano-SiO_2, glass, Al_2O_3, $Mg(OH)_2$ and $CaCO_3$ particles, carbon nanotubes and layered silicates, are often added to process polymer composites, which normally combine the advantages of their constituent phases.

Although the reinforcements play a dominant role in determining the stiffness and strength of a composite, the choice of the matrix will determine maximum service temperature, viable processing approaches, and long-term durability. Matrix materials can be divided into two categories: thermosetting and thermoplastic. Thermosetting materials are characterized by having a low-viscosity, reactive, starting oligomer that cures (reacts) to form an insoluble network. The cure temperature and time influence many matrix properties. Thermoplastics are linear or slightly branched polymers of relatively high molecular weight. They are of significant interest because they can be remelted, thus easing repair in the field, and because they are melt-processable. The use of thermoplastics also allows other composite processing techniques such as injection molding of short fibre composites and extrusion of long fibre composites. Thermoplastic polymer morphology may be either amorphous or semicrystalline. The semicrystalline and even liquid crystalline morphologies can impart superior solvent resistance to the overall matrix resin. Semicrystalline polymers display a melting temperature for the crystalline regions as well as a glass transition, and processing must be performed in excess of the melting temperature. Amorphous thermoplastics, on the other hand, are processed above the glass transition temperature. A possible limitation for some applications of semicrystalline polymers concerns the morphological changes that may occur during processing or in the service environment, particularly due to the application of heat or exposure to solvent while under stress. These changes in the crystalline structure and/or content may cause changes in the overall composite properties and are highly undesirable (National Research Council (US). Committee on High-Performance Structural Fibers for Advanced Polymer & Board, 2005).

Few polymers are thermally stable by comparison with metals or ceramics and even the most stable, like the polyimides, or poly(ether ether ketone) (known as PEEK) are degraded by exposure to temperatures above about 300°C. There is no reinforcement that can avoid chemical degradation, but the associated fall in strength and increase in time-dependent (creep or visco-elastic) deformation, a feature common to all polymers, though less serious in cross-linked resin systems than in thermoplastics, can be delayed by fibre reinforcement. Another serious problem with polymers is their very low mechanical strength and stiffness in bulk form: the weakest plastics tend to be ductile but the strongest tend to be brittle, although there are exceptions. Because of the

general good plastics properties (e.g. low densities and relative cheap production costs) nowaday is in the reinforcing of polymers that most important developments have been made.

2.2.3. CERAMIC MATRIX COMPOSITES

The word “ceramics” is intended, in the field of composites, as technical ceramics, such as alumina, silicon carbide, zirconia, carbon… They are generally stiff, hard and strong materials, but brittle, so that the main goal in the making of a ceramic matrix composite (CMC) is to increase its toughness with respect to the monolithic material. Often the composites present both a toughness and a strength improvement, but the most important fact is that the toughness increase may reduce the risk of a catastrophic failure; thus if the reinforcement is conveniently chosen, the composite may sustain much damage before collapsing. The desirable characteristics of CMCs include high-temperature stability, high thermal-shock resistance, high hardness, high corrosion resistance, light weight, nonmagnetic and nonconductive properties, and versatility in providing unique engineering solutions. The combination of these characteristics makes ceramic matrix composites attractive alternatives to traditional processing industrial materials such as high alloy steels and refractory metals. For the processing industry, related benefits of using ceramic composites include increased energy efficiency and increased productivity.

Ceramic matrix composites development has lagged behind metal and polymeric matrix composites for two main reasons, both linked to the fact that, generally, processing routes for the synthesis of CMCs involve high temperatures. Reinforcements are required that are able to sustain such temperatures, and there have been the need to wait until the technology to prepare such reinforcement was sufficiently developed. Then, since the processing temperatures are so high, all the factors that commonly affect composite preparation, like unwanted reactions or development of residual stresses during the cooling step, are enhanced with respect to other kind of composites. Moreover, if in a metal matrix composite plastic deformation of the matrix can relieve up to some extent these effects, in the case of brittle materials as ceramics are, cracking of the matrix may result. Clearly, in order to limit these inconveniences, there has to be some matching of the coefficients of thermal expansion.

2.3. COMPOSITE MATERIALS REINFORCED BY CARBON NANOTUBES

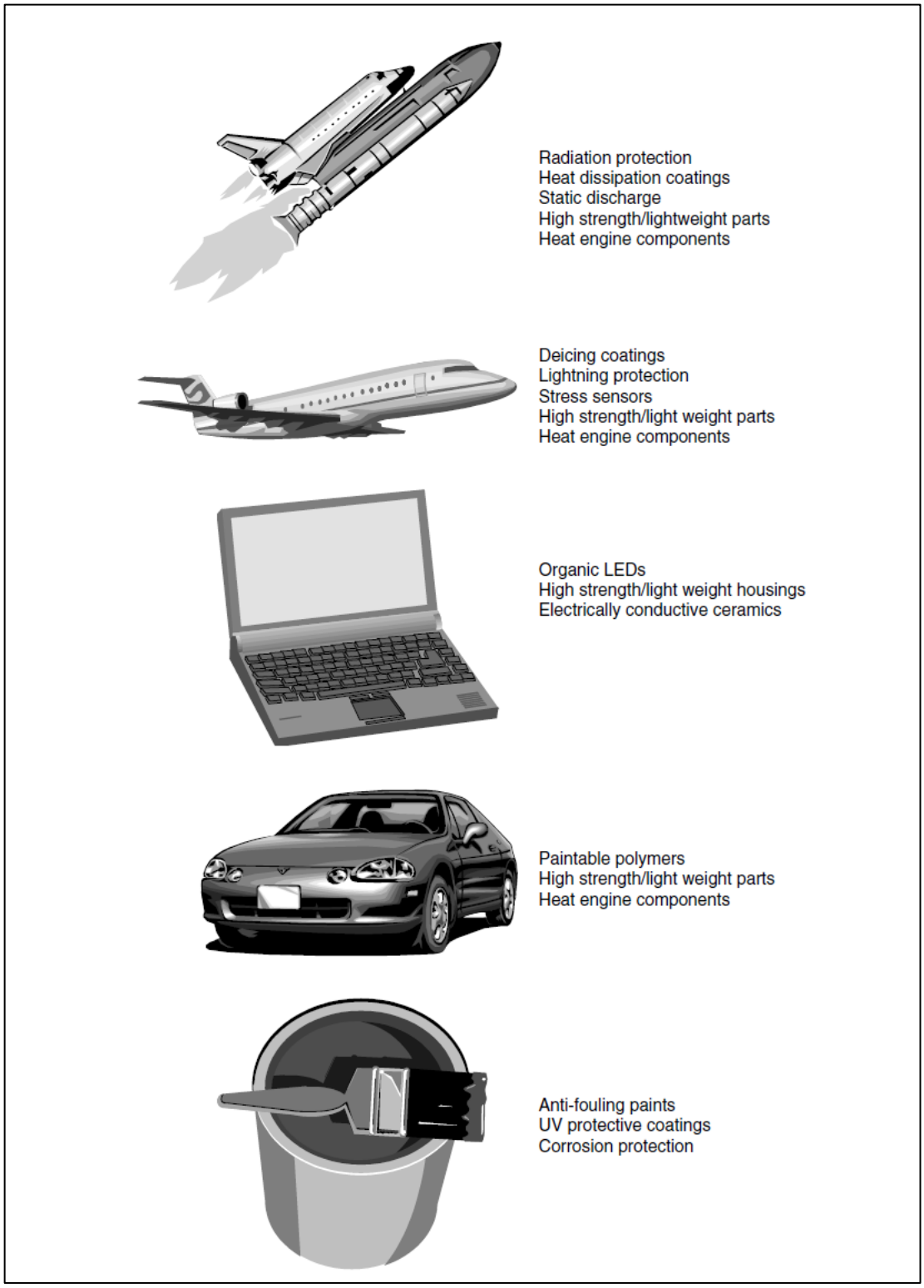

Figure 14 - Examples of CNTs composites applications (Meyyappan, 2005)

In last decades many research efforts have been directed toward the production and characterisation of composite materials reinforced by carbon nanotubes, in order to take advantage

of the extraordinary properties of these carbonaceous species. New conducting polymers, multifunctional polymer composites, conducting metal matrix composites, higher fracture-strength ceramics, electrical and structural high conductors, highly anisotropic insulators and high-strength, porous ceramics are just few examples of the possible new materials that can come from nanotubes (other specific examples in

Figure **14**).

The origin of nanotube-reinforced composites is the nanotubes themselves, but processing them into various matrices has been a spin-off from earlier work on incorporation of fullerenes into composite matrices. Nanotube composites can replace existing reinforcement materials with properties not as good as CNTs ones or can create nanocomposites for applications where composites have traditionally not been used before.Certainly, it would be useful and more economical if the conventional production techniques would work for producing new nanotube composites.

The evolution of nanotube processing, along with continued advances in purification, functionalization, and separation, have produced numerous starting conditions for composite development. The continued interest in developing longer nanotubes, similar to continuous reinforcements, will further enable the materials that can be produced with nanotubes. One of the most important aspect during the project and realization of composites reinforced by CNTs is certainly their dispersion and distribution: the outstanding properties of nanotubes have given cause for the development of composite materials however their agglomeration could negatively affect the final behavior of the material, i.e. modeling of electrical conduction has shown that because of the small size of nanotubes, a network will form at very low concentrations (about 1 wt.%) and may affect multifunctionality (Fournier, Boiteux, Seytre, & Marichy, 1997; Ounaies, 2003). The network that forms, particularly at high concentrations, may limit homogeneous dispersion. Because of the importance of this aspect a special attention will be paid to carbon nanotubes dispersion in section 1.4.

Composite materials reinforced by carbon nanotubes are generally categorized along similar classes of conventional composites and will be identified by the matrix materials. Altough, in particular in a first time, the largest efforts have been focused on polymer matrix composites, in last years a great interest has grown on metal and ceramic matrix composites reinforced by CNTs. Polymer nanocomposite studies have, in many cases, focused on nanotube dispersion, untangling, alignment, bonding, molecular distribution, and retention of nanotube properties. Studies of metal and ceramic systems have had additional issues of high-temperature stability and reactivity. The central goals have been the identification of new process techniques and of new nanotube chemistries able to provide stabilization and bonding to the high temperature matrices, namely materials that melt or

soften at temperatures higher than the nanotube degradation temperatures. Most studies treat nanotube addition in the same way for any micron-size additive.

2.3.1. POLYMER MATRIX COMPOSITES

Polymer composites, consisting of additives and polymer matrices, including thermoplastics, thermosets and elastomers, are considered to be an important group of relatively inexpensive materials for many engineering applications. Unlike traditional polymer composites containing micron-scale fillers, the incorporation of carbon nanotubes into a polymer results in very short distance between the tubes, thus the properties of composites can be largely modified even at an extremely low content of filler. For example, the electrical conductivity of CNT/epoxy nanocomposites can be enhanced several orders of magnitude with less than 0.5 wt.% of CNTs (J. Li et al., 2007).The excellent properties of CNTs have spawned huge potential applications in polymer nanocomposites. Ongoing experimental works in this area have shown some exciting results, although the much-anticipated commercial success has yet to be realized in the years ahead. In addition, CNT/polymer nanocomposites are one of the most studied systems because the polymer matrix can be easily fabricated without damaging CNTs using conventional manufacturing techniques, as discussed before, a potential advantage of reduced cost for mass production of nanocomposites in the future (P.-C. Ma, Mo, Tang, & Kim, 2010). A particular interest has been focused on understanding the structure–property relationship between CNTs and polymer matrix and also on finding useful applications in different fields for their composites, since the first report on preparation of CNTs/polymer composites (Ajayan, Stephan, Colliex, & Trauth, 1994).

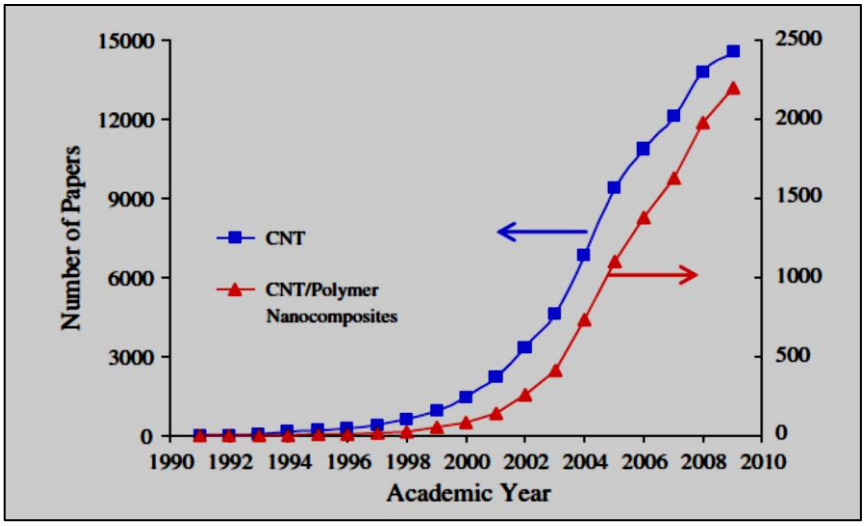

Figure 15 - Number of published papers related to CNT and CNT/polymer nanocomposites as a function of academic years (P.-C. Ma, Mo, et al., 2010)

A sensible increasing of the interest on this kind of composites is shown in Figure 15: the number of published papers related to both carbon nanotubes and CNTs/polymer composites has increased since 1999. This phenomenon is strictly related to the realization of CNT fabrication inindustrial scale with lower costs in the beginning of the 21st century (P.-C. Ma, Mo, et al., 2010).

According to the specific application, CNT/polymer nanocomposites can be classified as structural or functional composites (Du, 2007). For the production of structural composites, the unique mechanical properties of CNTs, i.e. the high modulus, tensile strength and strain to fracture, are exploited to develop structural materials with superior mechanical properties. Also many other properties of CNTs, such as electrical, thermal, optical and damping properties, are utilized to obtain multifunctional composites for applications in the fields of heat resistance, chemical sensing, electrical and thermal management, photoemission, electromagnetic absorbing and energy storage performances, etc.

A model developed by Cox (Cox, 1952) is very handy to relate the reinforcement to the shape factor. i.e. the length to radius ratio λ, for the simplest composite: a single filament embedded in a cylindrical matrix (Figure 16).

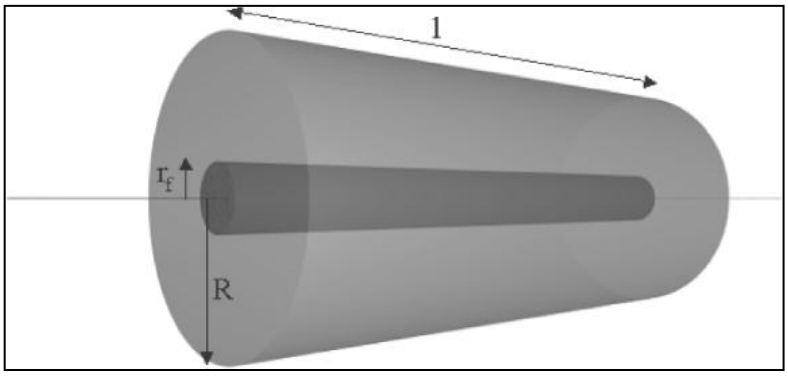

Figure 16 - Geometry of the Cox model (Cox, 1952)

The Cox model allows to calculate the shear strain (stress) axial component in the matrix and the tensile strain (stress) in the fibre. It cannot totally describe stress and strain fields in specimens which are triaxial (axisymmetric), and neglects:

– The influence of radial and orthoradial stresses on interfacial and longitudinal shear

– The elasto-visco-plastic behaviour of the polymer in polymer matrix composites (PMCs)

– The highly anisotropic structure of carbon fibres or nanotube ropes.

Nevertheless, the Cox model is not so far from more sophisticated analysis.

Load is applied to the matrix cylinder and a perfect interface is supposed, so that matrix strain is transferred to the fibre. This ensures continuity of displacement at each point of the interface. The axial strain in the fibre is given by:

$$\epsilon(x) = \epsilon_\infty \left(1 - \cosh\beta\left(\frac{l}{2} - x\right) \Big/ \cosh\beta\left(\frac{l}{2}\right)\right)$$

With $\beta = \left[2\, G_m / r_f^2 E_f \ln\left(R/r_f\right)\right]^{1/2}$. E_f , r_f and *l* are the fibre axial modulus, radius and length; *R* and G_m are the radius and the shear modulus of the matrix. The axial strain at the centre of a very long fibre is very close to that of the matrix ϵ_m both being equal to ϵ_∞ for infinite length. Thus $l_0 = 2/\beta$ appears as a characteristic length of the model composite. In Figure 17 $\epsilon_m/\epsilon_\infty$ is reported as a function of the reduced length l/l_0.

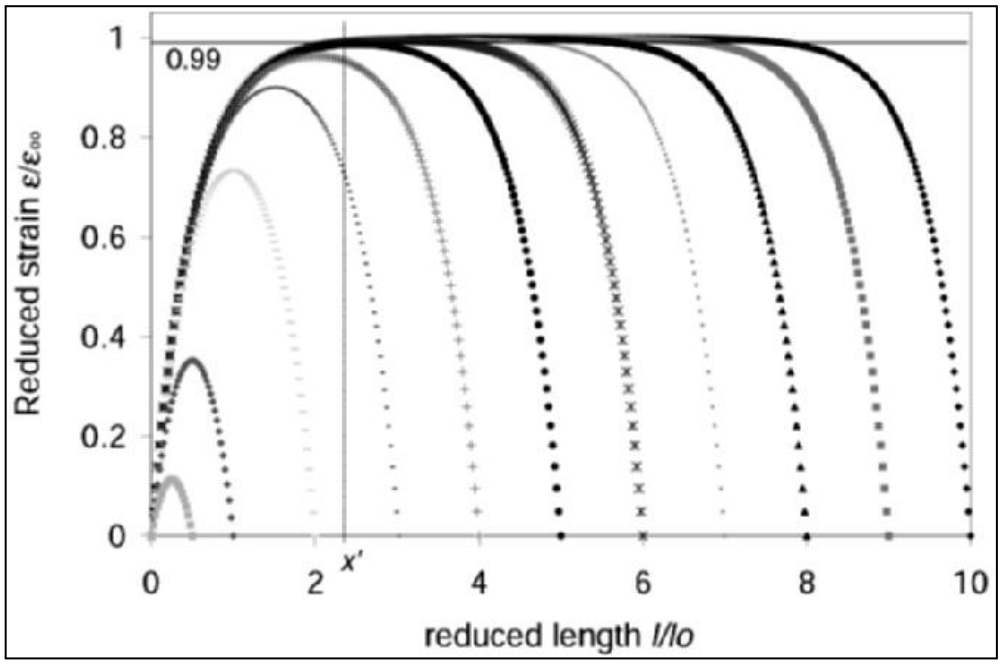

Figure 17 - Strain transfer reduced curves in the Cox model. The reduced strain along the fibre Is plotted for different values of the reduced length

Strain is maximised at the centre of the fibre (and zero at its ends) and strictly depends on l/l_0 for small values of this parameter, i.e. when l/r_f is small. The quantity $\eta = \epsilon_{1/2}/\epsilon_\infty$ reaches 0.99 for $l = 2x'$ where $x' \approx -(\ln 0.01)/\beta$ is a loading length. The strain transfer efficiency ξ can be defined simply as the ratio between the mean strain value $\bar{\epsilon}$ and ϵ_∞.

Several techniques have been developed for the production of carbon nanotubes/polymer composite materials:

- **Solution mixing**

Solution mixing is one of the most common techniques used to produce CNTs/polymer composites because it is fairly suitable for small size samples (Du, 2007; Grossiord, Loos, Regev, & Koning, 2006;

Moniruzzaman & Winey, 2006).Typically, this approach involves three major steps: dispersion of CNTs in a proper solvent by mechanical mixing, magnetic agitation or sonication. The solvent should also be compatible with polymer resins. After that, the dispersed CNTs are mixed with polymer matrix at room or elevated temperatures. The nanocomposite is finally obtained by precipitation or casting. This method is very useful to prepare composite films starting form a slurry.

- **Melt blending**

Melt blending is another widespread method for fabrication of CNT/polymer nanocomposites. Thermoplastic polymers, such as polypropylene (Q.-H. Zhang & Chen, 2004), polystyrene (Hill, Lin, Rao, Allard, & Sun, 2002), poly(ethylene 2,6-naphthalate) (J. U. N. Y. Kim & Kim, 2005), can be processed as matrix materials in this method. The major advantage is that it is a solvent-free approach. The dispersion of CNTs in the polymer matrix is carried by a high temperature and a high shear forces applied. Generally the process is conducted using special equipment, raising the temperature and working in high shear force conditions, such as extruders and injection machines. The melt blending is often used to produce CNTs/polymer composite fibres. Compared with solution mixing, this technique is less effective on carbon nanotubes dispersion and distribution inside the polymer matrix. Moreover its application is limited to low amount of filler in thermoplastic matrices (Moniruzzaman & Winey, 2006).

- **In situ polymerization**

In situ polymerization is an efficient method to realize uniform dispersion of CNTs in a thermosetting polymer. CNTs are mixed with monomers, either in the presence or absence of a solvent, and then the monomers are polymerized via addition or condensation reactions at an elevated temperature (in presence of hardeners or curing agents). One of the major advantages of this method is the possibility to create covalent bonds between the functionalized carbon nanotubes and polymer matrix chains, resulting in strong interfacial bonds and much improved mechanical properties of the final product. The main application of the in situ polymerization technique is certainly the production of epoxy-based nanocomposites (Gojny, Wichmann, Köpke, Fiedler, & Schulte, 2004; Kosmidou, 2008; P. C. Ma, Kim, & Tang, 2007; P.-C. Ma et al., 2009; Moisala, Li, Kinloch, & Windle, 2006), for which it is reported (in Figure 18) the typical process flowchart.

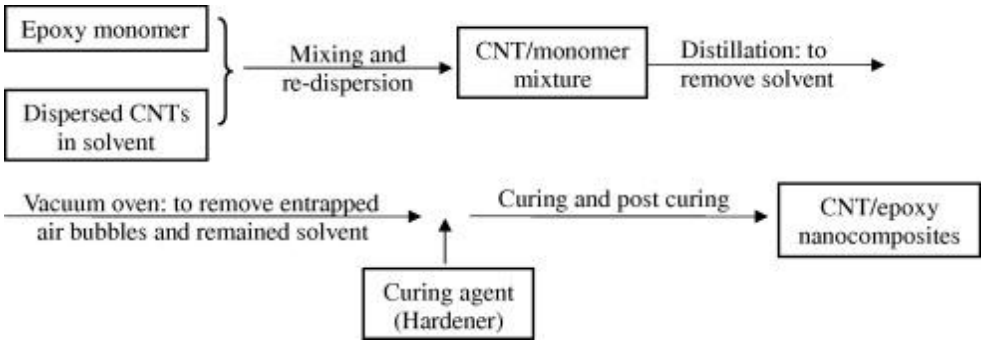

Figure 18 - Schematics of CNT/epoxy nanocomposites fabrication (P.-C. Ma et al., 2009)

- **Latex technology**

A relatively particular and new approach to disperse CNTs into a polymer is based on the latex technology (Du, 2007; Grossiord et al., 2006; Moniruzzaman & Winey, 2006). Latex is a colloidal dispersion of discrete polymer particles, usually in an aqueous medium. By this method it is possible to disperse both single and multi-walled CNTs in most of polymers that are produced by emulsion polymerization, or that can be brought into the form of an emulsion. CNTs are added only after the polymer synthesis. The first step of the process consists of dispersion of CNTs in an aqueous surfactant solution. Then the stable dispersion of surfactant covered carbon nanotubes is mixed with a polymer latex. After freeze-drying and subsequent melt-processing, the nanocomposite can be obtained. The advantages of this technique are obvious (Du, 2007; Grossiord et al., 2006): the whole process consists of simple mixing steps and therefore it is relatively easy. Moreover, it is versatile, reproducible, and reliable, and most of all it allows distribution of individual tubes into a viscous polymer matrix. All the dispersion process is totally carried in water, thus the process is a safe, environmentally friendly and low-cost method. Due to these advantages the possible scale-up of the technique is easily conceivable.

- **Other techniques**

In recent years many new methods have been developed to obtain CNT/polymer nanocomposites, especially with very high filler content or for some specific applications. They include:

- densification, in which CNT forests are prepared and transferred to a pool of uncured epoxy resin. The matrix is infused into the CNT forest and then cured. The advantage of this technique is the possibility to work with high percentage of carbon nanotubes and control their amount during the forest synthesis (Wardle et al., 2008).
- spinning of coagulant, in which, after a proper pre-dispersion in presence of a surfactant, the CNTs are coagulated into a mesh by wet spinning into a polymer solution, and then the mesh

is converted into a solid fibre by a slow draw process. It is clearly particularly useful for fibres production (Vigolo, 2000).

- layer-by-layer deposition involves, after a CNTs pre-dispersion in solvent, the dipping of a solid substrate (glass slides, silicon wafers) into the CNT/polymer solutions and a following curing. A method of this kind minimises structural defects that are originated from the phase segregation of the polymer/CNT and high loading of CNT (up to 50 wt.%) could be incorporated in the matrix (Mamedov et al., 2002).
- pulverization in which polymer and CNTs (without any kind of pre-treatment) are mixed and pulverized by pan mill or twin screw. The main advantages of this technique are the absence of solvents and the possible easy scale-up of the system (Xia, Wang, Li, & Hu, 2004).

With a tensile modulus on the order of 1 TPa and a tensile strength 100 times greater than steel at one sixth the weight, single-walled carbon nanotubes are ideal reinforcements for polymer matrix composites, but to fully exploit their exceptional properties, CNTs should be homogeneously dispersed and aligned within a polymer matrix. Composites containing isotropically oriented nanotubes generally possess lower mechanical properties than composites with aligned nanotubes (Andrews, Jacques, Minot, & Rantell, 2002; Shofner, Rodríguez-Macías, Vaidyanathan, & Barrera, 2003). Static and dynamic mechanical property improvements have been observed in nanotube-reinforced polymers compared with the neat polymers, and anisotropic nanotube orientation has shown greater improvements over isotropic nanotube orientations in polymers. Enhancements of about 450% in tensile modulus have been observed at CNTs amounts of 20 wt.% (Haggenmuller, Zhou, Fischer, & Winey, 2003). In composite fibres containing highly aligned nanotubes, simultaneous increases in tensile strength, tensile modulus, and strain to failure have been realized (Kumar et al., 2002).

Both SWCNTs and MWCNTs have been utilized as reinforcements in thermosetting polymers, such as epoxy, polyurethane, and phenol–formaldehyde resins, as well as thermoplastic polymers, including polyethylene, polypropylene, polystyrene, nylon, and so on. The CNTs reinforced nanocomposites can be considered as a kind of particular composites with the filler dimensions on the nanometre scale and a high aspect ratio. The mechanical properties of nanocomposites depend strongly on the characteristics of reinforcement and matrix and also on the dispersion state of the fillers. In addition to dispersion, the nanoparticles (particularly CNTs) should exhibit a high aspect ratio, alignment and interfacial interactions with the polymer matrix to act as effective reinforcement (J. Kim & Mai, 1998).

The aspect ratio must be sufficiently large to maximize the load transfer between the CNTs and matrix material and thus to achieve enhanced mechanical properties. For example, polystyrene nanocomposites reinforced with well-dispersed 1.0 wt.% carbon nanotubes of a high aspect ratio had

more than 35% and 25% increases in elastic modulus and tensile strength, respectively (Qian, Dickey, Andrews, & Rantell, 2000). Also good results have been reported by other research groups (J. Coleman, Khan, Blau, & Gunko, 2006; Jiang, Liu, Zhang, Wang, & Wang, 2007), but other reports demonstrated only modest improvements in mechanical properties. For example, the great impact of aspect ratio on mechanical properties of CNT/epoxy nanocomposites is reported by Hernandez-Pérez (Hernández-Pérez et al., 2008). Epoxy resin has been reinforced by two types of MWCNTs with different aspect ratios. It resulted that the impact resistance and fracture toughness were significantly improved only for those containing CNTs of a higher aspect ratio. At the same time, however, the corresponding tensile modulus and strength showed very limited improvements of less than 5%, probably due to weak bonds between the CNTs and polymer matrix and agglomeration of CNTs.

Indeed, dispersion is the foremost important condition in CNT/polymer nanocomposites production. Many different techniques are generally adopted to obtain carbon nanotubes dispersion, as it is going to be discussed in section 1.4. A good dispersion is necessary to make more reinforcement material surface area available for bonding with polymer matrix, and prevents the aggregated filler from acting as stress concentrator, crack generators and defects, with a consequent decreasing of mechanical performance of composites (L. Liu & Wagner, 2005).

Other major issues are CNT content in composites, length and entanglement of CNTs as well as viscosity of matrix. Regarding CNTs content in polymer matrix many studies show that there is a critical value below which the strengthening effect increases with increasing CNT content. On the other hand, above this critical CNT content the mechanical properties of composites decrease, and in some cases, they worsen those of the neat matrix material. This effect can be related to the difficulties associated with uniform dispersion of CNTs at high CNT contents and lack of polymerization reactions that are adversely affected by the high CNT content (Kosmidou, 2008; P. C. Ma et al., 2007; P.-C. Ma et al., 2009).

From the geometrical point of view, the difference between random orientation and alignment of carbon nanotubes can significantly change several properties of composites (J. Kim & Mai, 1998). For example the storage modulus of the polystyrene composite films containing random and oriented CNTs were 10% and 49% higher than the unreinforced bulk polymer, respectively (Erik T Thostenson & Chou, 2002). Several techniques, including mechanical stretching (Jin, Bower, & Zhou, 1998), melt-spinning (Fornes, Baur, Sabba, & Thomas, 2006), application of electrical or magnetic field (Steinert & Dean, 2009), have been employed during the composite production of aligned CNTs in a polymer matrix. The carbon nanotubes alignment in the composite can be governed by at least two factors: the diameter of the tubes and the CNTs content. A smaller diameter of CNT can enhance the degree of CNT alignment due to the greater extensional flow; and a higher CNT content decreases their

alignment because of the CNT agglomeration and restrictions in motion from neighbouring CNTs (Desai & Haque, 2005). While alignment can act to maximize the strength and modulus, at the same time the aligned composites exhibit very anisotropic mechanical properties: the mechanical properties along the alignment direction can be enhanced, whereas along the direction perpendicular to this orientation they could result not improved or even worsened.

Matrix		Dispersion technique	Functionalization technique	CNT content	Enhancement on mechanical properties[a]		
					Modulus (%)	Strength (%)	Toughness (%)
Thermo-plastic[b]	PA	Twin-screw extruder	Diamine treatment	1.0 wt.%	6.1 (42)	−5.3 (18)	–
	PB	Shear mixing	Polymer grafting	1.5 wt.%	18 (91)	−27 (61)	−40 (67)
	PE	Shear mixing	Maleic anhydride and amine treatment	1.5 wt.%	22 (75)	−17 (33)	−69 (61)
	PI	Ultrasonication	Acid treatment	7.0 wt.%	39 (61)	19 (31)	–
	PP	Ultrasonication and stir	Undecyl radicals attachment	1.5 wt.%	55 (84)	−10 (13)	–
	PS	Probe ultrasonication	Butyl attachment	0.25 wt.%	−8.3 (25)	2.1 (50)	–
	PVA	Ultrasonication and stir	Polymer grafting	2.5 wt.%	35 (40)	−4.8 (17)	–
	PMMA	Ultrasonication	Polymer grafting	0.10 wt.%	57 (104)	−2.7 (86)	–
Thermo-set[c]	EP	Calendering	Amino treatment	0.10 wt.%	2.1 (6.7)	−2.2 (3.1)	17 (19)
		Probe ultrasonication	Surfactant treatment	0.25 wt.%	8.6 (24)	6.8 (20)	35 (60)
		Ultrasonication	Organic silane	0.25 wt.%	8.7 (22)	3.6 (18)	−22 (8.5)
	PU	Ball mill	Polymer grafting	0.7 wt.%	48 (178)	27 (23)	–
		Ultrasonication	Acid treatment	10 wt.%	340 (500)	51 (111)	–
	VR	Ball mill	Acid treatment	25 phr	444 (594)	175 (244)	–
		Roll mill	Organic silane	1 phr	35 (28)	−7.8 (25)	–

Table 2 - Effect of CNT functionalization on the mechanical properties of CNT/polymer nanocomposites (P.-C. Ma, Siddiqui, Marom, & Kim, 2010)

Finally a strong interfacial adhesion corresponds to high mechanical properties of composites through enhanced load transfer from matrix to CNT. Chemical and physical functionalization of CNTs has proven to enhance the interfacial adhesion. In Table 2 several results on the effects of CNT functionalization on the mechanical properties of CNT nanocomposites are reported. These results indicate clearly that functionalization of CNTs can enhance the modulus, strength as well as fracture resistance of nanocomposites.

2.3.2. METAL MATRIX COMPOSITES

Lightweight, high strength materials have been required since the invention of the airplane. Increasing the strength and stiffness of a material, the dimensions, and consequently, the mass, of the material required for a certain load bearing purpose is reduced. This leads to several advantages in the case of aircraft and automobiles such as increase in payload and improvement of the fuel efficiency. With global oil resources on a decline, increase in the fuel efficiency of engines has become highly desirable. Metals and alloys resulted inefficient in providing both strength and

stiffness and therefore the development of alternative materials has become necessary. Metal matrix composites (MMCs) could be a solution, with lightweight and ductility provided by the metal and the strength and stiffness by the reinforcement that is either a ceramic or high stiffness metal based particulate or fibre (Bakshi, Lahiri, & Agarwal, 2010). Since the beginning metal matrix composites have been largely employed in automotive and aerospace applications (Kelly, 2006; Kevorkijan, 1999; Rawal, 2001; Shelley, LeClaire, & Nichols, 2001). Because of the extraordinary properties of CNTs many studies have been conducted, since 2003 especially, concerning various metal matrices reinforced by these promising carbonaceous materials. Figure 19 shows the number of papers published on CNT-reinforced composites between 1997-2007 (the years in which mainly exploded the interest on CNTs composites). The majority of the researches has been focused on reinforcement of polymers by CNT. This is due primarily to the relative ease of polymer processing, which often does not require high temperatures for consolidation as needed for metals and ceramic matrixes. The relative small number of papers on metal matrix composites reinforced by CNTs is quite surprising considering the fact that most of the structural materials used in today's world are metals.

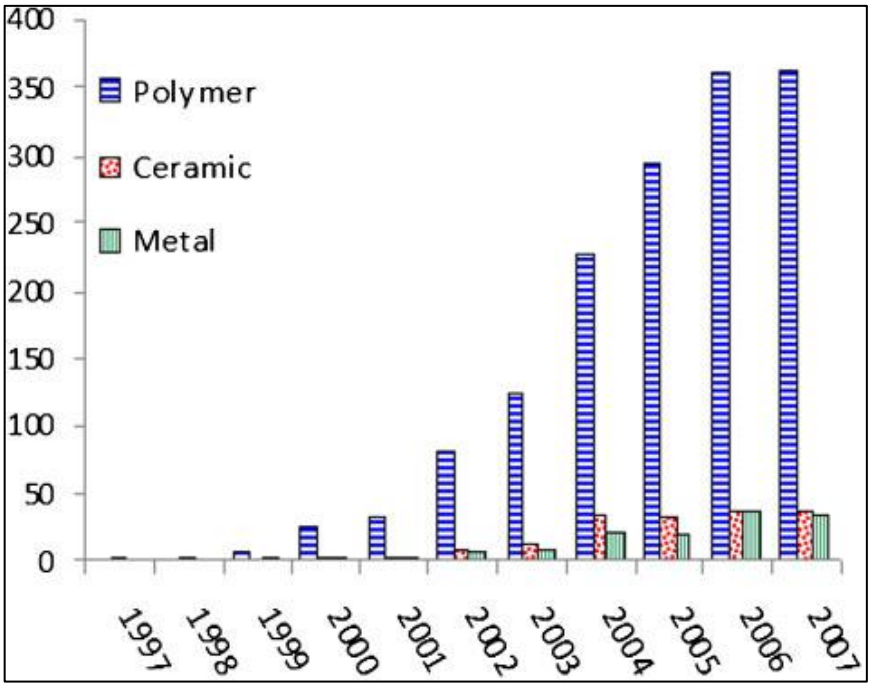

Figure 19 - Number of publications on CNTs composites between 1997-2008 (Bakshi et al., 2010)

Whether or not nanotubes in metals would overcome the problem of carbon reinforcement in metals is yet to be fully understood. The "no defect" description of SWNTs is probably what sparked an interest in developing nanotube-metal composites (NMCs). Carbon fibres have been avoided due to bonding and reaction issues in aluminium and other metals, and the absence of defects suggests these issues may be evaded (for example the Al_4C_3 formation between Al and carbon fibres). Wetting

and adhesion of metals to the nanotubes are outstanding peculiarity in order to obtain NMCs with improved properties. Dujardin and others (Andriotis, Menon, & Froudakis, 2000; E Dujardin, Ebbesen, Hiura, & Tanigaki, 1994; Ebbesen, 1996) showed that the determining factor for wetting metals to nanotubes is surface tension and resolved that a cut-off occurs between 100 and 200 mN/m. This limit implies that aluminium, copper, and iron (865 mN/m, 1270 mN/m, and 1700 mN/m, respectively) will not easily wet the nanotube surfaces. Therefore, various routes for improving the wetting are necessary in order to achieve strong interactions between the nanotubes and the matrix. Many of the processing modes used to improve the interaction between matrix and reinforcement involve processing below the melting temperature of the metals when in contact with the nanotubes to provide for nanotube stability. Few methods have involved the processing of nanotubes in molten metals because reactivity and potential nanotube degradation would be extremely high at these conditions. Carbon nanotube reinforced metal matrix composites are prepared through a variety of processing techniques. Powder metallurgy is the most popular and widely applied technique for NMCs preparation. Electro deposition and electroless deposition are used in particular for deposition of thin coatings of composites as well as for deposition of metals on to CNTs. Melting and solidification are good techniques for low-melting-point metals such as magnesium and bulk metallic glasses, as well as other several non-standard techniques experimented during last decade, i.e. molecular level mixing (Cha, Kim, Arshad, Mo, & Hong, 2005), sputtering techniques (Huang, Chen, & Zuo, 2006), vapor deposition (Y. Zhang, Zhang, Li, Wang, & Zhu, 2000) and nanoscale dispersion (Noguchi et al., 2004).

- **Powder metallurgy**

Powder metallurgy techniques are based on several process steps: mixing of CNTs with metal powder by grinding or mechanical alloying, consolidation of the composite powders by compaction and sintering, cold isostatic pressing, hot isostatic pressing, or spark plasma sintering. Generally, the compacted composite green specimens are subjected to post-sintering deformation processes such as rolling, equi-channel angular processing, extrusion, etc. These techniques are mainly applied to aluminium and copper matrix composites, however a few researchers have also prepared CNT composites based on magnesium, titanium, nickel, silver, tin and intermetallics through this route. The purpose is to obtain good reinforcement, by achieving homogeneous dispersion of CNT in the metal matrix and good bonding at the metal/CNT interface.

Mechanical alloying and sintering

The most critical issues in processing of NMCs are the dispersion of carbon nanotubes and the interfacial bond strength between CNT and the matrix. Researchers have tried different approaches

to solve these problems. For copper matrix composites (W. Chen et al., 2003; J. Tu, Yang, Wang, Ma, & Zhang, 2001) nanotubes were coated with nickel using electroless deposition to achieve good interfacial bond strength. Density of the composites was comparable up to 8 wt% CNT (beyond this value density decreased drastically due to agglomeration (He et al., 2007; J. Tu et al., 2001). No interfacial product formation was observed. To improve the dispersion of the filler inside aluminium matrix He et al. have grown CNT by chemical vapour deposition (CVD) process directly on Al powders which were then compacted and sintered at 913 K. For 5 wt% CNT relative density of 96% has been registered, and homogeneous dispersion of CNTs has been observed. Carbon nanotubes are responsible for increased hardness (4-8 times) and tensile strength (2-8 times) (He et al., 2007) on respect of pure aluminium. Yang et al. (Yang & Schaller, 2004) have obtained homogeneous distribution of nanotubes in magnesium matrix by mechanical mixing of the powders in presence of an alcohol and acid mixture. The powders are then sintered at 823 K. Ball milling has been exploited by Morsi and Esawi (Esawi & Morsi, 2007; Morsi & Esawi, 2007) for CNTs dispersion on Al particles. Milling for at least 48 hours lead to good dispersion of CNTs but resulted in formation of large spheres (larger than1 mm) due to cold welding.

Mixing/mechanical alloying and hot pressing

Instead of sintering, some researchers have used hot pressing consolidation of powder mixtures. This technique resulted inappropriate for fabrication of aluminium matrix NMCs (C. L. Xu et al., 1999; Zhong, Cong, & Hou, 2003), but it has been successfully applied to the fabrication of copper (C Deng, Zhang, Wang, & Ma, 2007), titanium (Kuzumaki, Ujiie, Ichinose, & Ito, 2000), magnesium (Carreño-Morelli et al., 2004) and iron-aluminium (L. X. Pang, Sun, Ren, Sun, & Bi, 2007) matrix composites. In the Fe_3Al-CNT case, composites synthesized via hot-pressing have shown improved mechanical properties (hardness, compressive strength and bend strength) due to uniform distribution of CNTs. The enhancement in the mechanical properties was attributed to grain growth inhibition caused by interlocking nanotubes (L. X. Pang et al., 2007).

Spark plasma sintering

In spark plasma sintering technique a pulsed direct current passed through the powder, producing rapid heating and thus greatly enhancing the sintering rate. This method is, generally, suitable for consolidation of nano powders, without allowing sufficient time for grain growth. The main applications of spark plasma sintering with NMCs are Cu-CNT (Cha et al., 2005; K. T. Kim, Cha, & Hong, 2007; K. T. Kim, Cha, Hong, & Hong, 2006) and in Al-CNT (H Kwon, Estili, Takagi, Miyazaki, & Kawasaki, 2009). Enhancement in mechanical strength by 129% with addition of 5 vol % of CNT has been reported for Al-CNT composite sintered by SPS and followed by hot extrusion of powders

prepared by a nanoscale dispersion Good dispersion and alignment of CNTs in the matrix as well as formation of Al_4C_3 at the CNT/matrix interface were the prime reasons for improvement is mechanical properties (Majkic & Chen, 2006). Spark plasma sintering has also been explored for synthesis of CNT-reinforced Ni–Ti alloys (Majkic & Chen, 2006) and Fe_3Al-CNT composites (L.-X. Pang et al., 2007). SPS, because of the high temperatures and high pressures reached during the process, allows good densification and mechanical properties. However, at these conditions could damage CNTs, which can also react with the matrix material.

- **Melting and solidification**

Melting and solidification represent the most conventional processing techniques for metal matrix composites. This route has also been utilised for synthesising CNT-reinforced composites. However, due to the high temperature required for melting, is not so commonly employed. The process could damage CNTs or lead to the formation of chemical reaction products at the CNT/metal interface. Whereupon, this technique is mainly used for composites with low melting point matrix. Another limitation is that carbon nanotubes in a liquid phase tend to form clusters because of their characteristics surface tension forces.

Casting

Pre-alloyed powders, mixed with CNTs, are compacted and then melted and casted and can eventually be followed by hot extrusion, so to achieve an improved reinforcement effect of the carbon nanotubes within the matrix. The main application of casting are zirconium matrix (B. Z. Bian, Wang, Wang, Zhang, & Inoue, 2004; Z. Bian, Pan, Zhang, & Wang, 2002) and magnesium (Goh, Wei, Lee, & Gupta, 2006, 2008; Kondoh et al., 2010).

Metal infiltration

At the base of metal infiltration there is the idea of prepare a porous solid structure with dispersed CNTs and then infiltrating liquid metal into the pores and solidify to prepare a composite structure (Figure 20).

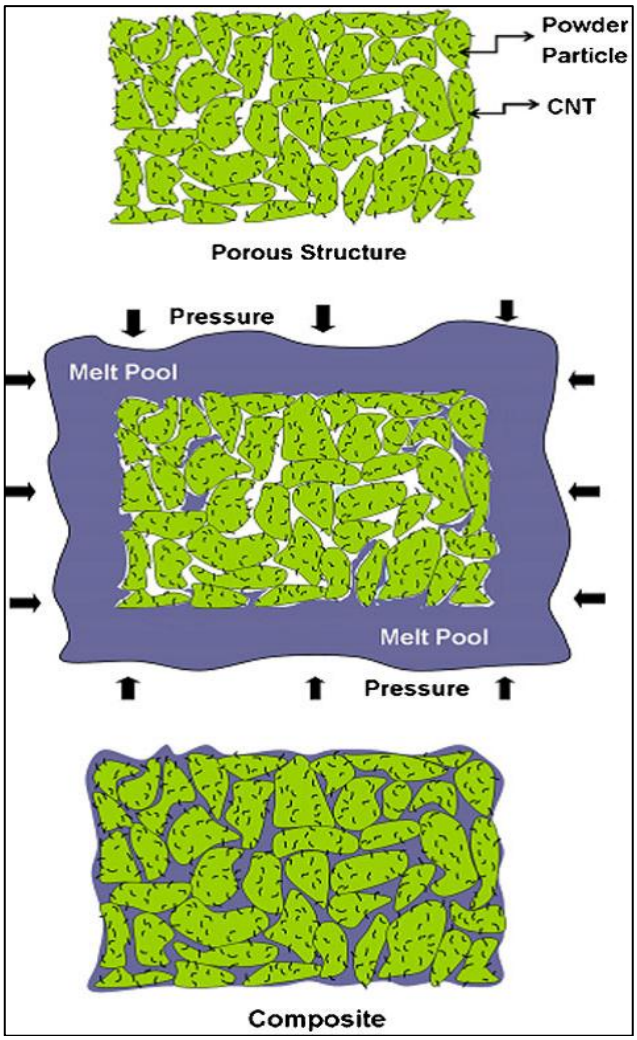

Figure 20 - Schematic of metal infiltration technique (Bakshi et al., 2010)

This technique has a higher chance to obtain uniform distribution of CNTs, but at the same time results critical to proper filling up of the pores and making a good and dense composite structure. There is a also probability of movement and thus agglomeration of CNTs due to high pressure application during infiltration. Yang and Schaller (Yang & Schaller, 2004) have used infiltration to synthesise magnesium matrix composite starting from CNTs grown by CVD on an Al_2O_3 fibres structure. Al-CNT composite has been produced by Zhou et al. (S. Zhou et al., 2007) through infiltration of a porous preform made by pressing a ball milled mixture of aluminium and magnesium powders and CNTs at 1073 K.

There are two mainly goals in adding carbon nanotubes to a metal matrix: to increase the tensile strength, and to increase the elastic modulus of the composite. Both of these effects are correlated with the fact that the CNTs have a higher stiffness and strength compared to the metal matrix. The critical issues in mechanical properties in NMCs are the homogeneous distribution of CNTs in the metal matrix, and the interfacial reaction and bonding with the matrix, necessary to achieve an

effective reinforcement. The percentage enhancement in mechanical property of NMCs is not just function of filler content or of the matrix material. The non-linearity in the trend of these data is correlated with the variance in the microstructural features, defects and porosity level of the samples. The difficulty in measuring the mechanical properties of CNTs reinforced can also affected the measurements.

Regarding aluminium matrix composites Kuzumaki et al. (Kuzumaki, Miyazawa, Ichinose, & Ito, 1998) were the first researchers to show a 100% increase of the tensile strength adding 10 vol.% CNT, while a maximum of 129% increase in the tensile strength has been reported with the addition of 5 vol. % CNT addition (C. F. Deng, Wang, Zhang, & Li, 2007; C Deng, Zhang, Ma, & Wang, 2007). On the contrary, Salas et al. (Salas, Alba-Baena, & Murr, 2007) have reported deterioration in hardness in a shock-wave-consolidated aluminium composite reinforced by 5 vol.% CNT composite. Agglomeration of CNTs in the matrix and weak interface bonding led to deterioration in the properties. Noguchi et al. (Noguchi et al., 2004) reported a 350% increase in the compressive yield strength in the case of 1.6 vol.% CNT addition, using the nanoscale dispersion method, which can provide a very satisfying dispersion and distribution of the reinforcements. He et al. (He et al., 2007) have also emphasised homogeneous distribution and good interfacial bonding of CNTs growing them directly on aluminium powder through the CVD method. After compaction they achieved 333% increase in hardness and 184% increase in tensile strength with 6.5 vol.%CNT addition (He et al., 2007). Hence, it is clear that homogeneous distribution of CNTs and strong bonding with the matrix are the main means to control the mechanical properties of the carbon nanotubes-metal matrix composites.

2.3.2.1. ALUMINIUM MATRIX COMPOSITES

Aluminium is one of the most important matrix materials for MMCs. Mechanical properties of carbon nanotubes reinforced Al matrix composites have been intensively studied. In fact in last decade the interest in CNT-reinforced aluminium composites has been grown considerably and the main purpose of the various groups has produced composites with enhanced mechanical properties. Such composites would make attractive novel materials with potential applications in the aerospace, automotive and sports industries where light weight combined with high stiffness and strength is desired.

The question of realizing nanoscale properties at bulk scale is an existing challenge for the scientific community. Though there is a fair degree of agreement that problems are largely associated with consolidation or processing of nanocomposites. Fabrication of bulk nanocomposite structure with CNT reinforcing aluminium has always become difficult, primarily due to the problem of inhomogeneous CNT distribution and retention, and the insufficient adhesion at the matrix–

reinforcement interface for effective load transfer. Because of these reasons, the evaluation of the mechanical properties of CNT-composites is considered extremely difficult and often ambiguous, attributed to the difficulties of preparing mechanical testing samples. Most of the mechanical property data reported on CNT reinforced nanocomposites has been based on microhardness, nanoindentation, miniaturized sample or computational theories (Laha, Chen, Lahiri, & Agarwal, 2009).

Samples	Composite processing technique	Tensile sample size	Mechanical properties (UTS, YS, E, strain to failure, hardness)		Reference
			With CNTs	Without CNTs	
Al + MWCNT (vol% – 0.5–2) & SWCNT (vol% – 1–2)	Al–CNT- mixed by ball milling, compacted and sintered at 580 °C and hot extruded at 560 °C	Not mentioned	(1) For MWCNT Y.S – 99 MPa, UTS – 150 MPa (2) For SWCNT Y.S. – 98.7 MPa, UTS – 181 MPa	Not mentioned	George et al.
Al + CNT(5–10 vol%)	Al–CNT, stirred in ethanol, dried in vacuum, compacted, hot extrusion	Tensile test pieces with a gage length of 15 mm and diameter of 3 mm	UTS (annealing at 873 K) = 80 MPa, for 0–100 h of annealing	UTS (annealing at 873 K) = 40–90 MPa (decreasing with annealing time)	Kuzumaki et al.
Al + MWCNT (0.8 vol% and 1.6 vol%)	Precursor with natural rubber, roll milled – compressed in mould, heated at 800 °C (for curing)	Compression test, dimensions not mentioned, may be 10 × 10 × 5 mm block	(1) For 0.8 wt% CNTs: YS = 150 MPa (2) For 0.16 wt% CNTs: YS = 225 MPa	Al < 50 MPa	Noguchi et al.
Al + 5 wt% CNT (1 wt% Ni)	CVD growth of CNT on Al powder – by Ni catalyst, pressing & sintering	Not mentioned	(1) CNT grown on powder (CVD): Hardness = 0.65 GPa, UTS = 398 MPa (2) CNT mixed powder: Hardness = 0.32 GPa, UTS = 213 MPa	Hardness = 0.15 GPa, UTS = 140 MPa	He et al.
2024 Al (Cu–Mg–Mn) + MWCNT (1 wt%)	Ball milling + cold isostatic press (CIP) + hot extrusion (460 °C, ratio 25:1) in Al case	Not mentioned	*E* = 102.2 GPa, UTS = 521.7 MPa, %El = 17.9, Hardness = 136 MPa	*E* = 72.3 GPa, UTS = 384.5 MPa, %El = 18.8, Hardness = 104	Deng et al.
Al powder + 2, 5 vol% MWCNT	Green compact, layers of pure Al, and Al + CNT, shock wave consolidation (SWC)	D638 type – V ASTM standard specifications (with gage length of 9 mm)	Rockwell hardness: E scale Al-2%CNT = 39 HRE, Al-5%CNT = 33 HRE UTS = 20 MPa, %El = 2	Al = 40 HRE, YS = 120 MPa, %El = 6.5	Salas et al.
2024 Al + 0–2 wt% MWCNT	Mixed & ultrasonicated + CIP + hot extrusion (460 °C, ratio 25:1) in Al case	Not mentioned	(1)F or 1% wt.CNT: UTS = 521.7 MPa, E = 102.2 GPa, %El = 19 (2) For 2% wt.% CNT: UTS = 350 MPa, *E* = 85 GPa, %El = 3	UTS = 385 MPa, *E* = 72 GPa %El = 20	Deng et al.
2024 Al + 1 wt% MWCNT	Mixed & ultrasonicated + CIP + hot squeeze	Dog bone shape sample with A gauge length of 15 mm	HV = 136 ± 5 MPa, YS = 336 MPa, UTS = 474 MPa, *E* = 88 GPa	HV = 104 ± 5 MPa, YS = 289 MPa, UTS = 384 MPa, *E* = 71 GPa	Deng et al.

Table 3 - Summary of tensile properties of carbon nanotube reinforced aluminum composites (C. F. Deng, Wang, Zhang, et al., 2007; C Deng, Zhang, Ma, et al., 2007; George, Kashyap, Rahul, & Yamdagni, 2005; He et al., 2007; Kuzumaki et al., 1998; Noguchi et al., 2004; Salas et al., 2007)

In Table 3 some data on the tensile properties of CNT reinforced aluminium composites are summarised. Few research groups have conducted tensile tests on relatively large (15 mm gauge length) aluminium/ carbon nanotubes composite but obtained very different yield strength values: Kuzumaki et al. (Kuzumaki et al., 1998) obtained the yield strength of 80 MPa for 5–10 vol% CNT whereas Deng et al. (Chunfeng Deng, Zhang, Wang, Lin, & Li, 2007) reported yield strength of 336 MPa using just 1 wt% CNTs as reinforcement. Looking at the data is evident that the tensile properties of CNT reinforced aluminium composites are influenced by the different processes used to synthesised them, attributed to the variance in the microstructural features, defects, porosity level

caused by processing and lack of consistency in mechanical testing techniques and samples (Suryanarayana, 1999).

In the field of CNTs reinforced aluminium matrix composites a big problem is constituted by the complexity of the interfacial reaction between CNTs and Al matrices, and lack of a suitable synthesis technique. In conventional carbon fibre/Al composites, aluminium carbide (Al_4C_3) grows on the prism plane of the carbon fibre. This reaction is serious due to the fact that growing Al_4C_3 needles result in a drastic decrease in the composites strength (Y. Zhou, Yang, Xia, & Mallick, 2003). In the CNT/Al system, an important issue of the chemical stability of the carbon nanotubes in the Al matrix is whether or not carbon nanotubes can be applied to the Al matrix as reinforcement. In general it is believed that under the proper processing condition the CNTs can be dispersed in the aluminium matrix and keep their good multiwalled structure and the properties of the aluminium matrix have been improved. Although the reaction product formed between carbon nanotubes and Al matrix is absent in CNT/Al composites (Kuzumaki et al., 1998; Noguchi et al., 2004; Zhong et al., 2003), Xu et al. reported some Al-carbide phases (an atomic ratio of Al:C = 1:1 or 1:2) in CNT/Al composites fabricated by hot pressing technique (C. L. Xu et al., 1999). However, Zhang et al. found that carbon nanotubes reacted with aluminium matrix and formed Al_4C_3 phases in CNT/Al composite when the composite was held at 800°C for 1 h (X.-X. Zhang, Deng, Wang, & Geng, 2005).

Other than the problems connected with dispersion of carbon nanotubes dispersion and with interfacial reaction and compatibility, CNTs-aluminium matrix composites are also affected by the choice of the proper production techniques, not also able to fulfil the dispersion and distribution requirements, but that also might provide a full densities of the material avoiding damages to the fillers. Several techniques have been experimented in last years, generally based on a pressure applied on powders in presence of an increased temperature. A very common approach is also to couple two or more techniques. The first carbon nanotube-aluminium composite fabrication was reported by Kuzumaki et al. (Kuzumaki et al., 1998). They used hot pressing and extrusion processes to produce aluminium with 10 vol% CNT as reinforcement. The final composites exhibit similar tensile strength as pure bulk aluminium (approximately 90 MPa) due to the poor dispersion of the CNTs. Esawi et al. fabricated an Al–CNT composite coupling planetary milling and rolling process. In that case the maximum obtained tensile strength of the pure aluminium in presence of 0.5, 1 and 2 wt% CNT composite was increased by 10% compared to that of pure bulk aluminium (Amal M.K. Esawi & El Borady, 2008). Esawi et al. also reported an approximately 50% increase in the tensile strength of the aluminium reinforced by 2 wt% CNTs prepared using the extrusion method (A.M.K. Esawi, Morsi, Sayed, Gawad, & Borah, 2009). Deng et al fabricated an alloy matrix with 2024Al with 1 wt% CNTs by mechanical milling and cold isotactic pressing. Specimens show about 35% increase in the tensile strength compared to the 2024Al alloy (C Deng, Zhang, Ma, et al., 2007; Chunfeng Deng,

Zhang, Wang, et al., 2007). Morsi et al. fabricated a pure aluminium matrix composite reinforced by 2.5 wt% CNT using their unique equipment for spark plasma extrusion (SPE), and they reported that this composite had a similar compressed strength value to that of the pure Al sample (Morsi, Esawi, Lanka, Sayed, & Taher, 2010; Morsi, Esawi, Borah, et al., 2010). A plasma spraying approach was experimented by Laha et al. to produce an Al–23 wt% silicon powder with 10 wt% CNT composite. They obtained a 78% improvement in the elastic modulus of the composite (Laha et al., 2009). Finally, another technique fully investigated is the spark plasma sintering (SPS). Kwon et al. demonstrated an approximately 400% increase in the tensile strength when the composites were fabricated coupling this sintering technique and hot extrusion processes on samples of pure aluminium reinforced by 1 and 5 vol% CNT (Hansang Kwon et al., 2009; Hansang Kwon, Park, Silvain, & Kawasaki, 2010).

2.3.3. CERAMIC MATRIX COMPOSITES

CNTs-reinforced ceramic matrix composites have become an intense field of research over the last decade (Zapata-Solvas, Gómez-García, & Domínguez-Rodríguez, 2012). CNTs have been used as reinforcement in a wide range of polycrystalline ceramic matrices, such as Al_2O_3 (J Sun, Gao, & Li, 2002), $MgAl_2O_4$ (Rul, Lefèvre-Schlick, Capria, Laurent, & Peigney, 2004), ZrO_2 (Shi & Liang, 2006), SiC (E T Thostenson, Karandikar, & Chou, 2005) and Si_3N_4 (Tatami, Katashima, Komeya, Meguro, & Wakihara, 2005). Among ceramics, Al_2O_3 is the most used for industrial applications due to its superior properties, such as hardness, chemical inertness and electrical/thermal insulation properties, which make alumina suitable for a wide range of applications, e.g. medical, aerospace and automotive industries. However brittle nature of Al_2O_3 is still a main issue (Ighodaro & Okoli, 2008).

Crucial conditions needed to obtain CNT-reinforced CMCs with superior mechanical properties and engineered electrical and thermal properties can be summarized as follows: (i) homogeneous dispersion of CNTs within the matrix ensuring the absence of CNTs agglomeration caused by van der Waals forces (J.-P. Salvetat et al., 1999) and intense entangling of CNTs throughout ceramic grains; (ii) avoiding damage of CNTs while processing, either during dispersion or consolidation; (iii) optimum bonding between CNTs and ceramic matrix interface with the aim of originating interfacial compatibility and strong adhesion. Gaining further control over challenging CNT-reinforced CMCs processing issues is a key to the future tailoring of physical properties, and is currently an active research field (Zapata-Solvas et al., 2012).

A range of dispersion techniques has been used with the aim of dispersing CNTs homogeneously inside the ceramic matrix, e.g. powder processing (Balázsi et al., 2005), colloidal processing (Poyato,

Vasiliev, Padture, Tanaka, & Nishimura, 2006), sol–gel processing (Mo, Cha, Kim, Lee, & Hong, 2005) and in situ growth of CNTs by catalytic chemical vapor decomposition (CCVD) (Flahaut et al., 2000). Consolidation of CNTs-reinforced CMCs has been carried out using pressureless sintering (S. C. Zhang, Fahrenholtz, Hilmas, & Yadlowsky, 2010), hot-isostatic pressing (HIP) (Balázsi et al., 2005), hot pressing (HP) (Flahaut et al., 2000) and spark plasma sintering (SPS) (Inam, Yan, Peijs, & Reece, 2010). However, pressureless sintering, HIP and HP might be avoided since large damages to CNTs during densification have been reported in multiple studies (Flahaut et al., 2000; Rul et al., 2004; Jing Sun & Gao, 2003). Thus, the critical processing

challenge for the fabrication of NT-CMCs is to minimize the reaction between the reinforcement and the matrix at the high temperatures required for ceramics processing. This challenge is similar to those encountered in the processing of traditional fibre-reinforced ceramic matrix composites except that the diameter of the reinforcement phase has changed from microns of traditional fibres (e.g. carbon and nicalon) to nanometres (E T Thostenson et al., 2005).

2.4. DISPERSION OF CARBON NANOTUBES

During last two decades many research efforts have been directed towards producing carbon nanotubes-based composites for functional and structural applications. However, even after a decade of research, the full potential of employing CNTs as reinforcements has been severely limited because of the difficulties associated with dispersion of entangled nanotubes during processing and poor interfacial interaction between CNTs and matrix materials. The dispersion problem for nanotubes is rather different from other conventional fillers, such as spherical particles and fibres, because CNTs exhibit small diameter in nanometre scale with high aspect ratio (>1000) and thus extremely large surface area. In addition, the dispersion states of carbon nanotubes involve complicated phenomena, since the carbon nanotubes are produced in bundles or bundle aggregations (P.-C. Ma, Siddiqui, et al., 2010; Xie, Mai, & Zhou, 2005). The states are affected by at least two competitive interactions: 1) the interactions of Van der Waals forces, among carbon nanotube threads; 2) the interactions between carbon nanotube threads and dispersion medium (J. N. Coleman, Khan, & Gun'ko, 2006; Erik T Thostenson et al., 2001). The characteristics of single carbon nanotube and of bundles of carbon nanotubes are completely different. CNTs must be uniformly dispersed to the level of isolated nanotubes individually wetted by the matrix. This is necessary in order to achieve efficient load transfer to the nanotubes network. This also results in a more uniform stress distribution and minimises the presence of stress concentration centres.

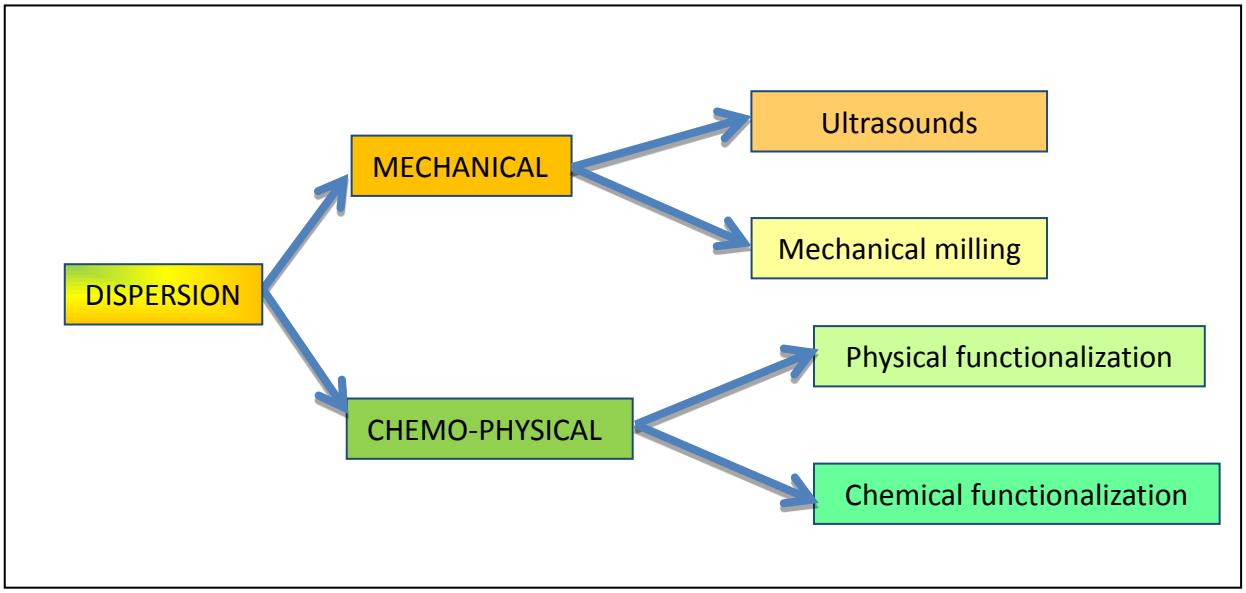

Figure 21 - Schematic resume of the principal dispersion approaches for CNTs

Several dispersion approaches have been proposed by numerous researchers. They are based on two different concepts: mechanical dispersion and chemo-physical dispersion (Figure 21). The former is based on the utilization of various techniques able to disperse CNTs right in a solvent or in a matrix, as ultrasound sonication or mechanical milling. The latter is based on the creation of a bond (of various strengths) between CNTs surfaces and a chemical agent. We can distinguish two kinds of approaches: a physical functionalization, based on low energy bonding with species as surfactants, and an actual chemical functionalization.

2.4.1. MECHANICAL DISPERSION

- **Ultrasonication**

Ultrasonication is an effective method to disperse CNTs in liquids having a low viscosity. It is a common tool usedto break up CNT agglomerates in solution based processing techniques but it could be used effectively also in presence of polymers, surfactants, acids and other compounds. For this reason is commonly used in conjunction with other dispersion techniques (Krause, Mende, Pötschke, & Petzold, 2010; H. Li, Nie, & Kunsági-Máté, 2010; Sato & Sano, 2008; Tang et al., 2011; X. Xu & Wang, 2012). Ultrasonication can be performed by different ways: using either an ultrasonic bath or an ultrasonic sonotrode (generally called probe or horn sonicators). Standard laboratory bath sonicators run at 20-23 kHz with a power less than 100 W. Commercial probe sonicators have adjustable amplitude, ranging from 20% to 70%, and a power of 100–1500 W. The probe is usually made of an inert metal such as titanium and the tips are exchangeable and with diameters between 1.6 and 12.7 mm. This tip oscillates at a fixed frequency and produces a conical field of high energy in the fluid. The solvent within this conical field undergoes nucleated boiling and bubble collapse. This phenomenon, known as cavitation, is the fundamental mechanism by which ultrasonic energy disperses particles (Hilding, Grulke, George Zhang, & Lockwood, 2003). This may help to debundle nanotubes by providing high local shear. However, the high energy produced by the sonicator and focused on the tip can generate substantial heat rapidly (causing problem in presence of volatile solvents) and CNTs can be easily and seriously damaged, especially when a probe sonicator is employed. The Raman spectroscopy (Figure 22) confirmed that ultrasonication of CNTs for a long time resulted in a significant increase in the intensity of D band (representing disordered sp^3 carbon on CNTs), suggesting the generation of defects on CNT surface. In extreme cases, the graphene layers of CNTs are completely destroyed and the nanotubes are converted into amorphous carbon nanofibers (Figure 23) (Lu, 1996). The damage to the carbon nanotubes clearly affected the electrical and mechanical properties and negatively influenced the final composites. The samples should be kept cold and the sonication must be performed for short times.

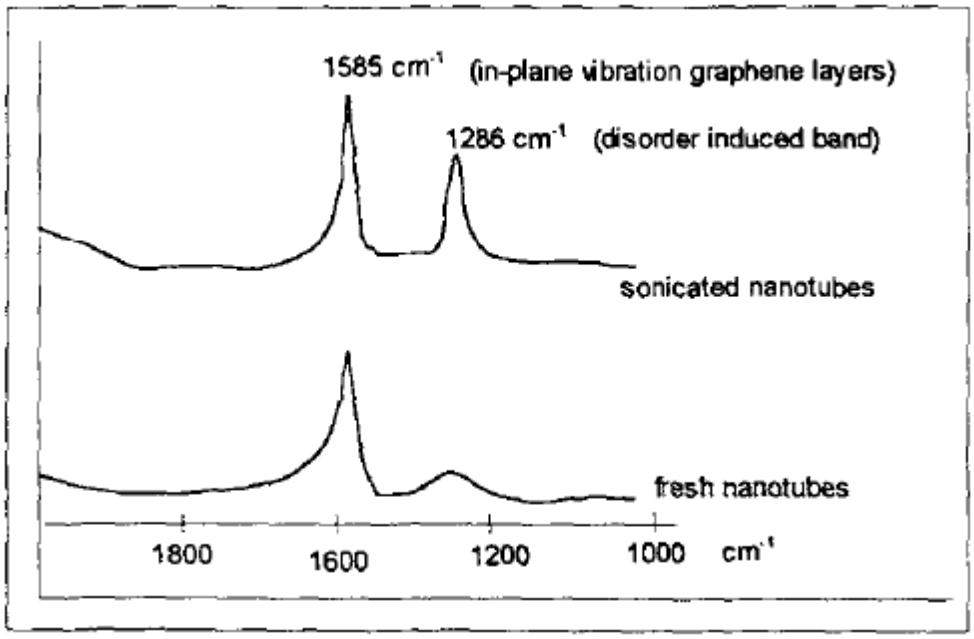

Figure 22 - Raman spectra of fresh and sonicated nanotubes (Lu, 1996)

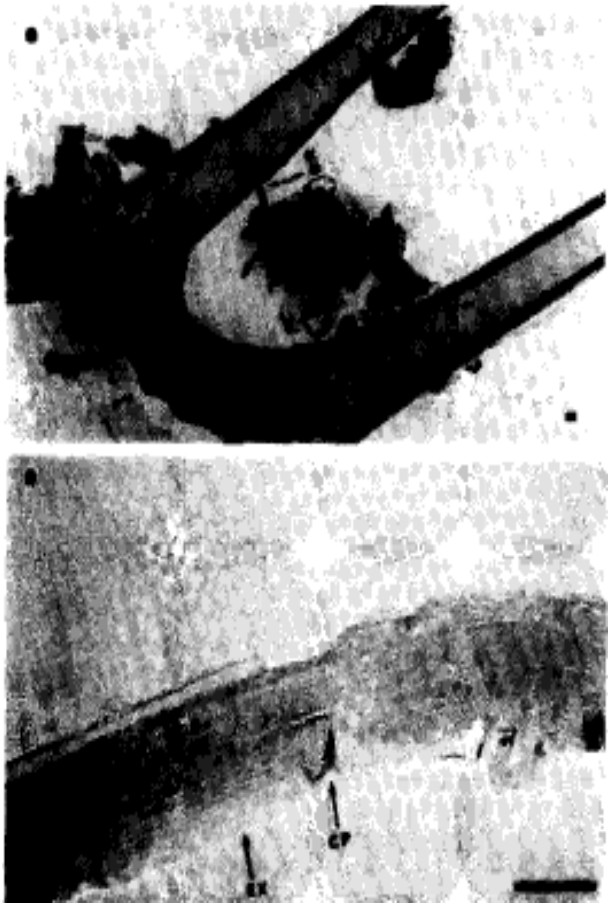

Figure 23 - Images of damaged carbon nanotubes after sonication (Lu, 1996)

- **Calendering**

The use of a three roll machine has recently provided good results for nano-reinforcement dispersion. The calender, or commonly known as three roll mills, is a machine tool that employs the force created by rollers to mix, disperse or homogenize viscous materials. The dispersion method exploits shear forces avoiding the presence of compression forces during the process and providing the dispersion of the carbon nanotubes without damages. A calendering machine consists of three adjacent cylindrical rollers running at different velocities (Figure 24). The first and third rollers, called the feeding and apron rollers, rotate in the same direction while the centre roller rotates in the opposite direction. The material is introduced in the system by a hopper directly between the feed and centre rollers. The material is then transported by the second roller it into the second gap. Here the filler is dispersed. Upon exiting, the material that remains on the centre roller moves through the second nip between the centre roller and apron roller, which subjects it to even higher shear force due to the higher speed of the apron roller. This milling cycle can be repeated several times to ensure the desired dispersion degree.

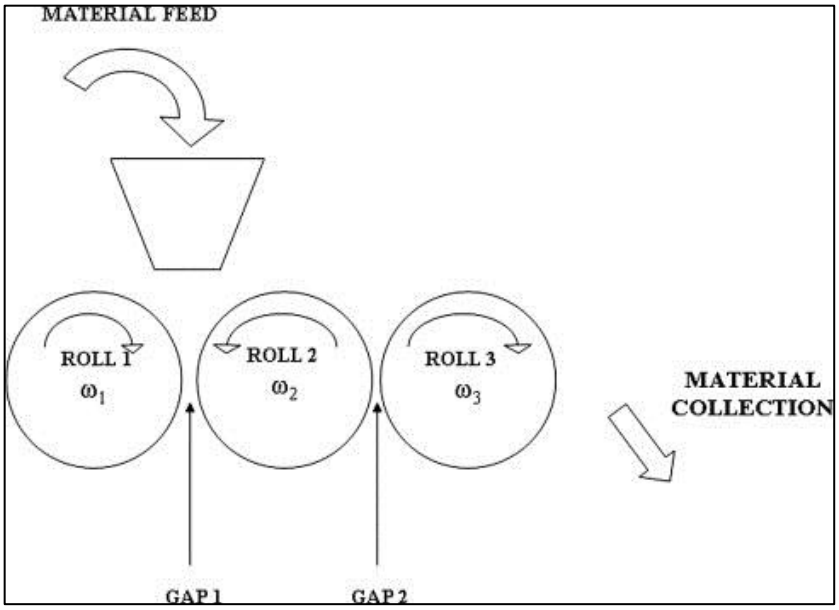

Figure 24 - Schematic of the three roll mill machine used for the calendering process (Jiménez-Suárez, Campo, Sánchez, Romón, & Ureña, 2012)

The employment of calendering to disperse CNTs in a polymer matrix has become a very promising approach to achieve a relatively good carbon nanotubes distribution and dispersion (Gojny et al., 2004; Sánchez, Campo, Jiménez-Suárez, & Ureña, 2012; E. Thostenson & Chou, 2006). However, there are several problems in using this technique: for example, despite of the unique advantage of calendaring to move the rollers and adjust their gap width, the minimum gap is about 1–5 μm, which is larger than the typical dimension of single nanotubes. Due to these characteristics calendaring can

better disperse the large agglomerated bundles of CNTs into small ones than dispersed them individually. In addition, the feeding materials should be in the viscous state thus this technique could not be used in presence of thermoplastic matrices.

- **Ball milling**

Mechanical milling, or mechanical grinding, is a common process to reduce the physical size of particles to extremely fine powder level. In ball milling, work materials are placed together with some milling balls in a proper container. The sample materials and the balls, also known as charge materials, are then moved upon the motion of the vial itself. Subsequently, the collision will create impact between the balls and a high pressure is generated locally. This generated energy is high enough to generate crack propagation and fracture leading to the breakage of the samples into smaller sizes (Budin, Almanar, Kamaruddin, Maideen, & Zulkifli, 2009). The higher the impact energy, the smaller the fragments produced. The typical motion of balls inside the container is shown in Figure 25. Different materials, including ceramic, flint pebbles and stainless steel, are used as balls.

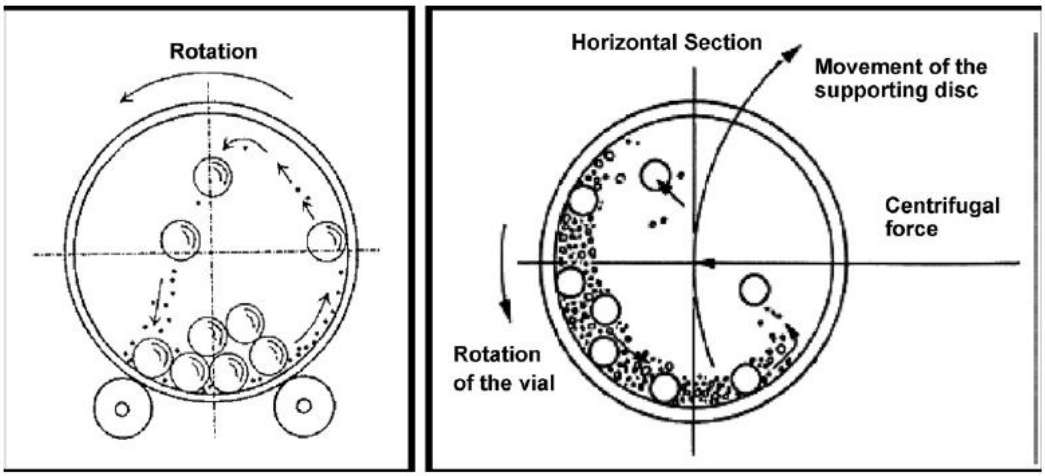

Figure 25 – Schematic representation of the balls motion during the milling process. On the left: vertical configuration (conventional ball mill). On the right: horizontal configuration (planetary ball mill) (Suryanarayana, 2001)

Ball milling has been used for a variety of applications related to carbon nanotubes: it has been used to obtain CNTs nanoparticles (Y. B. Li, Wei, Liang, Yu, & Wu, 1999), to enhance the saturation of lithium composition in SWCNTs (Gao et al., 2000), to modify the morphologies of cup-stacked CNTs (Y. A. Kim, Hayashi, Fukai, Endo, & Dresselhaus, 2002). Also chemo-mechanical reaction could be realised: ball milling of carbon nanotubes and chemical scan introduces some functional groups onto the CNT surface. For example in situ amino functionalization of CNTs using ball milling has been achieved (Singhal, Srivastava, Pasricha, & Mathur, 2011). Although this mechanical technique could be successfully used for several materials, one of the main applications of ball milling remains the

grinding of metal particles and carbon nanotubes to form composite powders. The mechanical alloying is used mainly for pure aluminium and aluminium alloys matrices (Choi, Shin, & Bae, 2012; a Esawi & Morsi, 2007; Liao & Tan, 2011; Z. Y. Liu et al., 2012; Pérez-Bustamante et al., 2012; Wu, Kim, & Russell, 2011).

Different kind of milling could be used on the basis of the material and of the purpose of the process. High energy milling (HEM) has high impact velocities and high impact frequencies of the grinding media. Due to the high energies reached during the milling mechanical alloying and very small particles size could be obtained and the process times are shortened. HEM, however, inevitably damages the CNTs, which is detrimental to the final composite mechanical properties (Darsono, 2008; A.M.K. Esawi et al., 2009; Liao & Tan, 2011). To prevent great damages to the material also a simple ball milling at lower energies could be led (Liao & Tan, 2011) or also alternative e more particular approaches as bead milling (Yoshio et al., 2011).

- **Other mechanical dispersion techniques**

With the aim of obtain a good dispersion of the carbon nanotubes inside a matrix also several less common techniques have been experimented.

For MMCs **friction stir processing** (FSP) has been tested. FSP is a solid-state joining and microstructural modification process (D. K. Lim, Shibayanagi, & Gerlich, 2009; Mishra & Ma, 2005), where a rotating tool pin is plunged into the surface of the metals to be processed and traversed along its surface. The friction and plastic deformation imposed by the tool heats and softens the specimen, and the tool pin caused intermixing of material in a local region. When reinforcing particles are introduced into the material they are dispersed by the tool (Mishra, Ma, & Charit, 2003). The main advantage of FSP is that it does not require multiple processing steps, rely on precursor metal powders, or involve melting. Moreover it can also refine the grain size in the metal matrix (Morisada, Fujii, Nagaoka, & Fukusumi, 2006).

Stir is a common technique to disperse particles in liquid systems and for this reason is commonly used to disperse carbon nanotubes in PMCs. After intensive stirring of CNTs in polymer matrix, a relatively fine dispersion can be achieved (Sandler et al., 1999), however, MWCNTs can be dispersed more easily than SWCNTs. This empirically observed event is mainly caused by frictional contacts and elastic interlocking mechanisms (Schmid & Klingenberg, 2000).

Extrusion is a popular technique to disperse CNTs into polymers (Benedito, Buezas, Gime, & Eiffel, 2011; Potschke, 2004; Villmow, Pötschke, Pegel, Häussler, & Kretzschmar, 2008) but also into metals

(H Kwon et al., 2009; Paramsothy, Chan, Kwok, & Gupta, 2011; Pérez-Bustamante et al., 2011). Pellets or powders of the matrix materials are mixed with the filler and are fed into the extruder hopper. Generally the instrument is characterized by twin screws that can rotate at a high speed, generating a high shear flow. This technique is particularly useful to produce carbon nanotubes composites with a high filler content.

Is very important to consider that, in order to overcome the problem associated with carbon nanotubes dispersion, many of the recent studies are based on the coupling of two or more mentioned technique.

2.4.2. CHEMO-PHYSICAL DISPERSION

As previously anticipated the performance of a CNT nanocomposite depends on the dispersion of CNTs in the matrix and interfacial interactions between the tubes and the surrounding material. Nevertheless, the carbon atoms on nanotubes walls are chemically stable because of the aromatic nature of the bond. Indeed, pristine CNT are insoluble in all organic solvents and aqueous solutions. They can be dispersed in some solvents by several techniques, e.g. sonication, but precipitation immediately occurs when the mechanical process is stopped. Their unwettability makes difficult to use them as fillers in composites and also complicates their chemical characterization. Despite that, carbon nanotubes can react with different classes of compounds (Balasubramanian & Burghard, 2005; Hirsch, Vostrowsky, Chemie, & Erlangen-nürnberg, 2005; Hirsch, 2002; Tasis, Tagmatarchis, Bianco, & Prato, 2006). A suitable functionalization of the nanotubes and the attachment of "chemical functionalities" is a good strategy to overcome these problems: functionalization can improve solubility, compatibility and processability, and allows the researchers to take advantage of the unique properties of nanotubes and of their new functional groups.

The main approaches for the functionalization of CNTs can be grouped into three categories:

- covalent functionalization, in which of chemical functional groups are attached to the carbon atoms of the tubes;
- non-covalent adsorption or wrapping of various macromolecules;
- the endohedral filling of their inner empty cavity. This approach has been extensively investigated for particular application as nanowires production or for efficient storage of liquid fuels. It was stated that any liquid having a surface tension below ~180 $mM \bullet m^{-1}$ could wet the inner cavity of tubes through an open end in atmospheric pressure (Gooding et al., 2003). In the case of high surface tension, a highly pressurized liquid must be used to force it

to enter inside the cavity. Since this particular approach is less common and less inherent with the present thesis work so it will not be investigated deeply.

2.4.2.1. COVALENT FUNCTIONALIZATION

A major milestone in the of nanotube chemistry was the development of an oxidation process involving ultrasonication of SWCNTs in concentrated nitric and sulfuric acids (J. Chen et al., 1998). Such drastic treatment can cause great damages to the nanotubes, e.g. opening of the tube caps, oxidative etching of the walls, shortening of the tubes up to obtain fragments with lengths in the range of 100 to 300 nm. Therefore it is obviously very important to keep the condition controlled. For example, using refluxing in nitric acid for the treatment of the CNTs, the shortening can be minimized. In this case the chemical modification is generally limited to the opening of the tube caps and the formation of functional groups at defect sites along the sidewalls. CNTs functionalized this way maintain their pristine electronic and mechanical properties (Jin Zhang et al., 2003). The oxidative treatment is always necessary before the actual functionalization reactions and it can be performed using several oxidants: nitric acid (Erik Dujardin, Ebbesen, Krishnan, & Treacy, 1998; M Holzinger, Hirsch, Bernier, Duesberg, & Burghard, 2000; Nagasawa, Yudasaka, Hirahara, Ichihashi, & Iijima, 2000; Rinzler et al., 1998; Vaccarini et al., 1999), sulfuric acid (Sumanasekera et al., 1999) or mixtures of both (Rinzler et al., 1998), “piranha” (sulfuric acid–hydrogen peroxide)(J. Liu et al., 1998) or gaseous oxygen (Morishita & Takarada, 1994; Tohji et al., 1996), ozone (J.-P. Deng, Mou, & Han, 1997; Mawhinney & Naumenko, 2000; Mawhinney, 2000) or air as oxidant (Ajayan & Iijima, 1993; Colomer et al., 1998; Ugarte, Chatelain, & De Heer Wa, 1996) at elevated temperatures, or combinations of nitric acid and air oxidation (Dillon et al., 1997). The introduction of carboxylic groups to nanotubes by oxidative procedures gives access to a large number of functionalizations by transformation of the carboxylic functions, and provides anchor groups for further modification. By this method the nanotubes can be provided with a wide range of functional moieties. The presence of (modified) carboxyl groups leads to a reduction of Van der Waals forces between the CNTs, and consequently an easier separation of nanotube bundles. Moreover, the attachment of suitable groups could modify the tubes solubility in aqueous or organic solvents, opening the possibility of further modifications through subsequent solution-based chemistry.

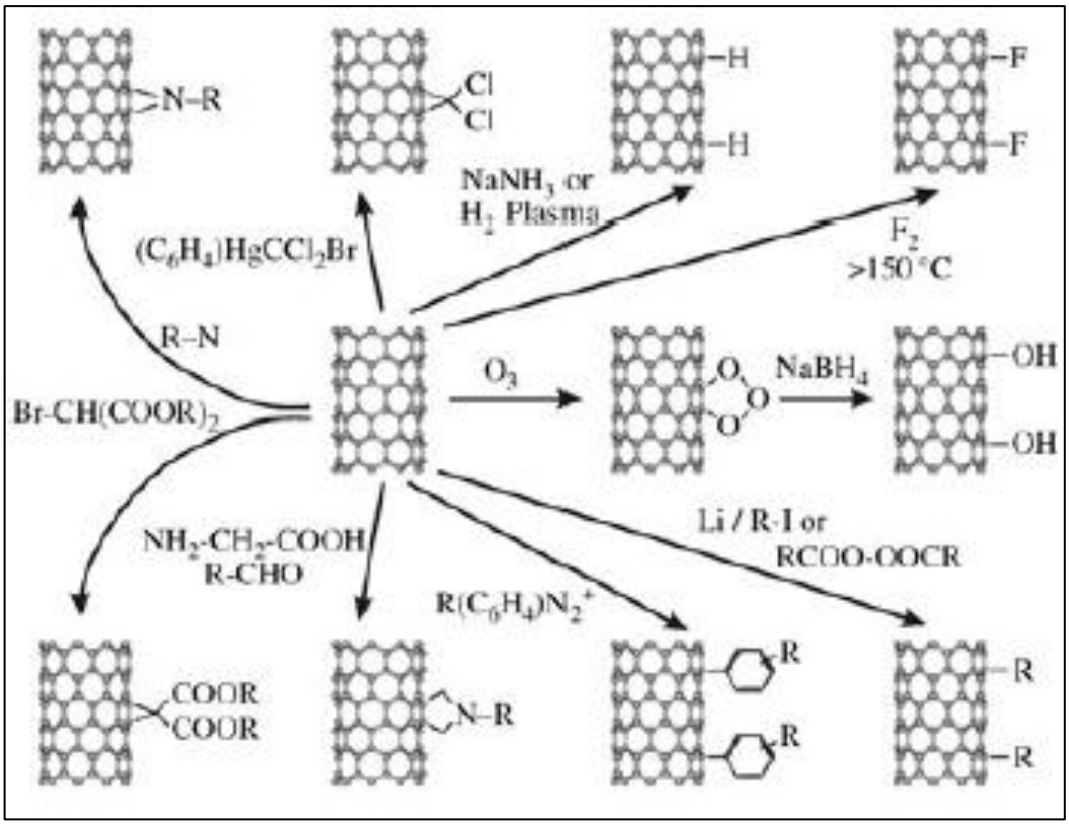

Figure 26 - Overview of possible addition reactions for the functionalization of the nanotubes sidewalls (Balasubramanian & Burghard, 2005)

Several functionalization have been experimented in last years, on the basis of the future applications of the modified CNTs: amidation (in which the carboxylic groups can be activated by conversion into acyl chloride groups with thionyl chloride (J. Chen et al., 1998; J. Liu et al., 1998), and the acyl chlorides formed can be transformed to carboxamides by amidation), esterification (acyl-chloride-functionalized CNTs could also react with nucleophile alcoholic groups (Hamon, Hui, Bhowmik, Itkis, & Haddon, 2002; Riggs, Guo, Carroll, & Sun, 2000)), thiolation (a particular reaction involving successive carboxylation (H_2SO_4/HNO_3; H_2O_2/H_2SO_4; sonication), reduction ($NaBH_4$), chlorination ($SOCl_2$) and thiolation ($Na_2S/NaOH$), to the open ends of CNTs (J. Lim, 2003)), fluorination (a complex reaction obtained using several approaches (Hamwi, 1997; Marcoux et al., 2002; Mickelson et al., 1998)), chlorination (Fagan, Da Silva, Mota, Baierle, & Fazzio, 2003), hydrogenation (obtained using different approaches as via dissolved metal reduction (Y. Chen et al., 1998), or electrochemical hydrogenation of open ended CNTs (Owens & Iqbal, 2002)), addition of radicals (e.g. the addition of perfluorinated alkyl radicals ,obtained by photoinduction from heptadecafluoro octyl iodide, to SWCNTs yielded perfluorooctyl-derivatized CNTs (Michael Holzinger et al., 2001), pristine SWCNTs and their fluorinated derivatives, F-SWCNTs, were reacted with organic peroxides to functionalize them by covalent sidewall attachment of free radicals (Peng, Reverdy, Khabashesku, & Margrave, 2003)) addition of nucleophilic carbenes (e.g. The reaction of a

nucleophilic dipyridyl imidazolidene with the electrophilic SWCNT p-system to give zwitterionic polyadducts (Michael Holzinger et al., 2001)) or the sidewall functionalization through electrophilic addition (Tagmatarchis, Georgakilas, Prato, & Shinohara, 2002). However, many other reactions have been attempted by several researchers (the main ones reported in the diagram in Figure 26).

2.4.2.2. PHYSICAL OR NON-COVALENT FUNCTIONALIZATION

Functionalization of CNTs using covalent method can provide useful functional groups onto the carbon nanotubes surface. Nevertheless, this kind of approach has two major drawbacks: firstly, during the functionalization reaction, especially if long ultrasonication steps are required, a large number of defects are inevitably created on the nanotubes sidewalls, and as anticipated in section 2.4.2.1, CNTs in some cases should be shortened into smaller pieces. These damages result in degradation in mechanical properties of carbon nanotubes as well as disruption of their p electron system, with severe consequences on electrical and thermal properties. Secondly, these chemical reactions often involve concentrated acids or strong oxidants, and so they are environmentally unfriendly. Hence, many efforts have been put forward to developing methods that are convenient to use, of low cost and less damage to CNT structure. Non-covalent functionalization is an alternative method for tuning the interfacial properties of nanotubes. Three main kind of physical functionalization have been studied: the first one is the so called polymer wrapping (Figure 27).

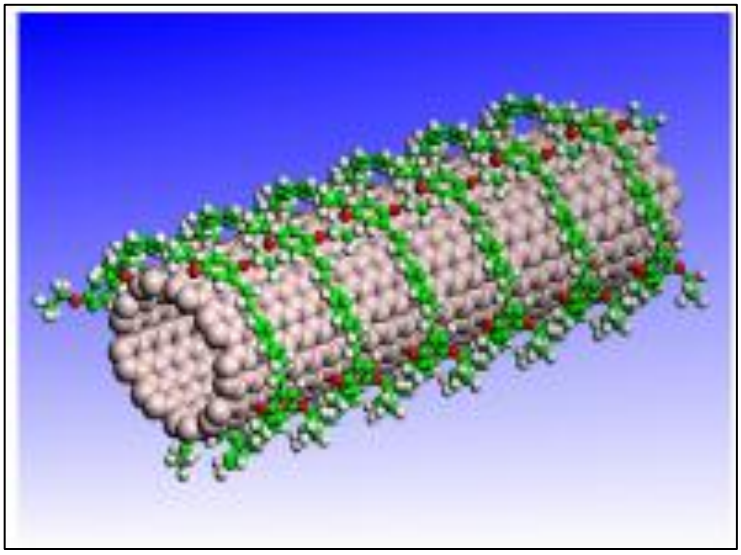

Figure 27 - Model of polymer wrapping

The suspension of CNTs in the presence of polymers, such as poly(phenylenevinylene) (Mc Carthy et al., 2001) or polystyrene (Hill et al., 2002), lead to the wrapping of polymer around the tubes to form

supermolecular complexes of CNTs. The polymer wrapping process is achieved through the van der Waals interactions and p–p stacking between CNTs and polymer chains containing aromatic rings. The second non-covalent approach is based on the use of surfactants (Figure 28). Several studies have been conducting on the effects of surfactant on dispersability and other property of CNTs (Cui, Canet, Derre, Couzi, & Delhaes, 2003; Geng, Liu, Li, Shi, & Kim, 2008; Gong, Liu, Baskaran, Voise, & Young, 2000; Grossiord et al., 2006; Islam, Rojas, Bergey, Johnson, & Yodh, 2003; T.-H. Kim, Doe, Kline, & Choi, 2007; L Vaisman, Marom, & Wagner, 2006; Linda Vaisman, Wagner, & Marom, 2006; Whitsitt & Barron, 2003; J. Yu, Grossiord, Koning, & Loos, 2007). The surfactants studied could be divided in three categories: non-ionic surfactants, such as polyoxyethylene-8-lauryl (Gong et al., 2000), nonylphenolethoxylate (Tergitol NP-7)(Cui et al., 2003), polyoxyethyleneoctylphenylether (Triton X-100) (Geng et al., 2008; L Vaisman et al., 2006); anionic surfactants, such as sodium dodecylsulfate (SDS), sodium dodecyl benzenesulfonate (SDBS), poly(styrene sulfate) (PSS) (Islam et al., 2003; Strano et al., 2003; J. Yu et al., 2007); cationic surfactants, such as dodecyl trimethyl ammonium bromide (DTAB) (Whitsitt & Barron, 2003), cetyl trimethyl ammonium 4-vinylbenzoate (CTVB) (T.-H. Kim et al., 2007). The physical adsorption of surfactant on the carbon nanotube surface lowered the surface tension of CNT, effectively preventing the formation of aggregates. Furthermore, the surfactant-treated CNTs overcome the Van der Waals attraction by electrostatic/steric repulsive forces.

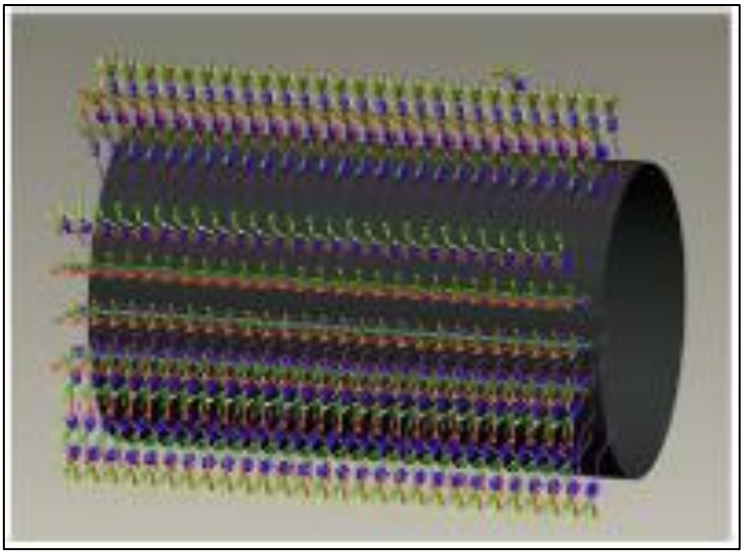

Figure 28 - Model of surfactant-functionalization

The efficiency of this method depended strongly on the properties of surfactants, medium chemistry and matrix. The disadvantage of this physical functionalization is that, because of the extremely high surface area of the carbon nanotubes, to obtain a good dispersion of the tubes a very large amount

of surfactant is required. The third method is the endohedral method (Figure 29), described in section 2.4.2.

Figure 29 - Model of endohedral method

Afterwards the searching for a way to disperse CNTs another important question is to consider: the dispersion evaluation. This is a big problem due to the dimensions, chemical and physical nature of carbon nanotubes. Several techniques are used but many issues remain unsolved with respect to the establishment of a straightforward, yet reliable method for the analysis of CNT dispersions, in particular one that can establish whether the CNTs are in fact well separated. Two kind of analysis approach are generally adopted: a direct method including morphological analysis, and an indirect method including rheological (Battisti, Skordos, & Partridge, 2009; Charman, Léonardi, Dominguez, Bissuel, & Derail, 2011; Kasaliwal, Göldel, Pötschke, & Heinrich, 2011; Semaan & Soum, 2012; Song & Youn, 2005; Sul, Youn, & Song, 2011), mechanical (Breton et al., 2004; Choi et al., 2012; a. M. K. Esawi, Morsi, Sayed, Taher, & Lanka, 2010; Kosmidou, 2008; L. Liu & Wagner, 2005; Z. Y. Liu et al., 2012; P. C. Ma et al., 2007), electrical (Chapartegui et al., 2010; Charman et al., 2011; Kosmidou, 2008; Lisetski, Minenko, Fedoryako, & Lebovka, 2009; Moisala et al., 2006) and thermal analyses (Fujigaya, Fukumaru, & Nakashima, 2009; Hong, Lee, Hong, & Shim, 2010; P. C. Ma et al., 2007; Moisala et al., 2006; Pöllänen, Pirinen, Suvanto, & Pakkanen, 2011; S. Wang, Liang, Wang, & Zhang, 2009). Direct observations are commonly performed using scanning electron microscopy (SEM) (J. Chen, Xue, Ramasubramaniam, & Liu, 2006; Jun, Jin, Park, Jeon, & Hong, 2012; C.-D. Liu et al., 2010; Loos, Grossiord, Koning, & Regev, 2007; Madni, Hwang, Park, Choa, & Kim, 2010; Schlea et al., 2010) or transmission electron microscopy (TEM)(Y. Kim, Kwon, Kim, Kim, & Jin, 2009; Mc Carthy et al., 2001; Oh, Jung, Lee, & Chang, 2010; Rastogi et al., 2008; Schwyzer, Kaegi, Sigg, Magrez, & Nowack, 2011; Jing Zhang & Gao, 2007), but also less common emerging techniques have been introduces in last years, e.g. atomic force microscopy (AFM) (Blanch, Lenehan, & Quinton, 2011; Foster, Singamaneni, Kattumenu, & Bliznyuk, 2005; Garate, Fascio, Mondragon, D'Accorso, & Goyanes, 2011; Potschke, 2004; Ryszkowska, Jurczykkowalska, Szymborski, & Kurzydlowski, 2007; Linda Vaisman et al., 2006). Also some kind of spectroscopy could be used, as UV-vis (Bai et al., 2011; Dong et al.,

2011; Ham, Choi, & Chung, 2005; Rastogi et al., 2008; Schwyzer et al., 2011) or light scattering (Jung et al., 2012; Y. Kim et al., 2009; Krause et al., 2010; Ntim, Sae-Khow, Witzmann, & Mitra, 2011; J. Wang, Früchtl, & Blau, 2010)) but only at very low CNTs concentrations and often coupled with microscopy.

REFERENCES

Ajayan, P. M., & Iijima, S. (1993). Capillarity-induced filling of carbon nanotubes. *Nature*, *361*(6410), 333–334. doi:10.1038/361333a0

Ajayan, P. M., Stephan, O., Colliex, C., & Trauth, D. (1994). Aligned carbon nanotube arrays formed by cutting a polymer resin--nanotube composite. *Science*, *265*(5176), 1212–1214.

Akbulut, H., Durmam, M., & Yilmaz, F. (1998). Dry wear and friction properties of alpha -Al2O3 short fiber reinforced Al-Si (LM 13) alloy metal matrix composites. *Wear*, *215*, 170–179.

Ando, Y. (1994). The Preparation of Carbon Nanotubes. *Fullerene Science and Technology*, *2*(2), 173–180. doi:10.1080/15363839408009542

Ando, Yoshinori, Zhao, X., Sugai, T., & Kumar, M. (2004). Growing carbon nanotubes. *Materials Today*, 22–29.

Andrews, R., Jacques, D., Minot, M., & Rantell, T. (2002). Fabrication of Carbon Multiwall Nanotube/Polymer Composites by Shear Mixing. *Macromolecular Materials and Engineering*, *287*(6), 395. doi:10.1002/1439-2054(20020601)287:6<395::AID-MAME395>3.0.CO;2-S

Andriotis, A. N., Menon, M., & Froudakis, G. E. (2000). Various bonding configurations of transition-metal atoms on carbon nanotubes: Their effect on contact resistance. *Applied Physics Letters*, *76*(26), 3890–3892. doi:10.1063/1.126811

Antes, H. (2003). Fundamental solution and integral equations for Timoshenko beams. *Computers & Structures*, *81*(6), 383–396. doi:10.1016/S0045-7949(02)00452-2

Arroyo, M., & Belytschko, T. (2002). An atomistic-based finite deformation membrane for single layer crystalline films. *Journal of the Mechanics and Physics of Solids*, *50*, 1941–1977.

Avigal, Y., & Kalish, R. (2001). Growth of aligned carbon nanotubes by biasing during growth. *Applied Physics Letters*, *78*(16), 2291. doi:10.1063/1.1365409

Bacon, R. (1960). Growth, Structure, and Properties of Graphite Whiskers. *Journal of Applied Physics*, *31*(2), 283. doi:10.1063/1.1735559

Bacsa, R. R., Laurent, C., Peigney, A., Bacsa, W. S., Vaugien, T., & Rousset, A. (2000). High specific surface area carbon nanotubes from catalytic chemical vapor deposition process. *Chemical Physics Letters*, *323*(June), 566–571.

Bai, Y., Park, I. S., Lee, S. J., Bae, T. S., Watari, F., Uo, M., & Lee, M. H. (2011). Aqueous dispersion of surfactant-modified multiwalled carbon nanotubes and their application as an antibacterial agent. *Carbon*, *49*(11), 3663–3671. doi:10.1016/j.carbon.2011.05.002

Bakshi, S. R., Lahiri, D., & Agarwal, a. (2010). Carbon nanotube reinforced metal matrix composites - a review. *International Materials Reviews*, *55*(1), 41–64. doi:10.1179/095066009X12572530170543

Balasubramanian, K., & Burghard, M. (2005). Chemically functionalized carbon nanotubes. *Small (Weinheim an der Bergstrasse, Germany)*, *1*(2), 180–92. doi:10.1002/smll.200400118

Balázsi, C., Shen, Z., Kónya, Z., Kasztovszky, Z., Wéber, F., Vértesy, Z., Biró, L. P., et al. (2005). Processing of carbon nanotube reinforced silicon nitride composites by spark plasma sintering. *Composites Science and Technology*, *65*(5 SPEC. ISS.), 727–733.

Bandow, S., Asaka, S., Saito, Y., Rao, a., Grigorian, L., Richter, E., & Eklund, P. (1998). Effect of the Growth Temperature on the Diameter Distribution and Chirality of Single-Wall Carbon Nanotubes. *Physical Review Letters*, *80*(17), 3779–3782. doi:10.1103/PhysRevLett.80.3779

Battisti, a., Skordos, a. a., & Partridge, I. K. (2009). Monitoring dispersion of carbon nanotubes in a thermosetting polyester resin. *Composites Science and Technology*, *69*(10), 1516–1520. doi:10.1016/j.compscitech.2008.05.012

Belytschko, T., Xiao, S., Schatz, G., & Ruoff, R. (2002). Atomistic simulations of nanotube fracture. *Physical Review B*, *65*(23), 1–8. doi:10.1103/PhysRevB.65.235430

Benedito, A., Buezas, I., Gime, E., & Eiffel, C. G. (2011). Dispersion and Characterization of Thermoplastic Polyurethane / Multiwalled Carbon Nanotubes by Melt Mixing. *Polymer*, 14–16. doi:10.1002/app

Berns, H. (2003). Comparison of wear resistant MMC and white cast iron. *Wear*, *254*(May 2002), 47–54.

Bethune, D. S., Klang, C. H., De Vries, M. S., Gorman, G., Savoy, R., Vazquez, J., & Beyers, R. (1993). Cobalt-catalysed growth of carbon nanotubes with single-atomic-layer walls. *Nature*, *363*(6430), 605–607. doi:10.1038/363605a0

Bian, B. Z., Wang, R. J., Wang, W. H., Zhang, T., & Inoue, A. (2004). Carbon-nanotube-reinforced Zr-based bulk metallic glass composites and their properties. *Advanced Functional Materials*, *14*(1), 55–63. doi:10.1002/adfm.200304422

Bian, Z., Pan, M. X., Zhang, Y., & Wang, W. H. (2002). Carbon-nanotube-reinforced Zr[sub 52.5]Cu[sub 17.9]Ni[sub 14.6]Al[sub 10]Ti[sub 5] bulk metallic glass composites. *Applied Physics Letters*, *81*(25), 4739. doi:10.1063/1.1530371

Blackwood, D. J., Chua, a. W. C., Seah, K. H. W., Thampuran, R., & Teoh, S. H. (2000). Corrosion behaviour of porous titanium–graphite composites designed for surgical implants. *Corrosion Science*, *42*(3), 481–503. doi:10.1016/S0010-938X(99)00103-1

Blanch, A. J., Lenehan, C. E., & Quinton, J. S. (2011). Parametric analysis of sonication and centrifugation variables for dispersion of single walled carbon nanotubes in aqueous solutions of sodium dodecylbenzene sulfonate. *Carbon*, 1–16. doi:10.1016/j.carbon.2011.07.039

Breton, Y., Desarmot, G., Salvetat, J., Delpeux, S., Sinturel, C., Beguin, F., & Bonnamy, S. (2004). Mechanical properties of multiwall carbon nanotubes/epoxy composites: influence of network morphology. *Carbon*, *42*(5-6), 1027–1030. doi:10.1016/j.carbon.2003.12.026

Breval, E. (1995). Synthesis routes to metal matrix composites with specific properties: A review. *Composites Engineering*, *5*(9), 1127–1133. doi:10.1016/0961-9526(95)00048-R

Budin, S., Almanar, I. P., Kamaruddin, S., Maideen, N. C., & Zulkifli, A. H. (2009). Modeling of vial and ball motions for an effective mechanical milling process. *Journal of Materials Processing Technology*, *209*(9), 4312–4319. doi:10.1016/j.jmatprotec.2008.11.016

Bundy, F. P. (1996). The pressure-temperature phase and transformation diagram for carbon; updated through 1994. *Carbon*, *34*(2), 141–153. doi:10.1016/0008-6223(96)00170-4

Buongiorno Nardelli, M., Yakobson, B., & Bernholc, J. (1998). Mechanism of strain release in carbon nanotubes. *Physical Review B*, *57*(8), R4277–R4280. doi:10.1103/PhysRevB.57.R4277

Callister, W. D. (2007). *Materials Science and Engineering: An Introduction*. (D. G. Rethwisch, Ed.)*Transport* (Vol. 6, p. 832). John Wiley & Sons, Inc. doi:10.1126/science.1213003

Carre�o-Morelli, E., Yang, J., Couteau, E., Hernadi, K., Seo, J. W., Bonjour, C., Forr�, L., et al. (2004). Carbon nanotube/magnesium composites. *Physica Status Solidi (a)*, *201*(8), R53–R55. doi:10.1002/pssa.200409045

Cassell, A. M., Raymakers, J. A., Kong, J., & Dai, H. (1999). Large Scale CVD Synthesis of Single-Walled Carbon Nanotubes. *The Journal of Physical Chemistry B*, *103*(31), 6484–6492. doi:10.1021/jp990957s

Cha, S. I., Kim, K. T., Arshad, S. N., Mo, C. B., & Hong, S. H. (2005). Extraordinary Strengthening Effect of Carbon Nanotubes in Metal-Matrix Nanocomposites Processed by Molecular-Level Mixing. *Advanced Materials*, *17*(11), 1377–1381. doi:10.1002/adma.200401933

Chapartegui, M., Markaide, N., Florez, S., Elizetxea, C., Fernandez, M., & Santamaría, a. (2010). Specific rheological and electrical features of carbon nanotube dispersions in an epoxy matrix. *Composites Science and Technology*, *70*(5), 879–884. doi:10.1016/j.compscitech.2010.02.008

Charman, M., Léonardi, F., Dominguez, S., Bissuel, C., & Derail, C. (2011). Dispersion of multiwalled carbon nanotubes in a rubber matrix using an internal mixer: Effects on rheological and electrical properties. *Journal of Polymer Science Part B: Polymer Physics*, *49*(22), 1597–1604. doi:10.1002/polb.22350

Chen, C., & Mansfeld, F. (1997). Corrosion protection of an Al 6092/SiCP metal matrix composite. *Corrosion Science*, *39*(6), 1075–1082. doi:10.1016/S0010-938X(97)00008-5

Chen, J., Hamon, M., Hu, H., Chen, Y., Rao, A., Eklund, P., & Haddon, R. (1998). Solution properties of single-walled carbon nanotubes. *Science*, *282*(5386), 95–8.

Chen, J., Xue, C., Ramasubramaniam, R., & Liu, H. (2006). A new method for the preparation of stable carbon nanotube organogels. *Carbon*, *44*(11), 2142–2146. doi:10.1016/j.carbon.2006.03.011

Chen, W., Tu, J., Wang, L., Gan, H., Xu, Z., & Zhang, X. (2003). Tribological application of carbon nanotubes in a metal-based composite coating and composites. *Carbon*, *41*, 215–222.

Chen, Y., Haddon, R. C., Fang, S., Rao, A. M., Eklund, P. C., Lee, W. H., Dickey, E. C., et al. (1998). Chemical Attachment of Organic Functional Groups to Single-walled Carbon Nanotube Material. *Journal of Materials Research*, *13*(09), 2423–2431. doi:10.1557/JMR.1998.0337

Choi, H. J., Shin, J. H., & Bae, D. H. (2012). The effect of milling conditions on microstructures and mechanical properties of Al/MWCNT composites. *Composites Part A: Applied Science and Manufacturing*, *43*(7), 1061–1072. doi:10.1016/j.compositesa.2012.02.008

Ci, L., Xie, S., Tang, D., Yan, X., Li, Y., Liu, Z., Zou, X., et al. (2001). Controllable growth of single wall carbon nanotubes by pyrolizing acetylene on the ¯ oating iron catalysts. *Chemical Physics Letters*, *349*(November), 191–195.

Cohen, M. L. (1994). Predicting properties and new materials. *Solid State Communications*, *92*(1–2), 45–52.

Cohen, M. L. (1998). Pergamon, *107*(11), 589–596.

Coleman, J., Khan, U., Blau, W., & Gunko, Y. (2006). Small but strong: A review of the mechanical properties of carbon nanotube–polymer composites. *Carbon*, *44*(9), 1624–1652. doi:10.1016/j.carbon.2006.02.038

Coleman, J. N., Khan, U., & Gun'ko, Y. K. (2006). Mechanical Reinforcement of Polymers Using Carbon Nanotubes. *Advanced Materials*, *18*(6), 689–706. doi:10.1002/adma.200501851

Colomer, J.-F., Piedigrosso, P., Willems, I., Journet, C., Bernier, P., Van Tendeloo, G., Fonseca, A., et al. (1998). Purification of catalytically produced multi-wall nanotubes. *Journal of the Chemical Society Faraday Transactions*, *94*(24), 3753–3758. doi:10.1039/a806804f

Cox, H. L. (1952). The elasticity and strength of paper and other fibrous materials. *British Journal of Applied Physics*, *3*(3), 72–79. doi:10.1088/0508-3443/3/3/302

Cui, S., Canet, R., Derre, A., Couzi, M., & Delhaes, P. (2003). Characterization of multiwall carbon nanotubes and influence of surfactant in the nanocomposite processing. *Carbon*, *41*(4), 797–809. doi:10.1016/S0008-6223(02)00405-0

Darsono, N. (2008). Milling and dispersion of multi-walled carbon nanotubes in texanol. *Applied Surface Science*, *254*(11), 3412–3419. doi:10.1016/j.apsusc.2007.11.028

Deng, C, Zhang, X., Ma, Y., & Wang, D. (2007). Fabrication of aluminum matrix composite reinforced with carbon nanotubes. *Rare Metals*, *26*(5), 450–455.

Deng, C, Zhang, X., Wang, D., & Ma, Y. (2007). Calorimetric study of carbon nanotubes and aluminum. *Materials Letters*, *61*(14-15), 3221–3223. doi:10.1016/j.matlet.2006.11.037

Deng, C. F., Wang, D. Z., Zhang, X. X., & Li, a. B. (2007). Processing and properties of carbon nanotubes reinforced aluminum composites. *Materials Science and Engineering: A*, *444*(1-2), 138–145. doi:10.1016/j.msea.2006.08.057

Deng, Chunfeng, Zhang, X., Wang, D., Lin, Q., & Li, A. (2007). Preparation and characterization of carbon nanotubes/aluminum matrix composites. *Materials Letters*, *61*(8-9), 1725–1728. doi:10.1016/j.matlet.2006.07.119

Deng, J.-P., Mou, C.-Y., & Han, C.-C. (1997). Oxidation of Fullerenes by Ozone. *Fullerene Science and Technology*, *5*(7), 1325–1336. doi:10.1080/15363839708013323

Desai, a. V., & Haque, M. a. (2005). Mechanics of the interface for carbon nanotube–polymer composites. *Thin-Walled Structures*, *43*(11), 1787–1803. doi:10.1016/j.tws.2005.07.003

Deuis, R., Yellup, J., & Subramanian, C. (1998). Metal-matrix composite coatings by PTA surfacing. *Composites science and …*, *3538*(97), 299–309.

Dillon, A. C., Jones, K. M., Bekkedahl, T. A., Kiang, C. H., Bethune, D. S., & Heben, M. J. (1997). Storage of hydrogen in single-walled carbon nanotubes. *Nature*, *386*(6623), 377–379. doi:10.1038/386377a0

Dong, B., Su, Y., Liu, Y., Yuan, J., Xu, J., & Zheng, L. (2011). Dispersion of carbon nanotubes by carbazole-tailed amphiphilic imidazolium ionic liquids in aqueous solutions. *Journal of colloid and interface science*, *356*(1), 190–5. doi:10.1016/j.jcis.2010.12.080

Donnet, J. B., Fousson, E., Samirant, M., Wang, T. K., Pontier-Johnson, M., & Eckhardt, A. (2000). Shock synthesis of nanodiamonds from carbon precursors: identification of carbynes. *COMPTES RENDUS DE L ACADEMIE DES SCIENCES SERIE II FASCICULE CCHIMIE*, *3*(5), 359–364.

Dresselhaus, M. S., Dresselhaus, G., & Saito, R. (1995). Physics of carbon nanotubes. *Carbon*, *33*(7), 883–891. doi:10.1016/0008-6223(95)00017-8

Du, J.-H. (2007). The present status and key problems of carbon nanotube based polymer composites. *eXPRESS Polymer Letters*, *1*(5), 253–273. doi:10.3144/expresspolymlett.2007.39

Dujardin, E, Ebbesen, T. W., Hiura, H., & Tanigaki, K. (1994). Capillarity and wetting of carbon nanotubes. *Science*, *265*(5180), 1850–1852.

Dujardin, Erik, Ebbesen, T. W., Krishnan, A., & Treacy, M. M. J. (1998). Purification of Single-Shell Nanotubes. *Advanced Materials*, *10*(8), 611–613. doi:10.1002/(SICI)1521-4095(199805)10:8<611::AID-ADMA611>3.0.CO;2-8

Dumitrică, T., Belytschko, T., & Yakobson, B. I. (2003). Bond-breaking bifurcation states in carbon nanotube fracture. *The Journal of Chemical Physics*, *118*(21), 9485. doi:10.1063/1.1577540

Ebbesen, T. (1996). Wetting, filling and decorating carbon nanotubes. *Journal of Physics and Chemistry of Solids*, *57*(6-8), 951–955. doi:10.1016/0022-3697(95)00381-9

Esawi, a, & Morsi, K. (2007). Dispersion of carbon nanotubes (CNTs) in aluminum powder. *Composites Part A: Applied Science and Manufacturing*, *38*(2), 646–650. doi:10.1016/j.compositesa.2006.04.006

Esawi, a. M. K., Morsi, K., Sayed, a., Taher, M., & Lanka, S. (2010). Effect of carbon nanotube (CNT) content on the mechanical properties of CNT-reinforced aluminium composites. *Composites Science and Technology*, *70*(16), 2237–2241. doi:10.1016/j.compscitech.2010.05.004

Esawi, A.M.K., Morsi, K., Sayed, A., Gawad, a. A., & Borah, P. (2009). Fabrication and properties of dispersed carbon nanotube–aluminum composites. *Materials Science and Engineering: A*, *508*(1-2), 167–173. doi:10.1016/j.msea.2009.01.002

Esawi, Amal M.K., & El Borady, M. a. (2008). Carbon nanotube-reinforced aluminium strips. *Composites Science and Technology*, *68*(2), 486–492. doi:10.1016/j.compscitech.2007.06.030

Fagan, S. B., Da Silva, A. J. R., Mota, R., Baierle, R. J., & Fazzio, A. (2003). Functionalization of carbon nanotubes through the chemical binding of atoms and molecules. *Physical Review B*, *67*(3), 1–4. doi:10.1103/PhysRevB.67.033405

Flahaut, E., Govindaraj, A., Peigney, A., Laurent, C., Rousset, A., & Rao, C. N. . (1999). Synthesis of single-walled carbon nanotubes using binary (Fe , Co , Ni) alloy nanoparticles prepared in situ by the reduction of oxide solid solutions. *Chemical Physics Letters*, *300*(January), 236–242.

Flahaut, E., Peigney, A., Laurent, C., Marlière, C., Chastel, F., & Rousset, A. (2000). Carbon nanotube-metal-oxide nanocomposites: Microstructure, electrical conductivity and mechanical properties. *Acta Materialia*, *48*(14), 3803–3812.

Fornes, T. D., Baur, J. W., Sabba, Y., & Thomas, E. L. (2006). Morphology and properties of melt-spun polycarbonate fibers containing single- and multi-wall carbon nanotubes. *Polymer*, *47*(5), 1704–1714. doi:10.1016/j.polymer.2006.01.003

Foster, J., Singamaneni, S., Kattumenu, R., & Bliznyuk, V. (2005). Dispersion and phase separation of carbon nanotubes in ultrathin polymer films. *Journal of colloid and interface science*, *287*(1), 167–72. doi:10.1016/j.jcis.2005.01.101

Fournier, J., Boiteux, G., Seytre, G., & Marichy, G. (1997). Percolation network of polypyrrole in conducting polymer composites. *Synthetic metals*, *84*, 839–840.

Fujigaya, T., Fukumaru, T., & Nakashima, N. (2009). Evaluation of dispersion state and thermal conductivity measurement of carbon nanotubes/UV-curable resin nanocomposites. *Synthetic Metals*, *159*(9-10), 827–830. doi:10.1016/j.synthmet.2009.01.019

Gao, B., Bower, C., Lorentzen, J. D., Fleming, L., Kleinhammes, A., Tang, X. P., Mcneil, L. E., et al. (2000). Enhanced saturation lithium composition in ball-milled single-walled carbon nanotubes, (September), 69–75.

Garate, H., Fascio, M. L., Mondragon, I., D'Accorso, N. B., & Goyanes, S. (2011). Surfactant-aided dispersion of polystyrene-functionalized carbon nanotubes in a nanostructured poly(styrene-b-isoprene-b-styrene) block copolymer. *Polymer*, *52*(10), 2214–2220. doi:10.1016/j.polymer.2011.03.032

Geng, Y., Liu, M., Li, J., Shi, X., & Kim, J. (2008). Effects of surfactant treatment on mechanical and electrical properties of CNT/epoxy nanocomposites. *Composites Part A: Applied Science and Manufacturing*, *39*(12), 1876–1883. doi:10.1016/j.compositesa.2008.09.009

George, R., Kashyap, K., Rahul, R., & Yamdagni, S. (2005). Strengthening in carbon nanotube/aluminium (CNT/Al) composites. *Scripta Materialia*, *53*(10), 1159–1163. doi:10.1016/j.scriptamat.2005.07.022

Gere, J. M., & Timoshenko, S. P. (1990). Mechanics of Materials. Amsterdam: KENT Publishing Company, Elsevier Science BV.

Goh, C. S., Wei, J., Lee, L. C., & Gupta, M. (2006). Simultaneous enhancement in strength and ductility by reinforcing magnesium with carbon nanotubes. *Materials Science and Engineering: A*, *423*(1-2), 153–156. doi:10.1016/j.msea.2005.10.071

Goh, C. S., Wei, J., Lee, L. C., & Gupta, M. (2008). Ductility improvement and fatigue studies in Mg-CNT nanocomposites. *Composites Science and Technology*, *68*(6), 1432–1439. doi:10.1016/j.compscitech.2007.10.057

Gojny, F. H., Wichmann, M. H. G., Köpke, U., Fiedler, B., & Schulte, K. (2004). Carbon nanotube-reinforced epoxy-composites: enhanced stiffness and fracture toughness at low nanotube content. *Composites Science and Technology*, *64*(15), 2363–2371. doi:10.1016/j.compscitech.2004.04.002

Gong, X., Liu, J., Baskaran, S., Voise, R. D., & Young, J. S. (2000). Surfactant-Assisted Processing of Carbon Nanotube/Polymer Composites. *Chemistry of Materials*, *12*(4), 1049–1052. doi:10.1021/cm9906396

Gooding, J. J., Wibowo, R., Liu, J., Yang, W., Losic, D., Orbons, S., Mearns, F. J., et al. (2003). Protein electrochemistry using aligned carbon nanotube arrays. *Journal of the American Chemical Society*, *125*(30), 9006–9007.

Grossiord, N., Loos, J., Regev, O., & Koning, C. (2006). Toolbox for dispersing carbon nanotubes into polymers to get conductive nanocomposites. *Chemistry of Materials*, *18*(5), 1089–1099.

Guo, T., Diener, M. D., Chai, Y., Alford, M. J., Haufler, R. E., McClure, S. M., Ohno, T., et al. (1992). Uranium stabilization of c28: a tetravalent fullerene. *Science*, *257*(5077), 1661–1664.

Haggenmuller, R., Zhou, W., Fischer, J. E., & Winey, K. I. (2003). Production and characterization of polymer nanocomposites with highly aligned single-walled carbon nanotubes. *Journal of Nanoscience and Nanotechnology*, *3*(1-2), 105–110.

Halpin, J., & Kardos, J. (1976). The Halpin-Tsai Equations: A Review. *Polymer Engineering Science*, *16*(5), 344–352.

Ham, H. T., Choi, Y. S., & Chung, I. J. (2005). An explanation of dispersion states of single-walled carbon nanotubes in solvents and aqueous surfactant solutions using solubility parameters. *Journal of colloid and interface science*, *286*(1), 216–23. doi:10.1016/j.jcis.2005.01.002

Hamada, N., Sawada, S., & Oshiyama, A. (1992). New One-Dimensional Conductors: Graphitic Microtubuleles. *Physical Review Letters*, *68*(10), 1579–1581. doi:10.1176/appi.neuropsych.242259

Hamon, M. A., Hui, H., Bhowmik, P., Itkis, H. M. E., & Haddon, R. C. (2002). Ester-functionalized soluble single-walled carbon nanotubes. *Applied Physics A Materials Science Processing*, *74*(3), 333–338. doi:10.1007/s003390201281

Hamwi, A. (1997). Fluorination of carbon nanotubes. *Carbon*, *35*(6), 723–728. doi:10.1016/S0008-6223(97)00013-4

Harik, V. . (2002). Mechanics of carbon nanotubes: applicability of the continuum-beam models. *Computational Materials Science*, *24*(3), 328–342. doi:10.1016/S0927-0256(01)00255-5

Harris, B. (1999). *Engineering composite materials*.

He, C., Zhao, N., Shi, C., Du, X., Li, J., Li, H., & Cui, Q. (2007). An Approach to Obtaining Homogeneously Dispersed Carbon Nanotubes in Al Powders for Preparing Reinforced Al-Matrix Composites. *Advanced Materials*, *19*(8), 1128–1132. doi:10.1002/adma.200601381

Hernández-Pérez, A., Avilés, F., May-Pat, A., Valadez-González, A., Herrera-Franco, P. J., & Bartolo-Pérez, P. (2008). Effective properties of multiwalled carbon nanotube/epoxy composites using two different tubes. *Composites Science and Technology*, *68*(6), 1422–1431. doi:10.1016/j.compscitech.2007.11.001

Hilding, J., Grulke, E. a., George Zhang, Z., & Lockwood, F. (2003). Dispersion of Carbon Nanotubes in Liquids. *Journal of Dispersion Science and Technology*, *24*(1), 1–41. doi:10.1081/DIS-120017941

Hill, D. E., Lin, Y., Rao, A. M., Allard, L. F., & Sun, Y.-P. (2002). Functionalization of Carbon Nanotubes with Polystyrene. *Macromolecules*, *35*(25), 9466–9471. doi:10.1021/ma020855r

Hirsch, A. (2002). Functionalization of single-□walled carbon nanotubes. *Angewandte Chemie International Edition*, (Cvd), 1853–1859.

Hirsch, A., Vostrowsky, O., Chemie, O., & Erlangen-nürnberg, U. (2005). Functionalization of Carbon Nanotubes, 193–237. doi:10.1007/b98169

Holzinger, M, Hirsch, A., Bernier, P., Duesberg, G. S., & Burghard, M. (2000). A new purification method for single-wall carbon nanotubes (SWNTs). *Applied Physics A: Materials Science & Processing*, *70*(5), 599–602. doi:10.1007/s003390051087

Holzinger, Michael, Vostrowsky, O., Hirsch, A., Hennrich, F., Kappes, M., Weiss, R., & Jellen, F. (2001). Sidewall Functionalization of Carbon Nanotubes . *Angewandte Chemie International Edition*, *40*(21), 4002–4005.

Hong, J., Lee, J., Hong, C. K., & Shim, S. E. (2010). Effect of dispersion state of carbon nanotube on the thermal conductivity of poly(dimethyl siloxane) composites. *Current Applied Physics*, *10*(1), 359–363. doi:10.1016/j.cap.2009.06.028

Huang, W., Chen, H., & Zuo, J.-M. (2006). One-Dimensional Self-Assembly of Metallic Nanostructures on Single-Walled Carbon-Nanotube Bundles. *Small*, *2*(12), 1418–1421. doi:10.1002/smll.200600241

Ighodaro, O. L., & Okoli, O. I. (2008). Fracture Toughness Enhancement for Alumina Systems: A Review. *International Journal of Applied Ceramic Technology*, *5*(3), 313–323. doi:10.1111/j.1744-7402.2008.02224.x

Iijima, S, & Ichihashi, T. (1993). SINGLE-SHELL CARBON NANOTUBES OF 1-NM DIAMETER (VOL 363, PG 603, 1993). *Nature*, *364*(6439), 737.

Iijima, Sumio. (1991). Helical microtubules of graphitic carbon. *Nature*, *354*, 56–58.

Inam, F., Yan, H., Peijs, T., & Reece, M. J. (2010). The sintering and grain growth behaviour of ceramic-carbon nanotube nanocomposites. *Composites Science and Technology*, *70*(6), 947–952.

Islam, M. F., Rojas, E., Bergey, D. M., Johnson, A. T., & Yodh, A. G. (2003). High Weight Fraction Surfactant Solubilization of Single-Wall Carbon Nanotubes in Water. *Nano Letters*, *3*(2), 269–273. doi:10.1021/nl025924u

Jiang, B., Liu, C., Zhang, C., Wang, B., & Wang, Z. (2007). The effect of non-symmetric distribution of fiber orientation and aspect ratio on elastic properties of composites. *Composites Part B: Engineering*, *38*(1), 24–34. doi:10.1016/j.compositesb.2006.05.002

Jiménez-Suárez, a., Campo, M., Sánchez, M., Romón, C., & Ureña, a. (2012). Dispersion of carbon nanofibres in a low viscosity resin by calendering process to manufacture multiscale composites by VARIM. *Composites Part B: Engineering*, *43*(8), 3104–3113. doi:10.1016/j.compositesb.2012.04.030

Jin, L., Bower, C., & Zhou, O. (1998). Alignment of carbon nanotubes in a polymer matrix by mechanical stretching. *Applied Physics Letters*, *73*(9), 1197. doi:10.1063/1.122125

Jun, G. H., Jin, S. H., Park, S. H., Jeon, S., & Hong, S. H. (2012). Highly dispersed carbon nanotubes in organic media for polymer:fullerene photovoltaic devices. *Carbon*, *50*(1), 40–46. doi:10.1016/j.carbon.2011.07.052

Jung, W. R., Choi, J. H., Lee, N., Shin, K., Moon, J.-H., & Seo, Y.-S. (2012). Reduced damage to carbon nanotubes during ultrasound-assisted dispersion as a result of supercritical-fluid treatment. *Carbon*, *50*(2), 633–636. doi:10.1016/j.carbon.2011.08.075

Kaczmar, J. W., Pietrzak, K., & Włosiński, W. (2000). The production and application of metal matrix composite materials. *Journal of Materials Processing Technology*, *106*(1-3), 58–67. doi:10.1016/S0924-0136(00)00639-7

Kasaliwal, G. R., Göldel, A., Pötschke, P., & Heinrich, G. (2011). Influences of polymer matrix melt viscosity and molecular weight on MWCNT agglomerate dispersion. *Polymer*, *52*(4), 1027–1036. doi:10.1016/j.polymer.2011.01.007

Kataura, H., Kumazawa, Y., Maniwa, Y., Ohtsuka, Y., Sen, R., Suzuki, S., & Achiba, Y. (2000). Diameter control of single-walled carbon nanotubes. *Carbon*, *38*(11-12), 1691–1697. doi:10.1016/S0008-6223(00)00090-7

Kataura, Hiromichi, Kimura, A., Ohtsuka, Y., Suzuki, S., Maniwa, Y., Hanyu, T., & Achiba, Y. (1998). Formation of Thin Single-Wall Carbon Nanotubes by Laser Vaporization of Rh/Pd-Graphite Composite Rod. *Japanese Journal of Applied Physics*, *37*(5B), L616–L618. doi:10.1143/JJAP.37.L616

Kelly, A. (2006). Composite materials after seventy years. *Journal of Materials Science*, *41*(3), 905–912. doi:10.1007/s10853-006-6569-9

Kennedy, F., Balbahadur, A., & Lashmore, D. (1997). The friction and wear of Cu-based silicon carbide particulate metaal matrix composites for brake applications. *Wear*, *204*, 715–721.

Kevorkijan, V. (1999). Aluminum composites for automotive applications: A global perspective. *JOM Journal of the Minerals, Metals and Materials …*, (November).

Kim, J., & Mai, Y. (1998). *Engineered interfaces in fiber reinforced composites*.

Kim, J. U. N. Y., & Kim, S. H. U. N. (2005). Influence of Multiwall Carbon Nanotube on Physical Properties of Poly (ethylene 2 , 6-naphthalate) Nanocomposites, 1062–1071. doi:10.1002/polb

Kim, K. T., Cha, S. Il, & Hong, S. H. (2007). Hardness and wear resistance of carbon nanotube reinforced Cu matrix nanocomposites. *Materials Science and Engineering: A*, *449-451*, 46–50. doi:10.1016/j.msea.2006.02.310

Kim, K. T., Cha, S. Il, Hong, S. H., & Hong, S. H. (2006). Microstructures and tensile behavior of carbon nanotube reinforced Cu matrix nanocomposites. *Materials Science and Engineering: A*, *430*(1-2), 27–33. doi:10.1016/j.msea.2006.04.085

Kim, T.-H., Doe, C., Kline, S. R., & Choi, S.-M. (2007). Water-Redispersible Isolated Single-Walled Carbon Nanotubes Fabricated by In Situ Polymerization of Micelles. *Advanced Materials*, *19*(7), 929–933. doi:10.1002/adma.200601991

Kim, Y. A., Hayashi, T., Fukai, Y., Endo, M., & Dresselhaus, M. S. (2002). Effect of ball milling on morphology of cup-stacked carbon nanotubes. *Chemical Physics Letters*, *355*(April), 279–284. doi:10.1016/S0009-2614(02)00248-8

Kim, Y., Kwon, S.-M., Kim, D.-Y., Kim, H.-S., & Jin, H.-J. (2009). Dispersity and stability measurements of functionalized multiwalled carbon nanotubes in organic solvents. *Current Applied Physics*, *9*(2), e100–e103. doi:10.1016/j.cap.2008.12.039

Kondoh, K., Fukuda, H., Umeda, J., Imai, H., Fugetsu, B., & Endo, M. (2010). Microstructural and mechanical analysis of carbon nanotube reinforced magnesium alloy powder composites. *Materials Science and Engineering: A*, *527*(16-17), 4103–4108. doi:10.1016/j.msea.2010.03.049

Korab, J., Stefanik, P., & KaveckÄ±, S. (2002). Thermal conductivity of unidirectional copper matrix carbon fibre composites. *Composites Part A: Applied …*, *33*, 577–581.

Kosmidou, T. V. (2008). Structural, mechanical and electrical characterization of epoxy-amine/carbon black nanonocomposites. *eXPRESS Polymer Letters*, *2*(5), 364–372. doi:10.3144/expresspolymlett.2008.43

Krause, B., Mende, M., Pötschke, P., & Petzold, G. (2010). Dispersability and particle size distribution of CNTs in an aqueous surfactant dispersion as a function of ultrasonic treatment time. *Carbon*, *48*(10), 2746–2754. doi:10.1016/j.carbon.2010.04.002

Kroto, H W, Heath, J. R., O'Brien, S. C., Curl, R. F., & Smalley, R. E. (1985). 1985 Nature Publishing Group. *Nature*, *318*(6042), 162–163. doi:10.1038/318162a0

Kroto, Harold W., Heath, J. R., O'Brien, S. C., Curl, R. F., & Smalley, R. E. (1985). C60: Buckminsterfullerene. *Nature*, *318*(14), 162–163.

Krätschmer, W., Lamb, L. D., Fostiropoulos, K., & Huffman, D. R. (1990). Solid C60: a new form of carbon. *Nature*, *347*(6291), 354–358. doi:10.1038/347354a0

Kumar, S., Dang, T. D., Arnold, F. E., Bhattacharyya, A. R., Min, B. G., Zhang, X., Vaia, R. A., et al. (2002). Synthesis, Structure, and Properties of PBO/SWNT Composites. *Macromolecules*, *35*(24), 9039–9043. doi:10.1021/ma0205055

Kuzumaki, T., Miyazawa, K., Ichinose, H., & Ito, K. (1998). Processing of carbon nanotube reinforced aluminum composite. *Journal of Materials Research*, *13*(9), 2445–2449. doi:10.1557/JMR.1998.0340

Kuzumaki, T., Ujiie, O., Ichinose, H., & Ito, K. (2000). Mechanical Characteristics and Preparation of Carbon Nanotube Fiber-Reinforced Ti Composite. *Advanced Engineering Materials*, *2*(7), 416–418. doi:10.1002/1527-2648(200007)2:7<416::AID-ADEM416>3.0.CO;2-Y

Kwon, H, Estili, M., Takagi, K., Miyazaki, T., & Kawasaki, a. (2009). Combination of hot extrusion and spark plasma sintering for producing carbon nanotube reinforced aluminum matrix composites. *Carbon*, *47*(3), 570–577. doi:10.1016/j.carbon.2008.10.041

Kwon, Hansang, Park, D. H., Silvain, J. F., & Kawasaki, A. (2010). Investigation of carbon nanotube reinforced aluminum matrix composite materials. *Composites Science and Technology*, *70*(3), 546–550. doi:10.1016/j.compscitech.2009.11.025

Laha, T., Chen, Y., Lahiri, D., & Agarwal, a. (2009). Tensile properties of carbon nanotube reinforced aluminum nanocomposite fabricated by plasma spray forming. *Composites Part A: Applied Science and Manufacturing*, *40*(5), 589–594. doi:10.1016/j.compositesa.2009.02.007

Landau, L. D., Lifshits, E. M., Kosevich, A. M., & Pitaevskii, L. P. (1986). *Theory of elasticity* (3rd editio.). Oxford: Pergamon Press.

Laplaze, D., Bernier, P., Barbedette, L., Lambert, J. M., Flamant, G., Lebrun, M., Brunelle, A., et al. (1994). Production de fullerenes à partir de l'énergie solaire: L'expérience d'Odeillo. *C.R. Acad. Sci. Paris*, *318*(2), 733–738.

Laplaze, D., Bernier, P., Maser, W. K., Flamant, G., Guillard, T., & Loiseau, A. (1998). Carbon nanotubes: The solar approach. *Carbon*, *36*(5-6), 685–688. doi:10.1016/S0008-6223(98)00025-6

Lauginie, P., & Conard, J. (1997). New growing modes for carbon: modelization of lattice, defects, structure of tubules and onions. *Journal of Physics and Chemistry of Solids*, *58*(11), 1949–1963.

Le Chatelier, H. (1926). *Leçons sur le carbone, la combustion, les lois chimiques, professées a la Faculté des sciences de Paris*. Paris: J. Hermann.

Li, H., Nie, J. C., & Kunsági-Máté, S. (2010). Modified dispersion of functionalized multi-walled carbon nanotubes in acetonitrile. *Chemical Physics Letters*, *492*(4-6), 258–262. doi:10.1016/j.cplett.2010.04.053

Li, J., Ma, P. C., Chow, W. S., To, C. K., Tang, B. Z., & Kim, J.-K. (2007). Correlations between Percolation Threshold, Dispersion State, and Aspect Ratio of Carbon Nanotubes. *Advanced Functional Materials*, *17*(16), 3207–3215. doi:10.1002/adfm.200700065

Li, S.-Y., Zhou, H.-H., Gu, J.-L., & Zhu, J. (2000). Does carbyne really exist? — carbynes in expanded graphite. *Carbon*, *38*(6), 934–937. doi:10.1016/S0008-6223(00)00056-7

Li, Y. B., Wei, B. Q., Liang, J., Yu, Q., & Wu, D. H. (1999). Transformation of carbon nanotubes to nanoparticles by ball milling process. *Carbon*, *37*(3), 493–497. doi:10.1016/S0008-6223(98)00218-8

Liao, J., & Tan, M.-J. (2011). Mixing of carbon nanotubes (CNTs) and aluminum powder for powder metallurgy use. *Powder Technology*, *208*(1), 42–48. doi:10.1016/j.powtec.2010.12.001

Lim, D. K., Shibayanagi, T., & Gerlich, a. P. (2009). Synthesis of multi-walled CNT reinforced aluminium alloy composite via friction stir processing. *Materials Science and Engineering: A*, *507*(1-2), 194–199. doi:10.1016/j.msea.2008.11.067

Lim, J. (2003). Selective thiolation of single-walled carbon nanotubes. *Synthetic Metals*, *139*(2), 521–527. doi:10.1016/S0379-6779(03)00337-0

Lisetski, L., Minenko, S., Fedoryako, a, & Lebovka, N. (2009). Dispersions of multiwalled carbon nanotubes in different nematic mesogens: The study of optical transmittance and electrical conductivity. *Physica E: Low-dimensional Systems and Nanostructures*, *41*(3), 431–435. doi:10.1016/j.physe.2008.09.004

Liu, C.-D., Shu, D.-Y., Tsao, C.-T., Han, J.-L., Tsai, F.-Y., Chen, F.-C., Chen, W.-C., et al. (2010). Synthesis and characterization of well-dispersed multi-walled carbon nanotube/low-bandgap poly(3,4-alkoxythiophene) nanocomposites. *Composites Science and Technology*, *70*(8), 1242–1248. doi:10.1016/j.compscitech.2010.03.012

Liu, J., Rinzler, A. G., Dai, H., Hafner, J. H., Bradley, R. K., Boul, P. J., Lu, A., et al. (1998). Fullerene Pipes. *Science* , *280* (5367), 1253–1256. doi:10.1126/science.280.5367.1253

Liu, L., & Wagner, H. D. (2005). Rubbery and glassy epoxy resins reinforced with carbon nanotubes. *Composites Science and Technology*, *65*(11-12), 1861–1868. doi:10.1016/j.compscitech.2005.04.002

Liu, Z. Y., Xu, S. J., Xiao, B. L., Xue, P., Wang, W. G., & Ma, Z. Y. (2012). Effect of ball-milling time on mechanical properties of carbon nanotubes reinforced aluminum matrix composites. *Composites Part A: Applied Science and Manufacturing*, *43*(12), 2161–2168. doi:10.1016/j.compositesa.2012.07.026

Llorca, J. (2002). High temperature fatigue of discontinuously-reinforced metal?matrix composites. *International Journal of Fatigue*, *24*(2-4), 233–240. doi:10.1016/S0142-1123(01)00077-9

Loiseau, A., Launois, P., Petit, P., Roche, S., & Salvetat, J. P. (2006). *Understanding Carbon Nanotubes*. (Annick Loiseau, P. Launois, P. Petit, S. Roche, & J.-P. Salvetat, Eds.)*Nature* (Vol. 677, pp. 153–153). Elsevier Ltd. doi:10.1007/b10971390

Loos, J., Grossiord, N., Koning, C., & Regev, O. (2007). On the fate of carbon nanotubes: Morphological characterisations. *Composites Science and Technology*, *67*(5), 783–788. doi:10.1016/j.compscitech.2005.12.029

Lu, K. (1996). Mechanical damage of carbon nanotubes by ultrasound. *Carbon*, *34*(6), 814–816. doi:10.1016/0008-6223(96)89470-X

Ma, P. C., Kim, J.-K., & Tang, B. Z. (2007). Effects of silane functionalization on the properties of carbon nanotube/epoxy nanocomposites. *Composites Science and Technology*, *67*(14), 2965–2972. doi:10.1016/j.compscitech.2007.05.006

Ma, P.-C., Liu, M.-Y., Zhang, H., Wang, S.-Q., Wang, R., Wang, K., Wong, Y.-K., et al. (2009). Enhanced electrical conductivity of nanocomposites containing hybrid fillers of carbon nanotubes and carbon black. *ACS applied materials interfaces*, *1*(5), 1090–1096.

Ma, P.-C., Mo, S.-Y., Tang, B.-Z., & Kim, J.-K. (2010). Dispersion, interfacial interaction and re-agglomeration of functionalized carbon nanotubes in epoxy composites. *Carbon*, *48*(6), 1824–1834. doi:10.1016/j.carbon.2010.01.028

Ma, P.-C., Siddiqui, N. a., Marom, G., & Kim, J.-K. (2010). Dispersion and Functionalization of Carbon Nanotubes for Polymer-based Nanocomposites: A Review. *Composites Part A: Applied Science and Manufacturing*, *41*(10), 1345–1367. doi:10.1016/j.compositesa.2010.07.003

Ma, Z. Y., & Tjong, S. C. (1999). The high-temperature creep behaviour of 2124 aluminium alloys with and without particulate and SiC-whisker reinforcement. *Composites Science and Technology*, *59*(5), 737–747. doi:10.1016/S0266-3538(98)00113-4

Mackay, A. L., & Terrones, H. (1991). Diamond from graphite. *Nature*, *352*(6338), 762.

Madni, I., Hwang, C.-Y., Park, S.-D., Choa, Y.-H., & Kim, H.-T. (2010). Mixed surfactant system for stable suspension of multiwalled carbon nanotubes. *Colloids and Surfaces A: Physicochemical and Engineering Aspects*, *358*(1-3), 101–107. doi:10.1016/j.colsurfa.2010.01.030

Majkic, G., & Chen, Y. (2006). Processing of Light-Weight Shape Memory Alloys Using Spark Plasma Sintering. *47th AIAA/ASME/ASCE/AHS/ASC Structures, Structural Dynamics, and Materials Conference14th AIAA/ASME/AHS Adaptive Structures Conference 7th*. American Institute of Aeronautics and Astronautics. doi:doi:10.2514/6.2006-1767

Mallik, S., Ekere, N., Best, C., & Bhatti, R. (2011). Investigation of thermal management materials for automotive electronic control units. *Applied Thermal Engineering*, *31*(2-3), 355–362. doi:10.1016/j.applthermaleng.2010.09.023

Mamedov, A. A., Kotov, N. A., Prato, M., Guldi, D. M., Wicksted, J. P., & Hirsch, A. (2002). Molecular design of strong single-wall carbon nanotube/polyelectrolyte multilayer composites. *Nature Materials*, *1*(3), 190–194.

Marcoux, P. R., Schreiber, J., Batail, P., Lefrant, S., Renouard, J., Jacob, G., Albertini, D., et al. (2002). A spectroscopic study of the fluorination and defluorination reactions on single-walled carbon nanotubes. *Physical Chemistry Chemical Physics*, *4*(11), 2278–2285.

Maser, W. K. (1998). Production of high-density single-walled nanotube material by a simple laser-ablation method, (August), 587–593.

Matthews, F. L., & Rawlings, R. D. (1999). *Composite materials: science and engineering*. (Springer, Ed.)*Engineering* (Vol. 2nd editio, p. 483). Springer. doi:10.1016/S0140-6736(00)67208-2

Mawhinney, D. (2000). Infrared spectral evidence for the etching of carbon nanotubes: ozone oxidation at 298 K. *Journal of American Chemistry Society*, (23), 2383–2384.

Mawhinney, D., & Naumenko, V. (2000). Surface defect site density on single walled carbon nanotubes by titration. *Chemical Physics Letters*, (June), 213–216.

Mc Carthy, B., Coleman, J. N., Czerw, R., Dalton, A. B., Carroll, D. L., & Blau, W. J. (2001). Microscopy studies of nanotube-conjugated polymer interactions. *Synthetic Metals*, *121*(1-3), 1225–1226. doi:10.1016/S0379-6779(00)00906-1

Merchan-Merchan, W., Saveliev, A. V., Kennedy, L., & Jimenez, W. C. (2010). Combustion synthesis of carbon nanotubes and related nanostructures. *Progress in Energy and Combustion Science*, *36*(6), 696–727. doi:10.1016/j.pecs.2010.02.005

Meyyappan, M. (2005). *Carbon Nanotubes Science and Applications*.

Mickelson, E. T., Huffman, C. B., Rinzler, A. G., Smalley, R. E., Hauge, R. H., & Margrave, J. L. (1998). Fluorination of single-wall carbon nanotubes. *Chemical Physics Letters*, *296*(1–2), 188–194.

Mishra, R. S., & Ma, Z. Y. (2005). Friction stir welding and processing. *Materials Science and Engineering: R: Reports*, *50*, 1–78.

Mishra, R. S., Ma, Z. Y., & Charit, I. (2003). Friction stir processing: a novel technique for fabrication of surface composite. *Materials Science and Engineering: A*, *341*(1–2), 307–310.

Mo, C. B., Cha, S. I., Kim, K. T., Lee, K. H., & Hong, S. H. (2005). Fabrication of carbon nanotube reinforced alumina matrix nanocomposite by sol – gel process, *395*, 124–128. doi:10.1016/j.msea.2004.12.031

Moisala, a, Li, Q., Kinloch, I., & Windle, a. (2006). Thermal and electrical conductivity of single- and multi-walled carbon nanotube-epoxy composites. *Composites Science and Technology*, *66*(10), 1285–1288. doi:10.1016/j.compscitech.2005.10.016

Moniruzzaman, M., & Winey, K. I. (2006). Polymer Nanocomposites Containing Carbon Nanotubes. *Macromolecules*, *39*(16), 5194–5205. doi:10.1021/ma060733p

Monthioux, M., & Kuznetsov, V. L. (2006). Who should be given the credit for the discovery of carbon nanotubes? *Carbon*, *44*(9), 1621–1623. doi:10.1016/j.carbon.2006.03.019

Morisada, Y., Fujii, H., Nagaoka, T., & Fukusumi, M. (2006). MWCNTs/AZ31 surface composites fabricated by friction stir processing. *Materials Science and Engineering: A*, *419*(1–2), 344–348.

Morishita, K., & Takarada, T. (1994). Scanning electron microscope observation of the purification behaviour of carbon nanotubes. *Journal of Materials Science*, *34*(6), 1169–1174. doi:10.1023/A:1004544503055

Morsi, K., & Esawi, a. (2007). Effect of mechanical alloying time and carbon nanotube (CNT) content on the evolution of aluminum (Al)–CNT composite powders. *Journal of Materials Science*, *42*(13), 4954–4959. doi:10.1007/s10853-006-0699-y

Morsi, K., Esawi, a. M. K., Borah, P., Lanka, S., Sayed, a., & Taher, M. (2010). Properties of single and dual matrix aluminum–carbon nanotube composites processed via spark plasma extrusion (SPE). *Materials Science and Engineering: A*, *527*(21-22), 5686–5690. doi:10.1016/j.msea.2010.05.081

Morsi, K., Esawi, a. M. K., Lanka, S., Sayed, a., & Taher, M. (2010). Spark plasma extrusion (SPE) of ball-milled aluminum and carbon nanotube reinforced aluminum composite powders.

Composites Part A: Applied Science and Manufacturing, *41*(2), 322–326. doi:10.1016/j.compositesa.2009.09.028

Munoz, E., Maser, W. K., Benito, A. M., Martinez, M. T., De La Fuente, G. F., Righi, A., Sauvajol, J. L., et al. (2000). Single-walled carbon nanotubes produced by cw CO2-laser ablation: study of parameters important for their formation. *Applied Physics A*, *70*(2), 145–151.

Nagasawa, S., Yudasaka, M., Hirahara, K., Ichihashi, T., & Iijima, S. (2000). Effect of oxidation on single-wall carbon nanotubes. *Chemical Physics Letters*, *328*(4–6), 374–380.

National Research Council (US). Committee on High-Performance Structural Fibers for Advanced Polymer, & Board, N. R. C. (US). N. M. A. (2005). *High-performance Structural Fibers for Advanced Polymer Matrix Composites*. National Academy Press.

Nikolaev, P., Bronikowski, M. J., Bradley, R. K., Rohmund, F., Colbert, D. T., Smith, K. A., & Smalley, R. E. (1999). Gas-phase catalytic growth of single-walled carbon nanotubes from carbon monoxide. *Chemical Physics Letters*, *313*(November), 91–97.

Ning, Y., Zhang, X., Wang, Y., Sun, Y., Shen, L., Yang, X., & Van Tendeloo, G. (2002). Bulk production of multi-wall carbon nanotube bundles on sol–gel prepared catalyst. *Chemical Physics Letters*, *366*(5-6), 555–560. doi:10.1016/S0009-2614(02)01647-0

Noguchi, T., Magario, A., Fukazawa, S., Shimizu, S., Beppu, J., & Seki, M. (2004). Carbon Nanotube/Aluminium Composites with Uniform Dispersion. *Materials Transactions*, *45*(2), 602–604. doi:10.2320/matertrans.45.602

Ntim, S. A., Sae-Khow, O., Witzmann, F. a, & Mitra, S. (2011). Effects of polymer wrapping and covalent functionalization on the stability of MWCNT in aqueous dispersions. *Journal of colloid and interface science*, *355*(2), 383–8. doi:10.1016/j.jcis.2010.12.052

Oberlin, A., Endo, M., & Koyama, T. (1976). Filamentous growth of carbon through benzene decomposition. *Journal of Crystal Growth*, *32*(3), 335–349. doi:10.1016/0022-0248(76)90115-9

Odegard, G. M., Gates, T. S., Nicholson, L. M., & Wise, K. E. (2002). Equivalent-continuum modeling of nano-structured materials. *Composite Science and Technology*, *62*, 1869–1880.

Oh, H., Jung, B. M., Lee, H. P., & Chang, J. Y. (2010). Dispersion of single walled carbon nanotubes in organogels by incorporation into organogel fibers. *Journal of colloid and interface science*, *352*(1), 121–7. doi:10.1016/j.jcis.2010.08.025

Ounaies, Z. (2003). Electrical properties of single wall carbon nanotube reinforced polyimide composites. *Composites Science and Technology*, *63*(11), 1637–1646. doi:10.1016/S0266-3538(03)00067-8

Owens, F., & Iqbal, Z. (2002). Electrochemical functionalization of carbon nanotubes with hydrogen. *23rd Army Science Conference, Session L …*, 1–2.

Pang, L. X., Sun, K. N., Ren, S., Sun, C., & Bi, J. Q. (2007). Microstructure, Hardness, and Bending Strength of Carbon Nanotube—Iron Aluminide Composites. *Journal of composite materials*, *41*(16), 2025–2031.

Pang, L.-X., Sun, K.-N., Ren, S., Sun, C., Fan, R.-H., & Lu, Z.-H. (2007). Fabrication and microstructure of Fe3Al matrix composite reinforced by carbon nanotube. *Materials Science and Engineering: A*, *447*(1-2), 146–149. doi:10.1016/j.msea.2006.11.070

Paramsothy, M., Chan, J., Kwok, R., & Gupta, M. (2011). Addition of CNTs to enhance tensile/compressive response of magnesium alloy ZK60A. *Composites Part A: Applied Science and Manufacturing*, *42*(2), 180–188.

Peng, H., Reverdy, P., Khabashesku, V. N., & Margrave, J. L. (2003). Sidewall functionalization of single-walled carbon nanotubes with organic peroxides. *Chemical Communications*, (3), 362–363.

Potschke, P. (2004). Melt mixing of polycarbonate with multiwalled carbon nanotubes: microscopic studies on the state of dispersion. *European Polymer Journal*, *40*(1), 137–148. doi:10.1016/j.eurpolymj.2003.08.008

Poyato, R., Vasiliev, A. L., Padture, N. P., Tanaka, H., & Nishimura, T. (2006). Aqueous colloidal processing of single-wall carbon nanotubes and their composites with ceramics. *Nanotechnology*, *17*(6), 1770–1777.

Purcell, S., Vincent, P., Journet, C., & Binh, V. (2002). Tuning of Nanotube Mechanical Resonances by Electric Field Pulling. *Physical Review Letters*, *89*(27), 1–4. doi:10.1103/PhysRevLett.89.276103

Pérez-Bustamante, R., Bueno-Escobedo, J. L., Jiménez-Lobato, J., Estrada-Guel, I., Miki-Yoshida, M., Licea-Jiménez, L., & Martínez-Sánchez, R. (2012). Wear behavior in Al2024–CNTs composites synthesized by mechanical alloying. *Wear*, *292-293*, 169–175. doi:10.1016/j.wear.2012.05.016

Pérez-Bustamante, R., Pérez-Bustamante, F., Estrada-Guel, I., Santillán-Rodríguez, C. R., Matutes-Aquino, J. A., Herrera-Ramírez, J. M., Miki-Yoshida, M., et al. (2011). Characterization of Al2024-CNTs composites produced by mechanical alloying. *Powder Technology*, *212*(3), 390–396.

Pöllänen, M., Pirinen, S., Suvanto, M., & Pakkanen, T. T. (2011). Influence of carbon nanotube–polymeric compatibilizer masterbatches on morphological, thermal, mechanical, and tribological properties of polyethylene. *Composites Science and Technology*, *71*(10), 1353–1360. doi:10.1016/j.compscitech.2011.05.009

Qian, D., Dickey, E. C., Andrews, R., & Rantell, T. (2000). Load transfer and deformation mechanisms in carbon nanotube-polystyrene composites. *Applied Physics Letters*, *76*(20), 2868. doi:10.1063/1.126500

Rastogi, R., Kaushal, R., Tripathi, S. K., Sharma, A. L., Kaur, I., & Bharadwaj, L. M. (2008). Comparative study of carbon nanotube dispersion using surfactants. *Journal of colloid and interface science*, *328*(2), 421–8. doi:10.1016/j.jcis.2008.09.015

Rawal, S. (2001). Metal-matrix composites for space applications. *JOM Journal of the Minerals, Metals and Materials …*, (April), 14–17.

Riggs, J. E., Guo, Z., Carroll, D. L., & Sun, Y.-P. (2000). Strong Luminescence of Solubilized Carbon Nanotubes. *Journal of the American Chemical Society*, *122*(24), 5879–5880. doi:10.1021/ja9942282

Rinzler, a. G., Liu, J., Dai, H., Nikolaev, P., Huffman, C. B., Rodríguez-Macías, F. J., Boul, P. J., et al. (1998). Large-scale purification of single-wall carbon nanotubes: process, product, and characterization. *Applied Physics A: Materials Science & Processing*, *67*(1), 29–37. doi:10.1007/s003390050734

Robertson, D. H., Brenner, D. W., & Mintmire, J. W. (1992). Energetics of nanoscale graphitic tubules. *Physical Review B*, *45*(21), 12592–12595.

Rul, S., Lefèvre-Schlick, F., Capria, E., Laurent, C., & Peigney, A. (2004). Percolation of single-walled carbon nanotubes in ceramic matrix nanocomposites. *Acta Materialia*, *52*(4), 1061–1067.

Ryszkowska, J., Jurczykkowalska, M., Szymborski, T., & Kurzydlowski, K. (2007). Dispersion of carbon nanotubes in polyurethane matrix. *Physica E: Low-dimensional Systems and Nanostructures*, *39*(1), 124–127. doi:10.1016/j.physe.2007.02.003

Salas, W., Alba-Baena, N. G., & Murr, L. E. (2007). Explosive Shock-Wave Consolidation of Aluminum Powder/Carbon Nanotube Aggregate Mixtures: Optical and Electron Metallography. *Metallurgical and Materials Transactions A*, *38*(12), 2928–2935. doi:10.1007/s11661-007-9336-x

Salvetat, B. J., Kulik, A. J., Bonard, J., Briggs, G. A. D., Stöckli, T., Møtønier, K., Bonnamy, S., et al. (1999). Elastic Modulus of Ordered and Disordered Multiwalled Carbon Nanotubes. *Advanced Materials*, (2), 161–165.

Salvetat, J.-P., Briggs, G. A. D., Bonard, J.-M., Bacsa, R. R., Kulik, A. J., Stöckli, T., Burnham, N. A., et al. (1999). Elastic and Shear Moduli of Single-Walled Carbon Nanotube Ropes. *Physical Review Letters*, *82*(5), 944–947.

Sandler, J., Shaffer, M. S. P., Prasse, T., Bauhofer, W., Schulte, K., & Windle, A. H. (1999). Development of a dispersion process for carbon nanotubes in an epoxy matrix and the resulting electrical properties. *Polymer*, *40*(21), 5967–5971. doi:10.1016/S0032-3861(99)00166-4

Sato, H., & Sano, M. (2008). Characteristics of ultrasonic dispersion of carbon nanotubes aided by antifoam. *Colloids and Surfaces A: Physicochemical and Engineering Aspects*, *322*(1-3), 103–107. doi:10.1016/j.colsurfa.2008.02.031

Schanz, M., & Antes, H. (2002). A Boundary Integral Formulation for the Dynamic Behavior of a Timoshenko Beam. *Electronic Journal of Boundary Elements, BETEQ 2011* (p. 348).

Schlea, M. R., Renee Brown, T., Bush, J. R., Criss Jr., J. M., Mintz, E. a., & Shofner, M. L. (2010). Dispersion control and characterization in multiwalled carbon nanotube and phenylethynyl-terminated imide composites. *Composites Science and Technology*, *70*(5), 822–828. doi:10.1016/j.compscitech.2010.01.019

Schmid, C., & Klingenberg, D. (2000). Mechanical flocculation in flowing fiber suspensions. *Physical Review Letters*, *84*(2), 290–3. doi:10.1103/PhysRevLett.84.290

Schwarz, H. (1890). *Gesammelte mathematische Abhandlungen. 2 Bande.* (Springer-Verlag, Ed.). Berlin.

Schwyzer, I., Kaegi, R., Sigg, L., Magrez, A., & Nowack, B. (2011). Influence of the initial state of carbon nanotubes on their colloidal stability under natural conditions. *Environmental pollution (Barking, Essex : 1987)*, *159*(6), 1641–8. doi:10.1016/j.envpol.2011.02.044

Semaan, C., & Soum, A. (2012). Dispersion of Carbon Nanotubes Through Amphiphilic Block Copolymers : Rheological and Dielectrical Characterizations of Poly (ethylene oxide) Composites. *Polymer*, 1–9. doi:10.1002/pc

Sen, R., Ohtsuka, Y., Ishigaki, T., Kasuya, D., Suzuki, S., & Kataura, H. (2000). Time period for the growth of single-wall carbon nanotubes in the laser ablation process : evidence from gas dynamic studies and time resolved imaging, *332*(December), 467–473.

Shelley, J., LeClaire, R., & Nichols, J. (2001). Metal-matrix composites for liquid rocket engines. *JOM Journal of the Minerals, Metals …*, (April), 1–4.

Shi, S.-L., & Liang, J. (2006). Effect of multiwall carbon nanotubes on electrical and dielectric properties of yttria-stabilized zirconia ceramic. *Journal of the American Ceramic Society*, *89*(11), 3533–3535.

Shimizu, Y., Nishimura, T., & Matsushima, I. (1995). Corrosion resistance of Al-based metal matrix composites. *Materials Science and Engineering: A*, *198*(1-2), 113–118. doi:10.1016/0921-5093(95)80065-3

Shofner, M. ., Rodríguez-Macías, F. ., Vaidyanathan, R., & Barrera, E. . (2003). Single wall nanotube and vapor grown carbon fiber reinforced polymers processed by extrusion freeform fabrication. *Composites Part A: Applied Science and Manufacturing*, *34*(12), 1207–1217. doi:10.1016/j.compositesa.2003.07.002

Singhal, S. K., Srivastava, A. K., Pasricha, R., & Mathur, R. B. (2011). In-situ amino functionalization of carbon nanotubes using ball milling. *Journal of Nanoscience and Nanotechnology*, *9*(2), 749–753.

Song, Y., & Youn, J. (2005). Influence of dispersion states of carbon nanotubes on physical properties of epoxy nanocomposites. *Carbon*, *43*(7), 1378–1385. doi:10.1016/j.carbon.2005.01.007

Speer, W., & Es-Said, O. S. (2004). Applications of an aluminum–beryllium composite for structural aerospace components. *Engineering Failure Analysis*, *11*(6), 895–902. doi:10.1016/j.engfailanal.2004.02.002

Srolovitz, D. J., Safran, S. A., & Tenne, R. (1994). Elastic equilibrium of curved thin films. *Physical Review E*, *49*(6), 5260–5270.

Steinert, B. W., & Dean, D. R. (2009). Magnetic field alignment and electrical properties of solution cast PET–carbon nanotube composite films. *Polymer*, *50*(3), 898–904. doi:10.1016/j.polymer.2008.11.053

Strano, M. S., Moore, V. C., Miller, M. K., Allen, M. J., Haroz, E. H., Kittrell, C., Hauge, R. H., et al. (2003). The role of surfactant adsorption during ultrasonication in the dispersion of single-walled carbon nanotubes. *Journal of Nanoscience and Nanotechnology*, *3*(1-2), 81–86.

Sul, I. H., Youn, J. R., & Song, Y. S. (2011). Quantitative dispersion evaluation of carbon nanotubes using a new analysis protocol. *Carbon*, *49*(4), 1473–1478. doi:10.1016/j.carbon.2010.12.017

Sumanasekera, G. U., Allen, J. L., Fang, S. L., Loper, a. L., Rao, a. M., & Eklund, P. C. (1999). Electrochemical Oxidation of Single Wall Carbon Nanotube Bundles in Sulfuric Acid. *The Journal of Physical Chemistry B*, *103*(21), 4292–4297. doi:10.1021/jp984362t

Sun, J, Gao, L., & Li, W. (2002). Colloidal processing of carbon nanotube/alumina composites. *Chemistry of Materials*, *14*(12), 5169–5172.

Sun, Jing, & Gao, L. (2003). D evelopment of a dispersion process for carbon nanotubes in ceramic matrix by heterocoagulation. *Carbon*, *41*, 1063–1068.

Suryanarayana, C. (1999). *Non-equilibrium processing of materials*. (Pergamon, Ed.) (Vol. 2).

Suryanarayana, C. (2001). Mechanical alloying and milling. *Progress in Materials Science*, *46*(1-2), 1–184. doi:10.1016/S0079-6425(99)00010-9

Sánchez, M., Campo, M., Jiménez-Suárez, a., & Ureña, a. (2012). Effect of the carbon nanotube functionalization on flexural properties of multiscale carbon fiber/epoxy composites manufactured by VARIM. *Composites Part B: Engineering*. doi:10.1016/j.compositesb.2012.09.063

Tagmatarchis, N., Georgakilas, V., Prato, M., & Shinohara, H. (2002). Sidewall functionalization of single-walled carbon nanotubes through electrophilic addition. *Chemical Communications*, (18), 2010–2011.

Tang, C., Zhou, T., Yang, J., Zhang, Q., Chen, F., Fu, Q., & Yang, L. (2011). Wet-grinding assisted ultrasonic dispersion of pristine multi-walled carbon nanotubes (MWCNTs) in chitosan solution. *Colloids and surfaces. B, Biointerfaces*, *86*(1), 189–97. doi:10.1016/j.colsurfb.2011.03.041

Tasis, D., Tagmatarchis, N., Bianco, A., & Prato, M. (2006). Chemistry of carbon nanotubes. *Chemical reviews*, *106*(3), 1105–36. doi:10.1021/cr050569o

Tatami, J., Katashima, T., Komeya, K., Meguro, T., & Wakihara, T. (2005). Electrically conductive CNT-dispersed silicon nitride ceramics. *Journal of the American Ceramic Society*, *88*(10), 2889–2893.

Thess, A., Lee, R., Nikolaev, P., Dai, H., Petit, P., Robert, J., Xu, C., et al. (1996). Crystalline Ropes of Metallic Carbon Nanotubes. *Science*, *273*(5274), 483–487. doi:10.1126/science.273.5274.483

Thostenson, E T, Karandikar, P. G., & Chou, T.-W. (2005). Fabrication and characterization of reaction bonded silicon carbide/carbon nanotube composites. *Journal of Physics D: Applied Physics*, *38*(21), 3962–3965.

Thostenson, E., & Chou, T. (2006). Processing-structure-multi-functional property relationship in carbon nanotube/epoxy composites. *Carbon*, *44*(14), 3022–3029. doi:10.1016/j.carbon.2006.05.014

Thostenson, Erik T, & Chou, T.-W. (2002). Aligned multi-walled carbon nanotube-reinforced composites: processing and mechanical characterization. *Journal of Physics D: Applied Physics*, *35*(16), L77–L80. doi:10.1088/0022-3727/35/16/103

Thostenson, Erik T, Ren, Z., & Chou, T.-W. (2001). Advances in the science and technology of carbon nanotubes and their composites: a review. *Composites Science and Technology*, *61*(13), 1899–1912. doi:10.1016/S0266-3538(01)00094-X

Timoshenko, S., Young, D. H., & Weaver, W. (1964). *Vibration problems in engineering*. (D. Van Nostrand, Ed.). New York.

Tjong, S., & Ma, Z. (1997). The high-temperature creep behaviour of aluminium-matrix composites reinforced with SiC, Al2 O3 and TiB2 particles. *Composites science and technology*, *3538*(97), 697–702.

Tohji, K., Takahashi, H., Shinoda, Y., Shimizu, N., Jeyadevan, B., Matsuoka, I., Saito, Y., et al. (1996). Purification Procedure for Single-Walled Nanotubes. *The Journal of physical chemistry. B, Materials, surfaces, interfaces & biophysical*, *101*(11), 1974–1978.

Tu, J., Yang, Y., Wang, L., Ma, X., & Zhang, X. (2001). Tribological properties of carbon-nanotube-reinforced copper composites. *Tribology Letters*, *10*(4), 225–228.

Tu, Z., & Ou-Yang, Z. (2002). Single-walled and multiwalled carbon nanotubes viewed as elastic tubes with the effective Young's moduli dependent on layer number. *Physical Review B*, *65*(23), 1–4. doi:10.1103/PhysRevB.65.233407

Tucker, C. L., & Liang, E. (1999). Stiffness predictions for unidirectional short- fiber composites : Review and evaluation. *Composites Science and Technology*, *59*, 655–671.

Ugarte, D., Chatelain, A., & De Heer Wa. (1996). Nanocapillarity and Chemistry in Carbon Nanotubes. *Science*, *274*(5294), 1897–1899. doi:10.1126/science.274.5294.1897

Vaccarini, L., Goze, C., Aznar, R., Micholet, V., Journet, C., & Dernier, P. (1999). Purification procedure of carbon nanotubes. *Synthetic Metals*, *103*(1–3), 2492–2493.

Vaisman, L, Marom, G., & Wagner, H. D. (2006). Dispersions of Surface-Modified Carbon Nanotubes in Water-Soluble and Water-Insoluble Polymers. *Advanced Functional Materials*, *16*(3), 357–363. doi:10.1002/adfm.200500142

Vaisman, Linda, Wagner, H. D., & Marom, G. (2006). The role of surfactants in dispersion of carbon nanotubes. *Advances in colloid and interface science*, *128-130*(2006), 37–46. doi:10.1016/j.cis.2006.11.007

Vigolo, B. (2000). Macroscopic Fibers and Ribbons of Oriented Carbon Nanotubes. *Science*, *290*(5495), 1331–1334. doi:10.1126/science.290.5495.1331

Villmow, T., Pötschke, P., Pegel, S., Häussler, L., & Kretzschmar, B. (2008). Influence of twin-screw extrusion conditions on the dispersion of multi-walled carbon nanotubes in a poly(lactic acid) matrix. *Polymer*, *49*(16), 3500–3509. doi:10.1016/j.polymer.2008.06.010

Wang, J., Früchtl, D., & Blau, W. J. (2010). The importance of solvent properties for optical limiting of carbon nanotube dispersions. *Optics Communications*, *283*(3), 464–468. doi:10.1016/j.optcom.2009.10.020

Wang, S., Liang, R., Wang, B., & Zhang, C. (2009). Dispersion and thermal conductivity of carbon nanotube composites. *Carbon*, *47*(1), 53–57. doi:10.1016/j.carbon.2008.08.024

Ward, P., Atkinson, H., & Anderson, P. (1996). Semi-solid processing of novel MMCs based on hypereutectic aluminium-silicon alloys. *Acta Materialia*, *44*(5), 1717–1727.

Ward-Close, C. ., Chandrasekaran, L., Robertson, J. ., Godfrey, S. ., & Murgatroyde, D. . (1999). Advances in the fabrication of titanium metal matrix composite. *Materials Science and Engineering: A*, *263*(2), 314–318. doi:10.1016/S0921-5093(98)01162-9

Wardle, B. L., Saito, D. S., García, E. J., Hart, a. J., De Villoria, R. G., & Verploegen, E. a. (2008). Fabrication and Characterization of Ultrahigh-Volume- Fraction Aligned Carbon Nanotube-Polymer Composites. *Advanced Materials*, *20*(14), 2707–2714. doi:10.1002/adma.200800295

Weber, L., Dorn, J., & Mortensen, a. (2003). On the electrical conductivity of metal matrix composites containing high volume fractions of non-conducting inclusions. *Acta Materialia*, *51*(11), 3199–3211. doi:10.1016/S1359-6454(03)00141-1

Whitsitt, E. A., & Barron, A. R. (2003). Silica Coated Single Walled Carbon Nanotubes. *Nano Letters*, *3*(6), 775–778. doi:10.1021/nl034186m

Wong, E. W. (1997). Nanobeam Mechanics: Elasticity, Strength, and Toughness of Nanorods and Nanotubes. *Science*, *277*(5334), 1971–1975. doi:10.1126/science.277.5334.1971

Wu, Y., Kim, G. Y., & Russell, A. M. (2011). Mechanical alloying of carbon nanotube and Al6061 powderfor metal-CNT composite. *Materials Science and Engineering: A*.

Xia, H., Wang, Q., Li, K., & Hu, G.-H. (2004). Preparation of polypropylene/carbon nanotube composite powder with a solid-state mechanochemical pulverization process. *Journal of Applied Polymer Science*, *93*(1), 378–386. doi:10.1002/app.20435

Xie, X., Mai, Y., & Zhou, X. (2005). Dispersion and alignment of carbon nanotubes in polymer matrix: A review. *Materials Science and Engineering: R: Reports*, *49*(4), 89–112. doi:10.1016/j.mser.2005.04.002

Xu, C. L., Wei, B. Q., Ma, R. Z., Liang, J., Ma, X. K., & Wu, D. H. (1999). Fabrication of aluminum – carbon nanotube composites and their electrical properties. *Carbon*, *37*(5), 855–858. doi:10.1016/S0008-6223(98)00285-1

Xu, X., & Wang, Z. (2012). Non-covalent dispersed carbon nanotube–benzocyclobutene composites as a bonding interface material for three-dimensional integration. *Microelectronic Engineering*, *91*, 33–38. doi:10.1016/j.mee.2011.10.010

Yan, C., Lifeng, W., & Jianyue, R. (2008). Multi-functional SiC/Al Composites for Aerospace Applications. *Chinese Journal of Aeronautics*, *21*(6), 578–584. doi:10.1016/S1000-9361(08)60177-6

Yang, J., & Schaller, R. (2004). Mechanical spectroscopy of Mg reinforced with Al2O3 short fibers and C nanotubes. *Materials Science and Engineering: A*, *370*(1-2), 512–515. doi:10.1016/j.msea.2003.08.124

Yoshio, S., Tatami, J., Yamakawa, T., Wakihara, T., Komeya, K., Meguro, T., Aramaki, K., et al. (2011). Dispersion of carbon nanotubes in ethanol by a bead milling process. *Carbon*, *49*(13), 4131–4137. doi:10.1016/j.carbon.2011.05.033

Yu, J., Grossiord, N., Koning, C., & Loos, J. (2007). Controlling the dispersion of multi-wall carbon nanotubes in aqueous surfactant solution. *Carbon*, *45*(3), 618–623. doi:10.1016/j.carbon.2006.10.010

Yu, M.-F. (2000). Strength and Breaking Mechanism of Multiwalled Carbon Nanotubes Under Tensile Load. *Science*, *287*(5453), 637–640. doi:10.1126/science.287.5453.637

Zapata-Solvas, E., Gómez-García, D., & Domínguez-Rodríguez, A. (2012). Towards physical properties tailoring of carbon nanotubes-reinforced ceramic matrix composites. *Journal of the European Ceramic Society*, *32*(12), 3001–3020. doi:http://dx.doi.org/10.1016/j.jeurceramsoc.2012.04.018

Zhang, Jin, Zou, H., Qing, Q., Yang, Y., Li, Q., Liu, Z., Guo, X., et al. (2003). Effect of Chemical Oxidation on the Structure of Single-Walled Carbon Nanotubes. *The Journal of Physical Chemistry B*, *107*(16), 3712–3718. doi:10.1021/jp027500u

Zhang, Jing, & Gao, L. (2007). Dispersion of multiwall carbon nanotubes by sodium dodecyl sulfate for preparation of modified electrodes toward detecting hydrogen peroxide. *Materials Letters*, *61*(17), 3571–3574. doi:10.1016/j.matlet.2006.11.138

Zhang, Q.-H., & Chen, D.-J. (2004). Percolation threshold and morphology of composites of conducting carbon black/polypropylene/EVA. *Journal of Materials Science*, *10*(5), 1751–1757. doi:10.1023/B:JMSC.0000016180.42896.0f

Zhang, S. C., Fahrenholtz, W. G., Hilmas, G. E., & Yadlowsky, E. J. (2010). Pressureless sintering of carbon nanotube-Al 2O 3 composites. *Journal of the European Ceramic Society*, *30*(6), 1373–1380.

Zhang, X.-X., Deng, C.-F., Wang, D.-Z., & Geng, L. (2005). Synthesis and thermal stability of multiwall carbon nanotubes reinforced aluminum metal matrix composites. *Transactions of Nonferrous Metals Society of China (English Edition)*, *15*(SPEC. ISS. 2), 240–244.

Zhang, Y., Zhang, Q., Li, Y., Wang, N., & Zhu, J. (2000). Coating of carbon nanotubes with tungsten by physical vapor deposition. *Solid State Communications*, *115*(1), 51–55. doi:10.1016/S0038-1098(00)00125-3

Zhong, R., Cong, H., & Hou, P. (2003). Fabrication of nano-Al based composites reinforced by single-walled carbon. *Carbon*, *41*, 2001–2004.

Zhou, S., Zhang, X., Ding, Z., Min, C., Xu, G., & Zhu, W. (2007). Fabrication and tribological properties of carbon nanotubes reinforced Al composites prepared by pressureless infiltration technique. *Carbon Nanotubes*, *38*(2), 301–306. doi:10.1016/j.compositesa.2006.04.004

Zhou, Y., Yang, W., Xia, Y., & Mallick, P. K. (2003). An experimental study on the tensile behavior of a unidirectional carbon fiber reinforced aluminum composite at different strain rates. *Materials Science and Engineering: A*, *362*(1-2), 112–117. doi:10.1016/S0921-5093(03)00214-4

Zhu, H. W., Xu, C. L., Wu, D. H., Wei, B. Q., Vajtai, R., & Ajayan, P. M. (2002). Direct synthesis of long single-walled carbon nanotube strands. *Science*, *296*(5569), 884–886.

CHAPTER 3: MATERIALS AND METHODS

3.1. MATERIALS

3.1.1. POLYMER MATRIX COMPOSITES

Polyvinyl butyral (PVB) has been used in the form of the commercial Butvar product (produced by Solutia), and two kinds of PVB were used: PVB-98, containing between 18 and 20% of PVOH and with a molecular weight between 5000 and 6000; PVB-76, containing between 12 and 14% of PVOH and with a molecular weight between 10000 and 11000. Nanocyl™ NC7000 nanotubes (Figure 30) were used, with an average diameter of 9.5 nm, average length of 1.5 µm, 90% carbon purity, 10% metal oxide residuum after burning out of the carbon, and a surface are around 250-300 m^2/g. The ethanol used as dispersion mean for the dispersion tests and also as solvent for the slurries preparation is provided by Sigma Aldrich.

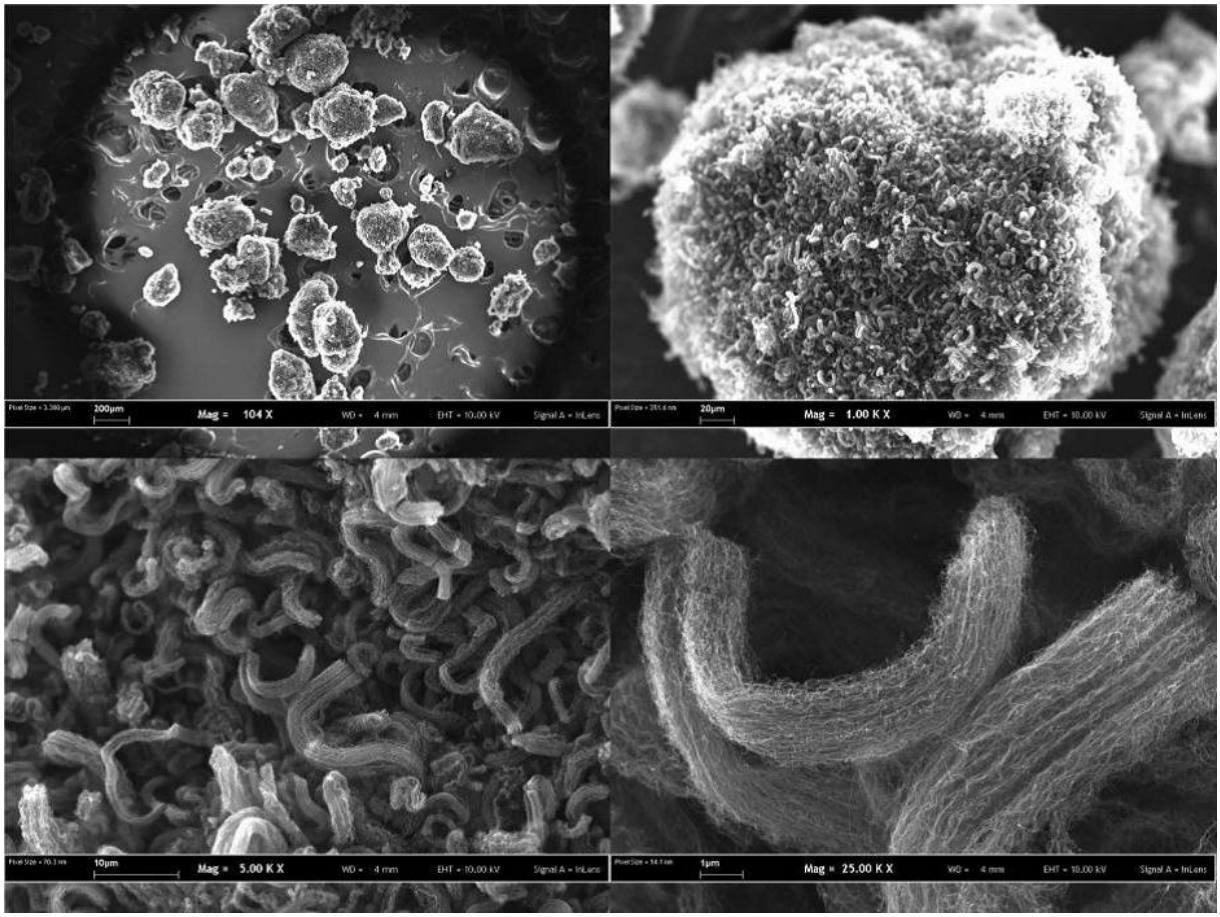

Figure 30 -Nanocyl™ NC7000 nanotubes in their different aggregation forms.

3.1.2. CERAMIC MATRIX COMPOSITES

Commercially available α-SiC powders (H.C. Starck UF-15, Germany with a mean particle size of 0.55 μm) were used in this study for the fabrication of multilayer ceramic composites. Carbon (Alfa Aesar flake 7–10 μm) and Boron (H.C. Starck amorphous grade I, 1–2 μm) were used as sintering additives for SiC in order to improve both its densification and mechanical properties of resulting materials, since they were adopted successfully for the sintering of SiC laminates (Badini, Fino, Ortona, & Amelio, 2002; Biamino et al., 2008). The slurry preparation consisted in mixing ceramic powders and multiwalled carbon nanotubes Nanocyl™ NC7000, solvent (ethanol by Sigma Aldrich) and fish oil (Sigma Aldrich) as a proper dispersant. Subsequently a plasticizer (polyethylene glycol, Bisoflex 102 Cognis) and a binder (polyvinyl butyral, Butvar B76 Solutia) were added to the slurry.

3.1.3. METAL MATRIX COMPOSITES

Micrometric aluminium powders (-365 mesh ≈ 44 μm, 99.5% purity) were supplied by Alfa Aesar (Figure 32), nanometric aluminium powders (spheres of 60-80 nm diameter, 99.9% purity) were supplied by SkySpring Nanomaterials Inc.. The multiwall carbon nanotubes were produced by Sigma Aldrich. They are characterized by O.D. 6-13 nm and 2.5-20 μm in length, with purity higher than 99%. As shown in Figure 31, they appear tangled and form sort of nuggets of a few micrometre size. Each nugget is made of several elongated snake-like bundles with diameter of a few tens of nanometres and length around the micrometre. Because of this characteristic a pre-dispersion step is needed before the powders mixing. As dispersion mean, 2-propanol by Sigma Aldrich was used.

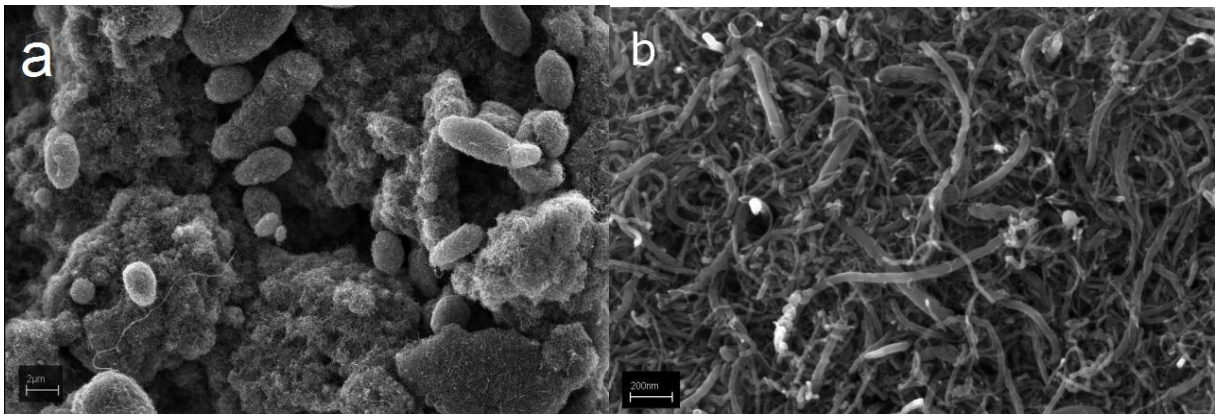

Figure 31 - (a) MWCNTs as received in nuggets shapes; (b) a magnification

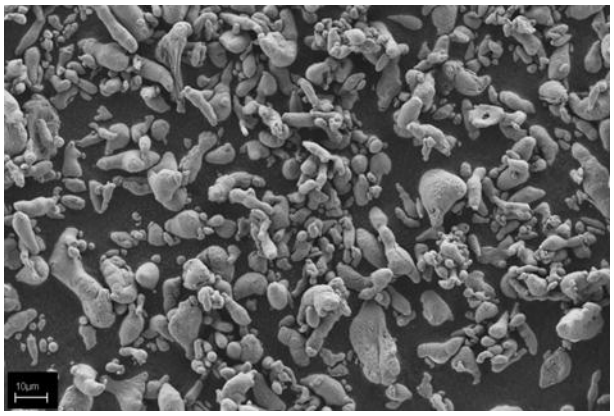

Figure 32 - SEM image of micro aluminium powder particles

3.2. CARBON NANOTUBES DISPERSION AND POWDERS PREPARATION

3.2.1. ULTRASONICATION

The principles of ultrasonication technique were extensively reported in section 1.4.1. In the present thesis work the sonication devices were used for the carbon nanotubes dispersion and distribution in proper solvents, as a preliminary step behind the production of PMCs and MMCs. The size of the cavitation bubble and, consequently, the dispersion grade of CNTs depends on sonication parameters of frequency and power. Lower frequency ultrasound, typical of tip/probe ultrasonicators, produces larger and more energetic cavitation bubbles and so a better CNTs dispersion (Hilding, Grulke, George Zhang, & Lockwood, 2003). Nevertheless the ultrasound tips are also responsible for an increased number of defects on the nanotubes, compared to the bath sonicators. Also an higher applied ultrasonication power, could correspond to a similar increase in the defect density and a reduction of the average length of the nanotubes (Vichchulada et al., 2010). The nanotube scission is thought to be due to fast collapsing cavitation bubbles that provide a high local solvent velocity, which could potentially produce a shear force exceeding the tensile strength of the nanotube and thus cause its fragmentation (Hennrich et al., 2007; Lucas et al., 2009).

During this research work two different sonicators were used: a probe ultrasound sonicator SONICS®, Vibra-Cell VCX 500 (Figure 33) and a lower energy bath sonicator SONICA Ultrasonic cleaner by Soltec™. Several dispersion tests were performed in order to adjust the different sonication steps and to obtain the higher dispersion level coupled with the minimum damage to the CNTs.

Figure 33 - SONICS®, Vibra-Cell VCX 500 probe sonicator

3.2.2. HIGH ENERGY MILLING

Figure 34- Planetary milling device

The milling process and principles have been depicted in section 1.4.1, because the milling technique is very commonly applied to the preparation of well dispersed carbon nanotubes composites. For the production of aluminium matrix composites a particular technique, known as high energy planetary milling has been used. Compared to the conventional ball mills which require a long milling time, modern high energy mills equipped with a high speed rotor rotating up to several thousand times per minute are known to be very effective for milling. Their high energy input and the use of small grinding media allow the achievement of a very small particle size in a very short processing time, especially in ceramic fields (Calka & Radlinski, 1991; Feng, Han, & Owen, 2004).

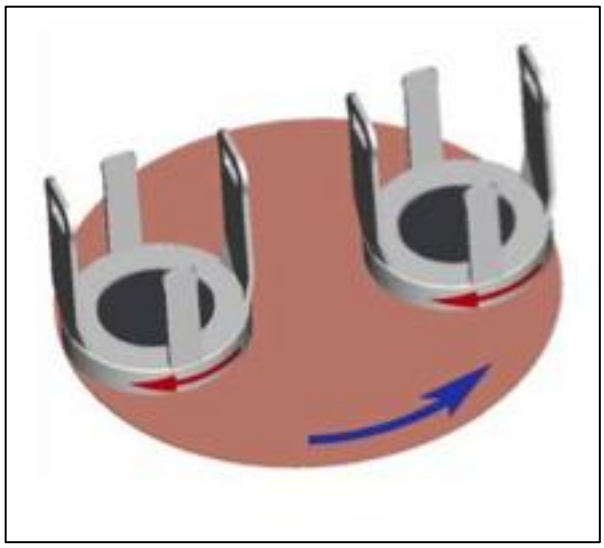

Figure 35 - The position and motion of the two pots on the rotating base of the HEM device

A planetary ball mill is generally constituted by two pots on a disk (as shown in Figure 35), and the pots and the disk are simultaneously and separately rotated at a high speed. The high rotation speed of the pot and the revolution of the disk make the balls move strongly and violently, leading to fine grinding of a product due to generation of large ball impact energy. The high-energy of balls during the milling is attributed to an extremely high centrifugal force acting on the balls by rotating a pot as well as a disk at high speeds (Mio, Kano, Saito, & Kaneko, 2002). The dynamic process of high energy ball milling, particularly planetary ball milling, is still far from fully understood. The difficulty is mainly associated with the complex physical phenomena involved in the process characterised by highly dynamic, non-linear behaviour of a multi-physics and multi-scale nature (Feng et al., 2004).
In this thesis work the High Energy Milling device used was a FRITSCH®, Pulverisette 5. For the operating conditions refer to the section of powder preparation, in chapter 4.

3.3. SINTERING: THE PRESSURE ASSISTED FAST ELECTRIC SINTERING (PAFES)

A large number of sintering techniques involves the consolidation of loose powders or a cold formed compact into a container which is heated to and then held at the desired temperature, while pressure is applied and maintained for a given period of time. When heat is provided by an electric current passing through the powders and/or their container, thus exploiting the consequent Joule effect, we can talk of Electric Current Activated/assisted Sintering (ECAS).

The **sintering process** is intended to materials that may belong to the class of ceramic, metallic, polymeric and composite materials, in the form of powder. The objective of this treatment is to eliminate the porosity existing between the various particles constituting the powder, and so to obtain the desired density values. The evolution of the structure of the powders starts from the movement of atoms, from positions close to those of contact between the particles, according to diffusion phenomena and facilitated by the high temperatures and pressure. Other streams of atoms that are removed from the surfaces of the particles and move toward the cavity to be filled are observed. In Table 4, with reference to Figure 36, are listed the transport phenomena that occur during sintering. As a result of all these motions of atoms, the formation of the "neck" among the particles is achieved. This process comes along up till the gaps present between the grains are completely filled (Anderson, 2003).

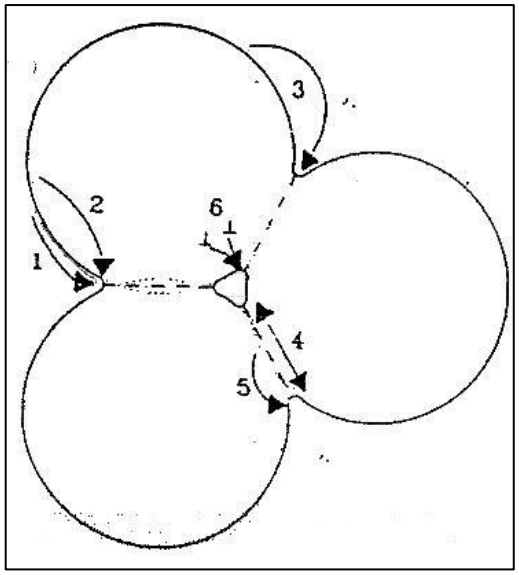

Figure 36- Phenomena involved during a typical sintering process

Phenomenon (with reference to Figure 36)	Kind of motion	Atoms origin
1	Surface diffusion	Surface
2	Lattice diffusion	Surface
3	Vaporisation	Surface
4	Contact diffusion	Contact zones among particles
5	Lattice diffusion	Contact zones among particles
6	Lattice diffusion	Dislocations

Table 4 - List of the phenomena occurring in a sintering process with reference to **Figure 36**

The use of the electric current, to aid pressure assisted sintering of materials, is characterized by technological and economic advantages over conventional sintering methods such as faster heating rate, lower sintering temperature, shorter holding time, consolidation of difficult-to-sinter-powders, elimination of the need of sintering aids, no need of cold compaction, less sensitivity to initial powders characteristics, and marked comparative improvements in the properties of materials consolidated. In particular, lower temperatures and shorter processing times give the possibility to sinter nanometric or metastable powders to near theoretical density with little grain growth or retention of metastability and cleaned grain boundaries (Orrù, Licheri, Locci, Cincotti, & Cao, 2009).

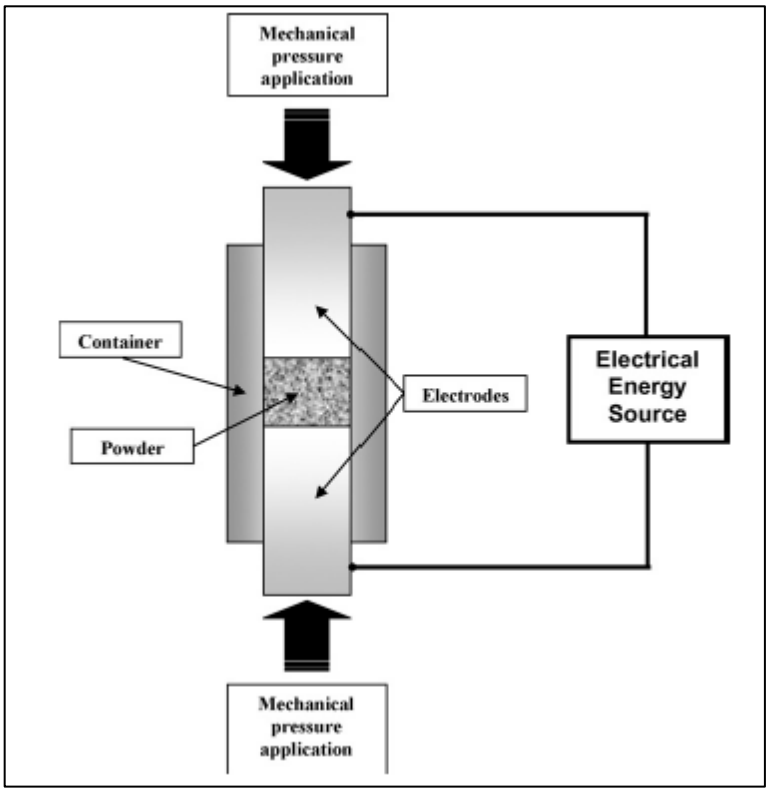

Figure 37- Schematic representation of ECAS process (Orrù et al., 2009)

The Electric Current Assisted Sintering (ECAS) process is schematically shown in Figure 37. It simultaneously applies an electric current along with a mechanical pressure in order to obtain theoretically full dense specimens. The applied electric current and mechanical load may be constant throughout the sintering process or may be tuned. In particular, the current may be adjusted with the aim of follow a specific temperature cycle. Materials to be consolidated can be electrically conducting or insulating, and are placed in a container (die, tube, etc.) and heated by applying the electric current. In most of cases the container material should be conducting in order to guarantee the electrical circuit closure. For the same reason, the electrodes carrying the current, and all blocks, spacers or plungers, inserted if necessary in the circuit, should be made of electrical conducting material (copper, graphite, stainless steel, etc.). The use of graphite containers, which are mostly applied in ECAS processes, limits the mechanical pressure levels to low values, generally 100 MPa, but provides a reducing component to the sintering environment.

The ECAS is very similar to Hot Pressing (HP), but the heating is induced by an electric current supply, leading to very rapid and efficient increment of temperature. The heating rate during the ECAS process can reach 1000°C/min and, as a consequence, the processing time varies from fraction of seconds to minutes depending on the material, part size, configuration, and equipment capacity.

The main problems of ECAS are the adequate electrical conductance of the powders and the homogenous temperature distribution inside the container. In fact, current and temperature gradients are very sensitive to the homogeneity of density distribution. Moreover, large density spatial variation, especially at the beginning of current flow, may result in high local overheating or even melting. For these reasons, generally the specimens sintered have small sizes and simple shapes (cylindrical or rectangular shape).

In the earliest period of ECAS development, the equipment's were fabricated and based on specific products and materials; the first specimens were produced in 1906 for the fabrication of incandescent lamps of tungsten or molybdenum, in vacuum with DC current and without an applied pressure. In 1913, the first apparatus with the application of a simultaneous electric current and mechanical pressure was used to sinter refractory metals and conductive carbide/nitride powders, with a boron nitride electrically insulated tube as a mould, the punches in graphite and high DC voltage 15 kV then decreased to 500 V (or 110 V). An important advance was obtained in 1927, when Davis increased sintering rates obtaining sintering of refractory metals in few minutes. The die was a silica tube with two electrodes made by water-cooled steel as punches to apply the pressure. The major contribution to the exploration and enhancement of the new technique had been the investigations about production and densification of tungsten carbide-cobalt tools, between 1920 and 1940. In 1945 Ross invented the first automated equipment. He used a pulses pressure and current, and both the parameters contributed to the improvement of the sintering process

generating a better densification and an increased heating control, respectively. Inoue has been the most important innovator of ECAS technique: in 1966, he developed an Electric discharge sintering or Spark Sintering, with an "impulsive spark discharge". The method consisted in apply a high frequency impulsive current and low pressure at the beginning of the process in which it is promoted the spark between particles, at local level. Then in a second step, the pressure is increased to help to obtain a fully dense material by the promotion of plastic deformation of the particles. Commercialization of this machine started when Inoue's patents expired in 1980s. Based in his inventions, PAS and SPS started to be produced. The most successful commercialization was made by Sumitomo Coal Mining Co. Ltd from 1990s with a SPS apparatus with DC pulse generator. The lasts years, researches have been focused on automation. The inventions patented are semi- or fully automated: multi-head (Sumitomo/SPSS), tunnel (Tokita 2002), rotary table (Tokita and Nakagawa, 2002) and shuttle (2004) systems. The last patent by Tokita in 2007 is for sintering of nanopowders in protective atmosphere (Grasso, Sakka, Maizza, 2009).

All the equipment above mentioned, can be used for Resistance Sintering (RS) or fast ECAS. In ultrafast ECAS or Electric Discharge Sintering (EDS), the machines could operate with one or a maximum of three capacitor discharges, where every capacitor has to be just for 0.1 s, and a current density of 10 kA/cm^2. The Joule heating effect occurs directly in the powder compact and it is not conducted by the die and punches, like in fast ECAS. In general, this technique uses a single current pulse with a relatively high mechanical pressure. The mould could be insulating (glass, Bakelite, alumina, etc) or conductive (graphite, steel, etc). The powders function as a resistance into the circuit. In the surface-surface contact among the particles, the heating is generated by Joule effect. It is a very fast method that does not need an inert gas to be performed (Grasso et al., 2009). The first device patented was register in 1933, by Taylor. Like many of the patents, this was created for fabrication of tungsten carbide-cobalt materials. A very fast sintering was planned to limit grain growth and enhance mechanical properties of the final product. The improvements in performance of ECAS machines were developed due to the necessity of reproducibility in sintering results and materials properties for an industrialization process.

With respect to the applied current characteristics, several classifications of the ECAS processes have been reported (Groza & Zavaliangos, 2000; Matsugi, Ishibashi, Hatayama, & Yanagisawa, 1996; Weissler, 1981). However, in Orrù et al. opinion (Orrù et al., 2009), two main categories can be identified:

- Resistance Sintering (RS)
- Electric Discharge Sintering (EDS)

RS involves the application of a low-voltage (of the order of few tens of volts), high current (of the order of thousands of amps) with a suchlike waveform (direct current (DC), alternate current (AC), rectified current (RC), pulsed, etc.). Higher voltages and currents are generally used during EDS, being the electric energy discharged through few heavy pulses. In addition, the change of current with time (dI/dt) during the EDS process has the potential to provide a significant contribution to the compaction by exploiting electromagnetic phenomena (Clyens, Al-Hassani, & Johnson, 1976; Johnson, Clyens, & Hassani, 1976). Another significant difference between EDS and RS processes is the characteristic processing time: the EDS processing time typically falls in the range 10^{-5} to 10^{-2} s, while the one of RS processes is of the order of 10^{0} to 10^{3} s.

In **Electric Discharge Compaction (EDC)**, also known as Environmental Electro-Discharge Sintering (EEDS), electrical energy is suddenly discharged from a capacitor bank. The powders are generally contained in an electrically non-conducting tube. The high transient current causes heating and sintering of sample particles. But simultaneously this current generates an intense magnetic field which can contribute to the sintering. The use of pressure is optional, and it can be both static and dynamic. For a proper densification, higher than 95%, is necessary a cold press preliminary step of the powders. Tuning some of the operating conditions, such as the variables of the electric circuit, powder properties, weight and geometry of the sample, is possible to obtain very good results in terms of density.

This process was from the beginning a promising candidate to enhance the processing materials routes because is easy, fast and with lower cost. However, few results have been satisfactory. These results depend on the instantaneous current density and only partially on the discharge energy. An example of method derived from EDS is High-Energy High-Rate (HEHR), that exploits Faraday effect to transform stored rotational kinetic energy in electrical one by a 10 MJ Homo-Polar Generator (HPG), which can operates with low voltage (5-25 V), in pulse mode and high current. The sintering process is achieved by a pulse resistive heating which is produced at the interface between the particles, with a current density between 100-500 MA/m^2, in more or less 3 s, and with a high amount of pressure from the beginning and hold for an estimated time of 3-5 minutes.

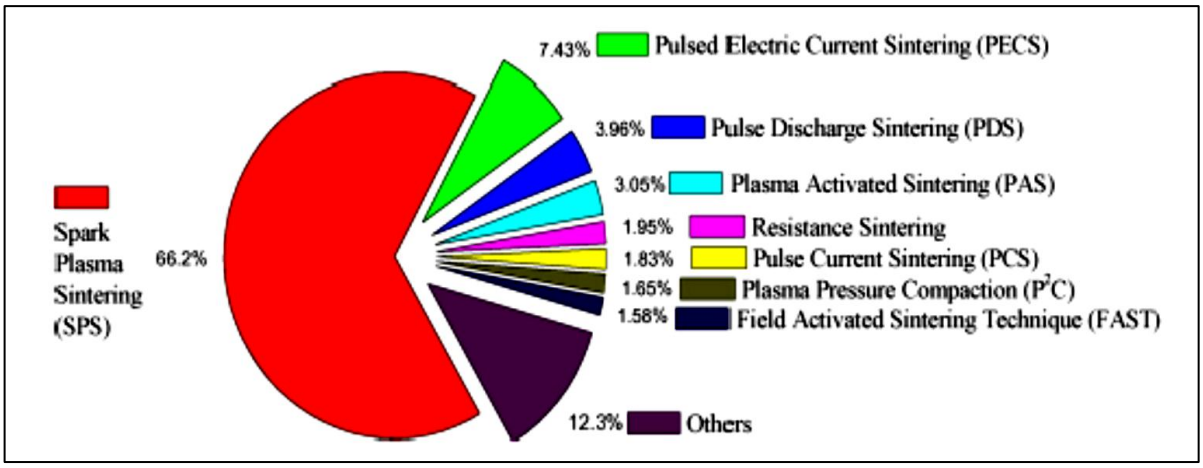

Figure 38 - RS processes designation (Orrù et al., 2009)

During more than 80 years, several devices based on the **Resistance Sintering (RS)** model have been projected and used. The main classified RS family techniques and their percentage of utilization are reported in the pie chart in Figure 38. Therefore, since the application of an electric current is the main feature of RS techniques a clear classification of them may be obtained by considering the electric current waveform that is applied during the process. The four waveforms mainly used by the scientific communities are reported in Figure 39, where the parameters needed for their characterization are also indicated.

The simpler current waveform is the constant DC (a), which is completely characterized by the current intensity I. The AC (b) is determined by maximum current intensity I_{max}, along with its frequency ω. The third waveform (c) is the pulsed DC, where the parameters needed for its complete definition are the maximum current I_{max}, the pulse duration t_{pulse}, and the on- and the off-time, t_{ON} and t_{OFF}, respectively. In portion d, a RS process two stages of applied current, is shown. During the first one, a pulsed electric current is imposed while a constant DC followed in the second stage. In addition to the parameters that characterize each stage, their relative duration, t_I and t_{II}, should be given.

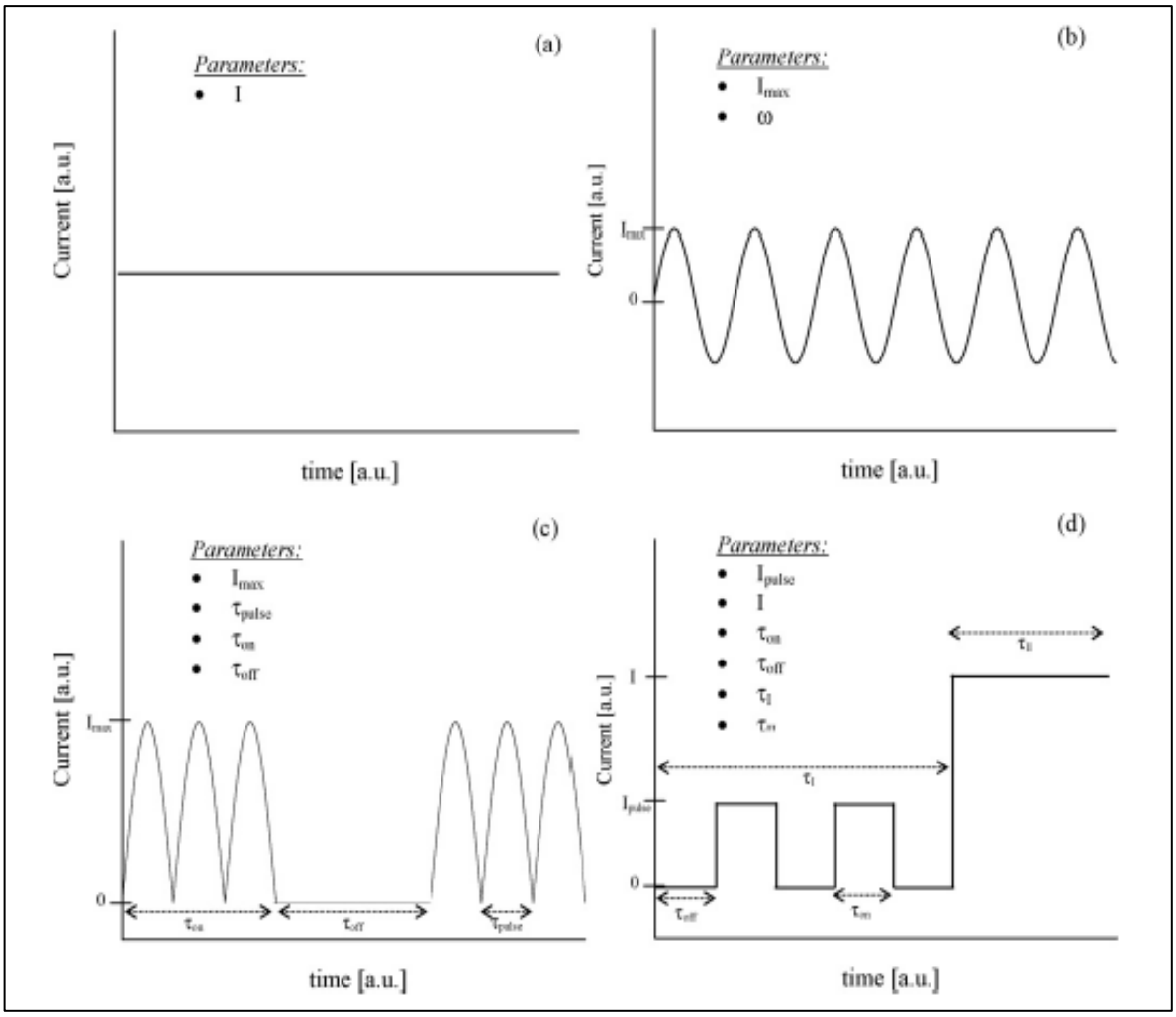

Figure 39 - Typical electric current waveforms applied in the RS processes:
(a) constant DC; (b) AC; (c) pulsed DC and (d) pulsed DC + DC.

The absence of rigid schemes of design means that different acronyms referred to the same procedure have been widespread: we can number among the RS processes SPS (Spark Plasma Sintering), FAST (Field Activated Sintering Technique), PPC (Plasma Pressure Compaction), PCS (Pulse Current Sintering), PAS (Plasma Activated Sintering), PDS (Pulse Discharge Sintering), PECS (Pulsed Electric Current Sintering). SPS, the most famous apparatus, is defined as a method in which is possible the consolidation of a fully dense material, by an extremely fast heating (> 500°C/min) and cooling rates, in very short holding times (minutes), and with a significant reduction of the sintering temperature compared with conventionally fabrication process. The heat is generated, as we mentioned before, in local and massive way by an electrical current of the type DC, AC, and/or pulse DC. The most applied is pulse DC (in general, 3.3 ms of 0.5 to 10 kA of intensity) (Riedel & Chen, 2008).

The sintering stage is reached by activation of more than one of the mechanisms related to surface oxide removal, electro-migration and electro-plasticity between the particles by combining electrical current to promoted resistive heat and load pressure to compact the sample. There is a local resistive

heat that helps to create the bonding between the particles, and a massive one for the continued plastic deformation until densification and consolidation (Grasso et al., 2009).

The device used in this thesis is called **Pressure Assisted Fast Electric Sintering (PAFES)** and it constituted by a hydraulic double effect press connected to an electric current generator, with waveforms of constant DC, AC, pulsed DC or combined cycles. The generator, with an Insulated Gate Bipolar Transistor, can work with a current intensity of 2000 A and voltage of 10 V for a maximum electrical power of 30 kVA. The frequency of the AC current is in the range of 1-800 Hz (Deorsola, Vallauri, Ortigoza Villalba, & Benedetti, 2010).

The sintering process, identified as "Fast Electric Pressure Assisted Sintering", uses the alternating current, whereby it is possible to control the electrical parameters as the wave shape and frequency. This technique, in a similar manner to the other belonging to the family of RS (in particular SPS and FAST), is coupled to the simultaneous application of uniaxial pressure. The remarkable similarities between the technique PAFES and the SPS allow to make comparisons between them, so as to understand the phenomena which lead to densification of the material. The technology SPS (Spark Plasma Sintering) was so named because, thanks to the use of continuous and pulsed current, it was assumed they came to pass phenomena of electric arc and transformation of the solid phase in the plasma. Plasma is a ionized gas phase containing ions and free electrons, which in total has neutral charge. Hulbert et al. (Hulbert et al., 2008) were the firsts to study the presence of these possible effects, generated in a sample following the passage of a current very intense, continuous type. In fact it was found that, during the sintering process, does not occur neither the formation of the plasma phase nor the generation of the electric arc. The assumptions, made regarding the plasma formation have lost over the years, consent and was thus possible to the spread of techniques that exploit other types of electric current, such that alternating, which leads to the birth of the technology PAFES. The sintering treatment of the powder with a dynamic technology that allows to adjust different parameters and to find the best compromise in all circumstances, has contributed to the use and dissemination of tools PAFES.

To perform the sintering of aluminium and composite aluminium-carbon nanotubes powders, using the technique PAFES, we used a special instrument, present at the Department of Applied Science and Technologyof the Politecnico di Torino (Figure 40). Such an instrument is divided into two main bodies: the pressing system hydraulic double effect, entirely designed and built by engineers of this institution, and by a current generator able to provide various types of waveform. The pressing system is constructed in such a way that the pistons can be carried through by the electric current.

Figure 40 - The PAFES apparatus. In the red panel the sintering chamber.

The experimental procedure with the PAFES was conducted on pre-treated powders. After a cold uniaxial pressing the green specimens were put inside a graphite cylindrical die of the same diameter; the temperature was monitored by a type K thermocouple in contact with one of the two graphite punches. The sintering was performed in a low vacuum atmosphere and it consisted in a cycle (AC current used, 50 Hz frequency): 15 minutes at 630°C (reached in a couple of minutes) with a 60 MPa pressure applied continuously. After that, pressure and current supplies were interrupted.

3.4. THE TAPE CASTING TECHNOLOGY

Tape casting technologies was introduced in the 1940s by Glenn Howatt as a new technique for the fabrication of ceramic sheet capacitors (Brook, Cahn, Haasen, & Kramer, 1996), however the technique was already very well known in other industries, like, paper, painting and plastic ones (Mistler & Twiname, 2000). This method is based on a suspension of a mix of ceramic powders and organics components (dispersant, binder and plasticizer) in a proper solvents, which is spread or "cast" on a flat moving support. After the actual casting step the solvents are slowly evaporated to obtained a "green ceramic tape" in form of a thin sheet. The thickness reported in tape casting go from 5 microns to some millimetres (Mistler & Twiname, 2000). The tape casting technique could be applied not only to the production of ceramic sheets but, applying proper modification to the method, also to metal ones.

In his first attempts, Howatt used a porous plaster to applied water as liquid media but, in 1950s, the American Lava Corporation introduced the use of a plastic carrier or "non-absorptive moving polymer carrier", tha tallowed mass casting films. Figure 41 reports the basic scheme of a typical tape casting apparatus. A stationary Doctor blade, which is the moving port of the slurry reservoir, can allow to the slurry to be cast on the moving carrier polymer film, when opened, and can also control the quantity of suspension involved in the process, and the final thickness of the tape. The reservoir, the carrier support and the slip complete the scheme. There are a lot of parameters to take into account during the tape casting process: the slurry formulation, its rheological properties, the gap of the doctor blade and its shape, the speed of the carrier, the reservoir depth, the drying conditions and so on.

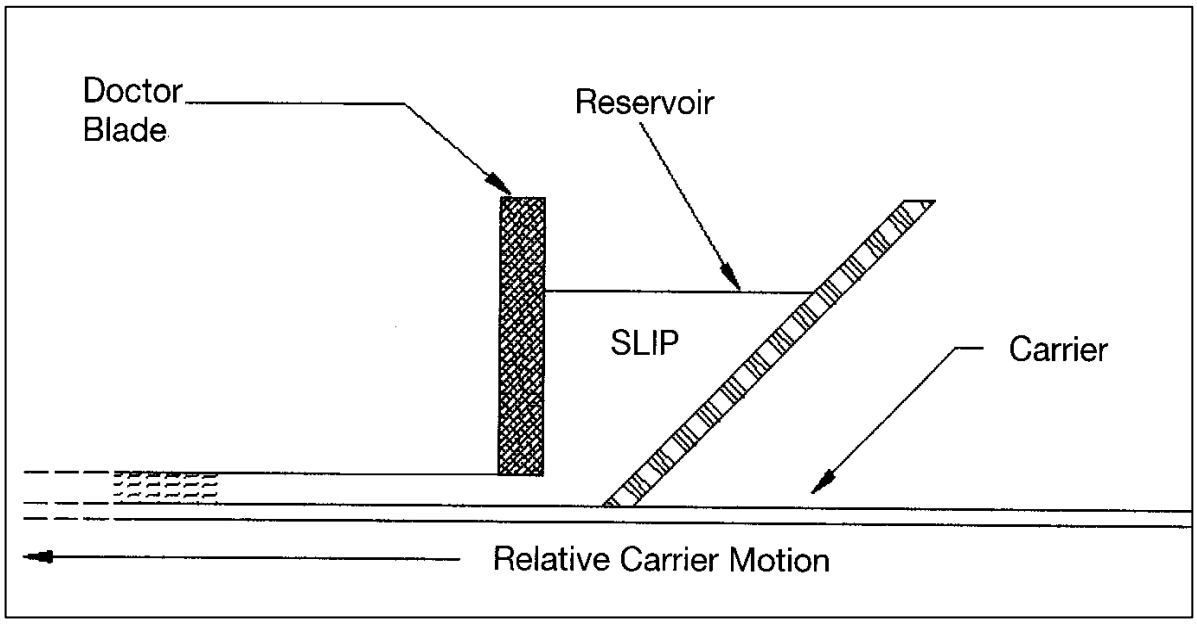

Figure 41 – Diagram of a typical tape casting apparatus

This process offers a low cost-effective application for industrial and laboratory testing technique. Is one of the best methods to fabricate ceramic layers large, thin and flat, and can be successfully used to produce multi-layered structures. The main advantage of tape casting is the possibility to obtain a homogeneous material, characterized by low density variations, and with controlled pore size distribution. However, this method is affected by the stability of the slurry, which can influence the homogeneity of the green specimen, and by the packing of the particles in the green tapes, which can determine the mode of sintering and the properties of the final products (Mukherjee, Maiti, Das Sharma, Basu, & Maiti, 2001). For this reason it is necessary to study and understand all aspect regarding every constituent of the slurries.

Because of the principle of the tape casting technique, the most important elements of the process are the **powders**. They can heavily determine the final product properties (Brook et al., 1996). The criteria for their selection depend on the properties required for the final material and its applications. Hence, before starting a new process, it would be necessary a complete and detailed characterization of the powders. In particular the parameters to be considered are:

- Chemical purity
- Particle size and size distribution
- Particle morphology
- Degree of segregation or agglomeration
- Compositional homogeneity
- Sintering activity
- Ability to be mass-produced
- Cost of production

For tape casting technology is required a very good knowledge of powder preparation, powder processing and packaging that will give the characteristic of the slurry, green body tape and final sintering product. The aim of an adequate preparation, processing and packaging is to avoid in homogeneity and segregation during slurry. When the “ideal” particle size, that in the case of tape casting have to reached a superficial area between 5 and 15 m^2/g (Mistler & Twiname, 2000) is possible to proceed to study the packaging of the powders. The surface area is a parameter very important because provide the best value for the interaction in what is possible to have a good dispersion, lubrication or binding qualities, because there is a direct relation between the total powder area and the quantity of organic have been necessary for the process reaction. The selection of the proper dispersant/solvent combination, as well as the proper dispersant and dispersant concentration, are all critical factors for the very high surface-area powders (Mistler & Twiname, 2000). Another general rule that can be useful for the powder choice is the packaging of the

particles. Two different approaches could be used for the evaluation of the packaging of the powders: the theoretical one was established by McGeary in 1961. He predicted a maximum packaging of 74 vol%, for mono-size particles with ideal sphere shape, and no Van der Waals interactions between the particles. The arrangement has to be octahedral or tetrahedral, with a coordination number of 12. For coordination number of 10, 8 and 6 theoretical calculation of the packing densities would be 69.8 vol.%, 60.5 vol.% and 52.4 vol.% respectively. On the contrary, experimental calculations indicate a packaging around 58 to 65 vol% when the coordination number is about 8. For liquid suspensions, a very good approximation for the values of packing density is established around 40-45 vol% with particles of approximated 1 μm of diameter. The most adequate is a narrow size distribution (Brook et al., 1996).

The **solvent** or mixture of solvents used to formulate tape casting, suspensions must have the following characteristics:

- Dissolving the organics components of the slurry: binder, plasticizers and additives.
- Dispersion of the powder (ceramic or intermetallic).
- Distribution of all ingredients homogeneously throughout the slip to create a homogeneous mixture.
- Giving the desired rheological properties to the suspension like suitable viscosity.
- Providing a good evaporation rate at moderate temperature.
- Ensuring consolidation of the tape.

Also other factors could influence the solvent selection as production costs, effects on health and environmental impact. All organics present in the slip, need to be dissolved as well, for that reason it is widely used a mixture of solvent. Water is a more environmental friendly solvent, however is difficult find binders and plasticizers water-soluble, and it also requires longer evaporation times. The most used solvents for tape casting and their properties are shown in

Table 5.

Another relevant parameter is the capability of the solvent to disperse the powders. The chemo-physical properties of the particles and of the liquid medium have to be taken into account but the most significant is the wettability. The wettability can be affected by capillary forces, because of the powder in general presents some agglomeration that produces caverns (like capillary tubes) where air is trapped, and the liquid needs some force to enter in. To provide a satisfactory wetting angle, it is possible to make use of wetting agents.

Solvent	Boiling Point [°C]	Evaporation rate [n-butylacet.=1]	Heat of vaporization [J/g]	Viscosity at 25°C [mPa s]	Polarity Et(30) [kJ/mol]	Relative permittivity	Surface tension [mN/m]
Water	100	0.16	2260	1	264	80	73
Methanol	65	3.70	1100	0.6	232	33	23
Ethanol	78	2.65	860	1.2	217	24	23
Butanol	118	0.44	578	2.9	210	18	22
Benzyl alcohol	205	<0.01	415	5.8	213	13	35
Isopropyl alcohol	82	2.08	578	2.4	204	18	22
Ethylene glycol	198	<0.01	800	20	236	37	48
Ethyl acetate	77	4.95	360	0.4	160	6	23
Butyl acetate	127	1.00	310	0.5	155	5	26
Methyl ethyl ketone	80	4.59	444	0.4	173	18	25
Acetone	56	7.70	524	0.3	177	21	25
Trichloroethylene	86	4.90	243	0.4	150	3	25
Toluene	110	1.96	352	0.6	142	2	29
o-/p-Xylene	140	0.55	327	0.7	141	2	28
Cycloexanone	155	0.24	427	0.8	171	18	35

Table 5 - List of the most common tape casting solvents and their properties

Surfactants are defined as chemical agents that alter the interaction between particles by modification of their surfaces properties. The literal meaning is SURFace – ACTive – AgeNTs. They include different chemical aids like dispersants, deflocculants, wetting agents, flattening agents, flocculants and many others. In tape casting, dispersant agents are used to control the natural tendency of the small powder particles to agglomerate into the slurry (Mistler & Twiname, 2000). This phenomenon is connected with the attractive and repulsive forces between the particles and can be analysed in terms of the sum (V_t) of their potential energies V_a (Van der Waals) and V_r (electrostatic and steric). The Van der Waals forces, are attractive forces generated by the interaction of atoms with permanent or induced electron/nucleus dipoles on the surface of the particles (Brook et al., 1996). The repulsive forces can be classified as electrostatic and steric ones. The former occurs when the particles have the same electric charges sign and it is most common in polar solvents like water-based slurries. The latter, are predominant in non-polar organic solvents, where the electrostatic forces should be smaller. The mechanism of response is related to the adsorption of the long chained macromolecules by the surface of the particle. The surfactant should be a molecule with a polar or ionic hydrophilic “head” and non-polar hydrophobic “tail”. They are classified as

anionic, cationic, zwitterionic, or non-ionic agents and are able to reduce surface and interface tensions of liquids (Brook et al., 1996).

The aim of adding surfactants is to obtain an electrosteric stabilization of the powder particles. The menhaden fish oil (MFO) is the most used surfactant for tape casting, due to its effectiveness, low costs and environmental compatibilities. Another widely used dispersant/deflocculant is phosphate ester. It is soluble in both water and in several organic solvents. However its main drawback is that it leaves phosphorus inside the specimens.

Even if it is well-known that binders tend to overlap the surfactants effects, it is necessary to add them to the slurries in order to obtain a good dispersion and wettability of the particles during the addition of the binder and also to prevent possible chemical reactions during the dispersion process.

Another fundamental component of the slip is the **binder**, because it is the holder of the powder particles into the green tape. After the evaporation of the solvent the organic resins form the matrix of the tape and the powders are entrapped into the their chains, producing a network and characterized by the presence of residual porosity, resulted from the drying process. Binders are responsible for the properties to the green tape such as strength, flexibility, plasticity, durability, toughness, printability, smoothness and ability to lamination. For all these properties, binder is the second factor with most influence in this processing route. For that reason, it will be required the identification of all the parameters to select a tape casting binder including solubility, viscosity, cost, strength, T_g or ability to modify T_g, firing atmosphere of the powder, ash residue, burnout temperature, among others (Brook et al., 1996; Mistler & Twiname, 2000). A large amount of binders can be classified in two groups: polyvinyls (vinyl) and polycrylates (acrylic). Both groups have the same ability to form a film. However, they have different burn-off/removal properties in different atmospheres. In general, there are long-chain polymers or precursors (monomers or emulsion particles) that become long-chain polymers during drying (Brook et al., 1996; Mistler & Twiname, 2000; Mukherjee et al., 2001).

The last organic additive is the **plasticizer**, which can improve the flexibility and/or plasticity of the green tape, so that it can be bended the tape without causing damages such as cracking. The mechanism consists in increasing the workability of the binder. The plasticizers generally exhibit molecular weight around 300-400 and boiling temperatures higher than 200°C, with a high efficiency, non-residues, stable chemo-physical properties, low cost and no hazardous impact. On the other hand, plasticizers have to be able to interact with the binder. They are classified in two types depending on the mechanism that can provide flexibility and/or plasticity to green tape. The first one, “Type I” is a plasticizer, that soften the polymer chains between particles allowing them to stretch. Plasticizers of the “Type II”, have the mission of introduce plasticity (plastic deformation) to the green tape matrix (Mistler & Twiname, 2000).

The slurry could be prepared in several ways (considering the properties desired) but in general two steps are fundamental:

- Milling of the powders with solvent and dispersing agent.
- Mixing the slurry, and the addition of binder and plasticizer

The first step of the slurry preparation pursues three objectives: breaking the agglomeration of the particles, wetting and dispersing them. The first one is possible by grinding action. The second one depends on the affinity between the solvent and the particles of the powder(s), and the use or not, of wetting agents. The third has the function of preserve the particles in suspension with some space between them by steric and/or electrostatic effects, or by their combination (Brook et al., 1996). For this step, it is very common the use of the ball-milling process. Even the high-specific gravity has to be well studied to decide the use of a specific grinding media. The shape of the milling media could be spherical, cylindrical, and "natural" shaped flint stones. The charge is in the range of one-third to one-half of the mill volume (Mistler & Twiname, 2000). One part of the solvent is added to the jar, already charged with the milling media, followed by the dispersant agent that needs to be dissolved and then by the rest of the liquid media. Then the eventual wetting agent is added, followed by the powder. Depending on the materials used, this process can take 4 hours or a maximum of 48 hours, but typically is 24 hours long. When a satisfying dispersion is reached, the plasticizer is added and after that, the binder. The final milling and mixing process is generally conducted for at least 24 hours, in order to obtain a homogeneous and stable slip to be cast. Following this procedure, the overall result is a tape free of defects and with a thickness that can be as low as less than 10 μm.

When the binder is in a powder form could be necessary a pre-dispersion step to avoid the formation of large clumps of non-dissolved binder. The dissolution of the binder takes between 4 to 12 hours. Air is entrapped in the slip during the milling and mixing process, and this can cause some defects in tape casting, such as pinholes (small pores left by air bubbles), crack foot (cracks generated radial to the pinholes), and elongate streaks or thin spot. To remove them, it is possible to use a partial vacuum chamber (with vacuum in the range of 635 and 700 of mm of Hg for laboratory desiccator) with low stirring rate. The necessary time for this step will depend on the quantity of slurry and viscosity.

Rheological properties of the slurry need to be known for a well performance during cast. The most suitable rheological behaviour for this process is the pseudoplasticity, in which the homogeneity if the slurry is maintained, without suffering sedimentation during the stage in which it lies into the reservoir. For that reason, it is necessary a slurry with high viscosity, and when the casting starts, the viscosity can diminish to the necessary level to be spread in the polymer support (Mistler & Twiname, 2000).

In the present thesis work the tape casting technique was used to produce carbon nanotubes-polymer composites and nanotube-ceramic ones. The method used has been developed after several attempts and is schematically reported in Figure 42.

For the PMCs after a pre-dispersion step, in which carbon nanotubes (1% in weight ratio with respect of SiC powders) were ultrasonicated in ethanol in presence of small amounts of polymer, proper quantities of polyvinyl butyral were added and the slurry maintained in agitation by a magnetic stirrer for 24 hours. After that the slurry were cast on a moving Mylar™ support at slow velocity. The CNTs-PVB composite strips were then let in a drying chamber at room temperature for at least 12 hours.

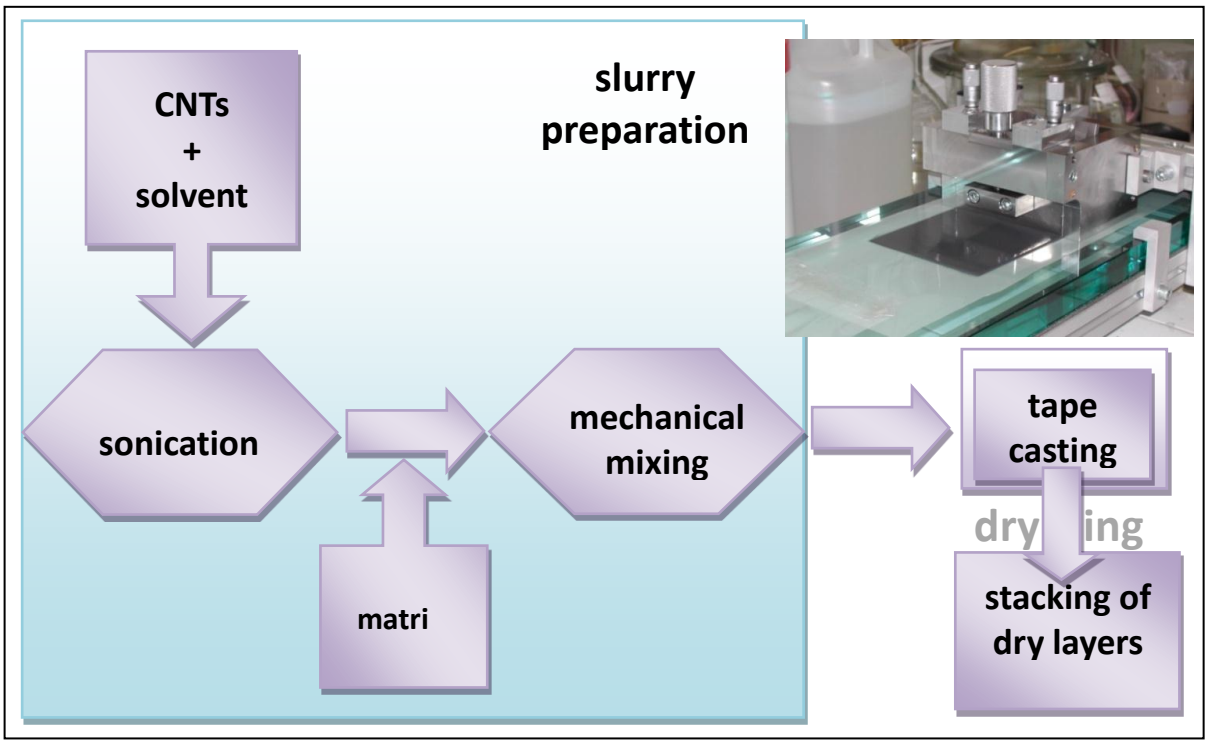

Figure 42 - Tape casting procedure for the production of CNTs-PVB composites

For CMCs preparation the same pre-dispersion process was used. The pre-dispersed CNTs-ethanol solution was then added to the ceramic powders (silicon carbide, boron amorphous and graphite flakes) in presence of fish oil as a dispersant. Mixing was carried out in an alumina jar for 2 hours using alumina balls as milling medium. Subsequently polyethylene glycol as plasticizer and the residual PVB were added to the slurry that was further mixed for at least 16 h, in order to ensure a homogeneous distribution of all the components. The resulting slurry (composition reported in Table 6) was then cast (advance speed of 100 mm/min).

After the slow evaporation of the ethanol, occurring at room temperature for about 24 hours, a green layer with a thickness of 200-250 µm and without defects was generally obtained. The sheets were cut and stacked in order to obtain a final architecture constituted by ten layers; the adhesion between the layers was ensured using a glue solution made of ethanol, water and polyvinyl alcohol (PVA by Sigma Aldrich).

The green tape underwent two heat treatments: a first de-binding cycle (performed in a furnace Elite thermal systems limited, Tersid s.r.l, Italy) up to 800°C in argon atmosphere caused the thermal decomposition of the organic components (binder, plasticizer and PVA from glue solution). During this thermal process a small quantity of carbonaceous solid residue was formed. Multilayer specimens were put on graphite supports during this treatment.

A final pressureless sintering (T.A.V. Cristalox, Italy) has been performed in argon atmosphere (99.99 purity, controlled pressure under 550 mbar) at 2200°C for 30 minutes.

Components		grams
Ceramic powder	Silicon carbide	15.025
Sintering aid	Boron amorphous	0.150
	Carbon	0.450
Solvent	Ethanol	22.543
Dispersant	Fish Oil	0.044
Binder	PVB	4.300
Plasticiser	Polyethylene glycol	2.238
Reinforcement	Carbon nanotubes	0.150

Table 6 - Slurry composition for CNTs-SiC composites

3.4.1. VISCOSIMETRIC INVESTIGATION OF THE SLURRIES

In order to tune the physical properties of the slurries required for an efficient casting process, an investigation of their viscosity has been conducted.

A viscous material is one in which the strain develops over a period of time and the material does not go to its original shape after the stress is removed. The development of strain takes time and is not in phase with the applied stress. Also, the material will remain deformed when the applied stress is removed (i.e., the strain will be plastic). A viscoelastic (or anelastic) material can be thought of as a material whose response is between that of a viscous material and an elastic material. The term

"anelastic" is typically used for metals, while the term "viscoelastic" is usually associated with polymeric materials. Many polymeric materials (solids and molten) are viscoelastic (Askeland, 1996).
While dealing with molten materials, liquids, and dispersions, such as paints or gels, a description of the resistance to flow under an applied stress is required. If the relationship between the applied stress (τ) and shear strain rate ($\dot{\gamma}$) is linear, we refer to that material as Newtonian. The slope of the shear stress versus the steady-state shear strain rate curve is defined as the viscosity (η) of the material. Water is an example of a Newtonian material. The following relationship defines viscosity:

$$\tau = \eta\dot{\gamma}$$

The units of η are Pa-s (in the SI system) or Poise (P) or $\frac{\mathrm{g}}{\mathrm{cm}-\mathrm{s}}$ in the cgs system. Sometimes the term centipoise (cP) is used, 1 cP=10^{-2} P.
The kinematic viscosity (ν) is defined as:

$$\nu = \eta/\rho$$

where viscosity (η) is in Poise and density (ρ) is in g/cm^3. The kinematic viscosity unit is in Stokes (St). In this, St is cm^2/s. Sometimes the unit of centiStokes (cSt) is used, 1 cSt =10^{-2}St.
For many materials the relationship between shear stress and shear strain rate is nonlinear. These materials are non-Newtonian. The stress versus steady state shear strain rate relationship in these materials can be described as:

$$\tau = \eta\dot{\gamma}^m$$

where the exponent m is not equal to 1.
Non-Newtonian materials are classified as shear thinning (or pseudoplastic) or shear thickening (or dilatant). The relationships between the shear stress and shear strain rate for different types of materials are shown in Figure 43.

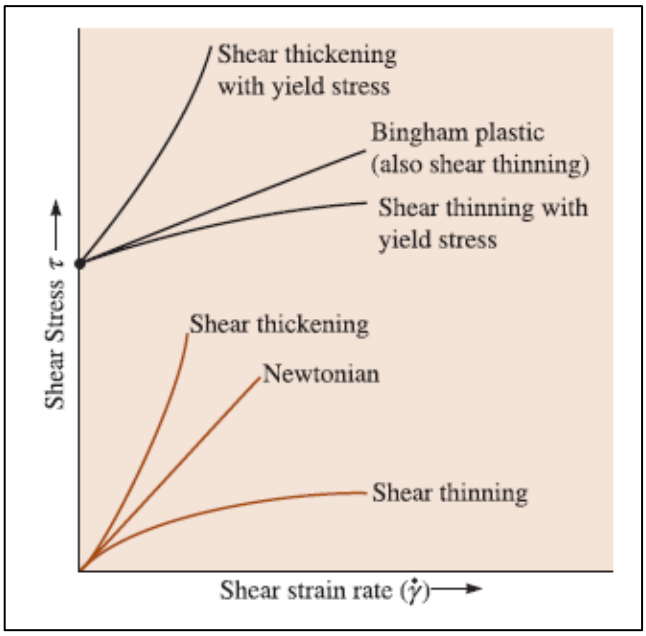

Figure 43 - Shear stress-shear strain rate relationships for Newtonian and non-Newtonian materials (Askeland, 1996)

Figure 44 - Brookfield viscosimeter

For the analysis of the slurries viscosity a Brookfield viscosimeter has been used (Figure 44). This type of viscometer measures the force required to maintain the rotation of a disc or a cylinder, with constant angular velocity, immersed in the fluid to be measured; in this case the force (and hence the choice of the proper impeller, disc or cylinder shaped) is strictly correlated with the fluid viscosity.

This property of a solution is extrapolated by the instrument on the basis of the torque applied to the impeller and after the comparison of the registered data with an internal data-base: for each value of regime N_i (in rpm) and torque α_i (percentage) corresponds a certain value of viscosity (in cP) (Mitschka, 1982). The torque values are converted into shear stress (in Pa) according to the formula:

$$\tau_i = k_{\alpha\tau}\alpha_i$$

The couples of values α_i/ N_i, valid for the impeller used, are put in a bilogarithmic graph; when the relation between the two parameters is close to the linear behaviour, the slope of the curve is simply correspondent to the fluidity index of the liquid *n*.
Using the values $k_{N\gamma}(n)$ associated to the viscosity and the type of impeller, it is possible to calculate the corresponding shear speed as:

$$\gamma_i = k_{N\gamma}(n) \cdot N_i$$

If it is not possible to approximate accurately the pairs $\log\tau_i$ / $\log N_i$ to a straight line, a curve is obtained, whose derivative point by point identifies the apparent viscosity n_i^* determined as:

$$n_i^* = d(\log \tau_i)/d(\log N_i)\,|_{N=N_i}$$

and therefore, the shear speed is calculated as:

$$\gamma_i = k_{N\gamma}(n_i^*) \cdot N_i$$

At this point it is possible to plot the function τ_i-γ_i characteristic of the fluid examined.
For low viscosity fluids the use of a disc-shaped impeller is required, and in this case the viscometer is not able to provide the values of γ_i, which are subsequently calculated using the formula:

$$\gamma_i = \frac{k_{\alpha\tau}\alpha_i}{\eta_i}$$

3.5. SPECIMENS CHARACTERIZATION

3.5.1. SCANNING ELECTRON MICROSCOPY AND EDS

Scanning electron microscopy (SEM) permits the observation of heterogeneous organic and inorganic samples on a nanometric and micrometric scale. The popularity of SEM is mainly due to its versatility and to the possibility to obtain three-dimension like images. The samples to be studied are irradiated with a highly focused electron beam. The interaction of electrons and specimen surface could generate several signals, including secondary electrons, backscattered electrons, characteristic X-rays. These signals are obtained from specific emission volumes within the sample and can be exploited to investigate different samples properties, e.g. topography, composition, crystallography, etc.

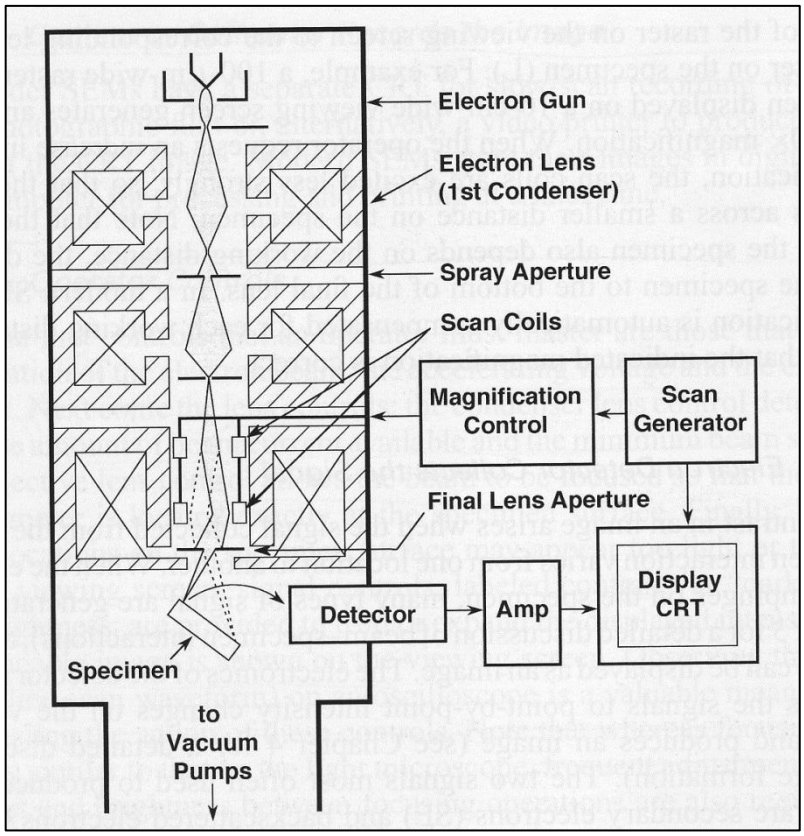

Figure 45 - A typical Scanning Electron Microscope configuration (Goldstein et al., 2003)

In Figure 45 are presented the basic components of a scanning electron microscopy. The system is divided in four main parts: the electron column, the specimen chamber, the vacuum pumping system and the electronic control of the imaging system. For the electron column, the most conventional gun is a tungsten wire of 0.25 mm of diameter as electron source, where the tungsten filament is heated to approximately 2500°C. The electrons are attracted to the anode, with a positive voltage in a range of 5 to 30 kV that can be controlled by the operator, and it is normally around 10-20 kV. The

vacuum system works at 10^{-3} Pa approximately, and provides the conditions for the beam to be scattered by gas atoms. The lenses are magnetic and have the function of reduce the diameter of the electron beam and to focus it on the sample surface, and can be adjusted by the current every time that the working distance is changed.

The signals of greatest interest for the image elaboration are the secondary (SE) and backscattered (BSE) electrons because their variations are strictly related with changes in surface topography. The former have low energy, and by putting an electrically charged grid near to the sample, it is possible to convoy them all toward a sensor, that counts their number. The latter, instead, have very high energy, and it is not possible to deflect them toward a sensor; thus only the fraction corresponding to the spatial angle covered from the sensor can be revealed. The image formation for the two signals is different and reported in Figure 46 and in Figure 47. The secondary electron emission, confined to a very small volume near the beam impact area, permits images with very high resolutions, approximating the size of the focused electron beam. The three-dimensional appearance of images is due to the large depth of field of the scanning electron microscope. While secondary electrons give only morphological information, backscattered ones give information about the atomic number of the interacting element; if a morphological effect is present however it is not easy to separate the two contributions, if the strategies shown in Figure 47 are not observed.

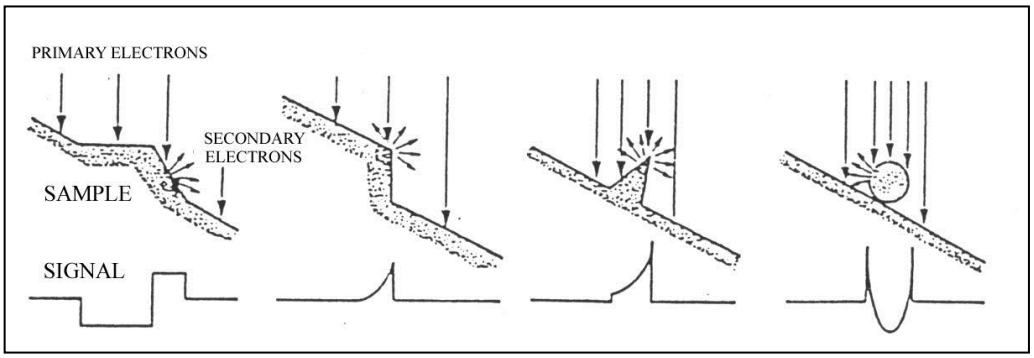

Figure 46 -Mechanism of image formation in the case of secondary electron revelation; secondary electrons are sensible only to the morphology of the sample (Lüth, 1995)

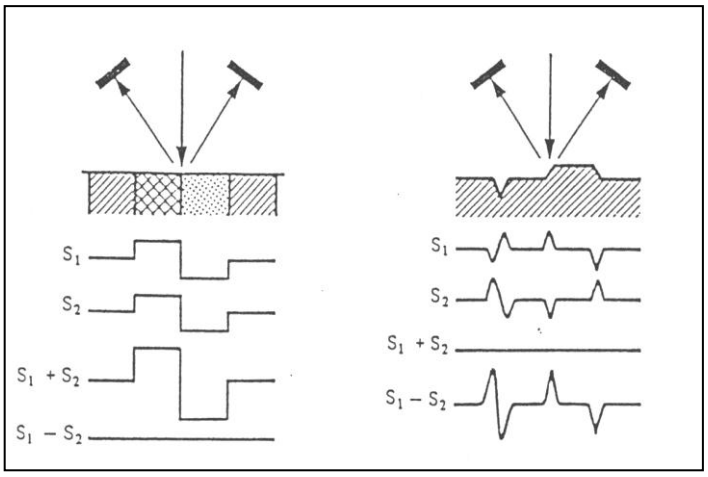

Figure 47 - Mechanism of image formation in the case of backscattered electrons revelation; there is the need of a couple of sensors in order to be able to distinguish between the composition, where the signal must be summed (a, on the left) and the morphology, where the signal must be subtracted (b, on the right) (Lüth, 1995)

In Scanning Electron Microscopy, characteristic x-rays are also emitted as a consequence of the electron beam impact. They are generated when the incident electron takes away a core electron from the atom; the equilibrium is re-established by the transition of an external electron to a core level: this phenomenon can cause the emission of a photon (X-Ray emission) or the generation of Auger electrons. Light elements prefer the latter mechanism, while heavier one the former. The analysis of the characteristic x-radiation emitted can yield both qualitative identification and quantitative elemental information from regions of a specimen nominally 1 µm and 1 µm in depth, even if these dimensions change with the operating conditions. It must not be forgotten though that the depth of emission of different signals varies: SE are emitted from the topmost layer of the sample, while both BSE and X-Ray are generated by atoms that can be quite deep inside the sample (Figure 48).

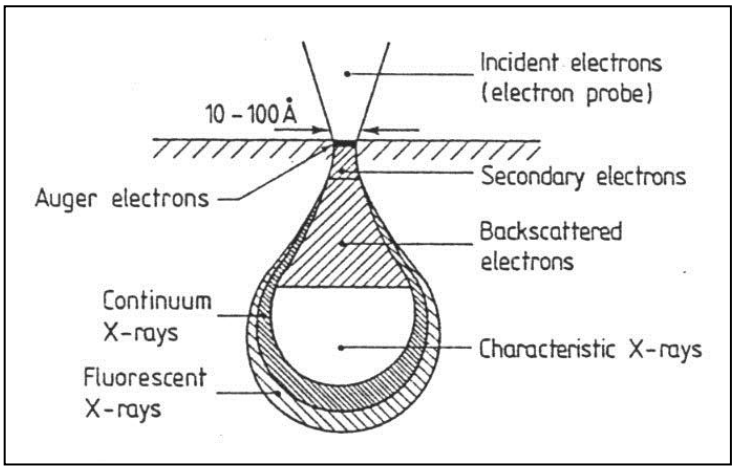

Figure 48 - Different emission zones for the signals produced after the impact of an electron on a surface (Lüth, 1995)

The chemical analysis in SEM is performed by measuring the energy and intensity distribution of the x-rays generated by the electron beam. One of the most common x-rays detectors are the so called Energy-Dispersive X-ray Spectrometer (EDS) and the Wavelength Dispersion Spectroscopy (WDS). In EDS, the impact of a X photon on the sensor generates an electron-hole couple with an energy proportional to that of the photon. In the second case the X-rays are separated by diffraction; by analysing the various diffracted signals it is possible to reconstruct the energy spectrum. The main characteristics of both the detectors are summarised in Table 7.

Feature	EDS	WDS
time required for quantitative analysis	minutes	hours
Sensibility	high (>10^4 cps nA^{-1})	low (<10^3 cps nA^{-1})
damage to the sample	Low	medium
focus problems	neglectable	high
spectral resolution	Low	optimum
signal to noise ratio	Low	high
revealable elements	Z > 10	Z > 4
accuracy of quantitative analysis	low	good

Table 7 - EDS and WDS comparison showing their different features

The mathematic model that allows a quantitative analysis by SEM and EDS/WDS is important to keep into account some corrections. Three different physical effects can alter a measurement:

- Atomic number (Z correction): different atoms emit different X photons quantities when hit by an electron.
- Absorption (A correction): if two elements A and B are close as atomic number, if hvB>Ek(A), where hvB is the energy of the X photon emitted by B and Ek(A) is the k level energy of atom A, the atom A may ionise itself and absorb the X photon. Therefore the number of resultant X photons for element B will be lower than the real.
- Fluorescence (F correction): if the atom A absorbs a photon emitted by B, it can re-emit another photon, that will be characteristic of A; in this case it will seem that the quantity of element A is higher than the real case.

The energy dispersive x-ray spectroscopy is the technique used during the present thesis work in addition to the scanning electron microscopy. This kind of detector allows micro chemical characterizations by the collection of the x-ray emitted by the elements of the structure under study, in general with an atomic number higher than sodium (Z = 11). As claimed before, for lighter elements Auger electrons emission is preferred, and only using EDS it results difficult to obtain a

complete quantification of light elements such as boron, carbon, nitrogen and oxygen. The X-rays are detected by a silicon diode, after the passage through a thick beryllium window (8 µm). The diode is generally cooled to reduce noise. The analysis of the revealed spectrum can ensure from a qualitative to a semi-quantitative characterization of the specimens. The qualitative identification of the elements is based on the fact that every element presents an X-ray emission with a specific wavelength. On the contrary, the quantification of the elements is quite difficult: the calculations are much more complex, because it is essential not only to integrate the peaks, but also to calculate the background signal, use correction for atomic number, fluorescence, adsorption (the so called ZAF correction) and tare the system with a known standard. The surface must also be extremely flat to avoid morphology effects on the signal (Echlin, 2009).

For the microstructural characterization of the materials and of the samples produced during the experimental work a Scanning Electron Microscope FEG ASSING SUPRA 25 was used. The SEM is equipped with an high-resolution EDS probe Oxford 7353 EDS, in addition to the SE and BSE detectors. The metal matrix composites, the metal powders and the carbon nanotubes have been analysed without the need of any kind of pre-treatment, whereas the polymer matrix composites requires a metallization process before the scanning electron microscopy investigation. The samples were covered by a very thick layer of chromium atoms so to improve the conductibility of the material, avoiding the accumulation of the incident electrons on the surface and allowing the emission of the secondary electrons.

3.5.2. UV-VISIBLE SPECTROSCOPY

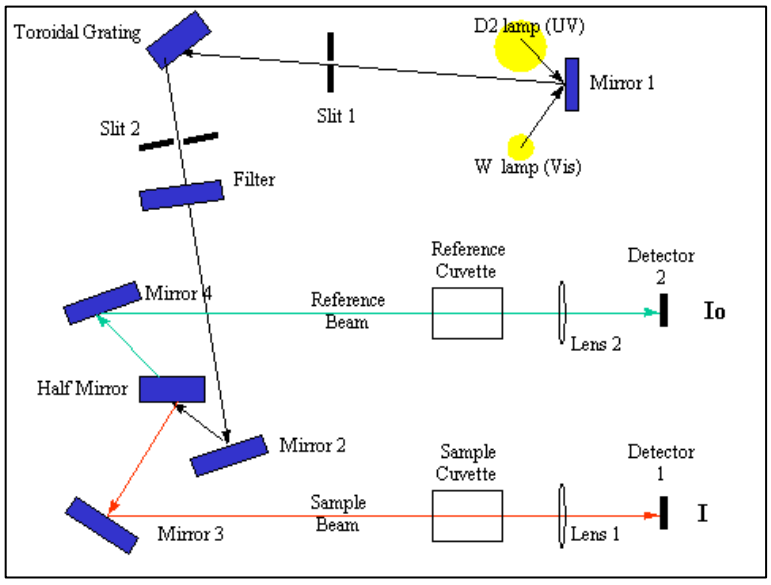

Figure 49- An example of double beam UV-visible spectrometer (Perkampus, Grinter, & Threlfall, 2012)

The Ultra Violet and visible spectroscopy is a particular spectroscopic technique in which the absorption of radiations in the range from the UV to the near infrared (from about 185 to 3000 nm wavelength) is measured. An example of UV-vis spectroscopy apparatus is reported in Figure 49.

The samples are generally in form of a liquid solution and put in transparent cells. A reflection phenomenon is observed both at the interface air/cell wall and at the interface liquid solution/ cell wall. A relevant attenuation of the transmitted ray light is observed because of these reflection phenomena and also because of the scattering of large molecules suspended in the solution. The emerging ray is collected by proper detectors and the absorbance *A* is evaluated using a very simple relation called Beer law, in which *A* is directly correlated with the step length *b*:

$$A = \varepsilon bc$$

Where *c* is the concentration and *ε* is the absorption coefficient of the material analysed.

The law is a good approximation of the absorbance behaviour however several limitations and deviations from the linearity have been reported (Skoog, Holler, & Crouch, 2007).

In my research work the UV-vis spectroscopy was used in order to evaluate the dispersion grade of carbon nanotubes after sonication and magnetic stirring in presence of PVB (polyvinyl butyral) as a surfactant. The idea is that big agglomerates of CNTs can increase the scattering effect of the solutions, while good dispersions exhibit a more intense absorbance around 250 nm (a typical absorbance peak of the CNTs). Because of their dark colour the CNTs can absorb intensely the UV-vis light, so the solution analysed were largely diluted with ethanol. To avoid the presence of large bundles the diluted samples were decanted for a week before their analysis.

The instrument used for the scattering evaluation is a UV–Vis double beam spectrophotometer Cary 500 (Varian Co., USA) equipped with a Varian DRA-2500 integrating sphere and the spectra were collected between 210 and 800 nm of wavelength.

3.5.3. X RAYs DIFFRACTION

X-Ray diffraction is used in order to analyse the phase composition of crystalline materials; the method is based on the Bragg Law:

$$n\lambda = 2d \sin \vartheta$$

where *n* is an integer, generally 1; *λ* is the wavelength of the incident X-Ray radiation, *ϑ* is the incident angle and *d* is the distance between identical planes reflecting the radiation, as reported in Figure 50.

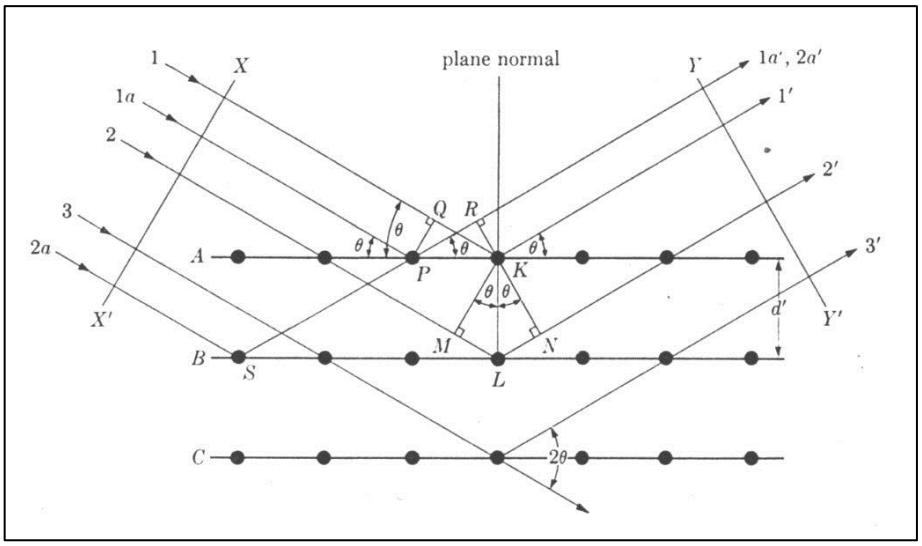

Figure 50- Mechanism of formation of diffracted wavelength explaining Bragg's Law (Cullity & Stock, 2001)

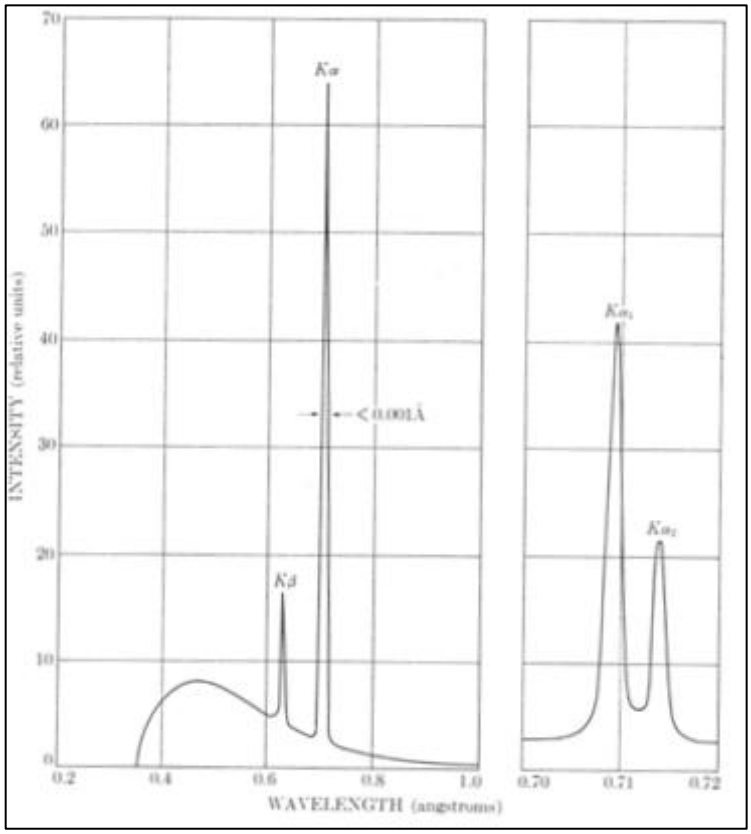

Figure 51 - X-Rays spectrum generated by the impact of electrons on a anode; it is possible to see the Bremsstrahlung and the characteristic peaks of the anode materials (Cullity & Stock, 2001)

Thus, if a X photon incises with angle ϑ on several atom planes separated by the distance *d*, a diffraction will take place, because of the constructive interference between the X photons and the atoms. From the distances *d* relative to each family of planes of a material, together with the intensities of the diffracted beams, it is then possible to know the exact lattice parameters and atoms

disposition of the crystal cell. All the diffractions of all the lattice planes create a pattern of diffraction signals that is specific for every material (Smallman & Bishop, 1999).

Since always $\lambda < 2d$, the wavelength must be rather low, and this is the reason why X radiation is used.

X-Rays are produced as a consequence of the impact of accelerated electrons toward an anode. The characteristic radiation spectrum emitted is characterized by a continuous radiation, called Bremsstrahlung, superimposed to peaks typical of the anode materials (Figure 51).

In X-Ray Diffraction it is needed a monochromatic radiation, so that filters are used to eliminate the not required contributions. The closer the peaks the more difficult the filtering, so that while K_α and K_β peaks are easily separated, $K_{\alpha1}$ and $K_{\alpha2}$ are very difficult to divide; in the instruments used during this thesis both the contribution are present in the spectra. In this case $K_{\alpha2}$ is half the height of $K_{\alpha1}$ and their separation is evident only at high diffraction angles.

One of the diffractometers used during this thesis was of the ϑ-2ϑ type (Figure 52), the other of the ϑ-ϑ type. The principle however is quite the same in the two cases.

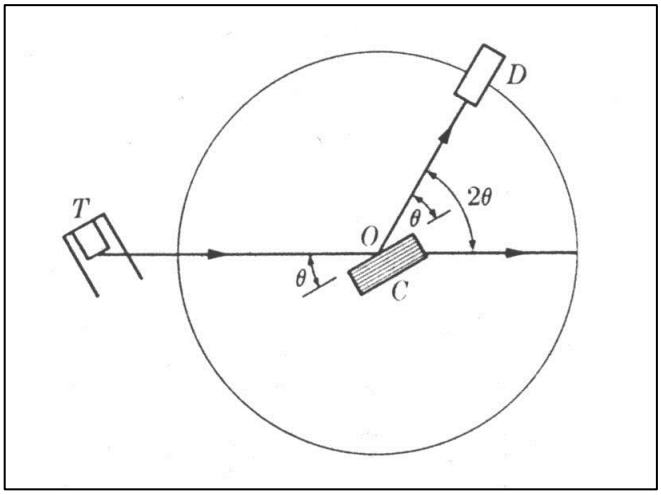

Figure 52- Diagram of a ϑ-2ϑ type diffractometer (Cullity & Stock, 2001)

There are different software to analyse the data, such as X-pert, used in this thesis, that takes the angles, intensities and potential constituents, and gives an estimation of the promising phases from the PCPDFWIN database (containing an extremely high quantity of identified and standard patterns), making a comparison between the experimental X-ray pattern and the reference one, so that it is possible to identify the phases present in the material under study. The X-ray diffraction can be realised on a massive material or on a powder; in the first case, if the material has an oriented crystallographic structure, this will influence much the measurement, since certain planes could not

be oriented as to diffract the incident radiation. In the case of powder instead it can be supposed that, if the powder is sufficiently fine, all possible diffracting planes are diffracting at the same time, and all possible reflections are reported.

The XRD characterizations were performed using a commercial X-ray diffractometer Philips PW 1710 CuK radiation in a range of 2θ between 20° and 80°, and a particular micro-XRD device in which a collimator of 0.3 mm is used to obtain a collimated ray of X radiation for the analysis of small samples or of small phases with an increased precision and accuracy. For the micro- XRD tests the samples were analysed by a Rigaku D/MAX Rapid microdiffractometer at a fixed 10° angle ω, while where rotated of a φ angle between -30° and 30°. The analyses were performed for 30 minutes in order to maximize the diffraction signals of the samples and minimize the noise level (due to the scattering of the sample).

3.5.4. MECHANICAL CHARACTERIZATIONS

3.5.4.1. MICROHARDNESS

The hardness of materials is usually determined by indentation. It consists in quantifying the resistance of a surface to the penetration of a harder object. Several methods have been developed and the main ones are Rockwell, Brinell, Vickers and Knoop. Recently also nanoindentation techniques have been spread. Each method differs from the others by a specific geometry and size of the indenter, has by its specific equation, and presents also specific load conditions.

In Table 8a list of these principals hardness tests and their main characteristics is reported (Askeland, 1996).

All these tests can be used to give indications about the effect of the specific fabrication technique, or thermal-treatment, and are often used for quality control and correlation with other properties of the materials.

Test	Indenter geometry and size	Load	Application	Equation
Brinell	Ball of 10 mm	3000 Kg	Cast and iron steel	$HB = \frac{2P}{\pi D(D - \sqrt{D^2 - d^2})}$
Brinell	Ball of 10 mm	500 Kg	Non-ferrous alloys	
Rockwell A	Diamond cone	60 Kg	Very hard materials	The instrument is equipped with a micrometer able to measure the penetration of the indenter and to evaluate the hardness of the material
Rockwell B	Ball of 1/6 in	100 Kg	Brass and low resistance steel	
Rockwell C	Diamond cone	150 Kg	High resistance steel	
Rockwell D	Diamond cone	100 Kg	High resistance steel	
Rockwell E	Ball of 1/8 in	100 Kg	Soft materials	
Rockwell F	Ball of 1/16 in	60 Kg	Aluminum and soft materials	
Vickers	Diamond pyramid	10 Kg	Hard materials	$HV = \frac{1.864P}{L^2}$
Knoop	Diamond pyramid	500 g	All materials	$HK = \frac{P}{C_p L^2}$

Table 8 - Indentation techniques and their features (*P*: load applied in kg, *D* diameter indenter in mm, *d* diameter of the imprint in mm, *L*: length of indentation along its long axis; C_p correction factor related to the shape of the indenter, ideally 0.070279. The factor 1.864 is cos (ϑ/2=136/2), where 136 is the angle of the pyramid.)

In this thesis, Vickers hardness test (ASTM E92-72) was used. Microhardness (HV) of aluminum matrix composites was measured using a LEICA micro HV indenter with a load of 50 g for a dwelling time of 10 s. At least 20 measurements were performed for each specimen, in order to obtain statistically representative results. The test consists in penetrate a surface under investigation by an indenter, in this case a diamond pyramid with square-base that forms an angle of 136° with the opposite side (Figure 53). The force applied is known, and by measuring the surface area of the imprint (the operator measures the imprint diagonal length, then the area of the imprint can be calculated by the simple geometrical formula shown in Table 8) it is possible to obtain the Vickers hardness. Vickers hardness test should be independent of the load, except in case of small loads (Dieter & Bacon, 1988).

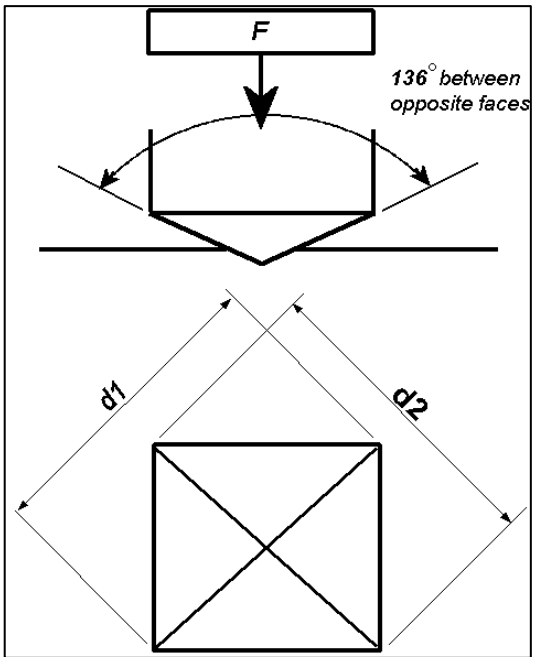

Figure 53- Schematic representation of a typical Vickers indenter

3.5.4.2. ELASTIC MODULUS

The elastic modulus can be estimated from the mechanical tensile tests, however it is easier and also gives better results to measure the fundamental resonant frequency of a test specimen by exciting it mechanically with an elastic impulse (ASTM standard C1259-01, "Standard test method for dynamic Young's modulus, shear modulus, and Poisson's ratio for advanced ceramics by impulse excitation of vibration", 2001). This technique, called "Impulse Excitation of Vibration", uses a transducer to sense the resulting mechanical vibrations of the impulse and isolate the fundamental resonant frequency. From this frequency values, knowing exactly the geometry of the specimen, it is possible to determine the dynamic Young's modulus (together with the dynamic shear modulus and Poisson's ratio).

The specimen must be in the form of a rod or a rectangular bar. In this latter case, the equation that can be used to calculate the Young's modulus *E* is:

$$E = 0.9465\left(\frac{mf_f^2}{b}\right)\left(\frac{L^3}{t^3}\right)T_1$$

where *E* is the Young's modulus (Pa), *m* the mass of the bar (g), *b* its width (mm), *L* its length (mm), *t* its thickness (mm) and f_f the fundamental resonant frequency (Hz) of the bar in flexure. T_1 is a correction factor that account for the finite thickness of the bar, the Poisson's ratio, etc.

$$T_1 = 1 + 6.585(1 + 0.2023\mu^2)\left(\frac{t}{L}\right)^2 - 0.868\left(\frac{t}{L}\right)^4 - \left[\frac{8.340(1 + 0.2023\mu + 2.173\mu^2)\left(\frac{t}{L}\right)^4}{1 + 6.338(1 + 0.1408\mu + 1.536\mu^2)\left(\frac{t}{L}\right)^2}\right]$$

where μ is the Poisson's ratio.

If the ratio *L* / *t* is greater than 20, T_1 can be simplified to the following:

$$T_1 = 1 + 6.585\left(\frac{t}{L}\right)^2$$

and *E* can be calculated directly.

If *L* / *t* is smaller than 20, either the Poisson's ratio is known or T_1 can be calculated with an iterative process; in this case however also the dynamic shear modulus *G* must be calculated, and must be used the equation

$$\mu = \frac{E}{2G} - 1$$

It is important to place correctly the microphone and to hit in the proper point the specimen, since the correct vibration mode must be excited.

If *E* is to be measured, the specimen must be hit on the centre of a face; if a contact transducer is used, it must not be placed in an antinode, since in this case the natural vibration can be modified, but as far as possible from the nodal points. If a non-contact transducer is used, on the contrary, it should be placed over an antinode point, close to the test specimen but not so close as to interfere with the free vibration. In this case the obtained frequency will be the flexural resonant frequency.

If the torsional frequency must be measured, so to be able to obtain *G*, the transducer must be located at one quadrant of the specimen, preferably at approximately 0,224 *L* from one end and toward the edge. This location is a nodal point of flexural vibration and will minimize the possibility of detecting a spurious flexural mode. The specimen must be hit on the quadrant diagonally opposite the transducer, at a specular position.

Young's modulus was measured on parallelepiped shaped samples according to ASTM C 1259-01 by using an impulse excitation technique, involving the analysis of the transient composite natural vibration (GrindoSonic MK5 Instrument).

3.5.4.3. THREE POINTS FLEXURAL TEST

The bending or flexural strength of the metal matrix composites were measured by three point flexural tests (configuration reported in
Figure 54). The samples preparation for this kind of measurements is easy: bars with a cross section either rectangular or circular with specific dimensions (ASTM standard C1161-94, “Standard test method for flexural strength of advanced ceramics at ambient temperature.”) that depends on the length of the span L. The specimen bar is placed between the span according to the three-point configuration, and then is applied a concentrated load in one point. The sample is in compression at the surface positioned in the load part and is in tension in the rear surface part.

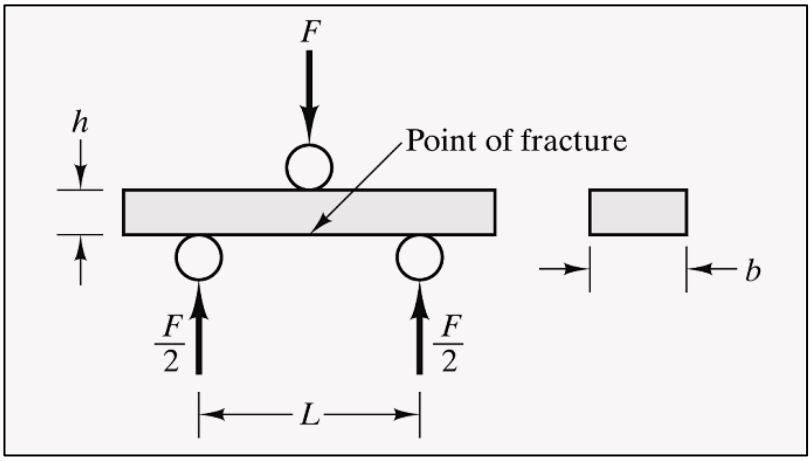

Figure 54 - Configuration for three-point bending test

The standard formula for the strength of a beam in three-point flexure is as follows (“ASTM standard C1161-94, Standard test method for flexural strength of advanced ceramics at ambient temperature.”):

$$\sigma = \frac{3FL}{2bh^2}$$

where *F* is the load, *L* is the outer support span, *b* the specimen width and *h* the specimen thickness.

Three-point bending strength was measured according to UNI EN 658.3 standard (Sintech 10D equipment), with a crosshead speed of 0.1 mm/min in stroke control and 20 mm span for MMCs, while for CMCs the crosshead spin was of 0.2 mm/min and the span of 40 mm.

3.5.4.4. TENSILE TEST

The tensile test measures the resistance of a material to a static or slowly applied force. Its popularity is due to the fact that the properties obtained could be applied to design different components. Typically, a tensile test is conducted on metals, alloys, and plastics. Tensile tests can also be used for ceramics, however, the test is not very useful for this kind of materials because the sample often easily fractures while it is being aligned. The strain rates in a tensile test are very small ($\dot{\varepsilon}=10^{-4}$ to 10^{-2} s^{-1}).

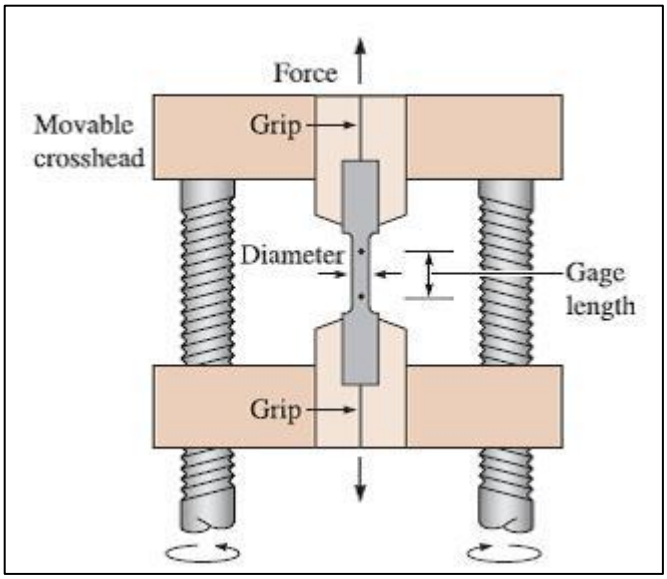

Figure 55 - A typical tensile test apparatus (Askeland, 1996)

In Figure 55 a typical tensile test apparatus is reported. The correctly placed specimen are subjected to a force *F*, called the load, and their amount of stretch between the gage marks when the force is applied is measured by a strain gage or an extensometer. Thus, what is measured is the change in length of the specimen (Δl) over a particular original length (l_0). Information concerning the strength, Young's modulus, and ductility of a material can be obtained from such a tensile test. When a tensile test is conducted, the data recorded includes load or force as a function of change in length (Δl). These data are then subsequently converted into stress and strain. The stress-strain curve is analysed further to the extract properties of materials, such as Young's modulus, yield strength, etc. (e.g. Figure 56). The results of a single test apply to all sizes and cross-sections of specimens for a given material if we convert the force to stress and the distance between gage marks to strain. Engineering stress σ and engineering strain ε are defined by the following equations:

$$\sigma = \frac{F}{A_0}$$

$$\varepsilon = \frac{\Delta l}{l_0}$$

where A_0 is the original cross-sectional area of the specimen before the test begins, l_0 is the original distance between the gage marks, and Δl is the change in length after force F is applied.

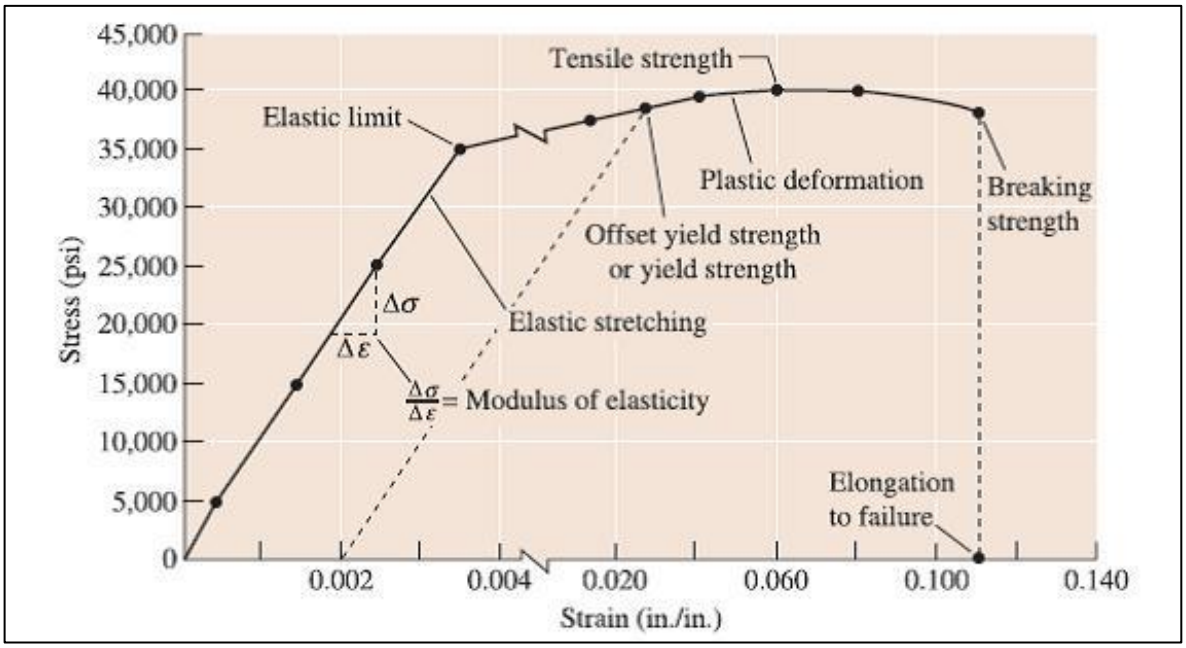

Figure 56 - Example of stress-strain curve for an aluminium alloy specimen (Askeland, 1996)

Mechanical performance of the tape cast PVB-CNTs composites was measured by Sintech 10D Dynamometer, and both maximum strength and Young's modulus were calculated.

REFERENCES

Anderson, J. C. (2003). *Materials Science: For Engineers*. CRC PressINC.

Askeland, D. R. (1996). *The Science and Engineering of Materials*. (B. Webster, Ed.)*Materials Science and Engineering A* (Vol. 212, pp. 186–187). Chapman and Hall. doi:10.1016/j.msea.2008.04.012

Badini, C., Fino, P., Ortona, A., & Amelio, C. (2002). High temperature oxidation of multilayered SiC processed by tape casting and sintering. *Journal of the European Ceramic Society*, *22*(12), 2071–2079. doi:http://dx.doi.org/10.1016/S0955-2219(01)00520-9

Biamino, S., Liedtke, V., Badini, C., Euchberger, G., Huertas Olivares, I., Pavese, M., & Fino, P. (2008). Multilayer SiC for thermal protection system of space vehicles: Manufacturing and testing under simulated re-entry conditions. *Journal of the European Ceramic Society*, *28*(14), 2791–2800. doi:http://dx.doi.org/10.1016/j.jeurceramsoc.2008.04.006

Brook, R. J., Cahn, R. W., Haasen, P., & Kramer, E. J. (1996). *Materials Science and Technology: A Comprehensive Treatment. Processing of ceramics, part II*. VCH.

Calka, A., & Radlinski, A. P. (1991). Universal high performance ball-milling device and its application for mechanical alloying. *Materials Science and Engineering: A*, *134*(0), 1350–1353.

Clyens, S., Al-Hassani, S. T. S., & Johnson, W. (1976). The compaction of powder metallurgy bars using high voltage electrical discharges. *International Journal of Mechanical Sciences*, *18*(1), 37–40.

Cullity, B. D., & Stock, S. R. (2001). *Elements of X-Ray Diffraction*. (M. Cohen, Ed.)*Elements* (Vol. USA, p. 664). Prentice Hall.

Deorsola, F. a., Vallauri, D., Ortigoza Villalba, G. a., & Benedetti, B. D. (2010). Densification of ultrafine WC–12Co cermets by Pressure Assisted Fast Electric Sintering. *International Journal of Refractory Metals and Hard Materials*, *28*(2), 254–259. doi:10.1016/j.ijrmhm.2009.10.007

Dieter, G. E., & Bacon, D. J. (1988). *Mechanical Metallurgy*. McGraw-Hill.

Echlin, P. (2009). *Handbook of Sample Preparation for Scanning Electron Microscopy and X-Ray Microanalysis*. Springer.

Feng, Y. T., Han, K., & Owen, D. R. J. (2004). Discrete element simulation of the dynamics of high energy planetary ball milling processes. *Materials Science and Engineering: A*, *375–377*(0), 815–819.

Goldstein, J., Newbury, D., Joy, D., Lyman, C., Echlin, P., Lifshin, E., Sawyer, L., et al. (2003). *Scanning Electron Microscopy and X-ray Microanalysis*. (J. Goldstein, Ed.)*Scanning Electron Microscopy* (Vol. 1, p. 689). Springer.

Grasso, S., Sakka, Y., & Maizza, G. (2009). Electric current activated/assisted sintering (ECAS): a review of patents 1906–2008. *Science and Technology of Advanced Materials*, *10*(5), 053001. doi:10.1088/1468-6996/10/5/053001

Groza, J. R., & Zavaliangos, A. (2000). Sintering activation by external electrical field. *Materials Science and Engineering: A*, *287*(2), 171–177.

Hennrich, F., Krupke, R., Arnold, K., Rojas Stütz, J. A., Lebedkin, S., Koch, T., Schimmel, T., et al. (2007). The mechanism of cavitation-induced scission of single-walled carbon nanotubes. *The Journal of Physical Chemistry B*, *111*(8), 1932–7. doi:10.1021/jp065262n

Hilding, J., Grulke, E. a., George Zhang, Z., & Lockwood, F. (2003). Dispersion of Carbon Nanotubes in Liquids. *Journal of Dispersion Science and Technology*, *24*(1), 1–41. doi:10.1081/DIS-120017941

Hulbert, D. M., Anders, A., Dudina, D., Andersson, J., Jiang, D., Unuvar, C., Anselmi-Tamburini, U., et al. (2008). The Absence of Plasma in " Spark Plasma Sintering. *Journal of Applied Physics*, *104*(3), 1–29. doi:10.1063/1.2963701

Johnson, W., Clyens, S., & Hassani, S. T. S. (1976). Compaction of metal powders using high voltage electrical discharges and rotary swaging. *Metallurgia*, *43*(11), 382–385.

Lucas, A., Zakri, C., Maugey, M., Pasquali, M., Schoot, P., & Poulin, P. (2009). Kinetics of Nanotube and Microfiber Scission under Sonication. *The Journal of Physical Chemistry C*, *113*(48), 20599–20605. doi:10.1021/jp906296y

Lüth, H. (1995). *Surfaces and interfaces of solid materials*. Springer.

Matsugi, K., Ishibashi, N., Hatayama, T., & Yanagisawa, O. (1996). Microstructure of spark sintered titanium-aluminide compacts. *Intermetallics*, *4*(6), 457–467.

Mio, H., Kano, J., Saito, F., & Kaneko, K. (2002). Effects of rotational direction and rotation-to-revolution speed ratio in planetary ball milling. *Materials Science and Engineering: A*, *332*(1–2), 75–80.

Mistler, R. E., & Twiname, E. R. (2000). *Tape Casting: theory and practice*. American Ceramic Society.

Mitschka, P. (1982). Simple conversion of Brookfield R.V.T. readings into viscosity functions. *Rheologica Acta*, *21*(2), 207–209 LA – English. doi:10.1007/BF01736420

Mukherjee, A., Maiti, B., Das Sharma, A., Basu, R. N., & Maiti, H. S. (2001). Correlation between slurry rheology, green density and sintered density of tape cast yttria stabilised zirconia. *Ceramics International*, *27*(7), 731–739.

Orrù, R., Licheri, R., Locci, A. M., Cincotti, A., & Cao, G. (2009). Consolidation/synthesis of materials by electric current activated/assisted sintering. *Materials Science and Engineering: R: Reports*, *63*(4-6), 127–287. doi:10.1016/j.mser.2008.09.003

Perkampus, H. H., Grinter, H. C., & Threlfall, T. L. (2012). *UV-VIS Spectroscopy and Its Applications*. Springer London, Limited.

Riedel, R., & Chen, I. W. (2008). *Ceramics Science and Technology: 4 Volume Set*. Wiley VCH Verlag GmbH.

Skoog, D. A., Holler, F. J., & Crouch, S. R. (2007). *Principles of Instrumental Analysis*. (H. B. Company, Ed.)*Publish* (Vol. 18, p. 1039). Thomson Brooks/Cole. doi:10.2307/1505543

Smallman, R. E., & Bishop, R. J. (1999). *Modern Physical Metallurgy and Materials Engineering*. *Management* (p. 368). Butterworth-Heinemann.

Vichchulada, P., Cauble, M. A., Abdi, E. A., Obi, E. I., Zhang, Q., & Lay, M. D. (2010). Sonication Power for Length Control of Single-Walled Carbon Nanotubes in Aqueous Suspensions Used for 2-Dimensional Network Formation. *The Journal of Physical Chemistry C*, *114*(29), 12490–12495. doi:10.1021/jp104102t

Weissler, G. A. (1981). Resistance sintering with alumina dies. *The International journal of powder metallurgy & powder technology*, *17*(2), 107–109,111.

CHAPTER 4: RESULTS AND DISCUSSIONS

4.1. CARBON NANOTUBES DISPERSION

Starting the experimental work on the production and characterization of composite materials reinforced by carbon nanotubes, a great importance has been devoted toward the comprehension of the state of the art of the topic. Due to the complexity and to the current interest on carbon nanotubes an extreme large number of papers and books has been published since the discover of carbon nanotubes 1991. The very first step of the work has been focused on a deep bibliographic investigation in order to fully understand the problem of CNTs. Several approaches are used in innumerable research works conducted all around the world (cf. chapter 2) but all of them have in common a fundamental aspect: the dispersion of the carbon nanotubes (section 2.4). For this reason the first step of my experimental work had been the deepening of the dispersion problem. We decided to start from low cost raw materials. Therefore we used for our experiments industrial grade nanotubes: the Nanocyl™ NC7000. These MWNT are produced by Nanocyl™ by CVD in large amounts and are low cost and low quality CNTs. We also determined to use a simple approach to avoid the use of expensive and complex processes: so we tried to disperse CNTs directly inside a proper solvent using only ultrasound sonication. The first attempts made concerned the direct dispersion of nanotubes in ethanol by sonicating them for several minutes with a probe sonicator. In a first moment different sonication-times have been experimented in order to determine the proper duration of the process. For very long sonication-times the CNTs could be damaged, the sample could be heated and evaporation of the solvent is observed. Moreover, for more concentrated samples, a particular phenomenon, that we called “gelification”, was observed after few minutes of sonication: the carbon nanotubes tend to form a sort of gel with the ethanol trapped inside, in which the propagation of the ultrasounds becomes impossible. This reaction could be connected with the presence of single nanotubes partially extracted from the CNTs bundles that try to re-aggregate with nanotubes of other bundles, creating a sort of net. This phenomenon is characteristic of concentrated dispersion of CNTs, in which the bundles results more close each other than in very diluted solutions. After several dispersion tests we decided to sonicate the carbon nanotubes and the solvent for 15 minutes, in order to maximize the dispersion effect of the ultrasound probe and minimize the damaging of the CNTs.

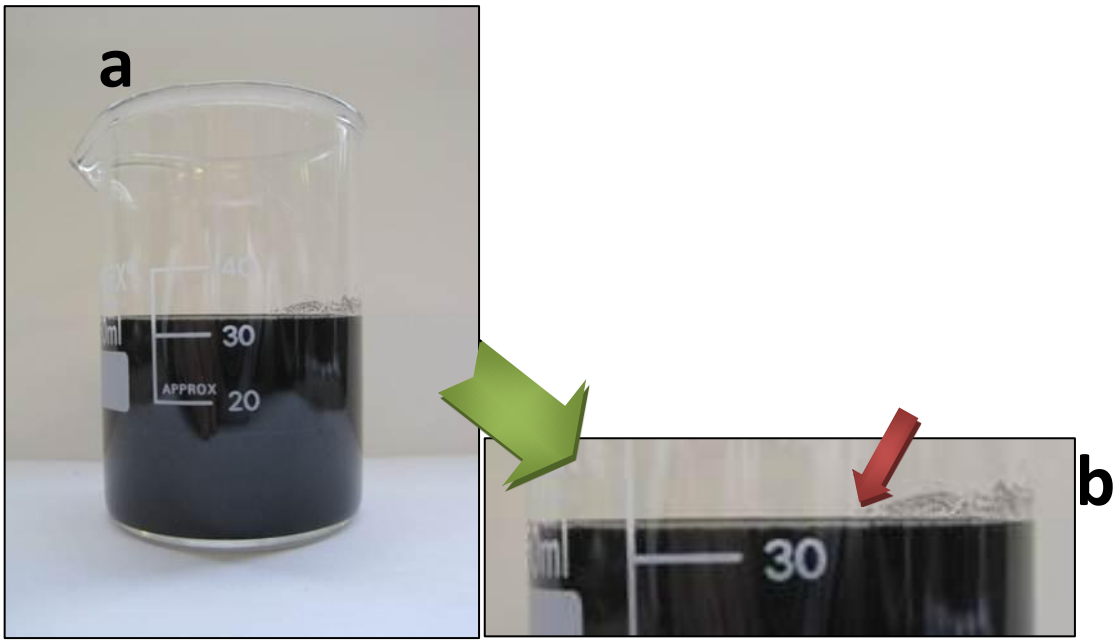

Figure 57 - A CNTs dispersion in ethanol after 15 minute of probe sonication (a) and a magnification of its meniscus (b) where the red arrow indicates the presence of pure ethanol.

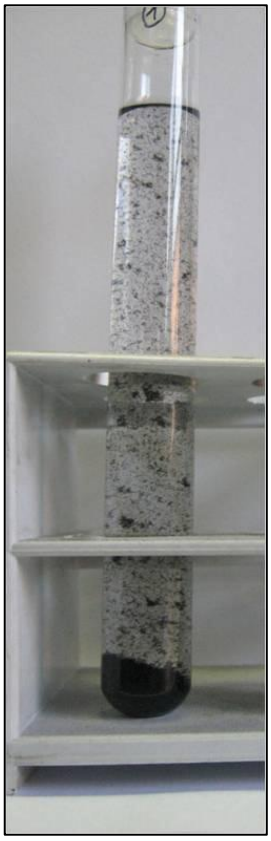

Figure 58 - Precipitation of the sonicated CNTs after dilution with pure ethanol

In literature it is possible to find that with this approach several researchers affirm to obtain a reasonable dispersion. Actually at a first sight the content of the beaker, in which the dispersion occurred, appeared black and uniform and generally the dispersion was maintained for several days (Figure 57a). But at the ethanol meniscus it was noted few millimeters of pure ethanol (Figure 57b). So it had been decided to try to dilute with ethanol a small quantity of this sonicated CNTs and after few minutes it was observed that they precipitated (Figure 58). So they were not completely well dispersed. The partially disaggregated bundles of carbon nanotubes have been used as reinforcements for the production of polyvinyl butyral matrix composites (cf. section 4.2). After the tape casting process and after the evaporation of the solvent, the obtained film of composite appeared macroscopically homogeneous, despite of the not satisfying dispersion of the fillers after the sonication step. In confirmation of this visual impression, small portions of composite were put in liquid nitrogen and a brittle fracture was caused. After metallization the fracture surfaces were observed by scanning electron microscopy. At the microscopic level, carbon nanotubes appeared uniformly dispersed within the polymer matrix, and a partial orientation is observed along the casting direction (the CNTs appeared as white spots on the polymer fracture surface) (Figure 59). Despite of the presence of few bundles, the general aspect of the tape cast composites was unexpectedly uniform and a good dispersion and distribution of the nanotubes is quite evident.

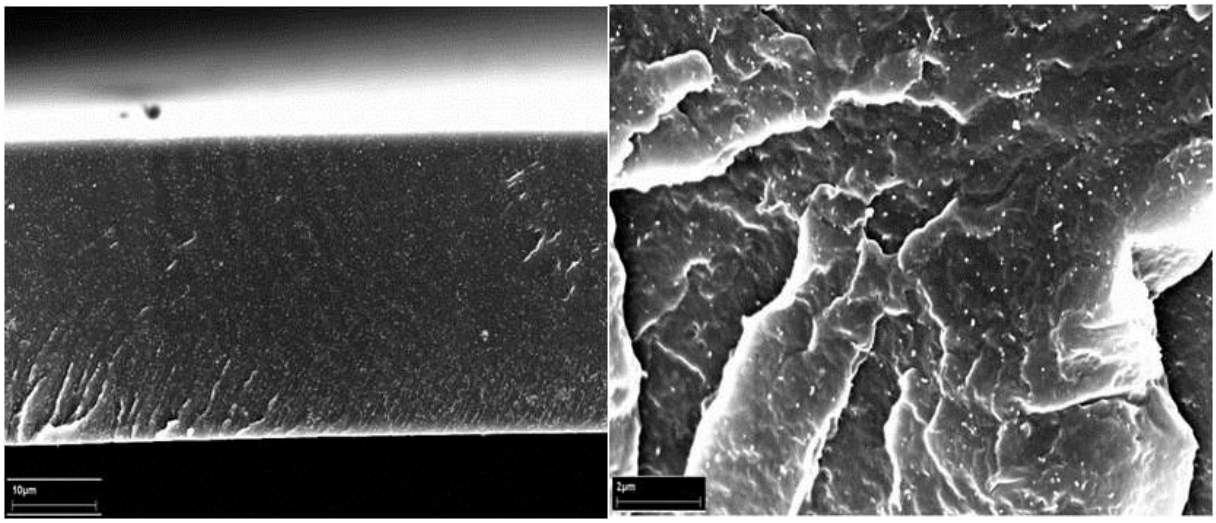

Figure 59 - Two different SEM magnification of PVB-CNTs tape cast composites.

Since the pre-dispersion step was the same adopted during the study of dispersion, it is clear that another effect contributed to the effective dispersion of the tubes. The main hypothesis to explain this dispersion phenomenon were two: the mechanical effect of the sliding under the blade and an

effect due to polyvinyl butyral, the thermoplastic resin commonly used as matrix in tape casting processes.

The polyvinyl butyral is the common name for poly[(2-propyl-1,3-dioxane-4,6-diyl)methylene], a polymer obtained from polyvinyl alcohol by reaction with butyraldehyde. It is characterized by the presence on its structure of a 1,3-dioxane, a cyclo-hexane ring with two substituent oxygen atoms in positions 1 and 3 (Figure 60). In literature, several studies were conducted on different polymers as dispersant of CNTs (cf. section 2.4). During the present experimental work, the tests conducted to demonstrate the effect of the polymer were: an optimization of the contact between PVB and CNTs and tests on the dispersion of CNTs with different quantities of polymer. All the experiments were conducted on 30 mg of Nanocyl™ NC7000 in 30 thousand milligrams of ethanol.

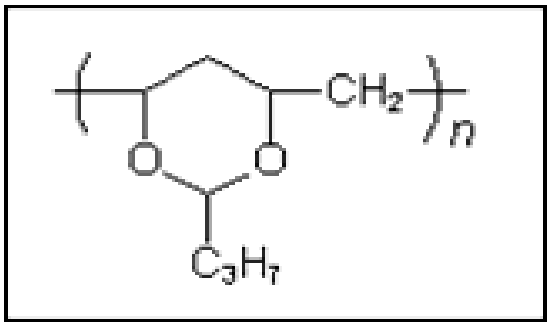

Figure 60 - Monomer of polyvinyl butyral

The first experiment involved an improvement of the contact between the polymer and the carbon nanotubes. We tried to increase the magnetic stirring time with respect to the one generally used for the preparation of the slurries. Experiments were realised by making polyvinyl butyral matrix composites with mechanical agitations of 1 to 72 hours, after the 15 minutes of ultrasonication. The slurries were tape cast, dried and finally were cut in small stripes, put in liquid nitrogen, broken and, after a metallization step, observed by scanning electron microscopy.

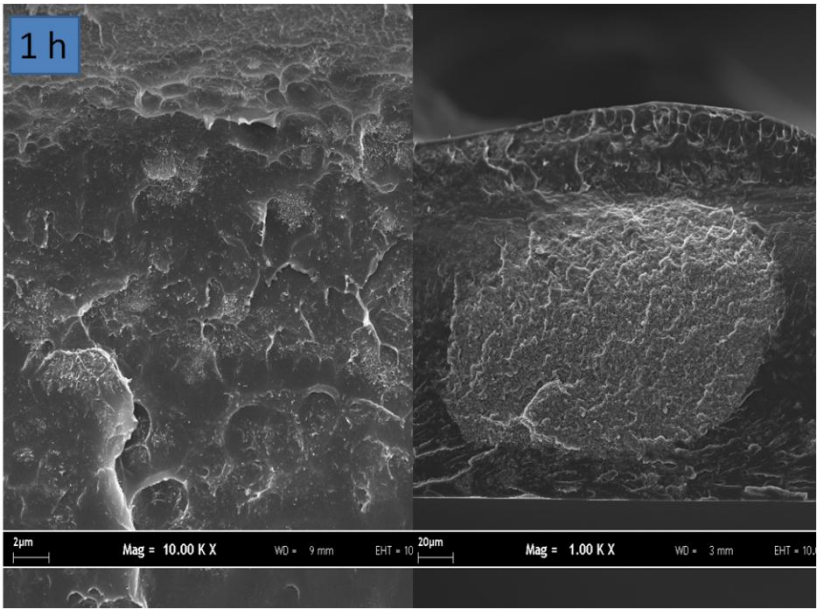

Figure 61 - Fracture surfaces of tape cast PVB-CNTs composite after 1 hour of magnetic stirring (two SEM magnifications)

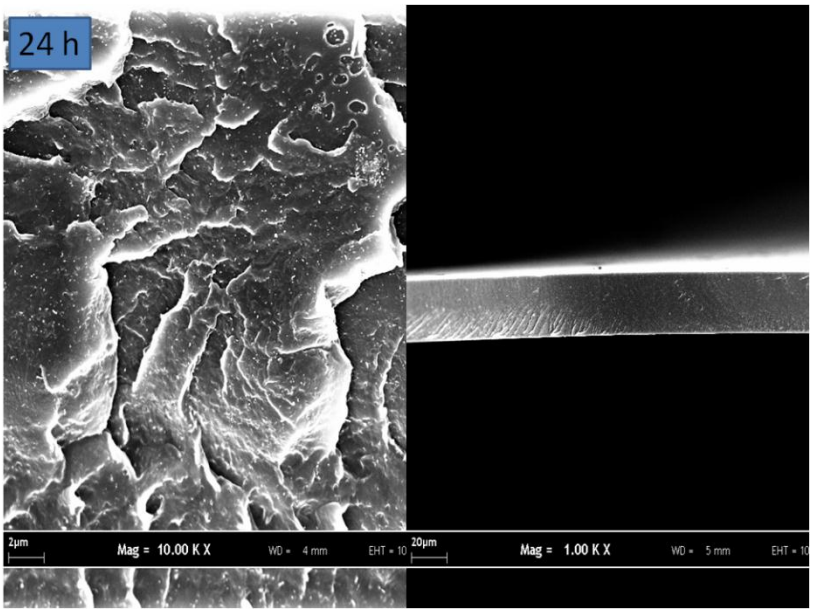

Figure 62 - Fracture surfaces of tape cast PVB-CNTs composite after 24 hours of magnetic stirring (two SEM magnifications)

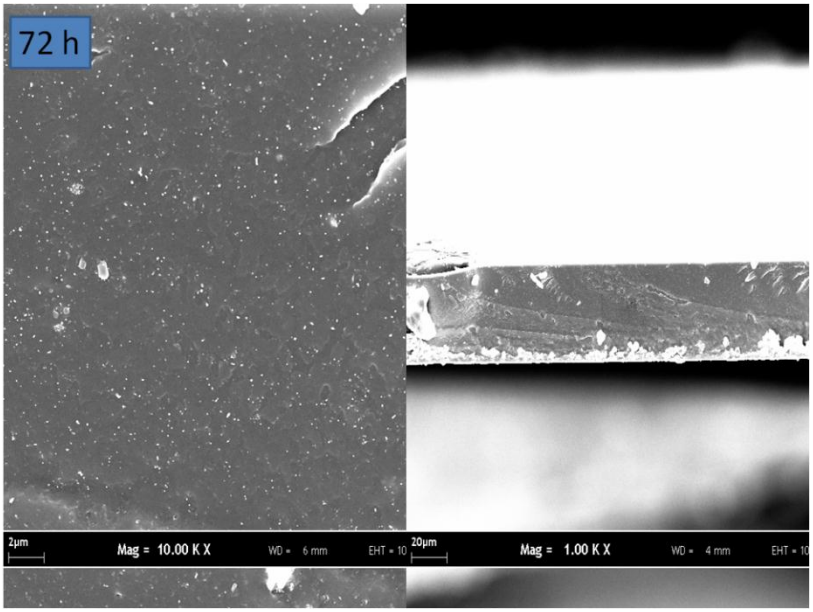

Figure 63 - Fracture surfaces of tape cast PVB-CNTs composite after 72 hours of magnetic stirring (two SEM magnifications)

The results are shown in Figure 61, Figure 62 and Figure 63 for samples stirred 1 h, 24 h and 72 h respectively: the samples with longer stirring times result more dispersed and the presence of bundles and aggregates are appreciably reduced. In particular large bundles are observed after only 1 h of magnetic stirring, with their number dwindling with increasing dispersion time. After one day it is possible to affirm that the dispersion is complete. Also considering the necessary optimisation of the process, it was decided to conduct all our experiments with a magnetic stirring step of 24 hours. This kind of test in any case showed that a better contact among the polymer and the nanotubes will improve the dispersion inside the composites, supporting the theory of a polymer effect.

A second test involved the dispersion of CNTs with different amounts of polyvinyl butyral. The study of PVB effect on CNTs dispersion was conducted dispersing 30 mg of Nanocyl™ NC7000 in 30 thousand milligrams of ethanol by 15 minutes of ultrasound sonication. After that different amounts of PVB were added and the suspensions were mechanically stirred for 24 hours, on the basis of the experimental data collected in the previous experiment. We used six different PVB amounts reported in Table 9 from 0 mg of polymer to the amount used in a normal slurry for tape casting. All the samples were then diluted 40 times with ethanol and put in test tubes for a better observation of precipitations. Our purpose was not only to detect a possible PVB effect, but also to identify the minimum quantity of polymer necessary to obtain it.

	PVB content / CNTs:PVB ratio
1	0 mg
2	30 mg (1:1)
3	150 mg (1:5)
4	600 mg (1:20)
5	2400 mg (1:80)
6	5010 mg (SLURRY amount)

Table 9 - PVB content in weight and CNTs:PVB weight ratio for the six samples prepared for the polymer effect study

Observing the test tubes with the diluted carbon nanotubes suspensions, of which the pictures are reported in Figure 64, several observation could be done: first of all, as expected, the sample prepared in absence of polyvinyl butyral resulted not dispersed and the CNTs completely precipitated on the bottom of the vial in few hours. The interesting effect correlated with the presence of PVB is already clear in the sample with a very small amount of polymer, equal to a ratio of 1 to 1 in weight with the CNTs. The suspension appears more homogeneous than the one without PBV and the supernatant ethanol appears black and not uncoloured as pure ethanol. The interesting thing is that after a quick precipitation of macro-agglomerates the supernatant maintain its dark colour for months. Increasing the PVB content we observed a decreasing amount of precipitated CNTs on the bottom of the test tube up to the sample prepared as a slurry where no visible agglomerates presence is observed.

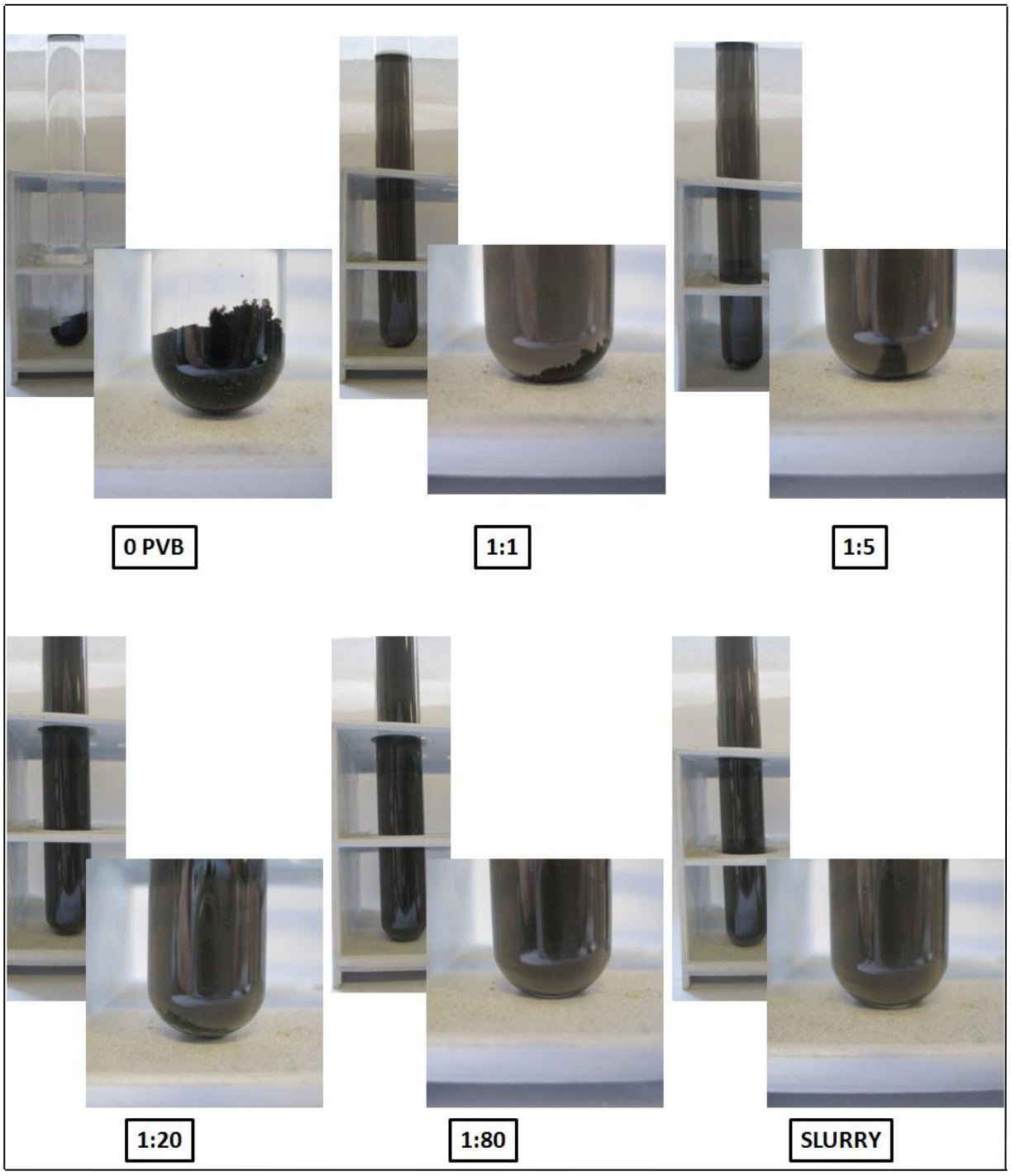

Figure 64 - Dispersions of CNTs in presence of different amounts of PVB after sonication, mechanical stirring and dilution with pure ethanol (1:40 vol)

The effect of the polymer polyvinyl butyral on the dispersion state of the carbon nanotubes has been demonstrated by these two simple tests but at this point of the dispersion investigation was useful to try to better understand which kind of effect the polymer could exert on the CNTs.

Polyvinyl butyral could be responsible for a polymer wrapping effect (extendedly discussed in section 2.4.2.2). This is a not well known interaction between carbon nanotubes and polymers. It is

considered a non-covalent functionalization and involves a nanotubes interfacial properties modification. The suspension of CNTs in the presence of some polymers leads to the wrapping of polymer around the CNTs to form supermolecular complexes (Figure 65). The polymer wrapping process is supposed to be achieved through the Van der Waals interactions and p–p stacking between CNTs and polymer chains containing aromatic rings. But the phenomenon should be also more general. In our hypothesis the wrap effect should involve the two oxygen atoms in the ring and their free electrons.

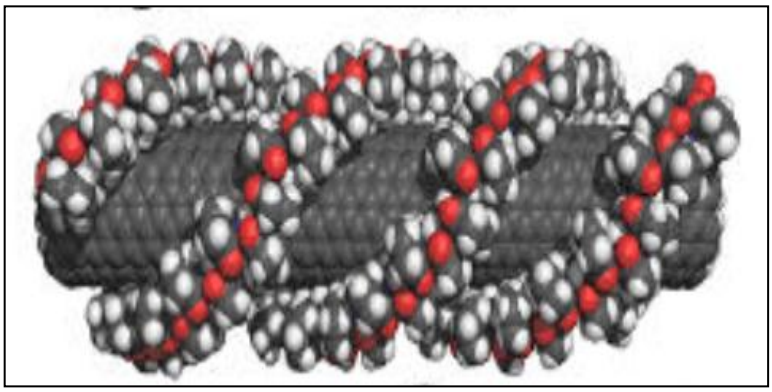

Figure 65 - Polymer wrapping model

We tried to create a very simple and easy model to evaluate the minimum quantity of polymer necessary to create a mono-layer on the CNTs. Our very basic calculations consider the surface area of the carbon nanotubes and an approximate “molecular area” for polyvinyl butyral. The results is that to create a monolayer of polymer on 30 mg of Nanocyl™ NC7000 about 6 mg of our polymer are required. Due to the statistical aspect of the effective wrapping (the polymer chains need to run into a tubes and then to start to wrap it, and this is a statistical phenomenon especially in very diluted solutions) and also considering the difficulty to weight and manipulate so small quantities of polymer, we decide to work with the 1 to 1 ratio but to try to improve the wrapping effect. The improvement starts from adding the PVB to the CNTs from the very start of the dispersion process. So the PVB is added to the nanotubes and ethanol and sonicated. An additional step of 30 minutes of ultrasounds bath sonication is inserted in our procedure to improve the contact between the nanotubes and the polymer chains (and so increase the probability of the beginning of a polymer wrapping phenomenon), also on the basis of the literature collected. A series of samples was prepared using the developed method, with the 15 minute ultrasonication and 30 minutes bath sonication steps, followed by 24 hours of magnetic stirring, only moving the insertion of the PVB from the stirring step to the probe sonication one. Other samples were only sonicated (both the 15

and 30 minutes steps and in presence of the polymer), others were prepared adding the polymer during the sonication and avoiding the mechanical stirring step 24 hours long.

From the test tubes we denoted immediately a precipitation of agglomerated carbon nanotubes lower than for the specimen only magnetic stirred (Figure 66).

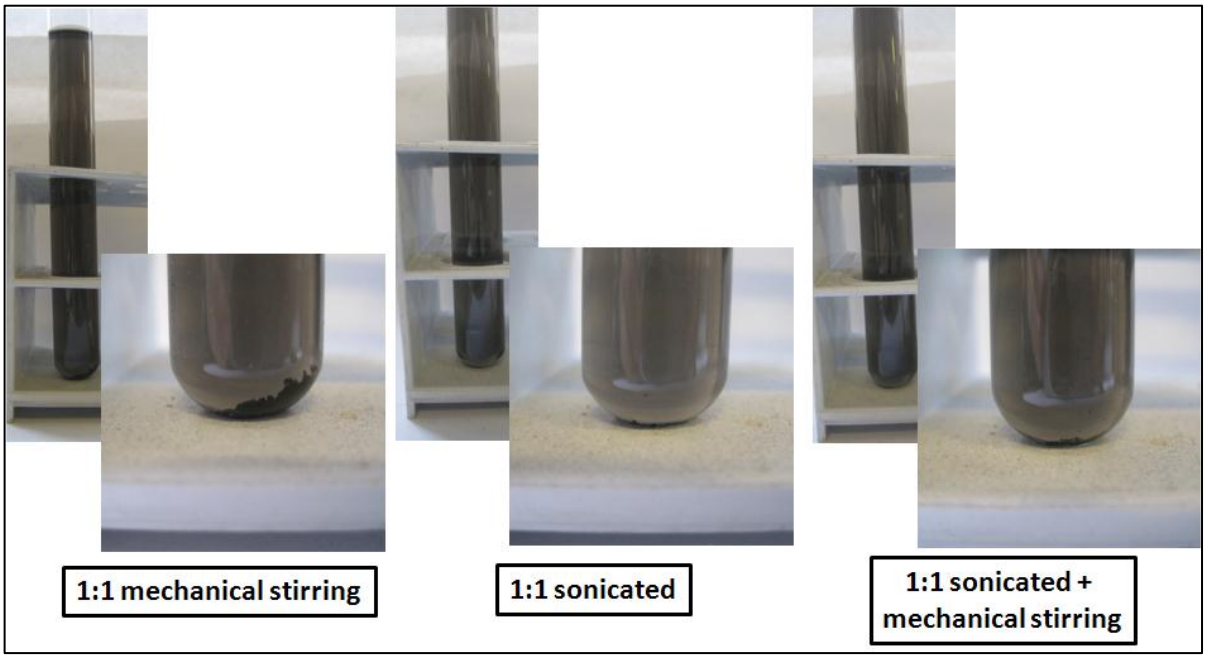

Figure 66 - Test tubes of differently treated CNTs-PVB samples. The first on the left is a dispersion in which the polymer was added in the stirring step, the central picture is for a dispersion in which the PVB is added during the sonication step and the mechanical stirring is eliminated; finally on the right a picture of a dispersion made adding the polymer during the ultrasonication and a 24 hours stirring also took place

To evaluate the dispersion state of the carbon nanotubes a drop of the three kind of samples and of pristine CNTs suspension is put on a SEM sample holder, evaporated and used for scanning electron microscopic investigation. Obviously some problems occurred due to the small excess of polymer present but the problem was not so serious to require a sample metallization for SEM analysis. In Figure 67a is reported a bundle of pristine Nanocyl™ NC7000 as bought and before every kind of manipulation. In Figure 67b is possible to observe Nanocyl™ NC7000 after the sonication process. The bundles are partially destroyed but a sort of tangled net is still present. Adding PVB after sonication, during the mechanical stirring process, the nanotubes assume the aspect registered in Figure 67c.

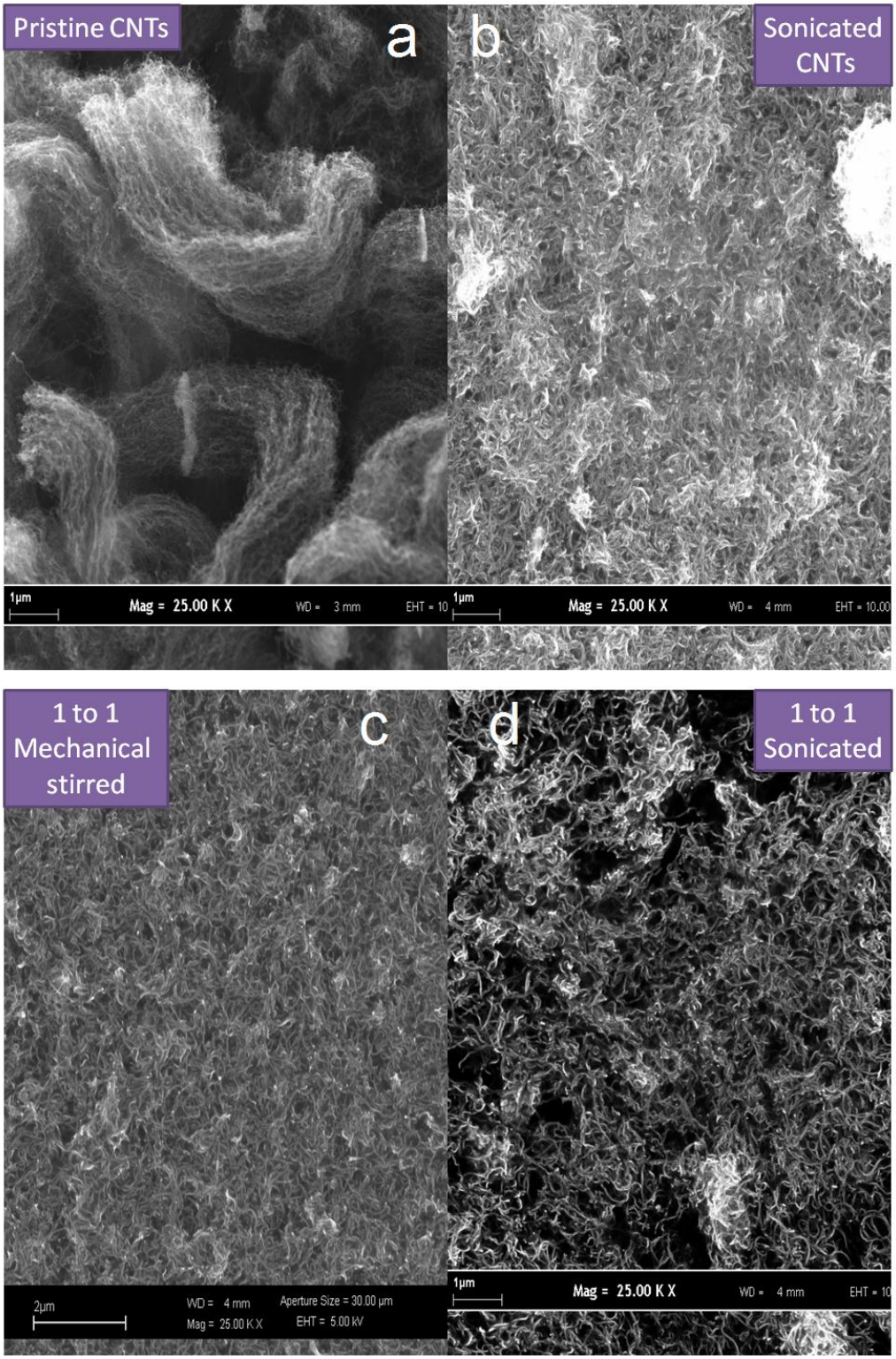

Figure 67 - SEM images of pristine CNTs (a), sonicated CNTs (b), CNTs sonicated and mechanically stirred with PVB (c) and CNTs sonicated in presence of PVB (d)

In this case single carbon nanotubes are present and they appeared well separated each other. Some bundle still hold tight but there are also zones with polyvinyl butyral agglomerates. Observing the CNTs where the polymer was added before sonication (Figure 67d) a very similar situation is reported. The problem of this kind of microscopic approach was the concentration of the

suspensions: despite of the dilution of the solutions, the number of CNTs present is very high and so is difficult well understand the dispersion and distribution state. Not significant differences were denoted for the sample with the additional stirring step after sonication of PVB.

Another approach to evaluate the dispersion state was used, i.e. UV-visible spectrometry. We tried to evaluate the presence of carbon nanotubes suspended (and so well dispersed) from a scattering effect on the light from 210 nm to 800 nm of wavelength. The samples in the test tubes were let stand still for two weeks, in order that all the agglomerates should precipitate and not interfere with the scattering test. A small amount of supernatant is taken and diluted ten times in ethanol. In our hypothesis the higher is the scattering effect the higher is the number of suspended (and so well dispersed) CNTs. The results are reported in Figure 68: the scattering effect is represented by the red line for the 1:1 ratio in weight PVB:CNTs with the polymer added after sonication, blue line is for the 1:1 ratio in weight PVB:CNTs with the polymer added during sonication. The scattering effect is correlated with the rising of the base line and the higher is the scattering the higher is the rising. In this case the two samples are not so different but the second one on the base of our hypothesis should be characterised by a better dispersion and thus a higher scattering effect. We also tested two other samples with higher content of PVB and the scattering is actually bigger. But the interesting thing is that the two samples resulted quite identical, as the effect of dispersion of PVB reach a maximum after a certain amount.

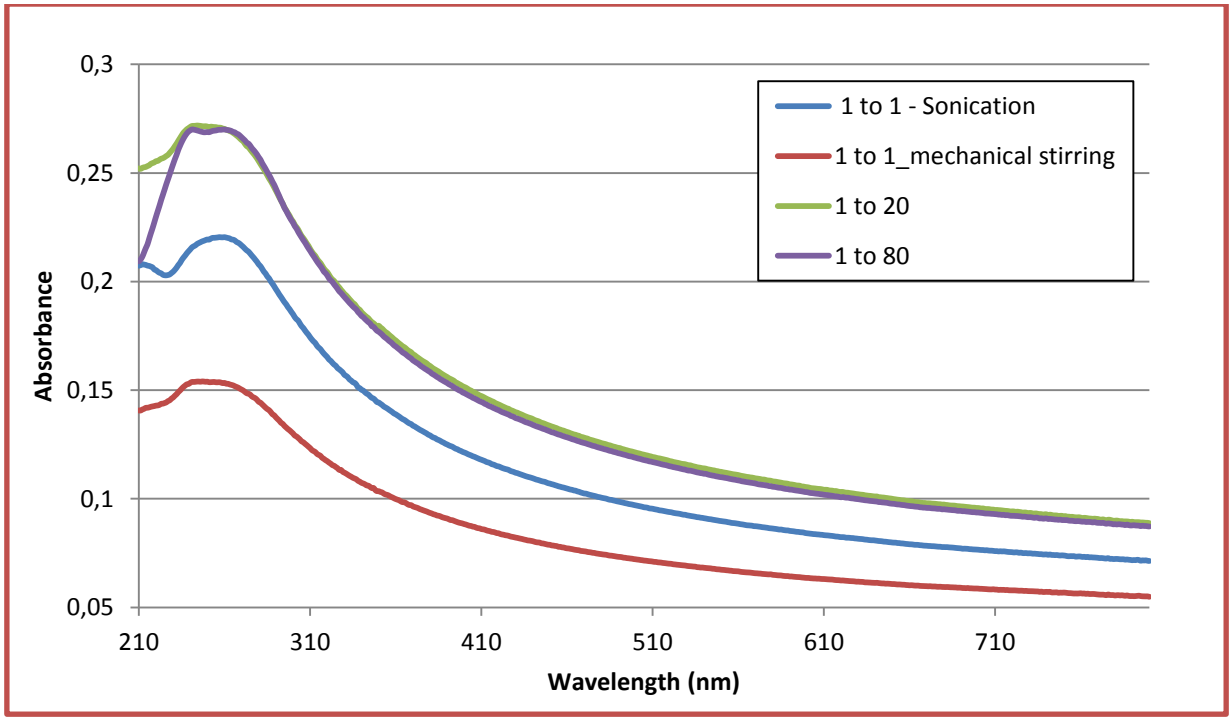

Figure 68 - UV-vis absorbance of different CNTs suspensions

Another study on the dispersant effect of polyvinyl butyral was made: instead of the PVB two different compounds: the 1,3-dioxolane and 1,3-dioxane (Figure 69). They have cyclic structures with two substituent atoms of oxygen, similar to the PVB one. These two compounds should help us to understand the effect on dispersion of the 2 oxygen atoms. A ratio of dioxolane and dioxane of 10 to 1 in weight on respect of CNTs was used. I added them before sonication so to improve the contact and I used a ratio of 10 to 1 considering the statistical aspect of a monomer linkage on respect of a polymer one. The result from a macroscopic point of view was not good and is similar to the sample sonicated without added compounds. The problem in the utilization of these two dispersant is certainly the absence of an actual polymer, which made the process of linkage on the carbon nanotubes surfaces more favourable.

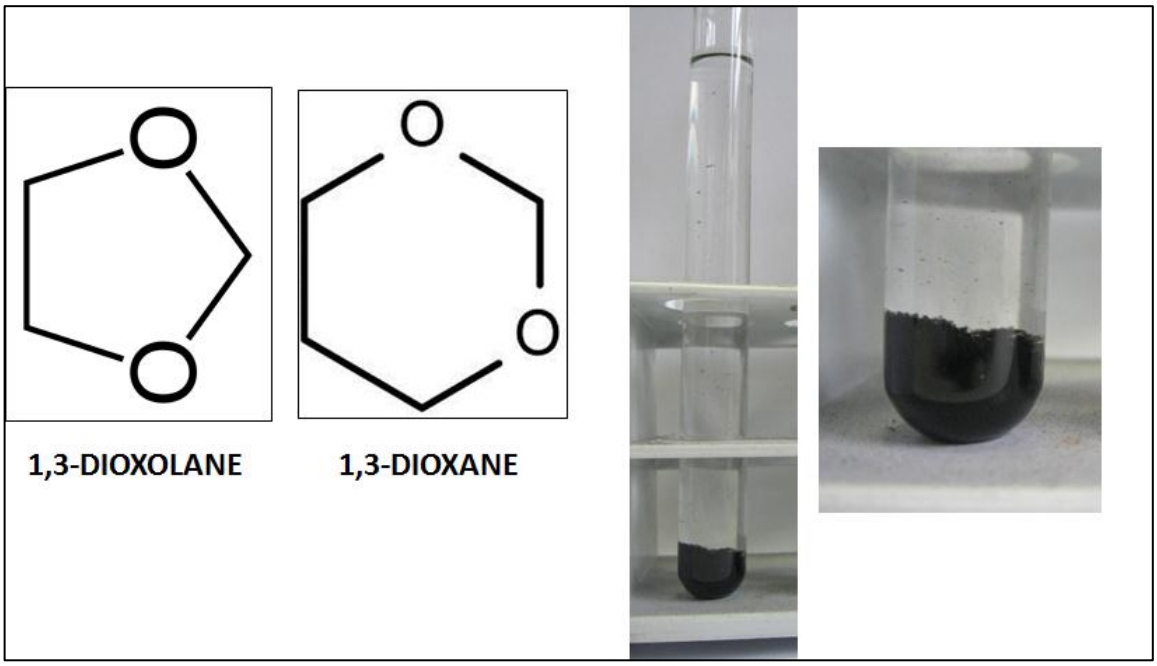

Figure 69 - 1,3-dioxolane and 1,3 dioxane structures and an example of not dispersed solution

Because of the excellent results obtained using the commercial grade multiwalled carbon nanotubes provided by Nanocyl™, we decided to use the same approach also for other kinds of CNTs, with different aspect and purity grade. We decided to adopt the dispersion technique with polyvinyl butyral 98 to Sigma Aldrich multiwalled nanotubes with high purity grade (Figure 70), with Future Carbon's MWCTs (Figure 71), and also with nanotubes produced by Arc Deposition at the National Laboratories of Frascati (Laboratori Nazionali di Frascati) - I.N.F.N. - Nanotechnology Laboratory (Rome) (in collaboration with Dr. Federico Micciulla). All the three kinds of nanotubes appear less entangled then the NC7000. The CNTs were treated as previously described for Nanocyl™ NC7000 by ultrasonication and in presence of PVB. After 24 hours of magnetic stirring the obtained slurries were

cast on the support and then dried in air at ambient temperature. The tape cast composites were then broken in liquid nitrogen, in order to avoid a plastic fracture surface, metallized with a very thin chromium layer and finally observed by Scanning Electron Microscopy.

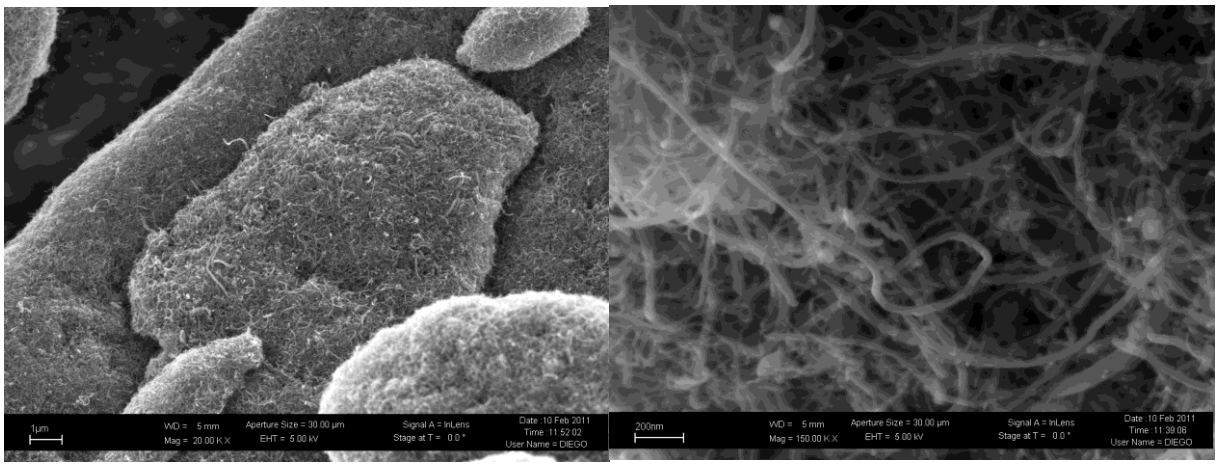

Figure 70 - Two different magnifications SEM images for Sigma Aldrich MWCNTs

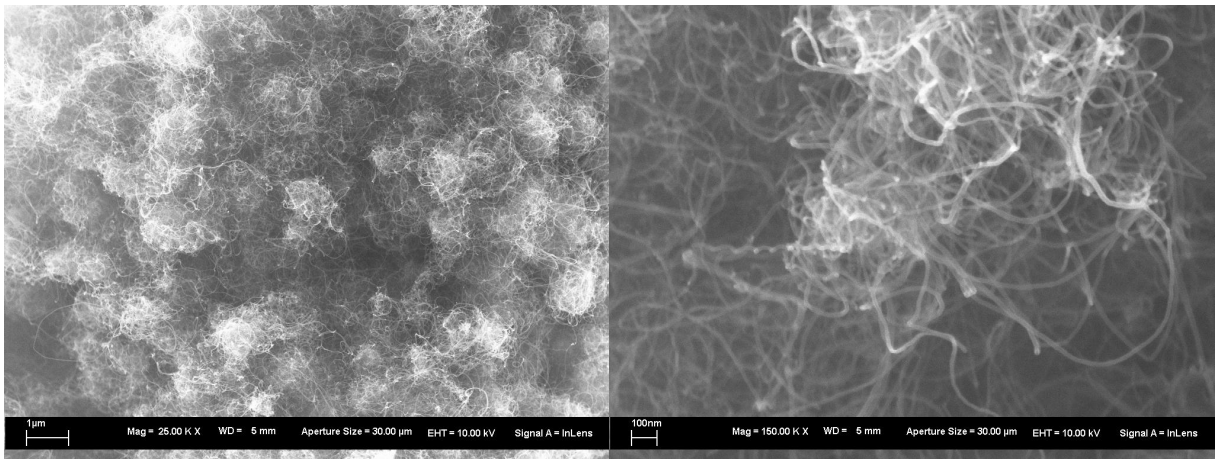

Figure 71 - Two different magnifications SEM images for Future Carbon MWCNTs

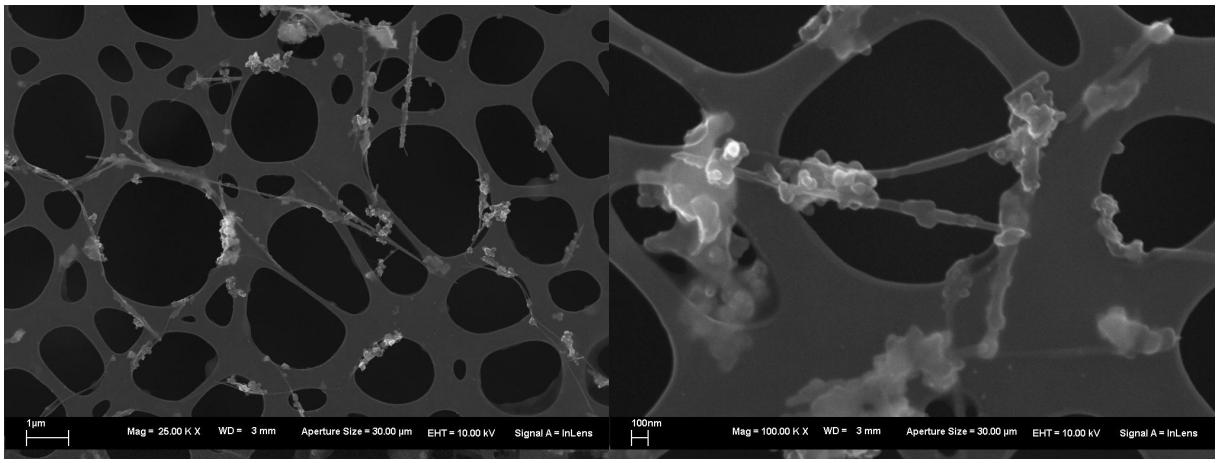

Figure 72 - Two different magnifications SEM images for MWCNTs by Arc Deposition at Laboratori Nazionali di Frascati - I.N.F.N. prepared on a TEM sample holder

The results are reported in Figure 73, Figure 74 and Figure 75, where several SEM images with different magnification are shown for each sample.

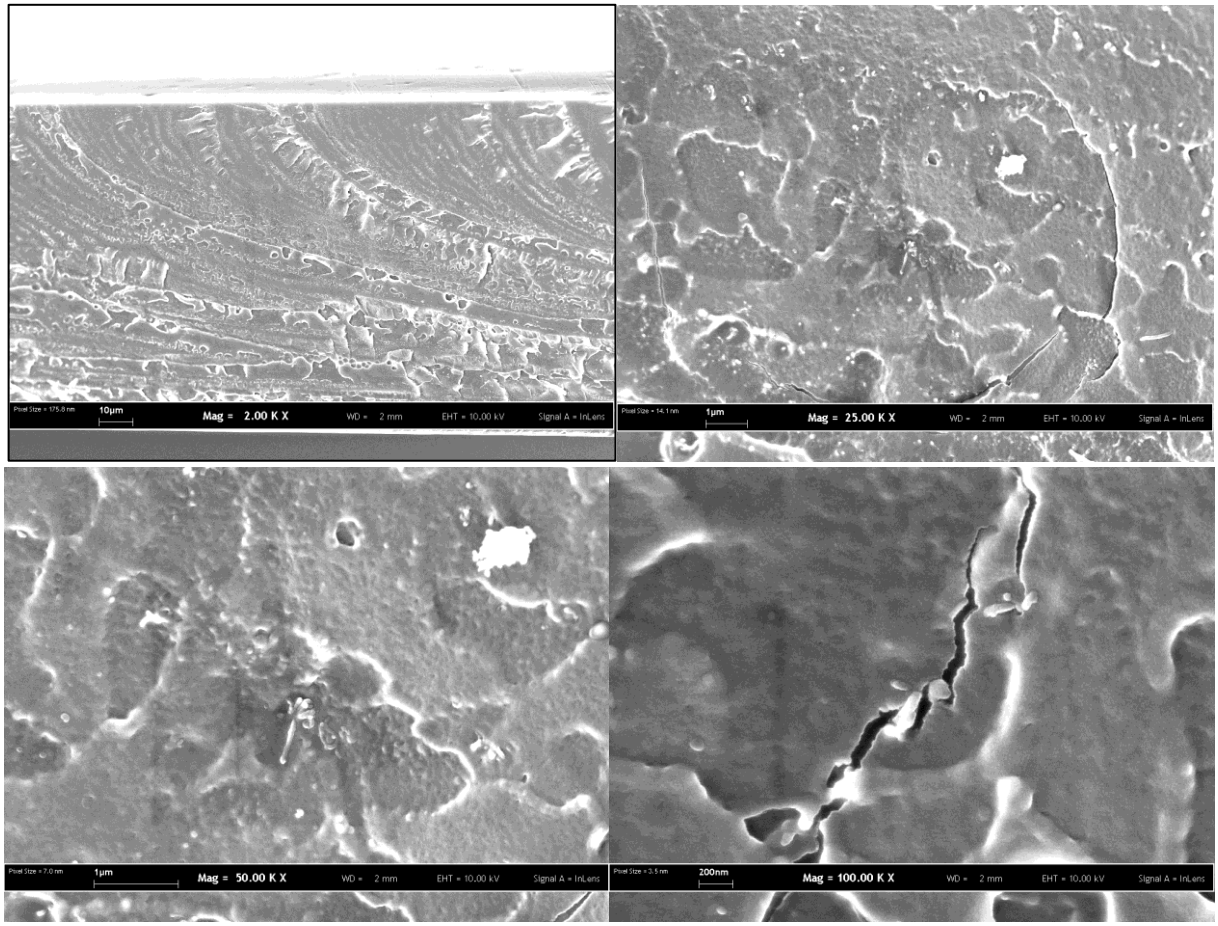

Figure 73 - Four SEM images at different magnifications for cast composites reinforced with Sigma Aldrich MWCNTs

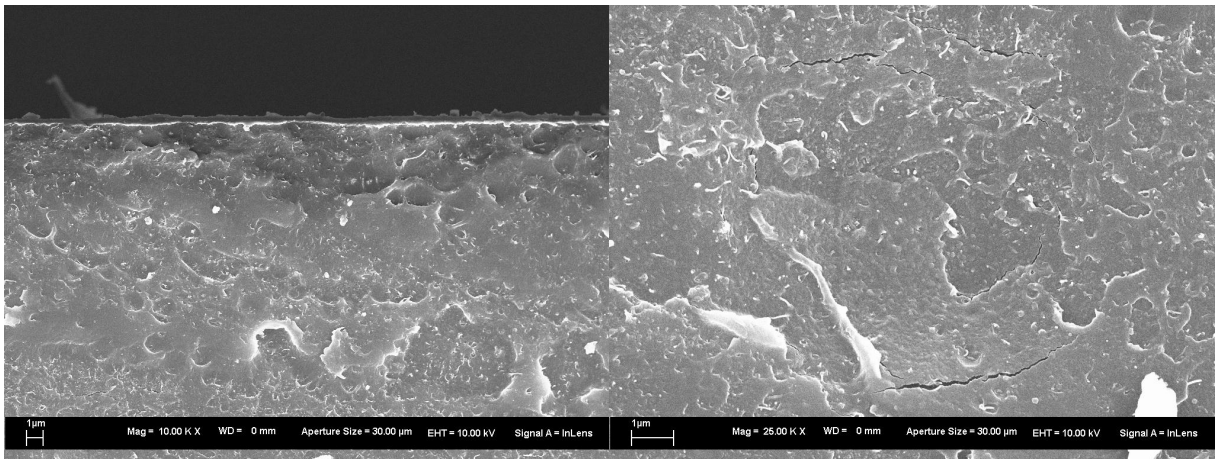

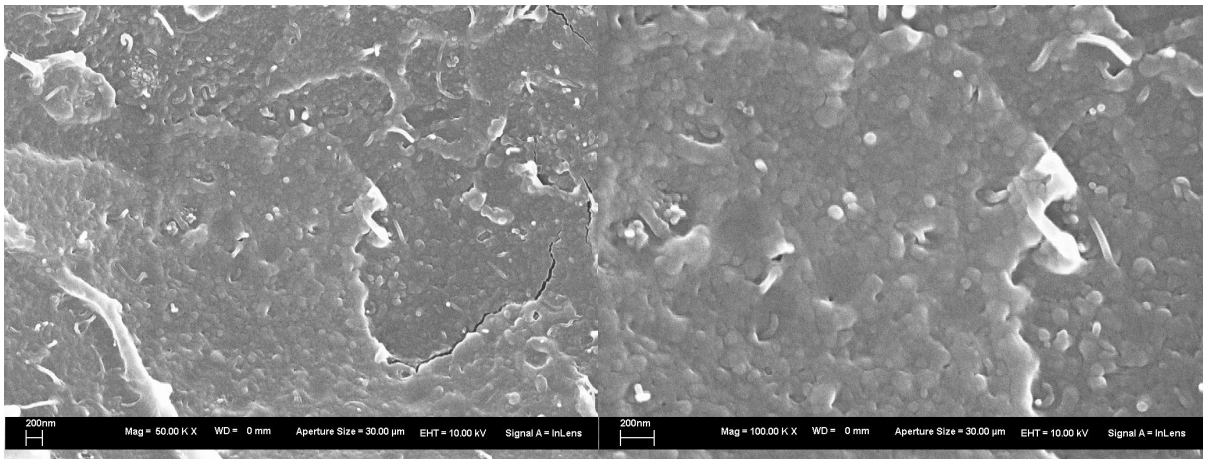

Figure 74 - Four SEM images at different magnifications for cast composites reinforced with Future Carbon MWCNTs

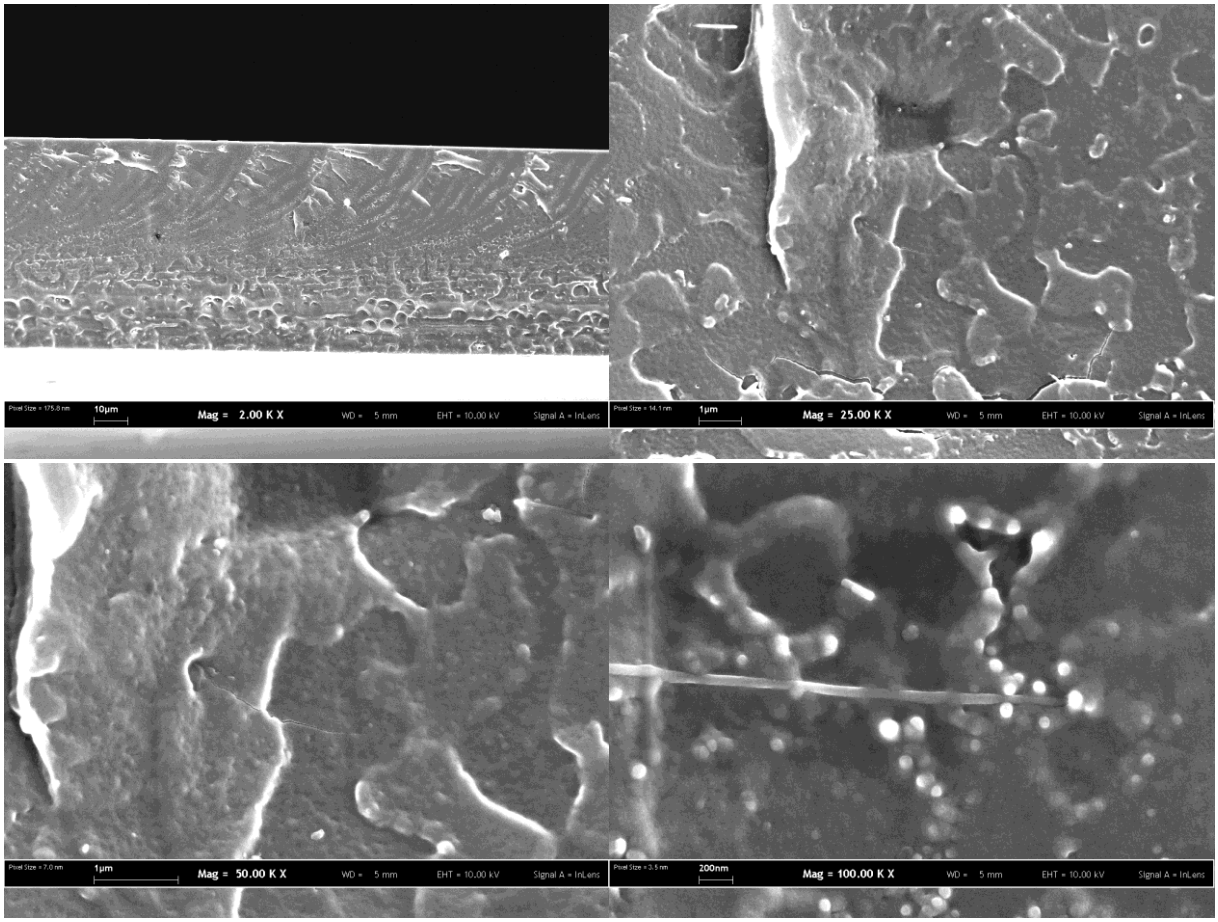

Figure 75 - Four SEM images at different magnifications for cast composites reinforced with MWCNTs by Arc Deposition At Laboratori Nazionali di Frascati - I.N.F.N.

All the three kinds of samples can be considered very similar to the composites obtained using carbon nanotubes Nanocyl™ NC7000: the nanotubes appear well dispersed and distributed on the fracture surface of the material, they are also partially orientated along the casting direction and we can observe especially their diameter (with spots and circles). Just few small bundles of not dispersed CNTs can be still identified. It is very interesting also to observe a diffuse phenomenon in which, in presence of cracks, the nanotubes are placed to form a bridge between the two edges of the crack.

In conclusion it is possible to affirm that the dispersion technique developed involving ultrasound sonication and use of polyvinyl butyral as a surfactant is successfully applicable to several kinds of MWCNTs, with different purity grade, diameter, length and aggregation state.

4.2. POLYMER MATRIX COMPOSITES

The dispersion of carbon nanotubes investigation was conducted in parallel to the production of composite materials, , to which is effectively strictly related. Indeed the efficient dispersion of CNTs and the establishment of a strong chemical affinity with the surrounding matrix are fundamental prerequisites for the production of high strength and stiffness composites. In the present experimental section the polyvinyl butyral has been used not only as dispersing agent, but also as the matrix in the preparation, by tape casting, of composite tapes with improved mechanical properties. The purpose of the work was not only to obtain carbon nanotubes-polymer composites with suitable characteristics, but also to produces them with low cost raw materials. Therefore we used for our experiments industrial grade nanotubes Nanocyl™ NC7000 and a commercial grade polymer.

As discussed in section 3.4, the preparation of tape cast polymer composites involved a pre-dispersion step of the carbon nanotubes in ethanol. The sonication step was initially conducted using a probe sonicator for 15 minutes. On the basis of the results obtained during the dispersion investigation the procedure has been modified and the final samples were prepared coupling a 15 minutes probe sonication step to a 30 minutes bath sonication one. An amount of 10% in weight of polyvinyl butyral, with respect to the solvent, was added to the ethanol before the sonication steps so to improve the contact among polymer chains and carbon nanotubes and to fully exploit the dispersant role of PVB. After that the remaining polymer was added during the 24 hours long mechanical stirring step. The development of the slurries production route occurred in parallel with the dispersion investigations, described in the previous section. It was decided to adopt a 24 hours magnetic stirring step not only to improve the contact between matrix and CNTs (indeed, our dispersion studies have proved that the crucial condition for an improved dispersion is the presence of PVB during sonication, more than the magnetic stirring time), but also to fully dissolve the PVB grains in the solvent and to homogenize the slurries. In any case, when a low stirring time was used (1hour), carbon nanotubes agglomerates were yet present inside the tape, as shown in Figure 76a. Here a light circular zone can be observed on the section of the tape, which corresponds to a bundle of nanotubes that does not contain any polymer. When the time was increased up to 24 hours all the agglomerates disappeared and the carbon nanotubes appear as white spots on the grey surface of the polymer. They appear well separated, distributed and partially orientated along the casting direction (Figure 76b).

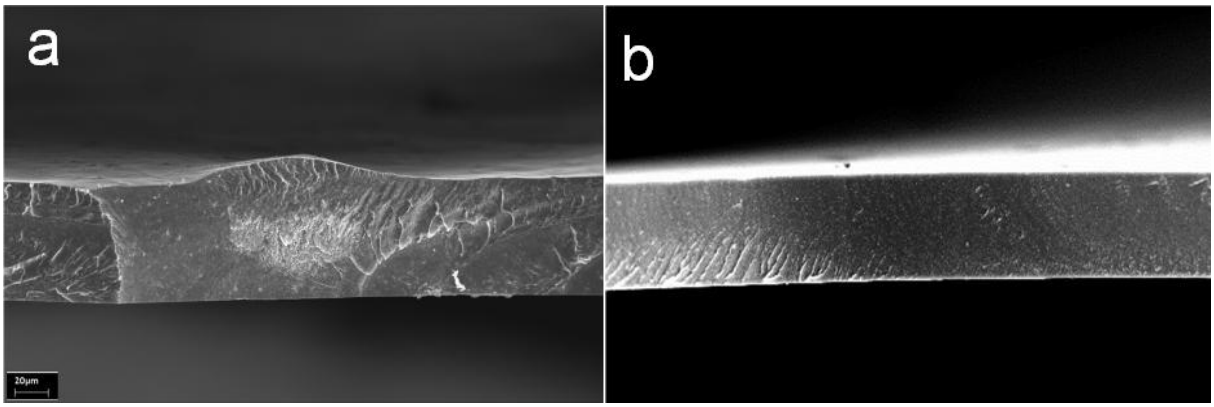

Figure 76 - Section of a 1 hour stirred 0.5% CNTs composite (a) and section of a 24 hours one (b)

The slurry was then cast on a Mylar support, moving with a controlled speed, and the layer thickness was controlled by the height of the blade and the viscosity of the slurry. The organic solvent was then slowly removed by controlled evaporation in air at ambient temperature. Different samples were prepared by modifying the amount of CNTs but maintaining constant their ratios with the solvent and the polymer.

As mentioned in the previous section the analysis of the dispersion was carried out mainly by SEM observation of the composite tapes.

After the process optimization several concentration of carbon nanotubes were used in order to obtain tape cast composites with different amount of reinforcement and so to study its effect on the final properties of the material. In Figure 77 it is shown the section of a PVB/CNT composite containing 0.5% of carbon nanotubes. In this case the nanotubes are uniformly dispersed within the polymer matrix, and a partial orientation is observed.

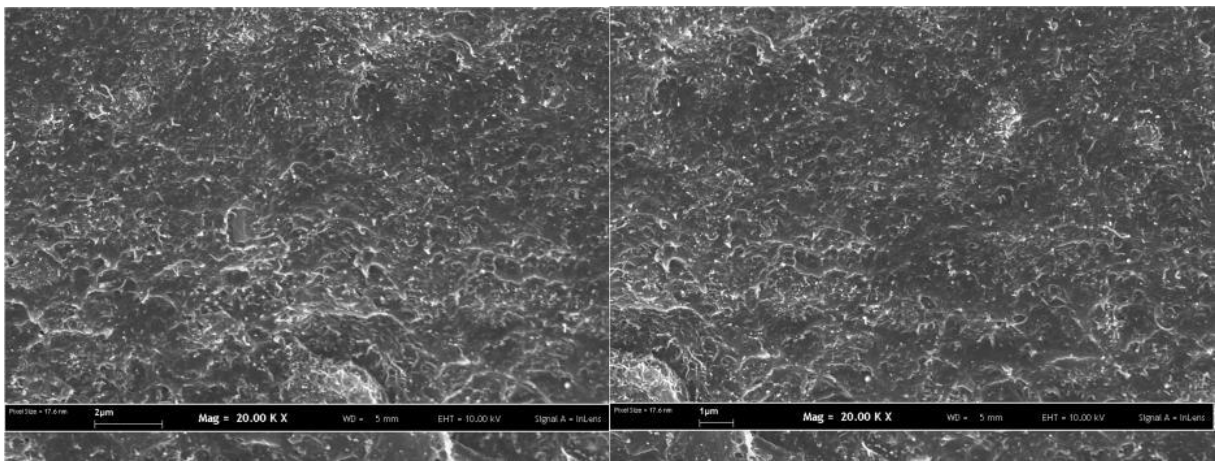

Figure 77 - PVB/CNT composite containing 0.5% of carbon nanotubes.

In a tape containing 1% in weight of carbon nanotubes (Figure 78) instead the dispersion is less good. Zones with CNTs agglomerates can be observed together with zones with a lower concentration of nanotubes. Small undispersed bundles can also be observed along the tape section. In a tape containing 2.5% of CNTs many nanotubes are present in very large not dispersed bundles, so that macroscopic defects are found, as can be observed in Figure 79. The presence of larger agglomerates can be probably related to the higher concentration of carbon nanotubes, that do not allow a complete dispersion during the ultrasonication step.

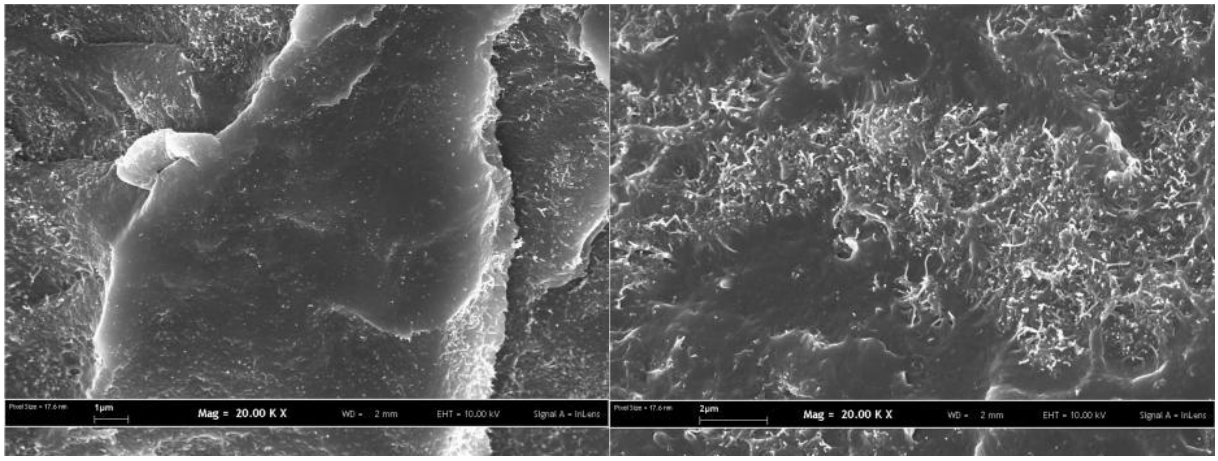

Figure 78 - PVB/CNT composite containing 1% of carbon nanotubes.

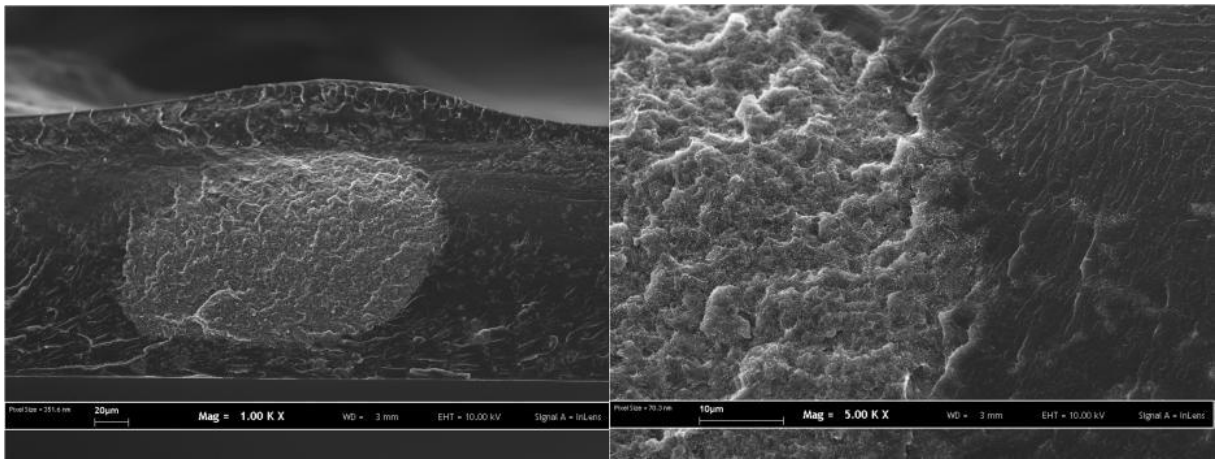

Figure 79 - PVB/CNT composite containing 2.5% of carbon nanotubes.

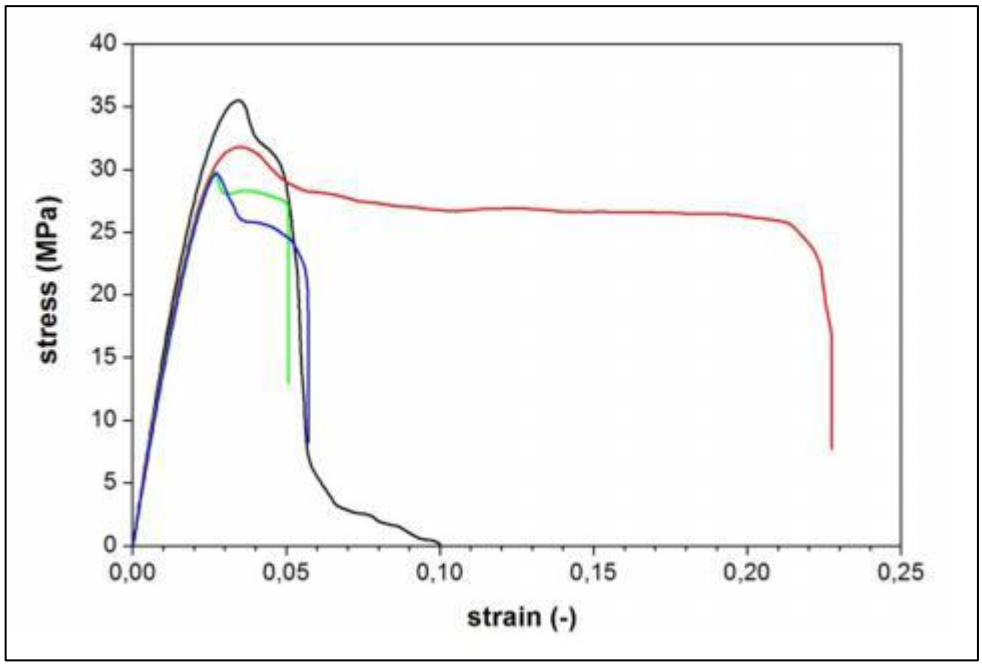

Figure 80 - Tensile tests of a PVB-98/CNT composite containing 2.5% of carbon nanotubes.

Mechanical performance of the composites was measured by tensile tests, and both maximum strength and Young's modulus were calculated. In Figure 80 it is possible to see a typical set of tests for a highly concentrated nanotubes solution (PVB-98, 2.5% of carbon nanotubes). The presence of defects inside the composites heavily influences the maximum strain registered during the mechanical tests. When a defect is present, a crack formation occurred at low strains, while if no defects are present, the strain at break results larger.

The maximum strength and Young's modulus are not affected by the nanotubes concentration in composites obtained with PVB-98 (the one generally used in the production of the tape cast composites since the start of this experimental work) (Figure 80). This was assumed to be due to the fact that adhesion between the carbon nanotubes and the polymer is not strong enough to transfer the mechanical load from the polymer matrix to the nanotubes. One of the reason for such a behavior could be that the chain length of this specific polymer is too short for both wrapping of the nanotubes and efficaciously entanglement with the other polymer chains. Thus the dispersion is good but the nanotubes are not effective in reinforcement.

For this reason we decided to change the polyvinyl butyral chain length and use a PVB-76 with higher average molecular weight (between 10000 and 11000, instead of values for the PVB-98 comprised between 5000 and 6000). With PVB-76 based composites, indeed, both strength and modulus increases substantially for low nanotubes concentration, where it is easier to obtain an optimal dispersion. For very high amounts of CNTs, instead, strength decreases substantially, due to the presence of defects. Young's modulus is less affected by the presence of defects, and only at very

high concentration a reduction is observed, due to the difficulties in dispersion in too concentrated suspensions. The higher chain length of PVB-76 it is thought to be the cause of a stronger interaction with nanotubes, thus providing an effective reinforcing mechanism.

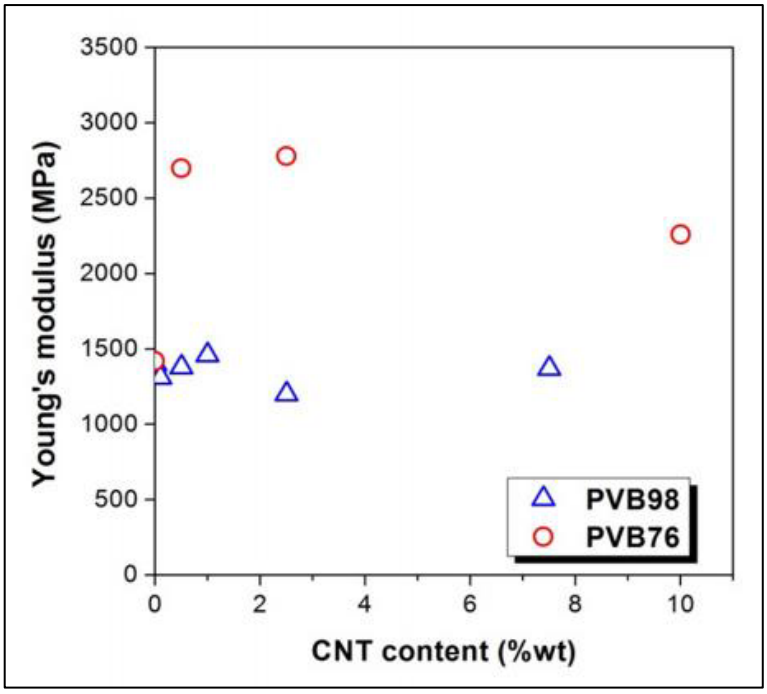

Figure 81 - Young's modulus VS CNT content (%wt) for PVB-98 and PVB-76 composites

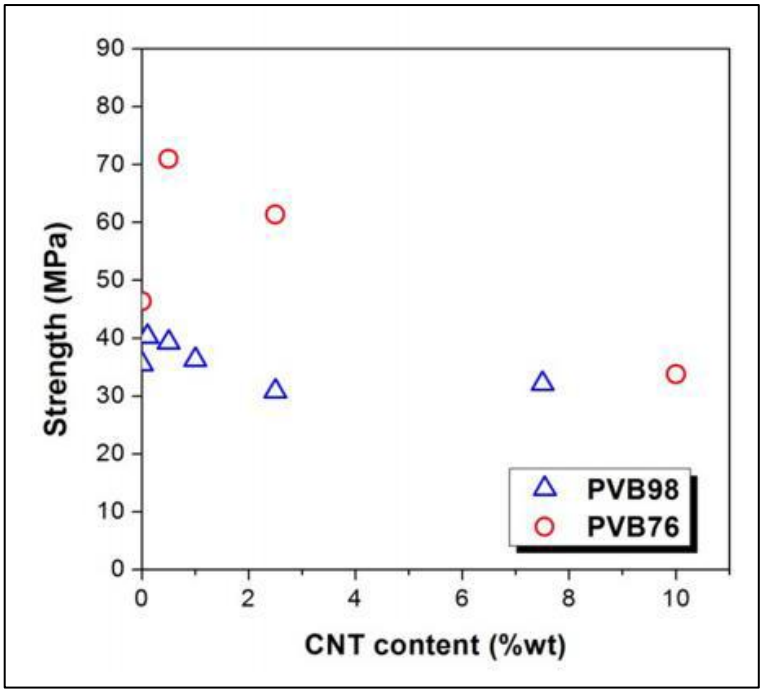

Figure 82 - Maximum strength VS CNT content (%wt) for PVB-98 and PVB-76 composites

Starting from the data of the PVB-76 reinforced with 0.5% CNTs the modulus and strength of the CNTs was calculated, using a simple law of mixtures and hypothesising a perfect alignment of the nanotubes along the casting direction. Since the alignment is not perfect, these values are a lowest limit for the mechanical performance of CNTs. The calculated values are 260 GPa for CNTs Young's modulus and 5.0 GPa for CNTs strength, that are reasonable lowest limit values for commercial low-cost nanotubes. By hypothesising that the CNTs are completely dispersed in the 0.5% sample, as is suggested by SEM observation, it was also possible to calculate the percentage of "active" CNTs in the different composites with PVB-76. The results suggest that the maximum concentration of well-dispersed nanotubes in the standard dispersing conditions is lower than 1%, and the other nanotubes are instead organised in bundles, that do not contribute to the overall mechanical properties, and can reduce substantially the strain at rupture by triggering cracks formation.

4.3. CERAMIC MATRIX COMPOSITES

The carbon nanotubes dispersion approach developed and described in section 4.1 can be successfully applied to the preparation not only of polymer matrix composites but also to ceramic matrix ones. Also for ceramic matrix materials the dispersion of the CNTs is fundamental for the improvement of the mechanical properties of the final composites and the use of PVB as a dispersant can solve the agglomeration problem.

The CMCs were produced using the tape casting technique and the production procedure and the slurries composition are deeply described in section 3.4. After pre-dispersion of CNTs (15 minutes of probe sonicator in presence of the 10% of the whole PVB matrix and 30 minutes of bath sonicator) SiC powders, sintering additives (carbon and boron), dispersant (fish oil), plasticizer (PEG) and the remaining binder were added and the slurry homogenised by mechanical mixing in alumina jars for at least 18 hours.

Whereas the tape cast polymer matrix composites were tested directly, for SiC-CNTs ones the cast films were used for the production of multilayer samples. The additives and the binder were eliminated by a thermal treatment at 800°C while the bar shaped green samples were sintered by a second pressureless treatment and at 2200°C maintained for 30 minutes. The whole process is the one developed by our research group for pure SiC multilayers production.

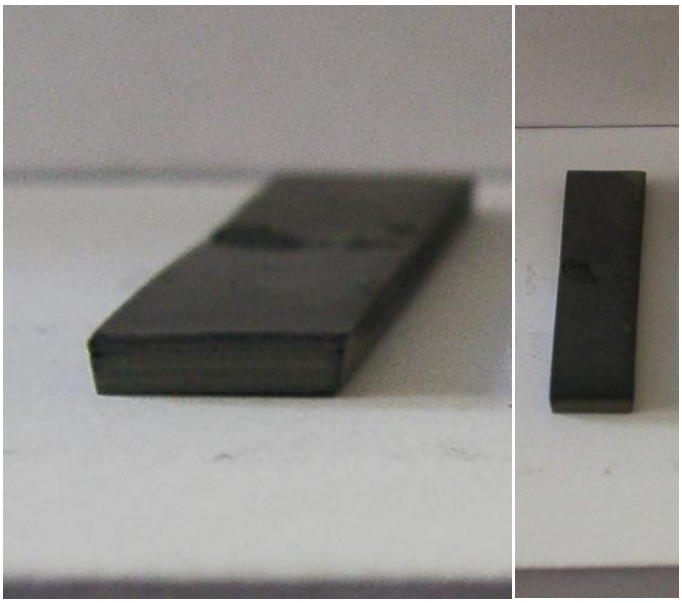

Figure 83 – Typical aspect of a bar shaped SiC-CNTs multilayer after pressureless sintering

The sintered specimens (Figure 83) were first characterized in terms of geometric density. In presence of 1% in weight of CNTs the theoretical density is expected to reach the value of 3.19 g/cm^3, whereas for pure SiC the density is 3.21 g/cm^3. The multilayer CMCs composites after

sintering showed an average density of 2.75 ± 0.02 g/cm^3, which corresponded to a relative density of 86%.

The Young's or elastic modulus of the SiC-CNTs composites were then measured and the samples exhibit an average value of 325 ± 1 GPa, a comparable value with respect to the pure SiC multilayer specimens measured in a previous work of the research group (Biamino et al., 2008). On the contrary a decreasing in the maximum bending strength had been registered for the SiC-CNTs materials (270 ± 10 MPa) with respect to the pure SiC multilayer specimens (321 MPa) (Biamino et al., 2008). This effect is probably related to the lower density of the multilayer composite samples with respect of the theoretical density.

The polished sections of the specimens and their fracture surfaces (after three point flexural tests) were finally investigate in terms of microstructure by scanning electron microscopy.

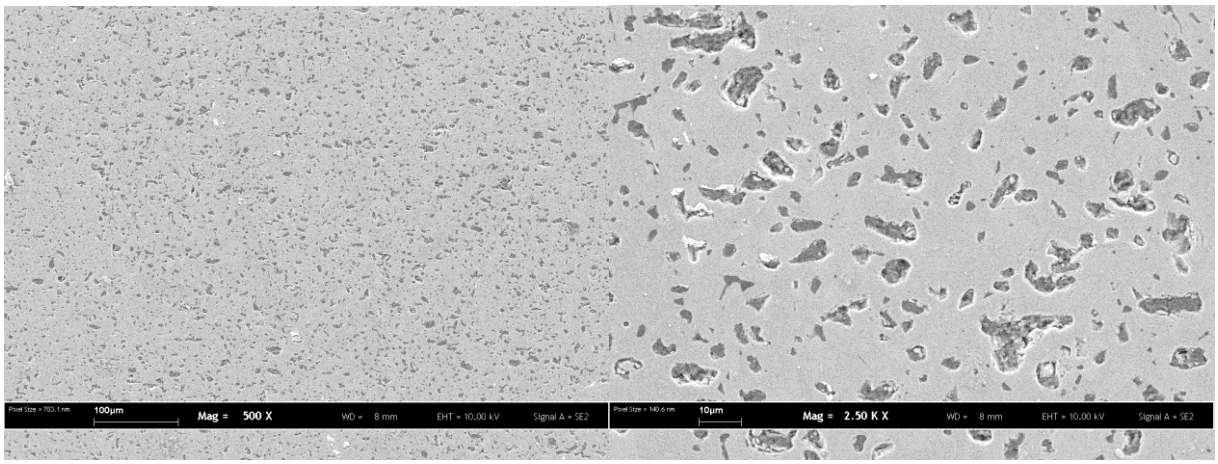

Figure 84 - SEM images of the polished section of SiC-CNTs multilayer composites

Despite of the presence of a large amount of porosity (predictable on the basis of the relative densities measured), the SiC-CNTs composites appeared quite homogeneous and it was impossible, also at very high magnifications, to pinpoint bundles of carbon nanotubes, which means that CNTs had been effectively and efficaciously dispersed.

These results represent at present a good starting point for the CMCs reinforced by carbon nanotubes production. Indeed, the future perspective of this branch of the work, now that a good dispersion and distribution of the reinforcement inside the SiC matrix has been achieved, will be the improvement of the sintering so to obtain more relevant increasing of the mechanical behaviour of the composites.

4.4. METAL MATRIX COMPOSITES

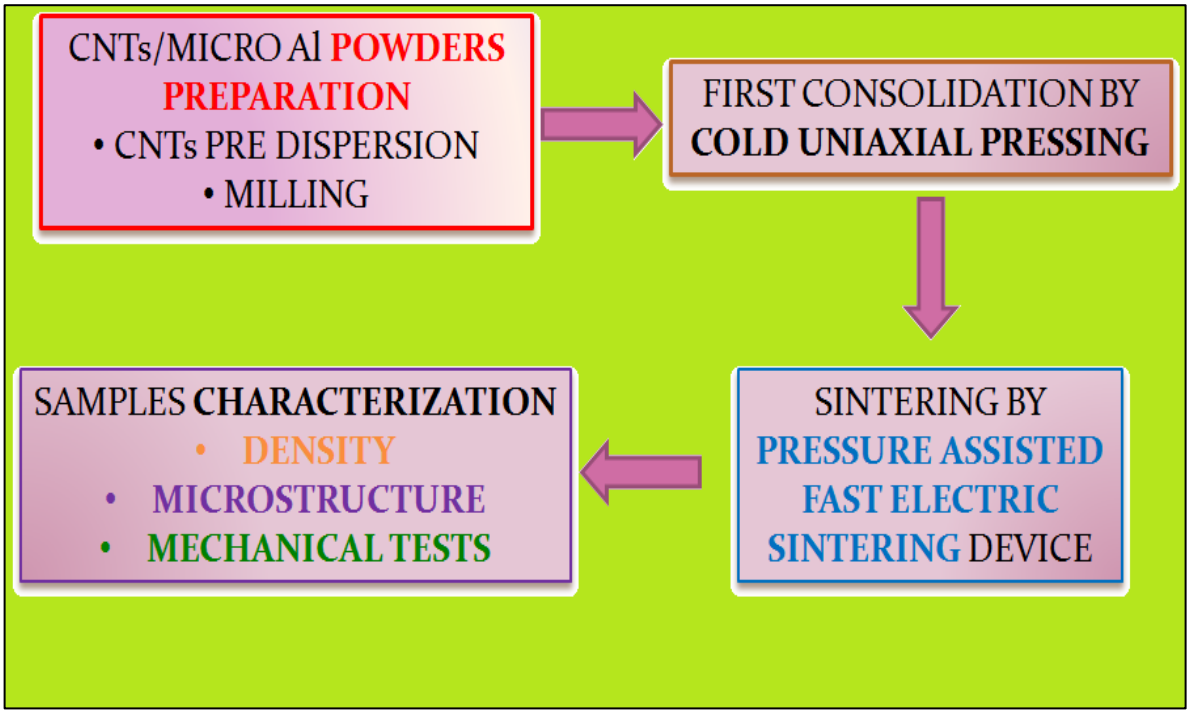

Figure 85 - Schematic overview of the preparation and characterization procedure for aluminium powder matrix composites reinforced by carbon nanotubes

The fourth part of my research work concerned the preparation and characterization of metal matrix composites reinforced by carbon nanotubes using the powder metallurgy technique. This kind of decision was brought to the great difficulty in dispersing carbon nanotubes in a molten metal matrix, especially aluminium; moreover, liquid aluminium and carbon nanotubes react with the formation of aluminium carbide (Al_4C_3) that is detrimental to the composite mechanical properties, due to its brittleness and to its reaction with water from the environment. The choice of aluminium as metal matrix is substantially due to its great technological interest: aluminium matrices have attracted great interest because of their excellent strength, low density and corrosion resistance and they result very promising for weight sensitive applications.

In Figure 85 is reported a schematic overview of the procedure for the preparation and characterisation of the composites obtained starting from aluminium powders and multiwall carbon nanotubes: the process always started from the powder preparation. The CNTs were pre-dispersed in a proper solvent by ultrasounds and then milled with the aluminium powders. After the evaporation of the solvent the powders were pressed by cold uniaxial pressing. The actual sintering was conducted by Pressure Assisted Fast Electric Sintering (PAFES), a particular technique of the Spark Plasma Sintering (SPS) family (cf. section 3.3). After sintering, the specimens were characterized in terms of density, microstructure and mechanical properties. Several samples were prepared and

characterized during the experimental work and the development of the research will be discussed in section 4.4.3.

4.4.1. POWDER PREPARATION

One fundamental step for the production of these composites is the powders preparation. The first attempt was made by milling together the aluminium powders and the carbon nanotubes by ball milling and in absence of any kind of solvent or liquid. The dry ambient and the small energy provided by the device did not ensure a good dispersion and distribution of the reinforcement and did not allow the preparation of homogeneous composite powders. The second attempt was made milling in dry ambient again the metal particles and the CNTs but by using a High Energy Planetary Milling device. Because of the high energies and local high temperatures reached during the process, in order to avoid oxidation reactions of the powders, the jars were filled with an inert gas. At the end of the process the powders resulted less stable and spontaneously flammable in calm air. Thus we decided to adopt the same process but adding a solvent in the jars and completely submerge the components of the mixture, in order to avoid overheating and undesired reactions; 2-propanol was added and the problem of flammability of the powders solved. Finally, on the basis of the dispersion study we decided to add a further step of pre-dispersion of the CNTs: the carbon nanotubes were ultrasonicated for 15 minutes by a ultrasound probe and 30 minutes in a bath sonicator in 2-propanol. After the dispersion of the CNTs the liquid was put in a jar and aluminium powders were added and mixed together by High Energy Milling process. Steel balls (5 mm diameter) with balls-to-powder ratio of 15:1 were used, and all the residual volume into the jar was filled by 2-propanol. Ball milling time was 1 h, with interim periods of 15 minutes every 15 minutes of milling, in order to avoid over-heating. The obtained powders were dried in an oven at 40°C for 12-24 hours. The final products were generally observed by Scanning Electron Microscopy. All the specimens produced in this section of the experimental work contained multiwall carbon nanotubes produced by Sigma Aldrich.

4.4.2. SINTERING PROCESS BY PAFES

The obtained Al-CNTs powders mix were first consolidated by cold uniaxial pressing (8 tons load and 30 seconds of loading time). Then the green disc-shaped specimens obtained (25 mm diameter, 2-4 mm height) were sintered by the PAFES device. The green specimens were put inside a graphite cylindrical die of the same diameter and in contact with two movable graphite punches (Figure 86); the temperature was monitored by a type K thermocouple in contact with one of the two punches.

The sintering was performed in a low vacuum atmosphere and it consisted in a cycle (AC current used, 50 Hz frequency): 15 minutes at 630°C (reached in a couple of minutes) with a 60 MPa pressure applied continuously. After that, pressure and current supplies were interrupted. A typical temperature versus time plot registered during a PAFES sintering is reported in Figure 87.

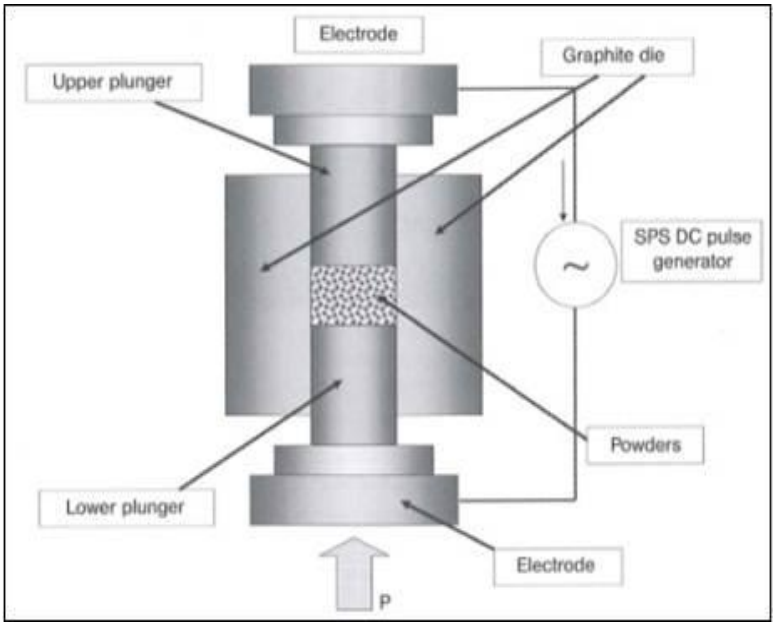

Figure 86 - A schematic representation of a graphite die and of two punches for ECAS applications

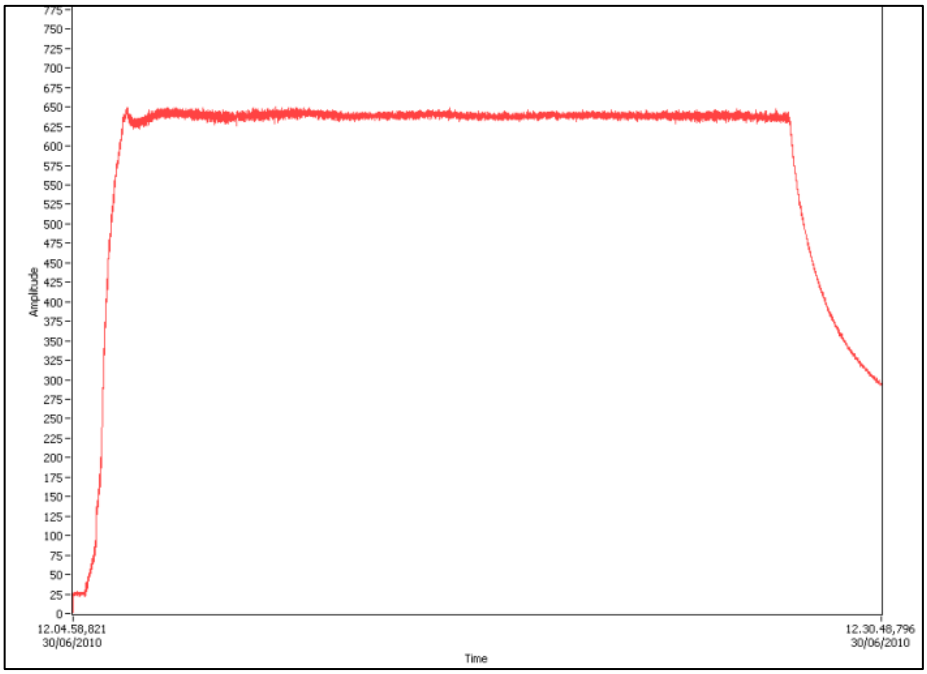

Figure 87 - A typical Temperature VS time plot registered during a PAFES process

Because of the position of the thermocouple on one of the graphite punches the registered temperature is slightly higher than the real one reached by the sample (positioned at the centre of

the die and in contact with the punches). To keep into account this effect, the first attempts when the die and punches were changed (because of the wear or breakage of the graphite) were used to calibrate the system, by trying to reach the full density of pure aluminium discs but at the same time avoiding their melting. All the temperature values that will refer to are the temperatures measured by the thermocouple and not the real temperature of the sample.

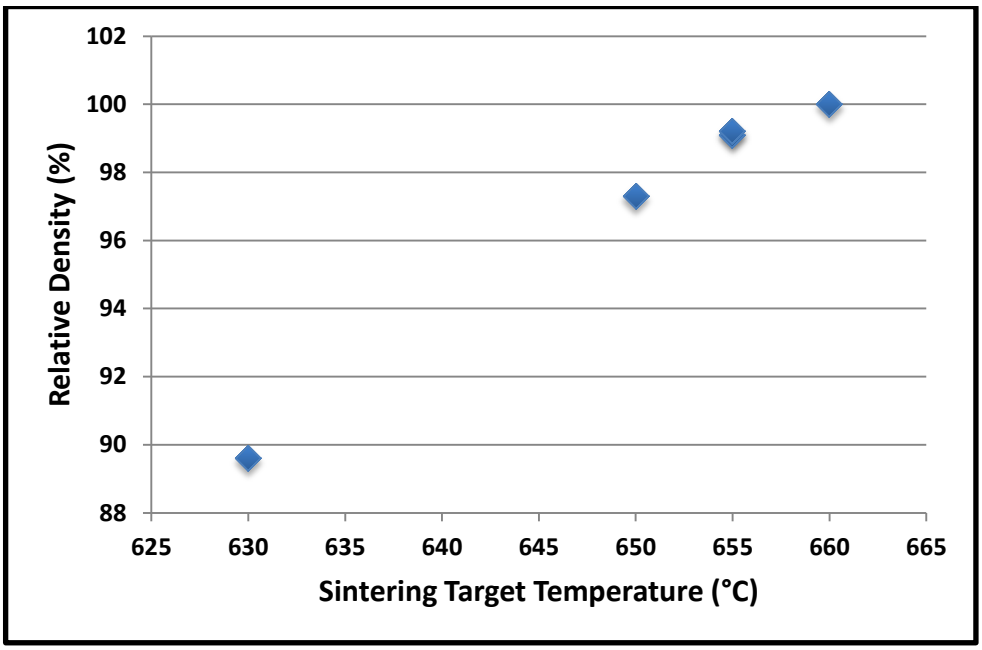

Figure 88 - Correlation between target temperature and density of the Al-CNTs specimens sintered by PAFES

The sintered specimens were characterized by density measurements (on the basis of ASTM C373). As it is possible to observe in Figure 88, the higher is the temperature reached during the PAFES process the higher is the density of the final sintered samples.

4.4.3. EXPERIMENTAL ROUTE

The work on carbon nanotubes reinforced aluminium composites started from the comparison between two aluminium powders with different grain size. In literature, the used aluminium grain size is generally of the order of micrometres (Bakshi & Agarwal, 2011; Choi & Bae, 2011; Liao, Tan, & Sridhar, 2010); we decided to work with both micro- (-325 mesh grain size) and nano-aluminium. The nanometric aluminium (spheres of 60-80 nm diameter, 99.9% purity) was supplied by SkySpring Nanomaterials Inc.

The first step was the powder preparation. The samples were prepared using an amount of the 3% in weight on respect of the aluminium content of Sigma Aldrich multiwall carbon nanotubes. For nanometric powder particular safety precautions were adopted and the jars for High Energy Milling

were prepared in a confined glove box, to avoid inhalation or environmental dispersion of nanoparticles. After milling, the micro- and nano-aluminium powders mixed with carbon nanotubes appeared as shown in Figure 89 and Figure 90.

Regarding micro-aluminium-CNTs powders (Figure 89), it is possible to observe a general decrease of the aluminium particles grain size and the powders appear as platelets. Despite the presence of few CNTs bundles, the micro aluminium particles appear covered by well-dispersed CNTs. The tubes appears also partially damaged by the HEM and partially incorporated in the aluminium particle surface. So this kind of powders is expected to provide a good distribution and dispersion of CNTs inside the sintered specimens.

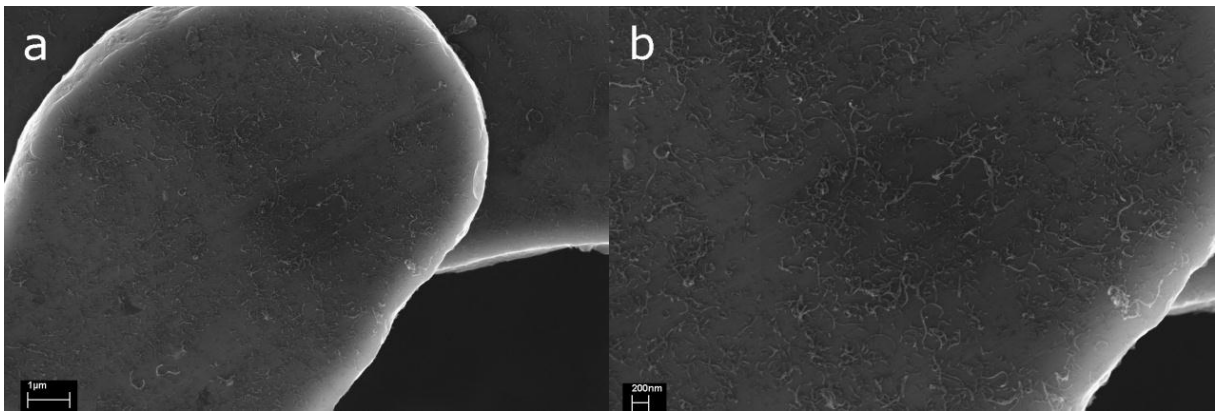

Figure 89 - SEM images at different magnification of micro-Al-CNTs powders after HEM process

With regards to nano-Al-CNTs powders the situation is completely different due to the comparable dimensions of the two components. The samples were prepared dispersing small quantities of HEM powders in acetone and then a drop of the solution in evaporated on a Transmission Electron Microscopy sample holder. The CNTs appear as tangled with nano-grains, which seem to cover the tubes (Figure 90). Furthermore if some CNT bundle is present, probably is covered by nanoparticles.

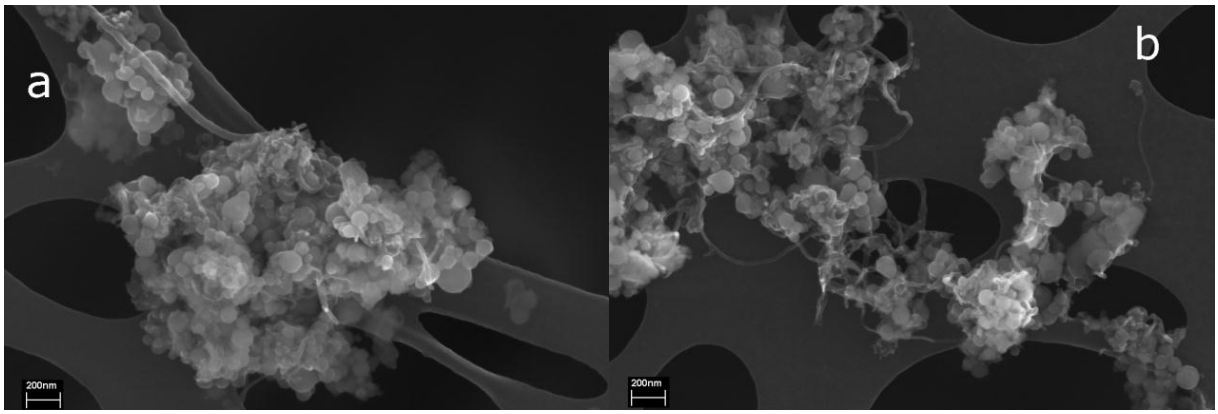

Figure 90 - SEM images at different magnifications of nano Al-CNTs powder after HEM process

In the case of micro-Al-CNTs samples, more than 99% density was obtained considering a theoretical density of 2.62 g/cm^3. Micro-indentation tests showed a mean value of about 40 HV (for pure Al ranges 15 to 35 HV after rolling (Kwon, Estili, Takagi, Miyazaki, & Kawasaki, 2009; Liao et al., 2010)). It is interesting to remark that in this case increased hardness values were obtained after PAFES process, without further treatments (e.g. hot extrusion process as reported by many authors (Esawi, Morsi, Sayed, Gawad, & Borah, 2009; Kwon et al., 2009; Liao et al., 2010)). The FESEM characterization of polished section of these specimens shows (Figure 91) a uniform surface, without porosities. It is also possible to observe some clusters of nanotubes bundles that assumed an oval shape in the direction of pressing (dark elongated spots on the image).

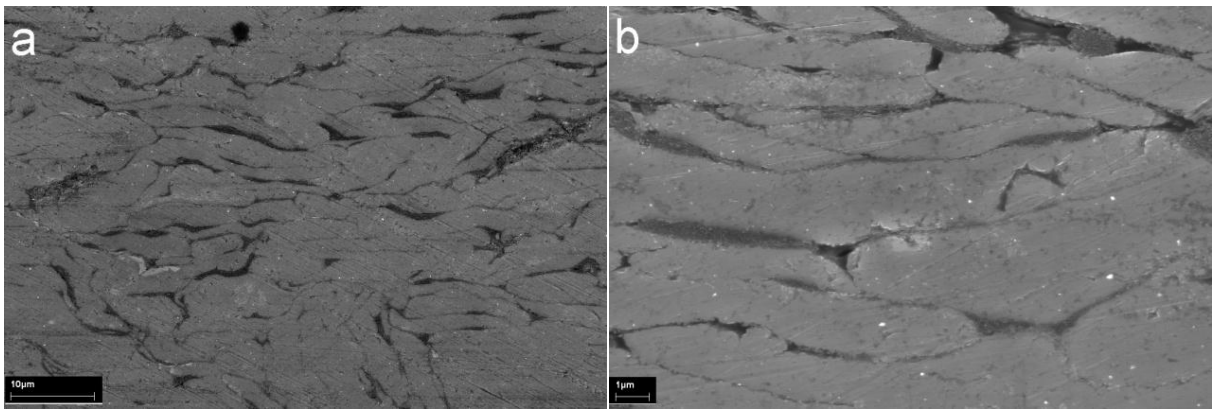

Figure 91 - Different magnification SEM images of CNTs/micro Al composites with a 3% in weight of CNTs

We can model the microstructure of the specimens 3% CNTs in micro aluminium powder with the simple scheme reported in Figure 92, in which the CNTs bundles appears as black spots, elongated to an oval shape in the direction of pressing.

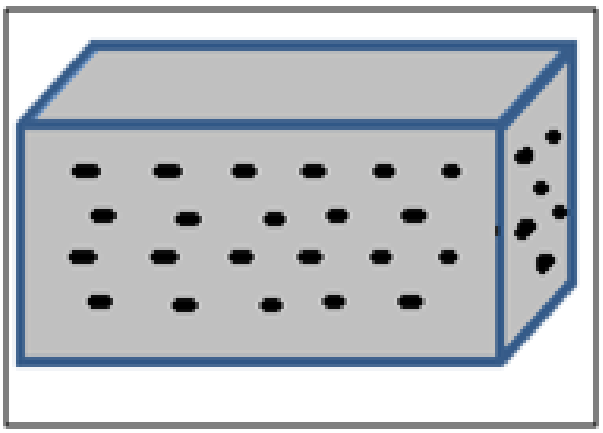

Figure 92 - Simple model of the micro Al-CNTs composites obtained by PAFES

For nano-Al-CNTs powders the sintering process is reasonable with densities of more than 80% (Figure 93). This lower density could be related to the higher oxidation percentage of aluminium nanopowder with respect to micrometric one, and to the difficulties to create a uniform sample made of two nano-components (even considering the CNTs content of 3% wt). In spite of the densities, the nano-Al-CNTs specimens show higher Vickers microhardness values compared to the micrometric ones: the mean value ranges from 80 to 90 HV, with peaks in hardness of 105-110 HV for more dense samples.

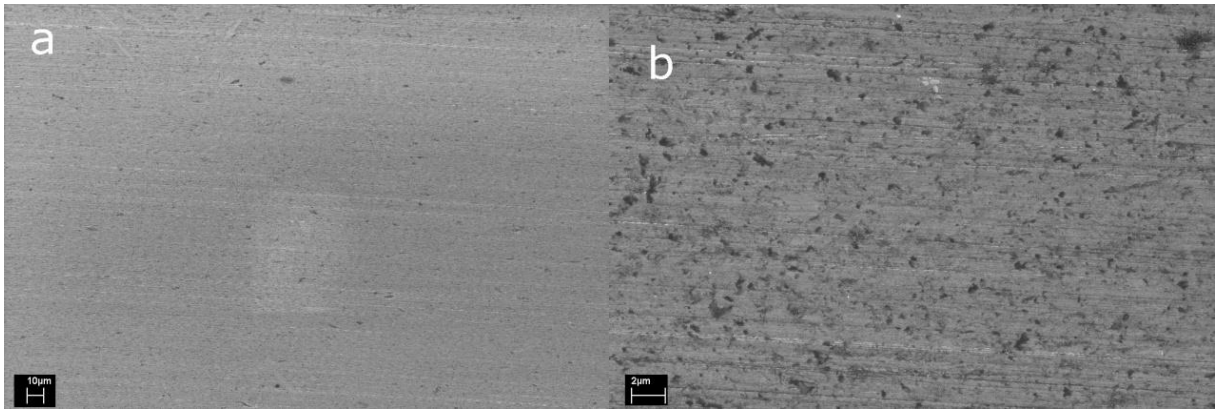

Figure 93 -Different magnification SEM images of CNTs/nano-Al composites with a 3% in weight of CNTs

Because of the presence of an oxidation layer on the nanometric powders it is impossible to obtain the full density of the specimens without the coupling of the PAFES technique with another technique. Also by increasing the sintering temperature it is impossible to observe relative densities higher than 90%, even when a partially melting of the specimens is reached.

A brief paragraph has to be dedicated to the polishing of the aluminium-CNTs powders. This kind of material require a long and difficult tuning. It was very easy to damage the samples with deep scratches during the polishing and also another problem arose with samples of nano-Al-CNTs and with micro-Al-CNTs ones with relative densities lower than 90%: the specimens in contact with water became very hot and small explosions occurred, with the destruction of the composites discs. This phenomenon is most probably due to the formation during the sintering of aluminium carbide. This carbide could react in a violent way with water and produce methane and aluminium hydroxide. To avoid this kind of destructive reaction the less dense specimens and the nano-aluminium based one were polished using ethanol as polishing mean and lubricant. For the dense micro-Al matrix samples water is instead normally used, since there is no possibility for water to come in contact with aluminium carbide. To obtain good results the specimens were polished for very short times and by applying a very low pressure. We started using polishing papers with very small roughness (2400 and 4000) and then we used diamond sticks with granulometry of 6, 3 and 1 µm. The final step was the use of a suspension of nanometric alumina particles to refine the polishing.

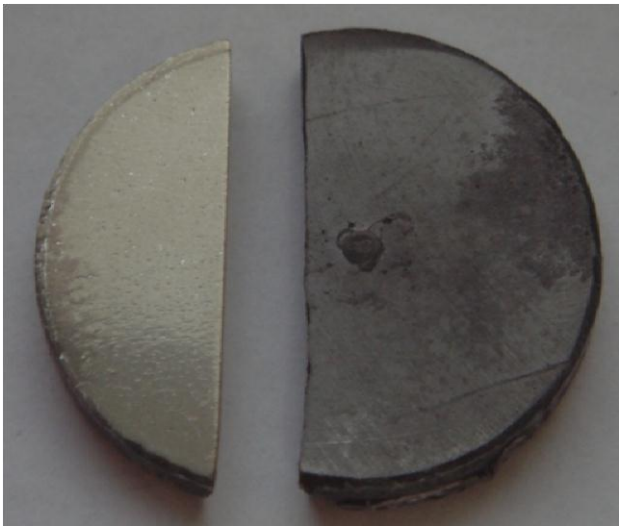

Figure 94 - A specimen before (right) and after (left) polishing

The nano-Al derived samples showed a very brittle and fragile behaviour during the three point flexural tests also because of the impossibility to reach the full density during the sintering process.
Because of the very fragile behaviour of the nano-Al-CNTs composites and also because of the difficulties associated with the sintering of this material we decided to abandon this aspect of the research and to concentrate the work on micro-aluminium powders.
After the decision to use micro-Al particles as matrix materials, the investigation on the composite Al-CNTs had concerned the modification of the content of carbon nanotubes. In addition to the already investigated 3% in weight specimens, 1.5 and 0.3% in weight samples were prepared. The collected values, showed in Figure 95, demonstrate that a sensible increasing of the microhardness is correlated with the presence of small amount of nanotubes on respect of pure aluminium (this kind of specimen is prepared starting from pristine Al particles without any kind of treatment and the powder underwent the same PAFES treatment of the composites). Increasing the nanotubes content also the HV values increased but a slight decreasing is observed for the 3% samples. This could be due to problem related to the dispersion of the filler inside the matrix and the nanotubes reinforcing/refining effect is thus partially compromised.

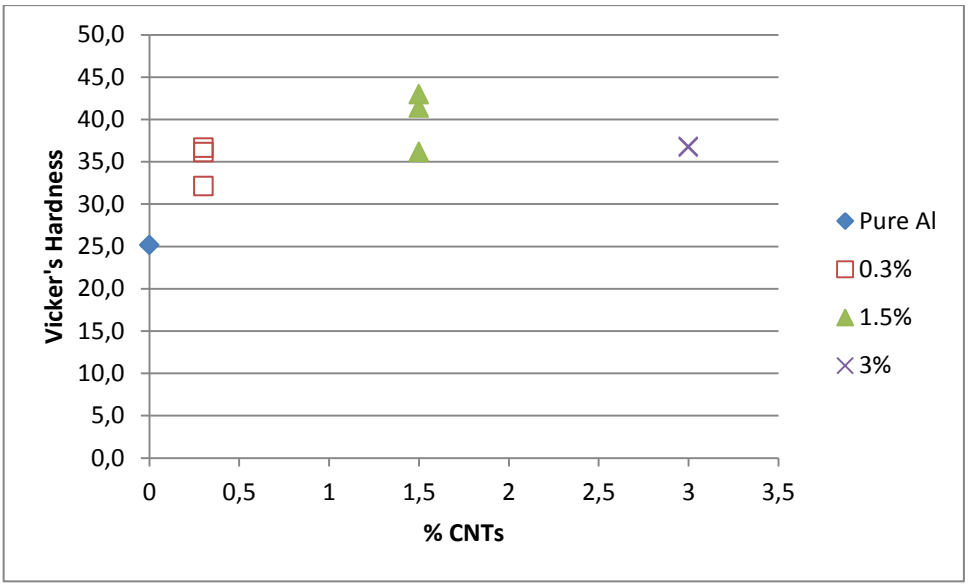

Figure 95 - Microhardness values for micro Al-CNTs composites with 0, 0.3,1.5,3% in weight of reinforcement

The polished sections of the samples were then analysed by SEM (Figure 96).

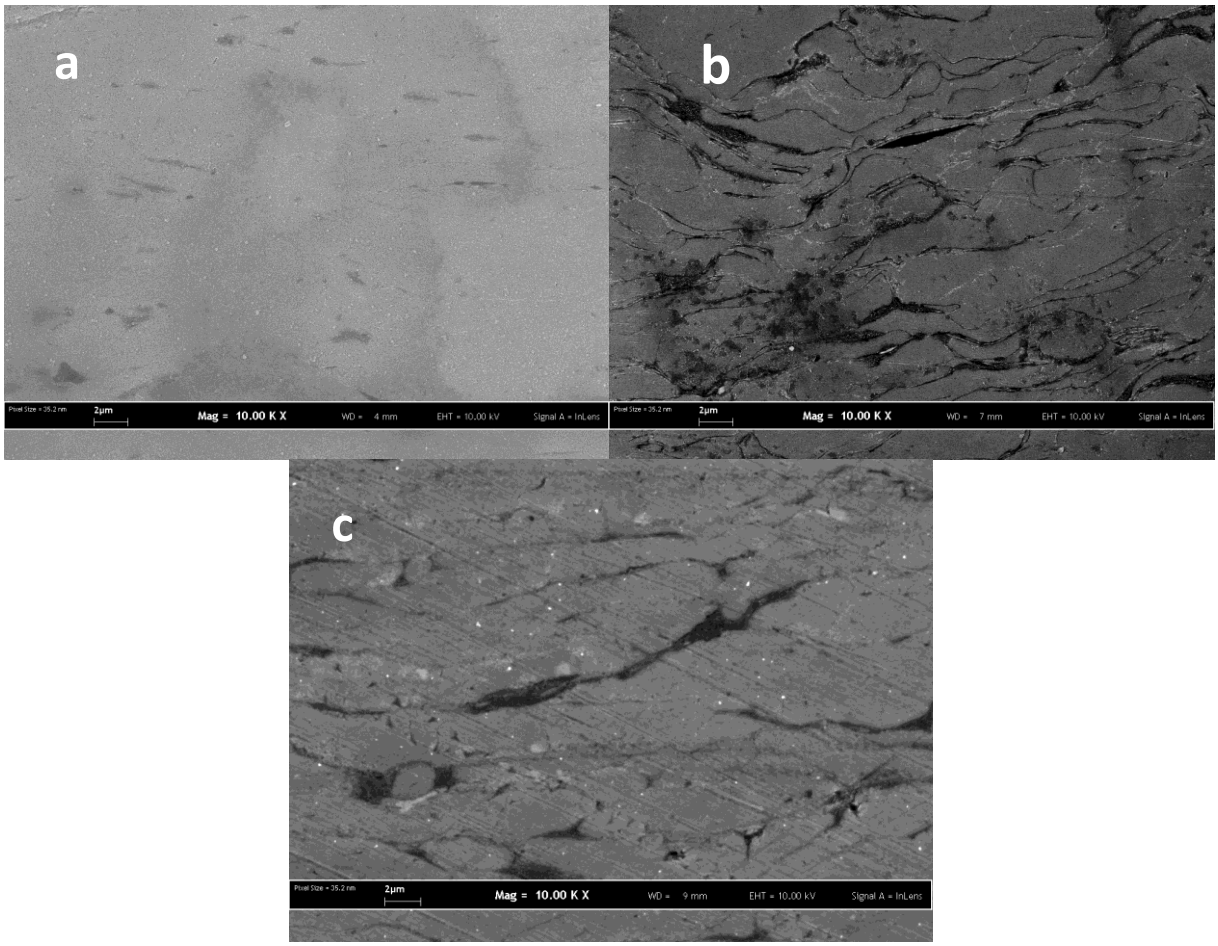

Figure 96 - SEM images for 0.3% CNTs in micro Al matrix (a), 1,5% (b) and 3% (c)

It is possible to observe that for 0.3% in weight of CNTs samples the section appears more homogeneous and a small number of bundles of not dispersed CNTs could be detected. For 1.5% samples the number of elongated black spots of CNTs increase sensibly and a very similar situation could be observed for the 3% in weight of CNTs specimens. The model represented in Figure 92 is valid for more concentrated samples, while for lower amounts of filler the dispersion resulted more efficient and a small number of aggregates and of reduced dimensions could be detected.

The disc-shaped specimens were then cut in order to obtain two small bars for each sample. The bars were then mechanical tested by three-point bending device. We used a three-points bending with 20 mm span configuration, suitable for our small samples.

The results obtained were not in accordance with the microhardness measured and a typical example for each sample is shown in Figure 97.

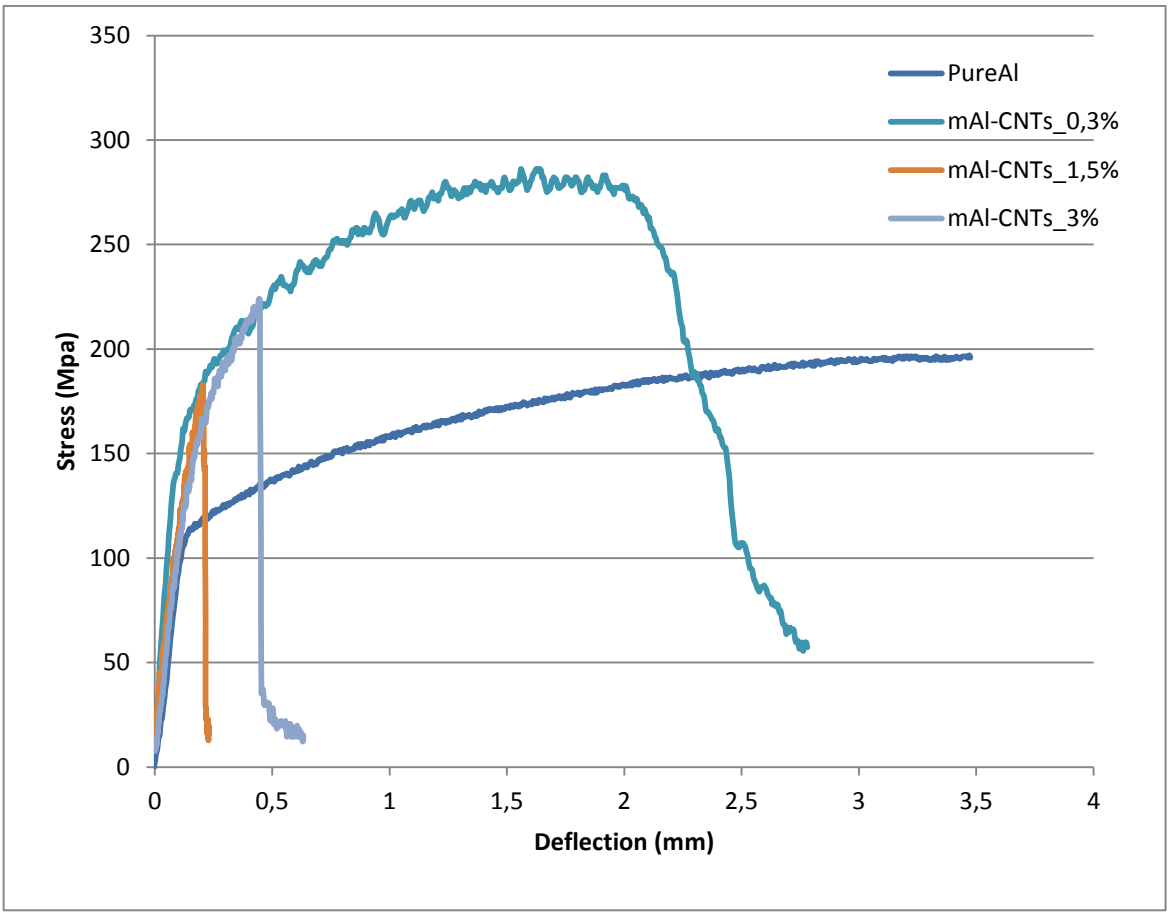

Figure 97 - Strength-stress plot for pure Al, 3, 1.5 and 0.3% CNTs-micro Al composites

The pure aluminium specimens showed maximum strength values lower than 200 MPa and the expected large deformation at fracture; the instrument reached the maximum elongation before fracture, so that at 3,5 mm extension no fracture was yet observed. A small quantity of CNTs could increase sensibly the maximum strength of the material and also its yield strength, with a reduction

of ductility. The higher is the content of CNTs the higher is the possibility to find defects and bundles of not dispersed nanotubes and for this reason both the 1.5 and the 3% samples showed higher maximum strength and lower toughness than pure aluminium but they showed overall mechanical properties not good as the 0.3% samples. It is interesting that the three curves for 0.3%, 1.5% and 3% follows the same trend; this suggests that the nano-structuring of the metal requires only a little fraction of nanotubes, while the others do not contribute to strengthening but instead they create defects that reduce ductility and bring to brittle failure of the material.

On the basis of these considerations we decided to try to improve the dispersion of the CNTs inside the metal powder matrix. The attempt was done by improving the CNTs dispersion before mixing the aluminium powders; 1% in weight of Sigma Aldrich multiwall carbon nanotubes, with respect to micro-aluminium powders, has been used. The composite powder has been prepared starting from nanotubes pre-dispersed in ethanol in presence of 1% of polyvinyl butyral, in order to improve the CNTs dispersion. After that the micro-aluminium powder was added to the mixture and the solvent slowly evaporated during a vigorous mechanical mixing process. The prepared powders were then pressed by cold uniaxial pressing and the green discs obtained were sintered by PAFES in the same conditions used for all the other samples. The choice of the amount of carbon nanotubes (1% in weight with respect to the aluminium) is due to a compromise between the possibility to reach a good dispersion and to introduce inside the composite material a significant quantity of reinforcement. As a comparison, also 1% in weight of CNTs - aluminium powders were prepared as usual by High Energy Milling

The two kinds of composite powders appeared extremely different and we report different scanning electron microscopy images for both the species in Figure 98 and Figure 99.

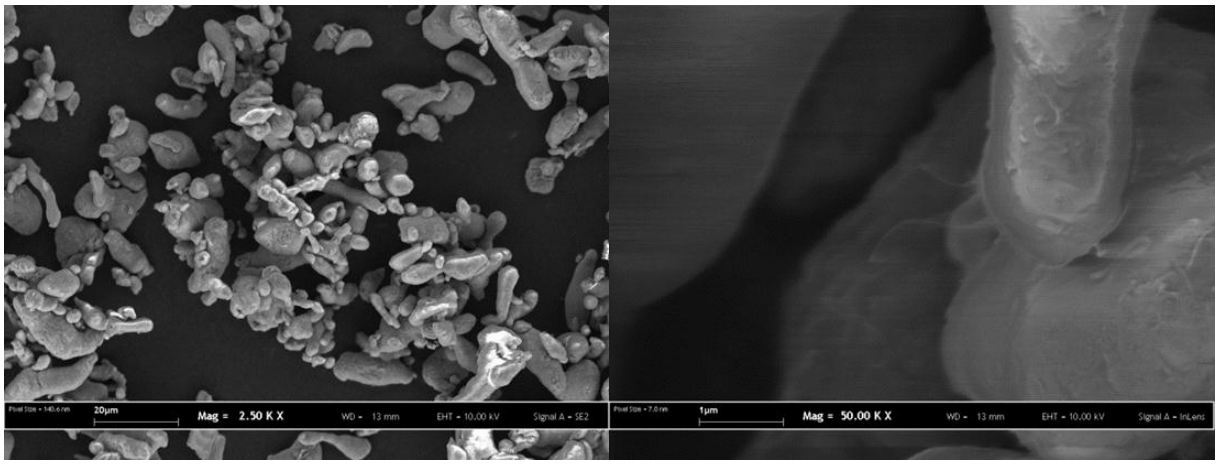

Figure 98 - SEM imagines of micro Al-CNTs dispersed with PVB

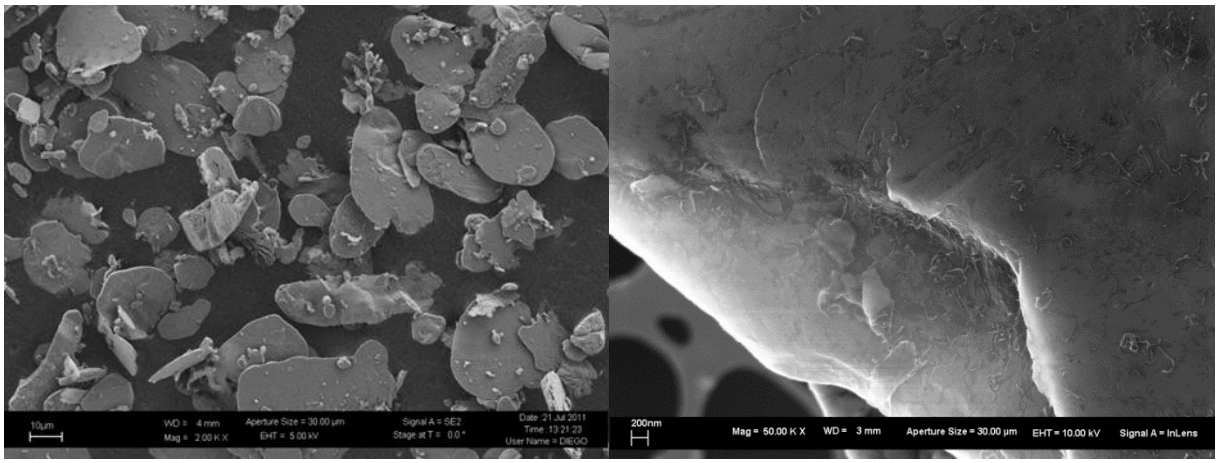

Figure 99 - SEM images of micro Al-CNTs high energy milled

In the case of micro-aluminium with 1% CNTs high energy milled (Figure 99), the particles have lost their spherical shape and they appear as platelets. The carbon nanotubes are well distributed and dispersed on the grain surfaces, they are also partially incorporated into the aluminium. The high energy milling process however not only modified the aluminium particles shape but also partially damaged the CNTs, by shortening them. Despite the presence of few bundles the reinforcements were effectively well dispersed and distributed. To represent the composite particles the model in Figure 100 has been hypothesised.

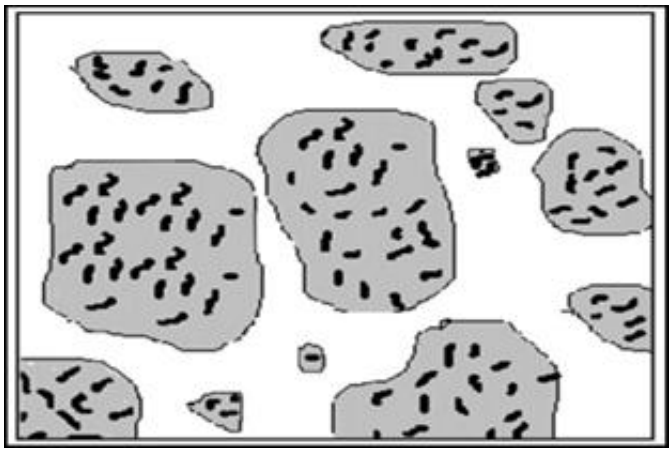

Figure 100 - Model for the HEM micro Al-CNTs particles

For the pre-dispersed carbon nanotubes (Figure 98) the aluminium particles are obviously not deformed and they maintained their spherical shape. The MWCNTs were well dispersed and they appeared just deposited on the aluminium, without any kind of damage and they are also not incorporated in the micro particles.

The HV microhardness for HEM samples with 1% in weight of carbon nanotubes, after PAFES, was of about 43 Vickers, while for the PVB-CNTs-micro Al the average value is 34 Vickers (against the 25 HV

for pure aluminium). The difference in hardness for the two samples could be related to two factors: first the work hardening of aluminium occurring during the high energy milling; second, the absence of grain growth due to the presence of the nano-structuring from carbon nanotubes.

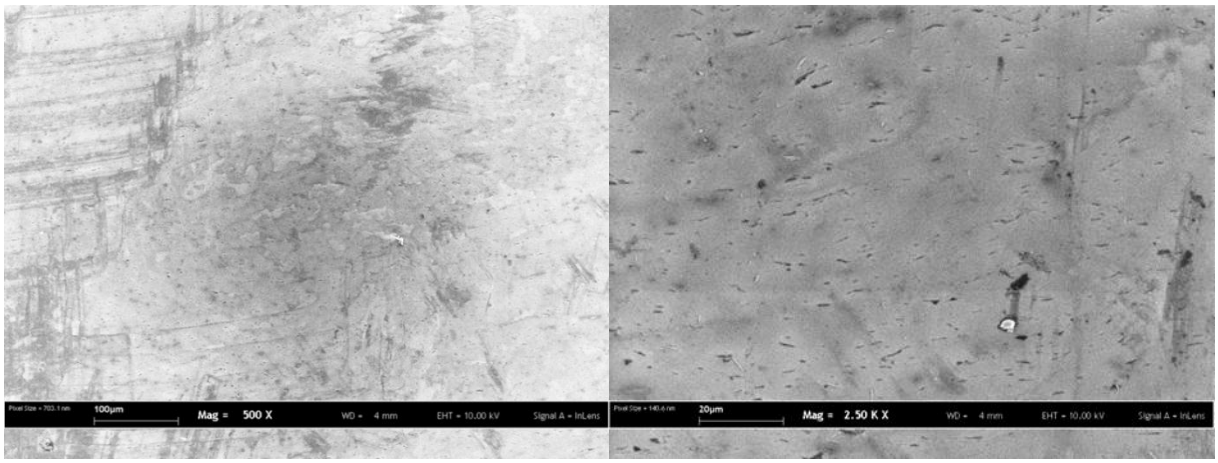

Figure 101 - Microstructure of 1% in weight CNTs Al composites, high energy milled

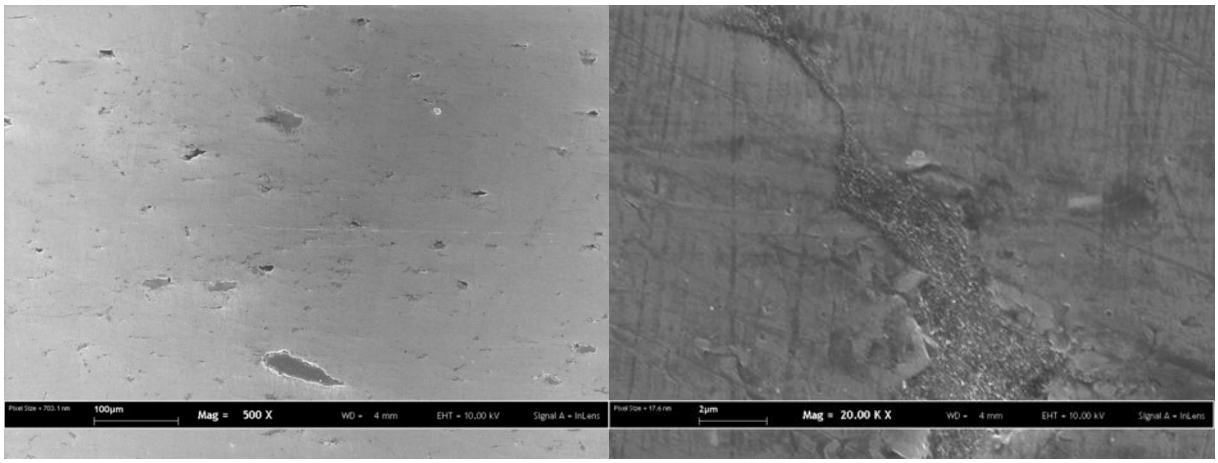

Figure 102 - Microstructure of 1% in weight CNTs Al composites, pre-dispersed using PVB as a surfactant

From the microstructural point of view the HEM sample appeared more homogeneous, with small bundles of not dispersed CNTs in black (Figure 101). In the case of 1% in weight CNTs Al composites with the filler pre-dispersed using PVB as a surfactant (Figure 102), the microstructure appeared less homogeneous: large agglomerates of carbon nanotubes can be detected in the SEM images, and also few pores. These defects were correlated with the formation of gaseous phase during the PAFES process, due to the degradation of the polymer.

The three-point flexural tests confirmed this difference between the two kind of specimens (Figure 103). Both the samples showed an increase of maximum strength and yield strength, and on the contrary a decreasing of the ductility with respect to pure aluminium, but for high energy milled samples the increment of the strength is much larger. In the case of powders treated by HEM, the

results are probably to be laid upon the good dispersion obtained allowed by the nanostructuring of the alloy and the effective reinforcing effect of the nanotubes. A consideration on the fracture surfaces of the specimens should also be done. After three-point flexural tests the fracture surfaces of the small specimens bars, that underwent failure, have been safeguarded by a protective lacquer. They have been finally observed by Scanning Electron Microscopy (Figure 104). The analysis by SEM confirms that, the High Energy Milling process is also responsible for the maintaining of a finer microstructure (Figure 104b).

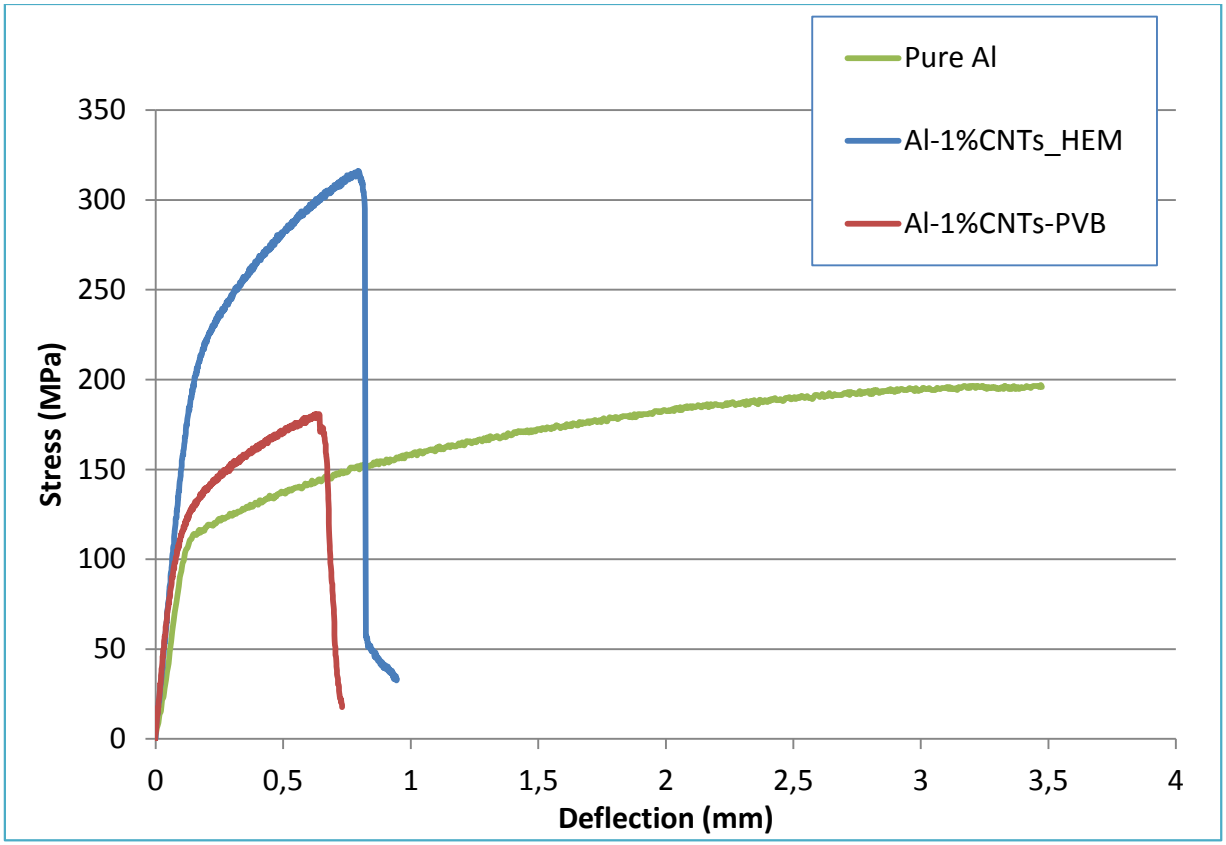

Figure 103 - Strength-stress plot for pure Al, 1% CNTs-micro Al composites prepared by HEM or after pre-dispersion with PVB

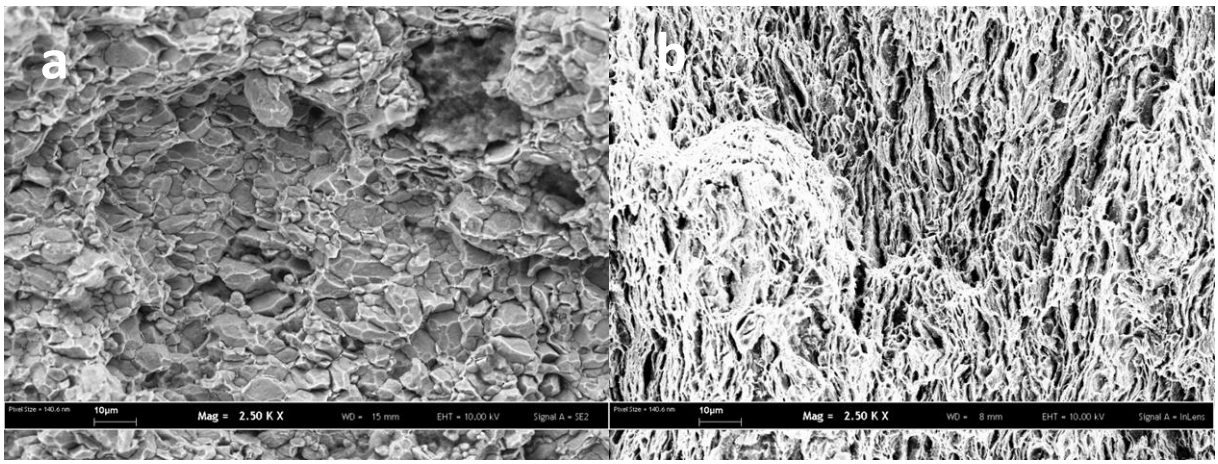

Figure 104 - Fracture surfaces for PVB-CNTs-micro Al composites (a) and HEM ones (b)

One of the most important evidence emerging from the data collected is the remarkable decrease of the toughness of the aluminium matrix in the final composite materials. If a good increase of yield strength and maximum strength could be observed after the addition of carbon nanotubes to the matrix, a considerable loss of toughness is observed. In material science and engineering this is a well-known phenomenon: in composites an increase in mechanical strength is very often accompanied by a reduction in toughness.

This problem of a too strong reduction in toughness when yield strength and hardness are increased is a typical problem observed in metal-matrix composite materials. Since the best toughening mechanism is the exploitation of plastic deformation inside the material, we tried to use this approach to recover the lost toughness and ductility. Several commercial composite materials are already designed including short metal fibres in the matrix, even if generally the matrix is a brittle material. An example of material based on this principle is the FIBERstone™ composite. It is a combination of high purity, refractory ceramic and up to 60% by weight of Custom Produced Stainless Steel Fibres. The combination of the materials is dependent upon the intended application of the composite product. The chart reported in Figure 105 compares the load-deflection curves, and thus the toughness of FIBERStone™ with those of a refractory castable containing a 4% stainless steel fibre addition and a castable with no addition of fibre.

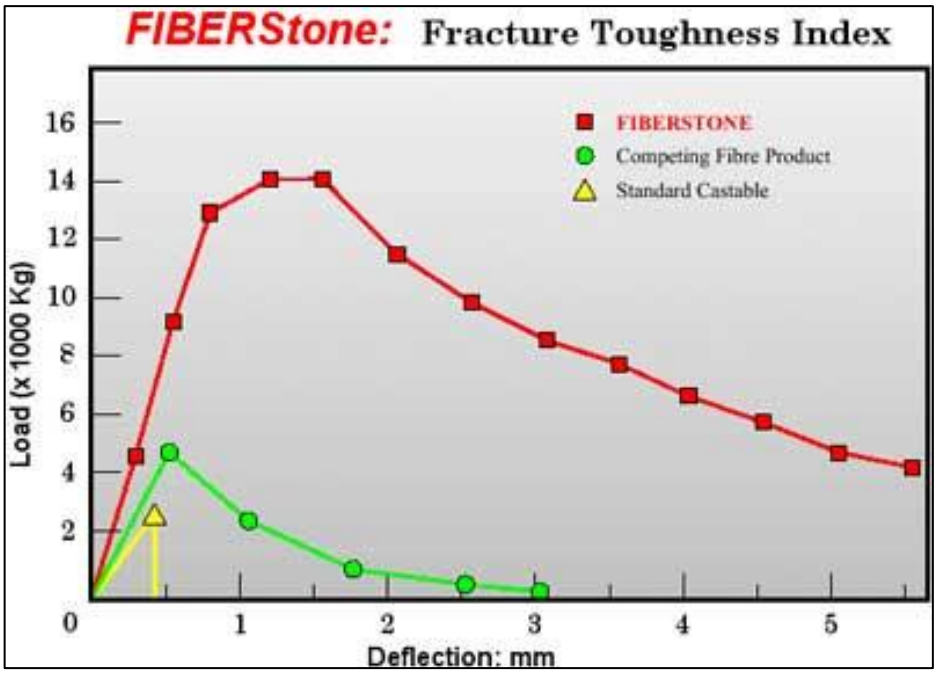

Figure 105 - Fracture toughness of FIBERstone™ composites

The presence of large amounts of short metal fibres allows a sensible increasing of the fracture toughness of the material.

We decided to apply the same idea of toughness improvement to the aluminium/CNTs composites: after high energy milling of pre-dispersed 1% in weight of CNTs and micro aluminium, the composite dried powders were mechanically mixed with micro stainless steel fibres (50% in weight). The prepared mix of powders and fibres were examined by Scanning Electron Microscopy and appeared homogeneous, despite of the large dimensional gap of the three components present in the final product (Figure 106).

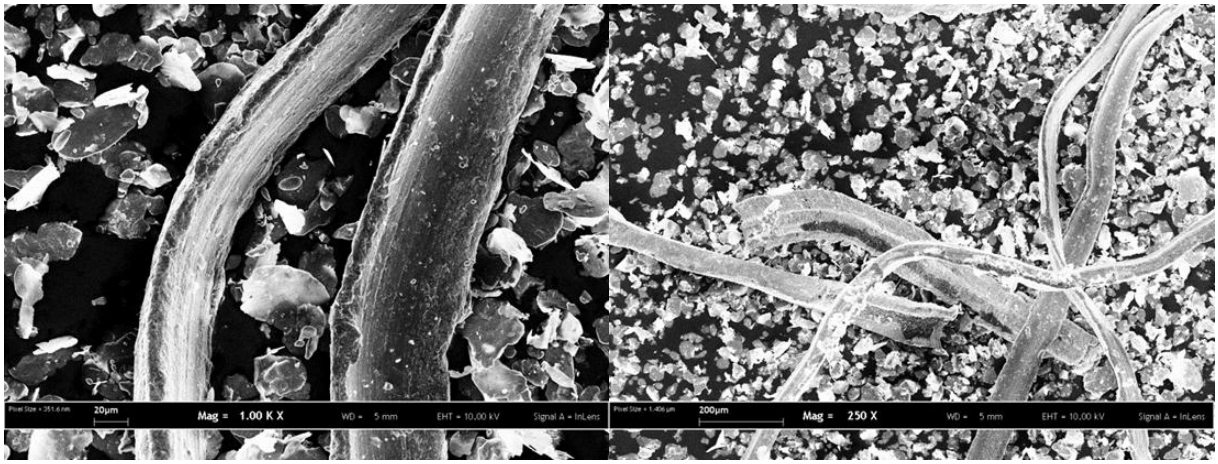

Figure 106 - Al-CNTs-stainless steel fibres composites before sintering process

The full dense samples after sintering were investigated in terms of microstructure. The Scanning Electron Microscopy images showed a very particular aspect, reported in Figure 107.

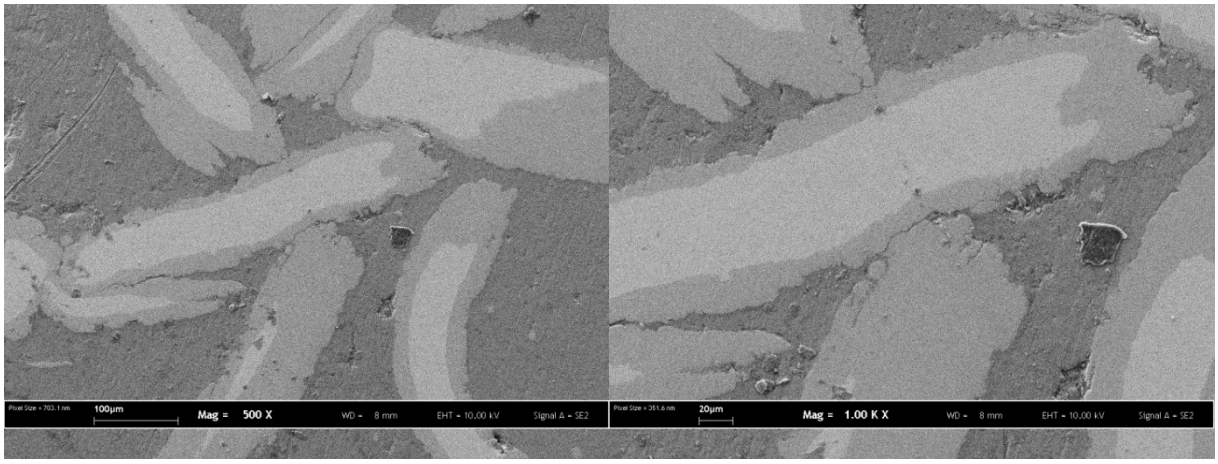

Figure 107 - Microstructure typical of Al-CNTs-stainless steel fibres composites after PAFES treatment

It is possible to observe three different zones in the samples in three different shades of grey. The EDS analysis conducted on the three zones showed the presence of different elemental compositions. In Figure 108 are reported the EDS spectra for the three zones and also the SEM images in which are shown the positions in which the analysis have been conducted.

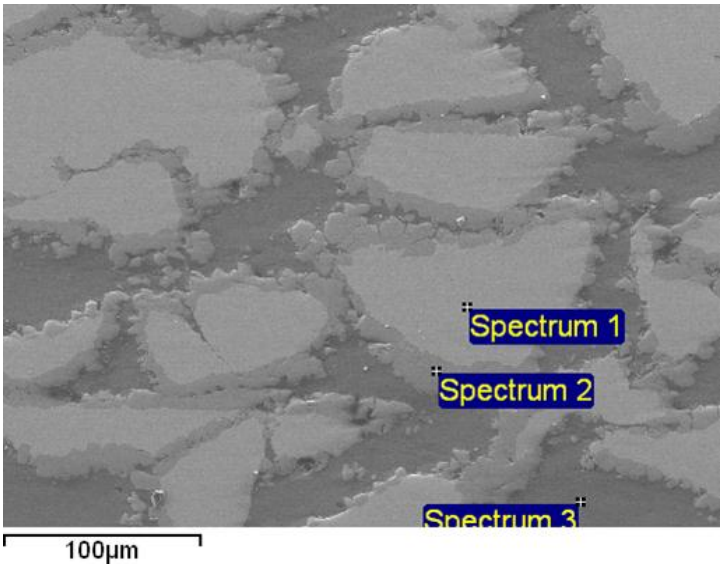

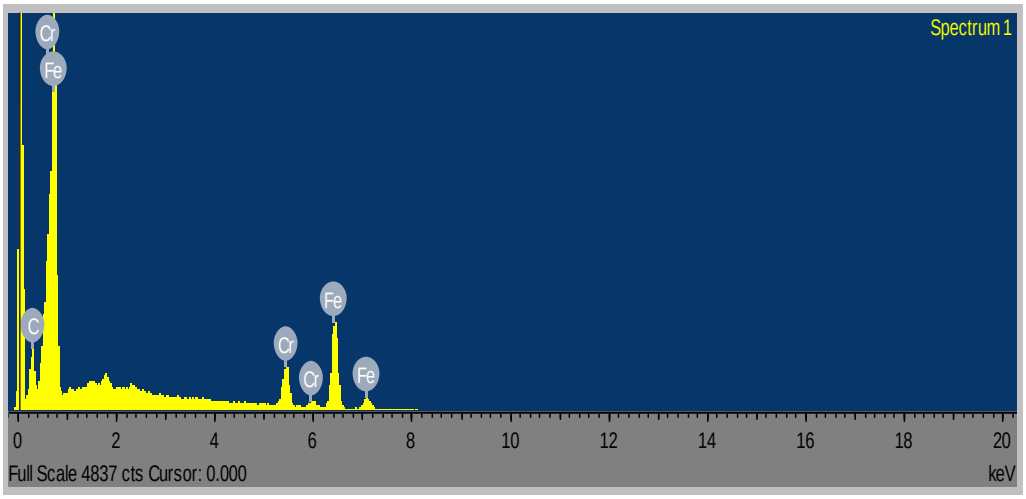

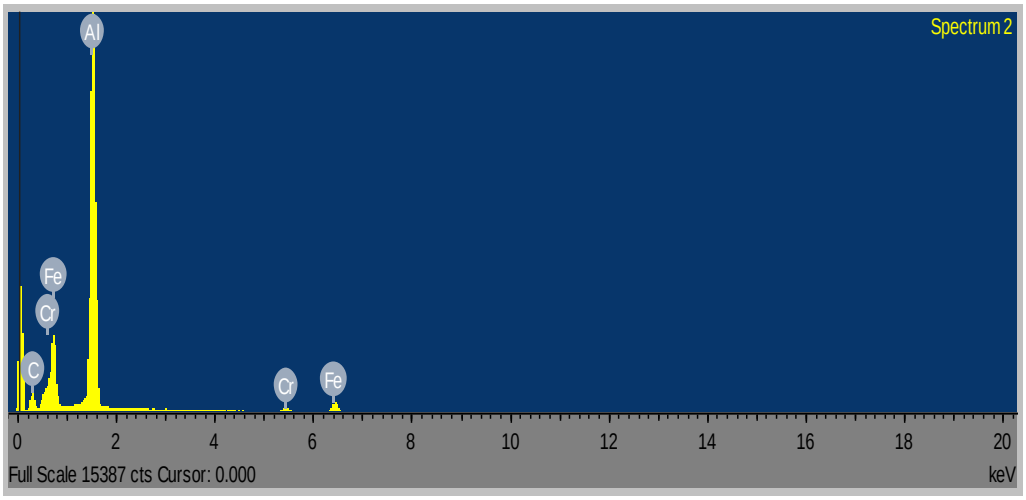

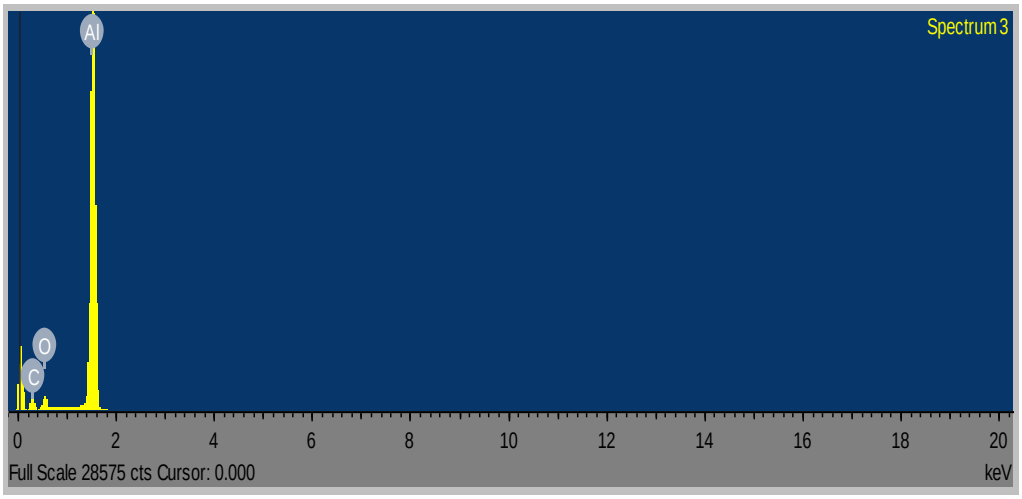

Figure 108 - EDS spectra for the three zones of the Al-CNTs-stainless steel fibres

The EDS elemental analysis shows that we can effectively recognise three compositional zones: the lightest one (Spectrum 1) corresponds to the core of the stainless steel fibres and the elements presents are mainly iron, chromium and carbon. The darkest zones are characterised by the presence of aluminium, with traces of carbon and oxygen, and so it is the composite matrix of aluminium (the presence of trace carbon, is due to the CNTs while the trace oxygen could be due to the small oxide contained in the powders or to a slight oxidation during the sample handling), while the interlayer between the fibres core and the matrix showed that both stainless steel elements and aluminium are present, suggesting a reaction with the formation of an intermetallic of the Fe-Al family. An XRD investigation on the specimens showed the presence of a new intermetallic phase, indicated in Figure 109 with the generic composition Al_xFe.

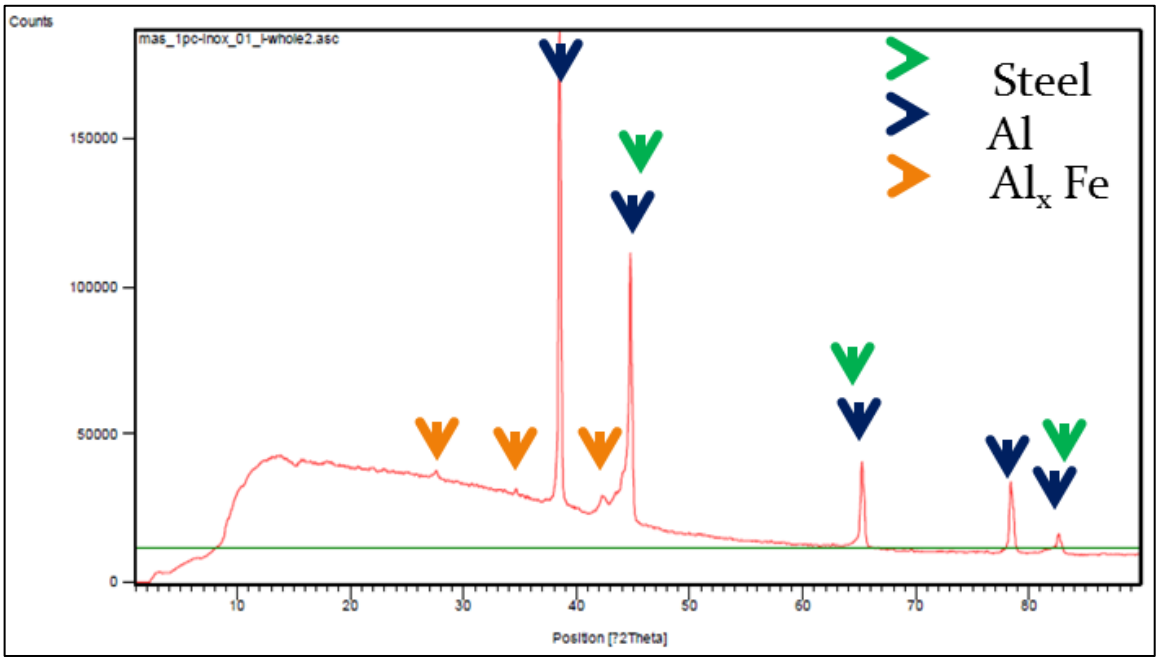

Figure 109 - X-ray diffractometric results for Al-CNTs-stainless steel fibres composites

Because of the formation of the Al-Fe intermetallics a very fragile and brittle behaviour was registered during the three point flexural tests (Figure 110).

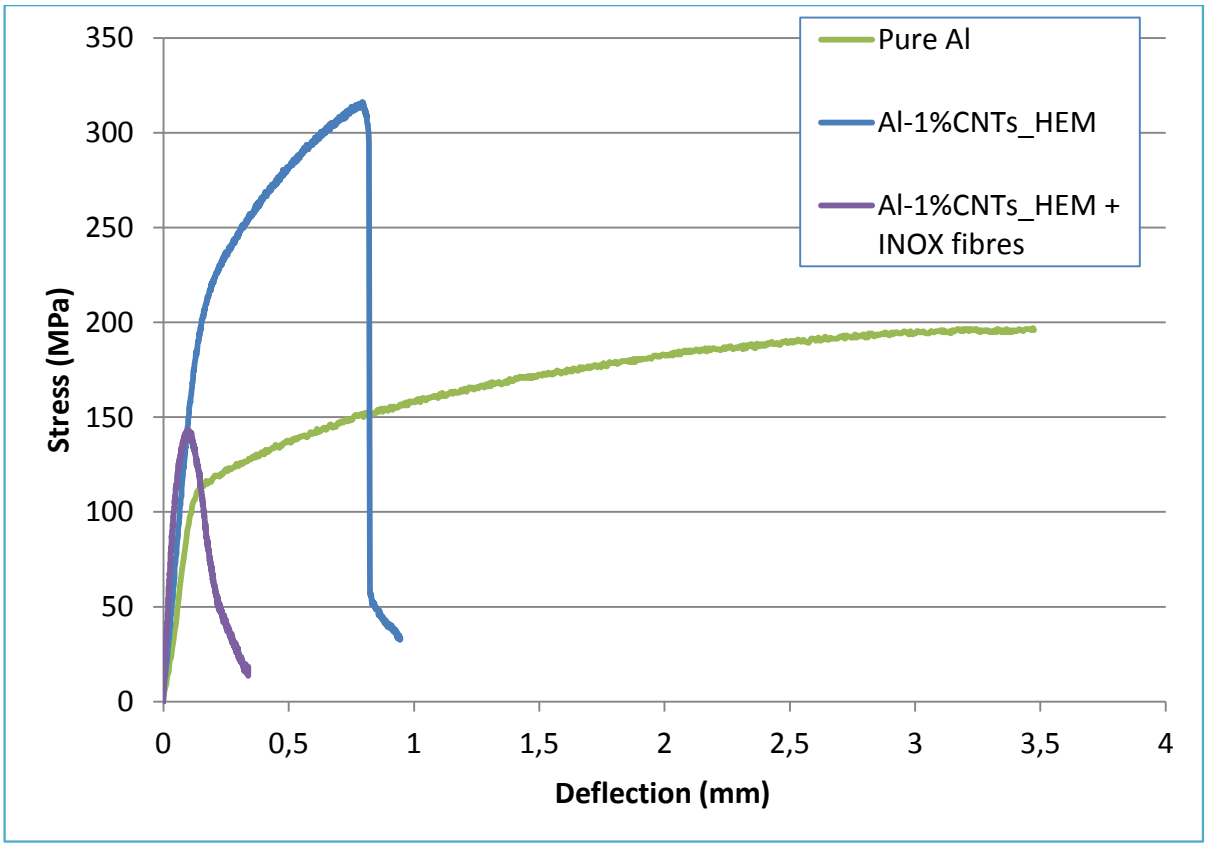

Figure 110 -Strength-stress plot for pure Al, 1% CNTs-micro Al composites prepared by HEM and 1% CNTs-micro Al composites prepared by HEM and sintered with 50% in volume of stainless steel fibres

Because of the reaction between iron and aluminium at the sintering temperature the use of stainless steel fibres to increase the toughness of the CNTs-aluminium composite materials is not efficient. Many tests were realised to optimise the sintering temperature without resulting in steel-Al reaction but no satisfying results were obtained.

Thus, we decided to change the micro-fibres added to the composite powders and try with pure aluminium ones. They are less tough than steel, but we can be sure that no reaction occurs. The composite powders (Figure 111) were prepared using both the powders prepared with the two approaches described before, the PVB approach and the high energy milling process. The 1% in weight of CNTs was added and the 20 and 10% in volume of aluminium powder were tested.

The microstructure of the samples appeared homogeneous and it is impossible to individuate the fibres in the matrix. Also in these cases the carbon nanotubes appeared as black elongated spots on the polished surface of the composite specimens (Figure 112).

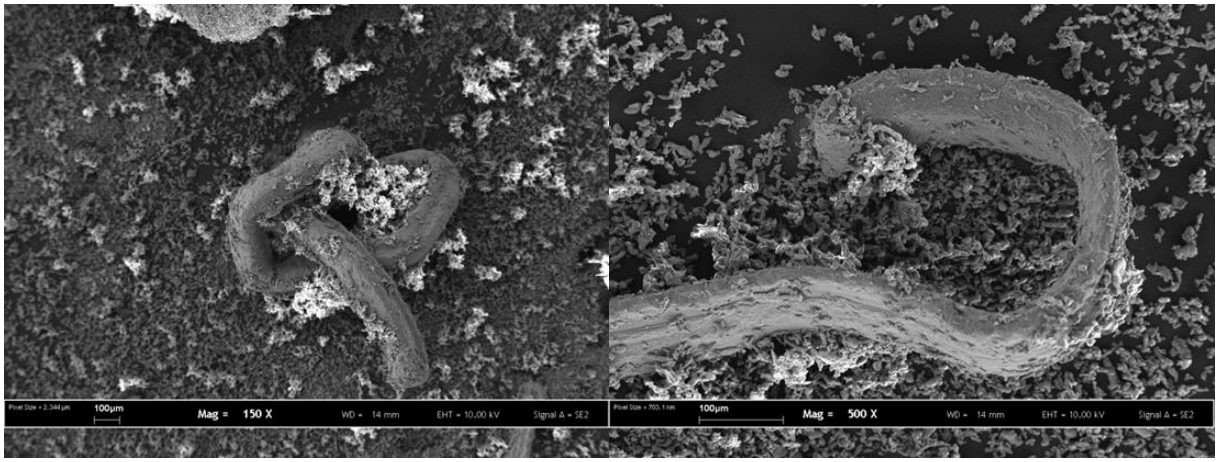

Figure 111 -Al-CNTs-aluminium fibres composites before sintering process

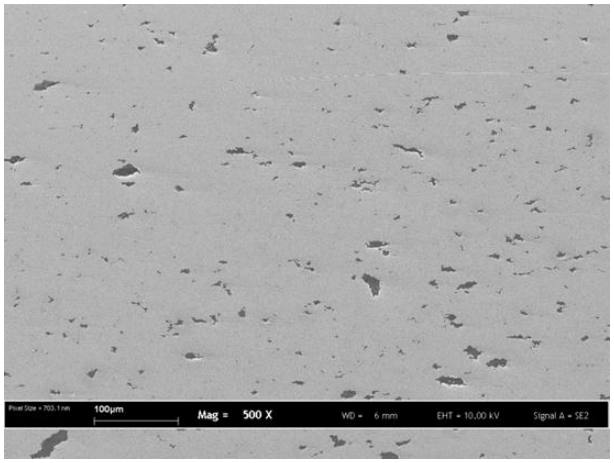

Figure 112 - SEM image of a polished section of the Al-CNTs-aluminium fibers composite

The three point flexural test results are showed in Figure 113. The addition of 10 or 20% in volume of aluminium microfibers increased sensibly the maximum strength (about 250 MPa) and the toughness of the composites on respect of pure aluminium. The metal fibres are responsible of these improvements of the composite properties provided that, during the sintering process, the reaction among aluminium matrix and the component of the fibres does not occur (with the formation of brittle intermetallic phases). In addition, both the kind of specimens showed an increasing of the maximum strength with respect to the pure matrix, but in case of high energy milled powder the specimens appear more resistant. However, slight decreasing of the yield strengths of the composites with aluminium microfibers could be observed, with respect to the 1% CNTs high energy milled composites. The effects of toughening, carried out by the fibres, and of reinforcing, carried out

by CNTs, are competitive and a compromise between them should be reached in order to obtain designed composites with pursued final properties.

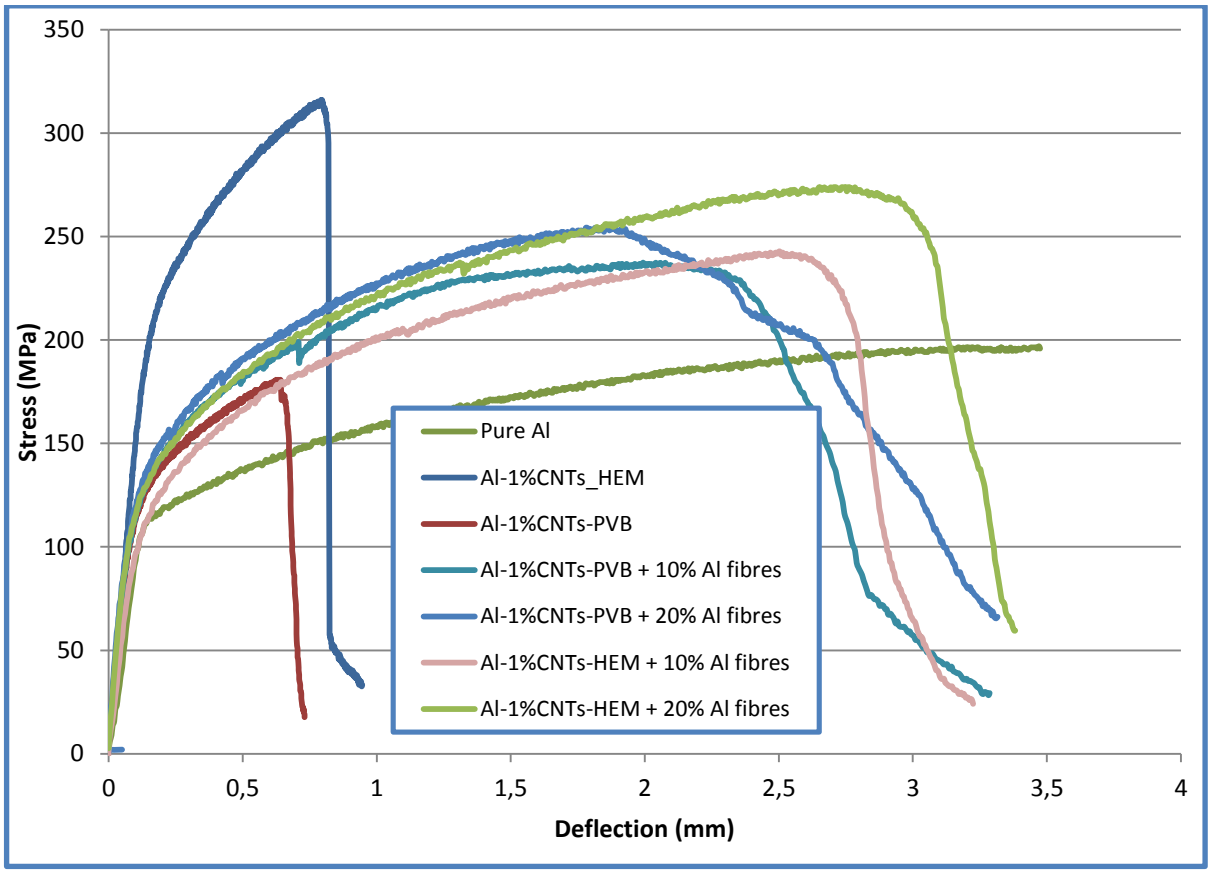

Figure 113 - Strength-stress plot for pure Al, 1% CNTs-micro Al composites prepared using PVB as a surfactant and 1% CNTs-micro Al composites prepared or using PVB as a surfactant or by high energy milling, and sintered with 20 and 10% in volume of stainless steel fibres

REFERENCES

Bakshi, S. R., & Agarwal, A. (2011). An analysis of the factors affecting strengthening in carbon nanotube reinforced aluminum composites. *Carbon*, *49*(2), 533–544. doi:10.1016/j.carbon.2010.09.054

Biamino, S., Liedtke, V., Badini, C., Euchberger, G., Huertas Olivares, I., Pavese, M., & Fino, P. (2008). Multilayer SiC for thermal protection system of space vehicles: Manufacturing and testing under simulated re-entry conditions. *Journal of the European Ceramic Society*, *28*(14), 2791–2800. doi:http://dx.doi.org/10.1016/j.jeurceramsoc.2008.04.006

Choi, H. J., & Bae, D. H. (2011). Strengthening and toughening of aluminum by single-walled carbon nanotubes. *Materials Science and Engineering: A*, *528*(6), 2412–2417. doi:10.1016/j.msea.2010.11.090

Esawi, A. M. K., Morsi, K., Sayed, A., Gawad, a. A., & Borah, P. (2009). Fabrication and properties of dispersed carbon nanotube–aluminum composites. *Materials Science and Engineering: A*, *508*(1-2), 167–173. doi:10.1016/j.msea.2009.01.002

Kwon, H., Estili, M., Takagi, K., Miyazaki, T., & Kawasaki, a. (2009). Combination of hot extrusion and spark plasma sintering for producing carbon nanotube reinforced aluminum matrix composites. *Carbon*, *47*(3), 570–577. doi:10.1016/j.carbon.2008.10.041

Liao, J., Tan, M.-J., & Sridhar, I. (2010). Spark plasma sintered multi-wall carbon nanotube reinforced aluminum matrix composites. *Materials & Design*, *31*, S96–S100. doi:10.1016/j.matdes.2009.10.022

CHAPTER 5: CONCLUSIONS

The carbon nanotubes issue represents a big dilemma for researchers all around the world since their discover, in 1991. The complexity of their physical and chemical properties makes them one of the most promising material in nature, but also one of the most arduous. In particular their aggregation states make them very hard to be dispersed and distributed inside a matrix (of various nature) and so it results complicated to exploit their potential as reinforcement materials in composites. During this Ph.D. work, the fundamental importance of the dispersion of the carbon nanotubes was understood and an easy and cheap way to obtain it was found: the polyvinyl butyral polymer can be successfully used as a dispersant for CNTs. It is a low cost material and the dispersion process in which it is implied is very simple: the ultrasounds can partially debundle the nanotubes aggregates and the polymer can wrap them assisting their dispersion. Despite the attempts conducted, the evaluation of the dispersion remains a considerable issue, mainly due to the nano-size of the CNTs and their chemo-physical properties. The best results can be obtained exploiting microscopy, and in particular, in the present research work, Scanning Electron Microscopy (SEM) was largely used. Moreover, good results can be reached by alternative techniques, i.e. UV-visible spectroscopy, which exploit the scattering effect of the dispersed carbon nanotubes in a solution.

The importance of the study of the carbon nanotubes dispersion is related to their application in composite materials, and during this Ph.D. work several attempts were made in order to cover the three main categories of composite materials: polymer matrix composites (PMCs), ceramic matrix composites (CMCs) and metal matrix composites (MMCs). In the first case the polymer polyvinyl butyral was used as a matrix and the composites investigated were produced using the tape casting technology. The experiments conducted showed increased dispersion grade of the CNTs increasing the contact between polymer and reinforcements. The ceramic matrix reinforced by CNTs during the present work is silicon carbide. The procedure implied the exploiting of the tape casting technology, to cast the SiC-CNTs composite and, after two proper thermal and sintering cycles, the final products were constituted by multilayer specimens. Finally, the investigation of MMCs involved a powder metallurgy approach for the mixing of CNTs and aluminium powders, which are then sintered using a very promising technique, based on electric current and pressure, the Pressure Assisted Fast Electric Sintering. It is interesting to remark that in this case PAFES allows to obtain satisfying mechanical behaviours, without further treatments, as generally reported in literature (e.g. hot extrusion process as reported by many authors). The carbon nanotubes are responsible for the increasing of the

maximum strength of the composites but to the detrimental of their toughness. To supply to this disadvantage the use of metal micro-fibres, in addition to the CNTs, was successfully experimented.

For all the three composites reinforced by carbon nanotubes good results have been registered. In particular, the improvement of the mechanical properties, with respect to the pure matrices ones, appeared to be strictly related to the dispersion state of the reinforcements. Indeed, bundles of CNTs not well dispersed, in all the three cases, act as defects and cracks generators. The use of PVB as a surfactant can help the dispersion of the carbon nanotubes and thus can improve their reinforcement action inside the composites. The excess of polymer can be easily eliminated by thermal treatments and so its use did not modify in a substantial way the processes of composite preparation.

Definitively, a good and cheap dispersion route for carbon nanotubes had been developed during the Ph.D. experimental work, and we demonstrated that it can be easily and successfully applied to the production of composites with improved mechanical properties.

ACKNOWLEDGEMENTS

I would like to express my sincere gratitude to Matteo Pavese for the possibility he gave me, almost four years ago, to work with him and join the HTMAT group. Thank you for all the things you taught me and for the patience demonstrated in the (numerous) moments I lost control. A special thanks to Professor Badini, Professor Paolo Fino and Sara Biamino for the scientific and human support. Thank you very much to Diego Manfredi, for his ideas on aluminium-CNTs composites, for his invaluable encouragements and for his patience during my “Bridget’s style” tales, and to Fabio Deorsola for the help with the PAFES device.

Thanks to all my colleagues of the last four years, for helping me in one way or another during this doctorate. Especially, Elisa, Veronica, Dreidy and Simona, the best office mates and friends I could desire; to Eleonora, Emiliano, Mathieu, Claudio D., Lorenzo, Simone, Andrea C. and Andrea R. for our wonderful lunch breaks and “briscole”; and finally to Andrea P., who stopped to be a colleague and he became a good friend.

My infinite gratitude and love to my family, for the support demonstrated during all my life and for the unconditional faith they always put in me. Thanks to Sara, because she is not only a sister but she is also my best friend, and to Andrea, apple of my eye.

A special mention to all my old friends of a life, because they have always been here for me since I was born, but also to the new wonderful people I met in last years and that became irreplaceable. Thank you so much to my very best friends Anlis, Sere, Stefi, Dani, Ciunny and Glò for our infinite chats and gossips and for our traditional Sunday breakfasts. And also a special and affectionate thought to Anna and Arianna for our amazing friendship, that made special my years at university, though we never talked about Chemistry.

And finally a special thanks to my beloved Matteo. You taught me the most important thing I could ever learn: what Love is. You are the starting and the arrival point of every future perspective and project.